Analysis of membrane protein translocation pathways in *Arabidopsis thaliana*

Dissertation

der Mathematisch-Naturwissenschaftlichen Fakultät

der Eberhard Karls Universität Tübingen

zur Erlangung des Grades eines

Doktors der Naturwissenschaften

(Dr. rer. nat.)

vorgelegt von

Dietmar Gerald Mehlhorn

aus Heidelberg

Tübingen

2021

Gedruckt mit Genehmigung der Mathematisch-Naturwissenschaftlichen Fakultät der Eberhard Karls Universität Tübingen.

Tag der mündlichen Qualifikation:	27.10.2021
Dekan:	Prof. Dr. Thilo Stehle
1. Berichterstatter:	Prof. Dr. Christopher Grefen
2. Berichterstatter:	Prof. Dr. Gerd Jürgens

Danksagung

Mein Dank geht zuerst an meinen Doktorvater Herrn Prof. Dr. Christopher Grefen. Nicht nur stellte er mir einen Platz für meinen PhD und Forschungen in seiner Gruppe zur Verfügung, sondern unterstützte mich auch mit Anregungen und konstruktiver Kritik. Seine Betreuung legte auch ein Augenmerk auf die zukünftigen Aufgaben in der Wissenschaftskarriere und seine freundlichen Ermunterungen halfen mir meine Englischkenntnisse zu verbessern. Auch ermutigte er mich, mich auf ein Forschungsstipendium zu bewerben.

Ebenfalls möchte ich mich bei Herrn Prof. Dr. Gerd Jürgens als Zweitgutachter und Mitglied meines Thesis-Berater Komitees für seine hilfreichen Anregungen und Diskussionen bedanken. Wäre er nicht, als ich noch im Masterstudiengang „Biomedical Technologies“ eingeschrieben war, so freundlich gewesen, mich in einem Praktikum der Entwicklungsgenetik willkommen zu heißen, hätte ich wahrscheinlich nie den Weg in Prof. Dr. Grefens Gruppe gefunden.

Auch geht mein Dank an Frau Prof. Dr. Claudia Oecking, die mir wie Prof. Dr. Jürgens in meinem Thesis-Berater Komitees mit Rat zu meiner Arbeit beiseite stand.

Mein persönlicher Dank geht auch an die Carl-Zeiss Stiftung für die finanzielle Unterstützung meiner Forschungsarbeit durch ein Stipendium.

Hervorheben möchte ich auch die unvergessliche Zeit am ZMBP. Dafür haben meine Arbeitsgruppenkollegen, insbesondere Prof. Dr. Shuping Xing, Niklas Wallmeroth, Dr. Lisa Asseck, Dr. Martiniano Ricardi und Dr. Ritwika Kar gesorgt. Meinen Dank auch an die vielen Mitglieder der anderen Gruppen, insbesondere an Dr. Sabine Brumm, Dr. Kerstin Huhn, Dr. Simone Frühholz, Dr. Tom Denyer, Dr. Matthias Karnahl, Dr. Theresa Lauster, Dr. Sandra Richter, Marika Kientz, Stefanie Zimmermann, Ulrike Herzog und vielen mehr. Ich glaube die Liste würde die Druckkosten der Dissertation immens in die Höhe treiben und diejenigen die nun nicht Erwähnung fanden sollen dennoch wissen, dass auch sie gemeint sind.

Weiterhin möchte ich meinen jetzigen Kollegen in Bochum, Danke sagen, dass sie mir den Umzug und die Eingewöhnung erleichtert und mich herzlich aufgenommen haben. Insbesondere möchte ich hier Frau Ingeborg Godehardt hervorheben, ohne die vieles im Labor einfach nicht möglich gewesen wäre.

Ich möchte auch meinen alten Schulfreunden danken, Daniel Kögel, Leonard Weidemann und Matthias Bohmke, die mir immer dann Ablenkung verschafften, wenn mein Kopf vor lauter GET/SND/TA-Proteine am Rauchen war.

„Last but not Least“ geht mein Dank an meine Familie, ohne deren Rückhalt und Hilfe ich das alles nicht geschafft hätte. Egal ob Hilfe beim Umzug, als Rückzugsort für Erholung und Jagd, Motivationsstützen oder als Unterstützung in jeder Lebenslage waren sie immer für mich da. Allen voran gebührt mein Dank meiner Frau Dr. Sonja Mehlhorn, die nie müde wurde mir zu helfen und einfach da war, wenn ich sie gebraucht habe.

Abschließend ein verändertes Zitat eines Autors, dessen Bücher mich durch den PhD begleiteten und vielleicht als Kredo für meinen weiteren wissenschaftlichen Werdegang gesehen werden kann: „Life before death, journey before destination, curiosity before discovery and science before knowledge.” DANKE!

Contents

ABBREVIATIONS

CaM	Calmodulin
CAML	calcium-modulating cyclophilin ligand
CLSM	confocal laser scanning microscopy
EMC	ER membrane protein complex
ER	endoplasmic reticulum
GET	guided entry of tail-anchored proteins
G-domain	GTPase domain
G1IP	*At*GET1-interacting protein
HSP	heat shock protein
IMP	integral membrane protein
IP-MS	immunoprecipitation-mass spectrometry
M-domain	methionine-rich domain
MOM	mitochondrial outer membrane
OEM	(plastid) outer envelope membrane
PPIs	protein-protein interactions
rBiFC	ratiometric bimolecular fluorescence complementation
RNC	ribosome-nascent chain
SEC61	secretory 61
SGT2	small glutamine-rich tetratricopeptide repeat-containing protein 2
SGTA	small glutamine-rich tetratricopeptide repeat-containing protein alpha
SNARE	soluble N-ethylmaleimide-sensitive factor attachment protein receptor
SND	SRP-independent
SR	SRP receptor
SRP	signal recognition particle
SS or SP	signal sequence or signal peptide
SYP123	syntaxin of plants 123
TA (-protein)	tail-anchored (-protein)
TEM	transmission electron microscopy
TMD	transmembrane domain
TRC	transmembrane domain recognition complex
TRC40	transmembrane domain recognition complex 40 kDa subunit
UBL4A	ubiquitin-like protein 4a
UBQ12	ubiquitin 12
WRB	Tryptophan-rich basic protein

SUMMARY

Insertion of proteins in the membrane of the endoplasmic reticulum is a pivotal process during their biogenesis. Tail-anchored (TA) proteins, a specific class of membrane proteins, play key roles in many vital cellular processes in almost all cellular membranes. Proper translocation is therefore pivotal. Their characteristic single carboxy-terminal transmembrane domain (TMD) dictates a post-translational translocation, as translation termination occurs concurrent with release from the ribosome. For that reason, TA proteins are prone to aggregation requiring accurate guidance to the destined membranes, and dedicated insertion pathways.

In this thesis, orthologues of one such pathway, the Guided entry of TA protein (GET) pathway was identified in *Arabidopsis thaliana*. Subcellular localisation, extensive interaction studies and characterization of T-DNA insertion lines revealed the conservation and importance of *At*GET1, *At*GET3a and *At*GET4 in a TA protein translocation pathway. Abolishing their function resulted in reduced root hair growth which coincided with reduced protein levels of the TA protein SYP123, which is important for root hair tip growth. However, *At*GET seemed to be dispensable and less than 5% of predicted TA proteins in *Arabidopsis* were shown to interact with *At*GET-proteins raising the question about alternative routes evolved in plants by which TA proteins can be targeted to the ER.

The investigation of *At*GET1-GFP interaction by an immunoprecipitation-mass spectrometry approach led to the discovery of a potential GET-receptor component, G1IP (*At*GET1-interacting protein). It did not share sequence homology with yeast GET2 or mammalian CAML yet its subcellular localisation and a functional analysis associated G1IP as an *At*GET1 co-receptor structurally and functionally related to GET2/CAML.

Furthermore, in this thesis one functional orthologue of the SRP-independent (SND) pathway was identified in *Arabidopsis thaliana*, that exists as two homologs. Investigation of T-DNA insertion lines and interaction screens implicated both proteins, *At*SND2a and *At*SND2b, as components of a sophisticated system for translocation and/or stress response. In this study we investigated similarities to the yeast/mammal SND2 but highlighted and discussed contrasts to these as well.

Large parts of this study were based on extensive protein-protein interaction (PPI) analyses. We made use of ratiometric Bimolecular Fluorescence Complementation (rBiFC), Förster Resonance Energy Transfer Acceptor Photobleaching (FRET-AB) and Fluorescent Lifetime Imaging (FRET-FLIM) and reported here on their recent improvements by incorporating a 2in1-cloning approach. Putative components of the *Arabidopsis* SEC61 translocon served as examples.

ZUSAMMENFASSUNG

Proteininsertion in die Membran des Endoplasmatischen Retikulums (ER) ist ein zentraler Prozess während der Proteinbiogenese. „Tail-anchored“ (TA) Proteine spielen eine wichtige Rolle in vielen lebensnotwendigen zellulären Prozessen und sind in fast jeder Membran vertreten. Bedingt durch ihre spezielle Topologie - eine Transmembrandomäne (TMD) erst nahe des C-terminus - ist die Translation meist zeitgleich mit der Freisetzung vom Ribosom abgeschlossen und eine sofortige Translokalisation zwingend notwendig. Bei dieser posttranslationalen Translokalisation müssen TA Proteine vor Aggregation im Zytosol geschützt und das neugebildete Protein zur gewünschten Membran geleitet werden. Zu diesem Zweck sind verschiedene Insertionspfade entstanden.

In dieser Arbeit wurden Orthologe eines dieser Insertionspfade, des „Guided Entry of TA protein“ (GET) Pfades in *Arabidopsis thaliana* identifiziert. Subzelluläre Lokalisation, intensive Analyse der Protein-Protein Interaktionen (PPI) und die Untersuchung von T-DNA Insertionslinien wiesen *At*GET1, *At*GET3a und *At*GET4 als Orthologe aus und deuteten auf ihre Rolle in der TA Protein Translokation hin. Das Ausschalten des GET Pfades in Pflanzen führte lediglich zu einer Verkürzung des Wurzelhaarwachstums. Dies ging auf zellulärer Ebene mit einer reduzierten Proteinmenge des TA-proteins SYP123 einher, welches für das Spitzenwachstum der Wurzelhaare verantwortlich ist. Jedoch zeigten unsere Forschungsergebnisse, dass der GET-Pfad in Pflanzen kompensiert werden kann. So interagierten zum Beispiel nur weniger als 5% der vermuteten TA Proteine überhaupt mit GET-Komponenten. Zusammengenommen deuteten diese Befunde auf das Vorhandensein eines alternativen Insertionsweges in das ER in Pflanzen hin.

Interaktionsanalysen mittels eines Immunoprezipitations - Massenspektroskopie (IP-MS) Verfahrens mit *At*GET1-GFP führten zur Entdeckung einer weiteren GET-Rezeptor Komponente, G1IP (GET1-Interagierendes Protein). Obwohl es keine Sequenzhomologie zu GET2 aus Hefe oder CAML aus Säugetieren aufweist, deuten die Lokalisierungs- und Funktionsanalysen dieser Arbeit darauf hin, dass es sich um den *At*GET1-Corezeptor handelt und um einen strukturellen und funktionalen Verwandten zu GET2/CAML.

Darüber hinaus wurde in dieser Arbeit ein funktionales Ortholog des „SRP-independent“ (SND) Insertionspfads in *Arabidopsis thaliana* identifiziert, welches als zwei Homologe vorliegt. Untersuchungen der Funktionsverlustmutanten und Interaktionsanalysen deuteten darauf hin, dass es sich bei den beiden Proteinen, *At*SND2a und *At*SND2b, um Kandidaten handeln, die in dem komplexen System der Translokation und/oder in der zellulären Stress-Antwort eine Rolle spielen könnten. Daher wurden in dieser Arbeit Gemeinsamkeiten zu den SND2 Proteinen aus Hefe und Säugetieren untersucht, aber auch Unterschiede verglichen und diskutiert.

Da viele Experimente dieser Arbeit auf Protein-Protein-Interaktionen (PPI) Analysen basierten, wurden im letzten Teil drei Methoden vorgestellt, die durch ein 2in1 basierendes Kloniersystem verbessert werden konnten: ratiometric Bimolecular Fluorescence Complementation (rBiFC), Förster Resonance Energy Transfer Acceptor Photobleaching (FRET-AB) und Fluorescent Liefetime Imaging (FRET-FLIM). Dabei dienten vorhergesagte Untereinheiten des SEC61-Komplexes als Interaktionsbeispiele.

LIST OF PUBLICATIONS

This cumulative thesis is based on following papers/manuscripts, which contain results and scientific input from D. G. Mehlhorn as explained in the chapter: **Personal Contribution**. The publications are attached within the **Appendices** of this thesis.

Accepted papers:

Asseck, L.Y., **Mehlhorn, D.G.**, Monroy, J.R., Ricardi, M.M., Breuninger, H., Wallmeroth, N., Berendzen, K.W., Nowrousian, M., Xing, S., Schwappach, B., Bayer, M., Grefen, C. (2021) "*Endoplasmic reticulum membrane receptors of the GET pathway are conserved throughout eukaryotes.*" Proceedings of the National Academy of Science 118 (**Appendices II**)

Mehlhorn, D.G., Wallmeroth, N., Berendzen, K.W., Grefen, C. (2018) "*2in1 Vectors Improve In Planta BiFC and FRET Analyses.*" Methods Mol Biol 1691: 139-158 (**Appendices IV**)

Xing, S., **Mehlhorn, D.G**., Wallmeroth, N., Asseck, L.Y., Kar, R., Voss, A., Denninger, P., Schmidt, V.A., Schwarzländer, M., Stierhof, Y.D., Grossmann, G., Grefen, C. (2017) "*Loss of GET pathway orthologs in Arabidopsis thaliana causes root hair growth defects and affects SNARE abundance.*" Proceedings of the National Academy of Science 114(8):E1544-1553 (**Appendices I**)

Review:

Mehlhorn, D.G., Asseck, L.Y., Grefen, C. (2021) *"Looking for a Safe Haven: Tail-anchored Proteins and their Membrane Insertion Pathways"* Plant Physiology (**Appendices V**)

Unpublished manuscripts:

Mehlhorn, D.G. and Grefen, C. "Conservation of SND2 in plants", *unpublished* (**Appendices III**)

PERSONAL CONTRIBUTION

Introduction: Looking for a Safe Haven: Tail-anchored Proteins and their Membrane Insertion Pathways (Mehlhorn et al., 2021)

Parts of the introduction were from the Plant Physiology Update: "*Looking for a Safe Haven: Tail-anchored Proteins and their Membrane Insertion Pathways*". Except for the paragraph on GET2/G1IP, the review was written by me with the support of Prof. Dr. Christopher Grefen. Conceptualisation aided by Prof. Christopher Grefen who also made the final editing. Parts of the introduction are from an early version of the manuscript which was completely written by me.

Chapter one: Loss of GET pathway orthologs in Arabidopsis thaliana causes root hair growth defects and affects SNARE abundance (Xing et al., 2017)

For this research article, I contributed the result which shows that the *At*GET homologues interact among one another as well as with some, but not all tail-anchored proteins. I also showed that in *Atget* T-DNA insertion lines compared to wild type plants, the SNARE SYP123 is less abundant within the membrane. For this, I developed the strategy, performed all required experiments, and analysed the observed results. Furthermore, I contributed to the writing of the manuscript for the paper.

Important Note: Results for Fig. S3A (see also Fig. 2 M) and Fig. S5B from this paper originated from my master thesis "Analysis of GET pathway components in *Arabidopsis thaliana*" and are therefore not pivotal as part of this thesis.

Chapter two: Endoplasmic reticulum membrane receptors of the GET pathway are conserved throughout eukaryotes (Asseck et al., 2021)

This research article illustrates the existence of a structural-functional homologue of yeast GET2 or human CAML in plants, G1IP. Here, I contributed results showing that GET1 is interacting with G1IP via its transmembrane domain and not the cytosolic part of G1IP. I planned the experiments, designed, and created the constructs of GIP1cyt,

G1IP-TMDs and others, performed the rBiFC and CoIP-experiments and evaluated the data. Furthermore, I designed and cloned constructs for GET1 coiled coil and generated the constructs for the mammalian insertion assay. Moreover, I verified the data from Dr. Lisa Y. Asseck and the above-mentioned interactions via reciprocal rBiFC fusions. Finally, I supported the first author with all needed information for the writing of the paper and gave input and comments on the manuscript.

Chapter three: Conservation of SND2 in plants (Mehlhorn and Grefen, unpublished manuscript)

Within this manuscript, I performed all experiments and their evaluation, except for the IP-MS analysis which was performed by the Proteome Center at the University of Tübingen of which I evaluated the data. *In silico* analysis of the maximum likelihood tree was shared between Prof. Dr. Christopher Grefen and me. Structural evaluation of SND2 orthologues (Fig. S1) was originated from Prof. Dr. Christopher Grefen and modified by me. The initial draft of the manuscript was prepared by me and reviewed by Prof. Dr. Christopher Grefen.

Chapter four: 2in1 vectors improve in planta BiFC and FRET analyses (Mehlhorn et al., 2018)

This book chapter describes the use of 2in1 vectors for transient use in tobacco rBiFC and FRET/FLIM analyses. Based on interaction studies between the *At*SEC61α1 subunit and other SEC61 subunits of the translocon, I demonstrated three different techniques for PPI. To this end, I performed all experiments, analyzed the data, and generated the reported genetic constructs. Protoplast experiments were performed with the aid of Niklas Wallmeroth and Dr. Kenneth W. Berendzen. The article was written by me together with Niklas Wallmeroth (section for protoplast transformation) and Prof. Dr. Christopher Grefen.

INTRODUCTION

Classification of membrane proteins

Membrane proteins have a substantial diversity of enzymatic, signalling, or structural functions reflecting their importance in cellular homeostasis. As diverse as their function is, so are the differences of how these proteins associate with membranes. In the classical fluid-mosaic membrane model (Singer and Nicolson, 1972), membrane-bound proteins can be classified in two types: peripheral and integral, however, more recently three additional basic types have been described: fatty acid-linked, phosphatidylinositol-anchored, and prenyl group-linked membrane proteins which are all linked to the bilayer by lipid tails (Nicolson, 2014; Buchana et al., 2015).

The fatty acid-linked and the prenyl group-linked proteins can cycle between a membrane-bound and a free cytoplasmic state. This reversible mechanism is often mediated by phosphorylation/dephosphorylation or in an GTP/GDP dependent manner. Contrary to the cytoplasmic faced orientation of this class of membrane-bound proteins, the phosphatidylinositol-anchored proteins bind the extracellular/luminal surface of membranes. They are derived from integral membrane proteins (IMPs) with one transmembrane domain (TMD) via enzymatic cleavage of the TMD and formation of a new C-terminus coupled to the lipid (Buchana et al., 2015).

Peripheral proteins are only transiently bound to membranes. They either bind to integral membrane proteins or to lipids through salt bridges, hydrogen bonds, electrostatic interactions, or a combination of these. Per definition, they do not penetrate the lipid bilayer and are water-soluble and therefore can be extracted easily from the bilayer without detergent. In contrast, integral proteins comprise hydrophobic domains which are sequestered in the lipid bilayer permanently anchoring these proteins, leading to amphipathy, and water-insolubility (Buchana et al., 2015).

One can classify integral membrane proteins by three different characteristics, the number of TMDs (single- or multi-spanning), the orientation after integration in the membrane (type I-III) and linked to temporal modes of integration (co- and post-translational) (Higy et al., 2004).

The topology of type I integral membrane proteins is defined by an N-terminus facing the lumen/extracellular space while the C-terminus is oriented towards the cytoplasm (**Figure 1**). The targeting information lies in a cleavable N-terminal signal sequence (SS) and translocation is conducted via the *Signal recognition particle* (SRP) pathway simultaneous to translation (Goder and Spiess, 2001; Park and Rapoport, 2012; Cournia et al., 2015).

By contrast, type II proteins are anchored within the membrane exactly the opposite direction as type I proteins (**Figure 1**). Type II proteins have a non-cleavable transmembrane signal-anchor which in most cases facilitates SRP-dependent translocation and sequesters them in the lipid bilayer (Goder and Spiess, 2001). A special subclass of type II membrane proteins features a single-spanning TMD close to their C-terminus and are referred to as tail-anchored (TA) proteins (Borgese et al., 2003). These proteins do not have an SS or TMD close to the N-terminus which is why they are not recognized by SRP and translocation occurs *post*-translationally via the *Guided Entry of Tail-anchored protein* (GET)/*Transmembrane domain Recognition Complex* (TRC) pathway or alternatives such as the *SRP-independent* (SND) pathway (Borgese and Fasana, 2011; Hegde and Keenan, 2011; Aviram et al., 2016).

Similar to type II, membrane proteins of type III possess a non-cleavable signal anchor. However, the signal-anchor sequence is reversed. As consequence, their N-terminal end gets translocated across the membrane, thus they adopt an orientation comparable to type I proteins (**Figure 1**) (Goder and Spiess, 2001). Insertion is directed by the machinery involving SRP and the SEC61 translocon (Goder and Spiess, 2001; Higy et al., 2004).

Multi-spanning membrane proteins may belong to either of these types (I-III) based on their first hydrophobic element (cleavable SS, signal-anchor, reverse signal anchor). Insertion is co-translationally directed by the SRP-dependent pathway while the *Endoplasmic Reticulum* (ER) *Membrane protein Complex* (EMC) is important for accurate insertion of the first TMD and defines the topology (Goder and Spiess, 2001; Chitwood et al., 2018).

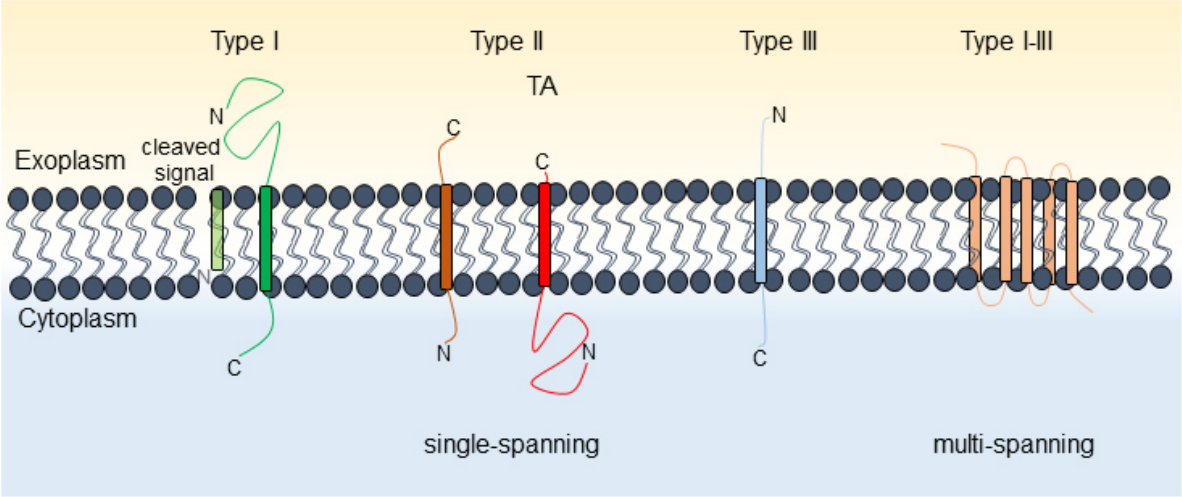

Figure 1: Topogenic classification of integral membrane proteins. The orientation within the lipid bilayer (type I and III: N_{Exo}/C_{Cyt} , type II (including TA proteins): N_{Cyt}/C_{Exo}) as well as the number of TMDs (single- or multi-spanning) defines the integral membrane proteins. Topogenic determinants are a cleaved signal sequence (transparent green) for type I, a signal-anchor for type II, and a reverse signal-anchor for type III IMPs.

Membrane protein translocation across the endoplasmic reticulum

Sustaining the homeostasis of an organism is defined by the precise delivery of newly translated proteins to the predestined location within a cell to retain their functionality. Roughly one third of the average eukaryotic proteome comprises IMPs that act for example as channels, transporters or receptors (Hegde and Keenan, 2011). Eukaryotic cells face many challenges in directing these proteins to their target membrane. The aqueous cytosol would lead to premature aggregation of hydrophobic signal peptides (SP) or transmembrane domains (TMD) of the nascent protein without the protection of chaperoning proteins (Whitley and Mingarro, 2014). Furthermore, navigation to the destined membrane and – once arrived - correct topological integration must be ensured, especially for IMPs with various numbers of TMDs and either cytosolically or luminally facing peptide stretches (Whitley and Mingarro, 2014; Aviram and Schuldiner, 2017). To cope with these challenges, various strategies evolved in eukaryotes ranging from temporal mechanisms (*co*-translational or *post*-translational insertion), chaperones to receptors, insertases and sophisticated translocation complexes (Paul et al., 2013) which will now be described in detail.

The Signal Recognition Particle (SRP)-dependent pathway

Co-translational translocation of most secretory and membrane proteins in or across the ER is mediated by the *Signal Recognition Particle* (SRP) – dependent pathway. This route targets pre-proteins during their synthesis at the ribosome and directly delivers them to the Sec61 translocon for ER-insertion (David J. Anderson et al., 1982) (**Table 1**).

Translocation starts with the recognition and binding of a nascent polypeptide chain by the SRP complex at the ribosome. SRP is composed of a 7SL RNA in complex with six protein subunits (SRP9 [mammals]/ SRP21 [yeast], SRP14, SRP19, SRP54, SRP68, and SRP72) (**Table 1**) (Nyathi et al., 2013). Functionality of SRP is ensured by different domains; among them an Alu domain, a methionine-rich (M) domain and a GTPase (G) domain. SRP binds ribosomes with low affinity which intensely increases when a signal peptide/signal sequence (SP/SS) or an N-terminal transmembrane domain (TMD) of a nascent protein emerges from the ribosome exit tunnel (**Figure 2**). Binding of the M-domain to the SP or TMD precludes its exposure to the aqueous cytosol thereby preventing their aggregation. Subsequent binding of the SRP Alu-domain to the ribosome transiently arrests synthesis by blocking further tRNA entry (Asvin K.K. Lakkaraju et al., 2008; Martinez-Gil et al., 2011; Shao and Hegde, 2011; Richter and Coller, 2015).

Targeting to the ER membrane of the SRP/ribosome-nascent chain (RNC) complex is induced by binding to the SRP-receptor (SR) in a GTP dependent manner (**Figure 2**) (Gilmore et al., 1982; Gilmore et al., 1982). SR is composed of a peripheral ER membrane protein, SRα, and an integral membrane protein SRβ. Binding of SRP-RNC with its receptor leads to conformational changes allowing interaction with the Sec61 translocon (consisting of Sec61α; Sec61β and Sec61γ). Subsequent unloading of the RNC from SRP to Sec61 terminates the translational pause and translation proceeds into the ER membrane or its lumen (**Figure 2**).

Enzymes such as the oligosaccharyl transferase (OST) or signal peptidase (SPase) associate with the translocon during the translocational process facilitating further modifications as N-glycosylation or cleavage of the SS (type I IMP) from the nascent protein, respectively (Nyathi et al., 2013). GTP hydrolysis triggers the disassembly of

SRP from its receptor and recycling of the components for additional rounds of protein targeting (Weiqun Song et al., 2000; Martinez-Gil et al., 2011).

For the discovery that proteins utilize an intrinsic signal to get recognized by the SRP-dependent pathway, Günter Blobel earned a Nobel prize. Later, Randy Schekman was prized as well for the discovery of the Sec61 translocon (Novick et al., 1980; Deshaies et al., 1991), and following research deciphered most of the sophisticated mechanism in yeast and mammals. Conservation of SRP-dependent ER-translocation is presumed in plants despite insufficient research. So far, intensive studies focused on a chloroplast SRP transport system derived from the prokaryotic SRP pathway, which is reviewed in (Ziehe et al., 2017). Currently, a plant SRP-complex has not been described for ER membrane translocation although homologues can be found based on sequence comparison (**Table 1**). Homologues of its receptor are encoded in the *Arabidopsis thaliana* genome and, for the translocon, three homologues of each, the core protein Sec61α and the two subunits Sec61β and Sec61γ can be found (**Table 1**). However, experimental evidence proving functionality is still lacking.

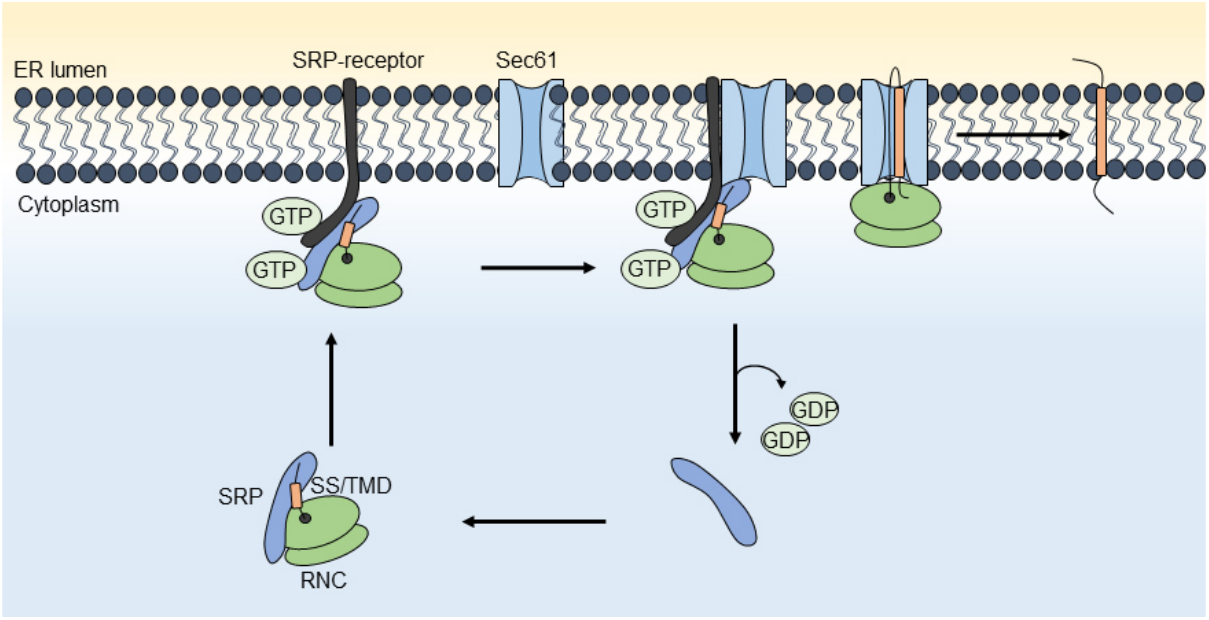

Figure 2: The SRP pathway. SRP binds the signal sequence (SS) or transmembrane domain (TMD) of nascent proteins emerging from the ribosomal exit tunnel and temporaryly arrests translation. Recruitment of the SRP-RNC complex is mediated by the SRP-receptor in a GTP dependent manner. Recognition and transfer of the RNC to the SEC61 translocon resumes translation through the membrane pore. Subsequent GTP-hydrolyses recycles SRP from its receptor.

Table 1: Overview of yeast, mammalian, and *Arabidopsis* SRP/Sec61-pathway orthologues.

SRP/Sec61-pathway		
Yeast	*Mammalian*	*Arabidopsis (AGI Code)*
SRP complex [a]	SRP complex [a]	SRP complex [d]
SRP21	SRP9	SRP9 subunit (At3g49100)
SPR14	SPR14	SRP14 subunit (At2g43640)
SRP19	SRP19	SRP19 (At1g48160)
SRP54	SRP54	SRP54 subunit (At1g48900)
SRP68	SRP68	SRP-*like* protein (At5g61970)
SRP72	SRP72	SRP72 (At1g67680)
SR-receptor [a]	SR-receptor [a]	SR-receptor [b, d]
SRα	SRα	*At*SRα1 (At4g30600)
		*At*SRα2 (At4g35070)
SRβ	SRβ	*At*SRβ1 (At5g05670)
		*At*SRβ2 (At2g18700)
Sec61 translocon [a]	Sec61 translocon [a]	Sec61 translocon [c, d]
Sec61p	Sec61α	*At*Sec61α1 (At2g34250) [c]
		*At*Sec61α2 (At1g29310) [d]
		*At*Sec61α3 (At1g78720) [d]
Sbh1p	Sec61β	*At*Sec61β1 (At2g45070) [c]
		*At*Sec61β2 (At5g60460) [d]
		*At*Sec61β3 (At3g60540) [d]
Sss1p	Sec61γ	*At*Sec61γ1 (At5g50460) [c]
		*At*Sec61γ2 (At3g48570) [d]
		*At*Sec61γ3 (At4g24920) [d]

[a] complex comprises various subunits

[b] see **Chapter 3**: "*Conservation of SND2 in plants*" (part of this dissertation)

[c] see **Chapter 4**: "*2in1 vectors improve in planta BiFC and FRET Analyses*" (part of this dissertation)

[d] based on PSI-Blast analysis (unpublished)

Limits of the SRP-dependent pathway – Tail anchored (TA) proteins

The SRP/Sec61 co-translational pathway reaches its limits when signal sequences or TMDs are absent from the N-terminal part of the protein. This is in particular the case for type II orientated membrane proteins that feature a TMD close to their C-terminal end and are referred to as tail-anchored (TA) proteins (Borgese et al., 2003). To distinguish these from other type II proteins, the C-terminal stretch following the TMD should by definition be no longer than 30 amino acids (Voss et al., 2006). This is roughly the length of a peptide stretch within the ribosomal exit channel. Proteins with such feature are released from the ribosome when their TMD is disclosed to the cytosolic environment requiring immediate action of chaperones to prevent aggregation of the hydrophobic TMD within the aqueous cytosol. Therefore, insertion of TA proteins occurs *post*-translationally (Pedrazzini, 2009; Johnson et al., 2013).

TA proteins make up to ~3-5% of all IMPs and can be found in almost all cellular membranes (Abell and Mullen, 2011). In *Arabidopsis thaliana*, around 500 TA proteins were predicted *in silico* (Kriechbaumer et al., 2009). They play key roles in many vital processes such as vesicle trafficking, apoptosis, translocation of other proteins, ubiquitination, signal transduction, enzymatic reactions, or regulation of transcription (Borgese et al., 2003; Kriechbaumer et al., 2009). Some TA proteins even take part in translocation of other membrane proteins as subunits of translocation machineries such as the Sec61β subunit of the SEC61 translocon, or Tom22 and Toc33 of the mitochondrial and chloroplast import machineries. Additionally, most of the soluble N-ethylmaleimide-sensitive factor attachment receptors (SNAREs) which facilitate vesicle fusion in eukaryotic cells, are TA proteins (Neveu et al., 2020). Their prominent role in many physiological processes is reflected by dramatic phenotypes upon impairment, ranging from conditional sensitivity towards pathogens to embryonic lethality (Lipka et al. 2007).

The Guided Entry of Tail-Anchored protein (GET) pathway

A possible post-translational pathway for TA proteins into the ER membrane is the *Guided Entry of Tail-anchored proteins* (GET) pathway (**Figure 3**) which was initially identified in mammals (as *Transmembrane domain Recognition Complex* (TRC) pathway) and yeast (Stefanovic and Hegde, 2007; Schuldiner et al., 2008) (**Table 2**).

In yeast, nascent TA proteins are recognized right after emergence from the ribosomal exit tunnel through a tripartite pretargeting complex consisting of the small glutamine-rich tetratricopeptide co-chaperone 2 (Sgt2), Get4 and Get5 (Chang et al., 2010; Wang et al., 2010). A functional mammalian homologue of Get4/5 is the BAG6 complex comprising BCL2-associated athanogene cochaperone 6 (BAG6), transmembrane domain recognition complex 35 (TRC35) and ubiquitin-like domain (UBL)-containing protein 4A (UBL4A), which works in cooperation with Small glutamine-rich tetratricopeptide repeat-containing protein α (SGTA), the mammalian Sgt2 orthologue (Mariappan et al., 2010; Johnson et al., 2013). While Sgt2 alone is ineffective in binding TA proteins, Get4/5 assist this process by bridging and facilitating TA protein transfer from Sgt2 to the cytosolic ATPase Get3 (in mammals TRC40 or Asna1) (Suloway et al., 2009; Simpson et al., 2010; Chartron et al., 2011; Gristick et al., 2014) (**Figure 3**).

Key-component of the pathway is the dimeric ATPase Get3. Its subunit interaction is stabilized by a Zn^{2+} ion coordinated by a CxxC motif (Mateja et al., 2009; Simpson et al., 2010). Get3 consists of a nucleotide-binding pocket and a TA protein binding domain and undergoes conformational changes dependent on its nucleotide-binding state (Wereszczynski and McCammon, 2012). In a nucleotide-free state, Get3 is in an open conformation while binding of ATP leads to a closed dimer, thereby creating a hydrophobic groove which binds and shields the TMD of TA proteins (Mateja et al., 2009; Wereszczynski and McCammon, 2012; Mateja et al., 2015). It was demonstrated that unlike SRP, Get3 does not associate with ribosomes (Stefanovic and Hegde, 2007).

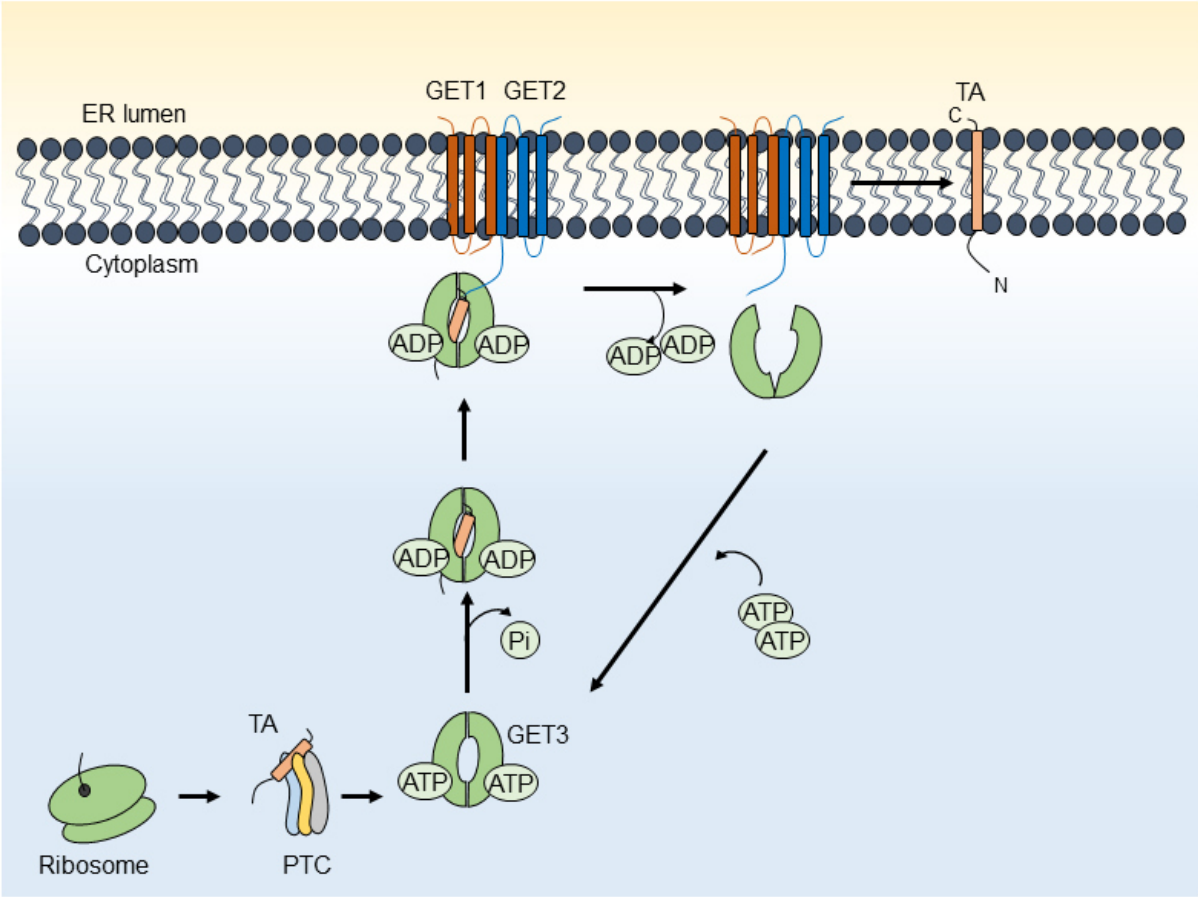

Figure 3: The GET-Pathway in yeast. Newly synthesized TA proteins are captured by the cytosolic pretargeting complex (PTC; comprising SGT2, GET4 and GET5) and transferred to the dimeric ATPase GET3 triggering ATP-hydrolysis. GET3 is tethered to the ER by the cytosolic domain of GET2. Release of ADP and interaction with the GET1-GET2 receptor complex leads to conformational change of GET3 leading to the release and insertion of the TA protein. Rebinding of ATP allows the dissociation of GET3 from the receptor and recycling to the cytosol.

Get3 shuttles the client protein to the ER membrane receptors consisting of a heteromeric complex of Get1 (WRB in mammals (Vilardi et al., 2011; McDowell et al., 2020)) and Get2 (CAML in mammals (Yamamoto and Sakisaka, 2012; Vilardi et al., 2014)) (**Figure 3, Table 2**). The long cytosolic N-terminal domain of Get2 mediates tethering of the Get3-TA protein complex (Mariappan et al., 2011; Wang et al., 2011). Interaction of Get2 only takes place with a nucleotide-bound Get3 which is also compatible with TA protein binding (Denic et al., 2013). Hydrolysis of ATP opens the Get3 dimer. This conformational change disrupts the hydrophobic groove releasing the bound TA protein and providing it for insertion by the Get1-Get2 insertase (Wang et

al., 2014; Zalisko et al., 2017). Intriguingly, Get1 and Get2 compete for Get3 binding via overlapping binding sites (Stefer et al., 2011; Denic et al., 2013), although interaction between Get3 and a coiled-coil domain of Get1 occurs only with an open, nucleotide-free Get3 (Mariappan et al., 2011).

Rebinding of ATP returns Get3 into a closed conformation, thereby weakening the Get3-Get1 interaction which leads to dissociation of Get3 from the membrane and recycling for another round of TA protein loading via the pretargeting complex Sgt2/Get4/Get5 (Stefer et al., 2011; Suloway et al., 2012) (**Figure 3**).

Table 2: Overview of yeast, mammalian, and *Arabidopsis* GET-pathway orthologues.

GET-pathway		
Yeast	*Mammalian*	*Arabidopsis (AGI Code)*
Get1	WRB	*At*GET1 (At4g16444) [a]
Get2	CAML	G1IP (At4g32680) [b]
Get3	TRC40/Asna1	*At*GET3a (At1g01910) [a] *At*GET3b (At3g10350) [a] *At*GET3c (At5g60730) [a]
Get4	TRC35	*At*GET4 (At5g632220) [a]
Get5	UBL4A	*At*GET5 (At1g55060) [c]
Sgt2	SGTA	*At*SGT2 (At4g08320) [c]
- [e]	BAG6	*At*BAG6 (At2g46240) [d]

[a] see **Chapter 1:** "*Loss of GET pathway orthologs in Arabidopsis thaliana causes root hair growth defects and affects SNARE abundance.*" (part of this dissertation)

[b] see **Chapter 2:** "*Endoplasmic reticulum membrane receptors of the GET pathway are conserved throughout eukaryotes.*" (part of this dissertation)

[c] according to (Srivastava et al., 2017)

[d] based on PSI-Blast analysis (unpublished)

[e] currently, no functional orthologue has been discovered

Alternative insertion pathways

The GET pathway is considered as a dominant route for post-translational TA protein insertion into the ER membrane. Contrary to such an implied vital role, the GET genes are not essential under normal conditions in yeast (Schuldiner et al., 2008). The observed lethality under oxidative stress likely relates to the additional function of *Sc*Get3 as chaperone holdase for unfolded soluble proteins (Powis et al., 2013; Voth et al., 2014; Dahl et al., 2015). A screen for TA protein dependency on an intact GET pathway revealed merely two out of 46 potential client proteins in yeast (Rivera-Monroy et al., 2016). It has been shown that the GET-pathway mainly handles ER-destined TA proteins with a high hydrophobicity while TA proteins with a lower hydrophobic TMD are unaffected upon GET-pathway inhibition (Guna et al., 2018). Nonetheless, knockout of the mammalian orthologue TRC40 leads to embryo lethality in mice (Mukhopadhyay et al., 2006) and severe organ defects in conditional *get* mutants (Lin et al., 2016; Norlin et al., 2016; Vogl et al., 2016). According to these observations, alternative pathways for TA proteins have been presumed and discovered. They potentially serve as compensation in case the GET is compromised (Casson et al., 2017) and will be introduced here briefly.

The SRP-dependent post-translational pathway

Even before the GET-pathway was discovered, it was shown *in vitro* that SRP can associate and translocate TA proteins in an SR-dependent manner (Abell et al., 2004). For that purpose, crosslinking experiments of the SRP54 subunit demonstrated its post-translational association with some TA proteins (Abell et al., 2004). As *co*-translational insertion cannot occur, it was presumed that SRP binding to TA proteins facilitates *post*-translational processes. Canine pancreas derived microsomes were trypsinised leading to reduced SRα level. Monitoring TA protein membrane integration in these microsomes revealed a pathway dependent on GTP and the SRP receptor (Abell et al., 2004). Some years later, TRC40 independent integration of TA proteins was demonstrated by competitively blocking the TRC40 (GET) pathway by expressing the cytosolic domain of the WRB receptor (WRBcc) or the cytosolic domain of CAML (CAMLcyt). A similar *in vitro* TA protein integration assay

as described by Abel et al., 2004 demonstrated that, indeed, TA proteins may utilise the SRP-dependent pathway *post*-translationally (Casson et al., 2017). However, the mechanistic details are still enigmatic.

The SRP-independent "post-translocon"

Connected to the discoveries of SRP-dependent TA protein insertion, the Sec61 translocon was considered to fulfil a role in post-translational translocation, therefore termed "*post-translocon*" (Harada et al., 2011; Schweiger and Schwenkert, 2013). The yeast Sec61-translocon was shown to form an alternate subcomplex with the auxiliary proteins Sec62p, Sec63p, Sec71p and Sec72p to provide another function in post-translational translocation (Deshaies et al., 1991; Panzner et al., 1995; McClellan and Brodsky, 2000; Reithinger et al., 2013; Wu et al., 2019) (**Table 3**). However, unlike the SRP-dependent post-translational translocation, it has been shown that substrate delivery is driven by an ATP-dependent reaction with the HSP70 family protein Kar2p (BiP in mammals) which is recruited by Sec63p to ratchet the nascent chain into the ER lumen (Panzner et al., 1995; Lyman and Schekman, 1997; Matlack et al., 1999). It has been noted that this pathway is mostly used by small pre-secretory proteins. For those, transcription of the SS is finished shortly before translation is entirely completed (Lakkaraju et al., 2012; Ast and Schuldiner, 2013). It seems that a molecular connection between TA protein translocation and the Sec61 post-translocon is still elusive.

In spite of their post-translocational role in yeast, both Sec62 and Sec63 (ERdj) have been reported to act also in a co-translational mode for some substrates in mammals (Müller et al., 2010; Lakkaraju et al., 2012; Lang et al., 2012).

While the SRP-independent translocon has been primarily studied in the context of translocation, the mammalian heat shock proteins BiP and Sec63 also partake in ER-stress recovery (Pobre et al., 2019). Furthermore, mammalian Sec62 is critical for maintenance and recovery of ER homeostasis (Denks et al., 2014). This indicates a strong connection between translocation and quality control.

In *Arabidopsis*, the ER membrane protein *At*TRP7 has been shown to functionally complement the yeast Δsec71 mutant, interact with HSP90 and HSP70 and is

associated with the *Arabidopsis* Sec63 homologue, *At*ERdj2A and *At*Sec62 (Schweiger et al., 2012; Schweiger and Schwenkert, 2013). This strengthens the hypothesis for it to be part of a putative Sec post-translocon yet an *in vivo* analysis of the functional conservation of such a translocon is still missing. So far, only a link between *At*Sec62 with ER-stress recovery, similar to mammals, has been proven (Hu et al., 2020). Furthermore, *At*Sec62 and the two *At*ERdj2 homologues (A and B) are connected to male fertility and plant development (Yamamoto et al., 2008; Mitterreiter et al., 2019).

Table 3: Overview of yeast, mammalian, and *Arabidopsis* post-translocon orthologues.

"Post-translocon"		
Yeast	*Mammalian*	*Arabidopsis (AGI Code)*
Sec62p	Sec62	*At*SEC62 (At3g20920)
Sec63p	Sec63/ERdj	*At*ERdj2A (At1g79940) *At*ERdj2B (At4G21180)
Sec71p	- [d]	*At*TRP7 (At5g21990) [a]
Sec72p	- [d]	- [d]
Kar2p	BIP	BIP1 (At5G28540) [b] BIP2 (At5g42020) [b] BIP3 (At1G09080) [b,c]

[a] has been shown to complement yeast Δsec71 mutant strains (Schweiger et al., 2012)

[b] based on (Noh et al., 2003)

[c] see **Chapter 3**: "*Conservation of SND2 in plants*" (part of this dissertation)

[d] currently, no functional orthologue has been discovered

The ER membrane protein complex (EMC) pathway

More recently, discoveries of a post-translational insertase for ER-destined TA proteins with TMDs of moderate to low hydrophobicity have been reported (Guna et al., 2018). Those proteins are preferably shielded in the cytosol by calmodulin (CaM), although SGTA might substitute in its absence. The exact mechanism of insertion is still unclear yet the mammalian ER-resident enzyme squalene synthase (SQS) and four other

TA proteins have been shown to utilize members of the *ER membrane protein complex* (EMC) for correct integration (Guna et al., 2018; Volkmar et al., 2019) (**Figure 4**). EMC consists of at least six proteins in yeast and ten in mammals (**Table 4**) and was demonstrated to be important for ER protein homeostasis (Jonikas et al., 2009). Moreover, EMC3 is a homologue of Get1 and both probably evolved from the ancestral prokaryotic insertase of the YidC family belonging to the "Oxa1 superfamily" (Anghel et al., 2017).

In addition to its post-translational insertion capacity, EMC cooperates with the SRP receptor to co-translationally insert the first transmembrane domain of multi- spanning membrane proteins thereby defining the accurate topology of many membrane proteins together with the SEC61 translocon (**Figure 4**) (Chitwood et al., 2018).

In *Arabidopsis thaliana*, orthologues for almost all components of the mammalian EMC can be found through PSI Blast *in silico* analysis (**Table 4**), however, functional characterisation is still pending.

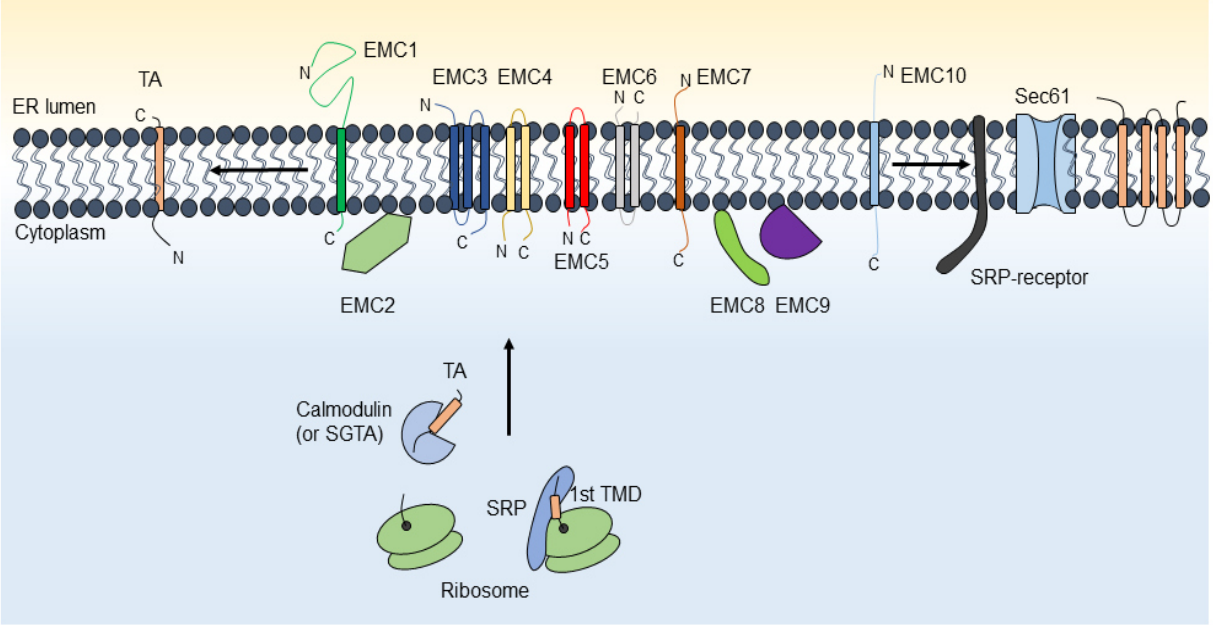

Figure 4: The EMC pathway in mammals. TA proteins with low hydrophobicity preferably delivered by Calmodulin (in its absence SGTA) to the ten-protein comprising EMC leads to its insertion. Moreover, EMC in cooperation with the SRP-dependent pathway defines the correct insertion of the first TMD of multi-spanning membrane proteins.

Table 4: Overview of yeast, mammalian, and *Arabidopsis* EMC orthologues.

ER Membrane Complex (EMC)		
Yeast	*Mammalian*	*Arabidopsis (AGI Code)* [a]
EMC1	EMC1	(At5g11560)
EMC2	EMC2	(At3g04830) (At5g28220)
EMC3	EMC3	(At4g12590)
EMC4	EMC4	(At5g10780)
EMC5	EMC5	(At5g03345)
EMC6	EMC6	(At5g49540)
Sop4	EMC7	(At4g32130) (At2g25310)
EMC8 [b]	EMC8/EMC9	(At5g55940)
YDR056C	EMC10	- [c]

[a] determined by PSI-Blast; see Appendices V (part of this dissertation)

[b] Lost in Ascomycetes (Wideman, 2015)

[c] currently, no functional orthologue has been discovered

The SRP-independent pathway

Not only EMC serves as an alternative for co- and post-translational insertion. The *SRP-independent* (SND) pathway, first identified in yeast, has been shown to have a wide substrate profile with a preference for proteins with central TMDs and can compensate for the loss of the SRP – and GET-pathway (Aviram et al., 2016). *Sc*SND comprises of 3 proteins, a putative peripheral ribosomal protein SND1 and two ER destined proteins SND2 and SND3 (**Table 5**). SND2 is predicted to contain four transmembrane domains while SND3 probably has one. Though mechanistic details are not ascertained yet, cytosolic SND1 is supposed to target nascent substrates for delivery to SND2 and SND3, both associated with the Sec61 translocon, acting as putative receptors (Aviram et al., 2016) (**Figure 5**). Loss of SND components leads to mislocalisation of IMPs with an internal TMD albeit not affecting overall viability in yeast (Aviram et al., 2016). In combination with deletion of Get components, double knockouts show lethality which strengthens the idea that in yeast both SND- and GET

pathways fulfil a compensatory role for TA protein delivery to the ER (Aviram and Schuldiner, 2017).

The human orthologue hSND2 was discovered as the first, and so far, only constituent of a putative mammalian SND pathway. Similar to yeast, hSND2 is localised to the ER and associates with many translocon components (Hassdenteufel et al., 2017). Its depletion leads to upregulation of the SRP-pathway associated with an increase of SRP-dependent substrate insertion while simultaneous hampering of TA protein insertion (Casson et al., 2017; Hassdenteufel et al., 2017). Initially, hSND2 was reported to regulate autophagy and ER stress, again showing a strong connection between translocation and protein quality control (Zhao et al., 2013).

Conservation of an SND2 homologue in plants had been noted but without further characterisation (Zhao et al., 2013). Therefore, the functional homology with regard to TA protein targeting to the ER membrane remained to be determined (**Table 5**).

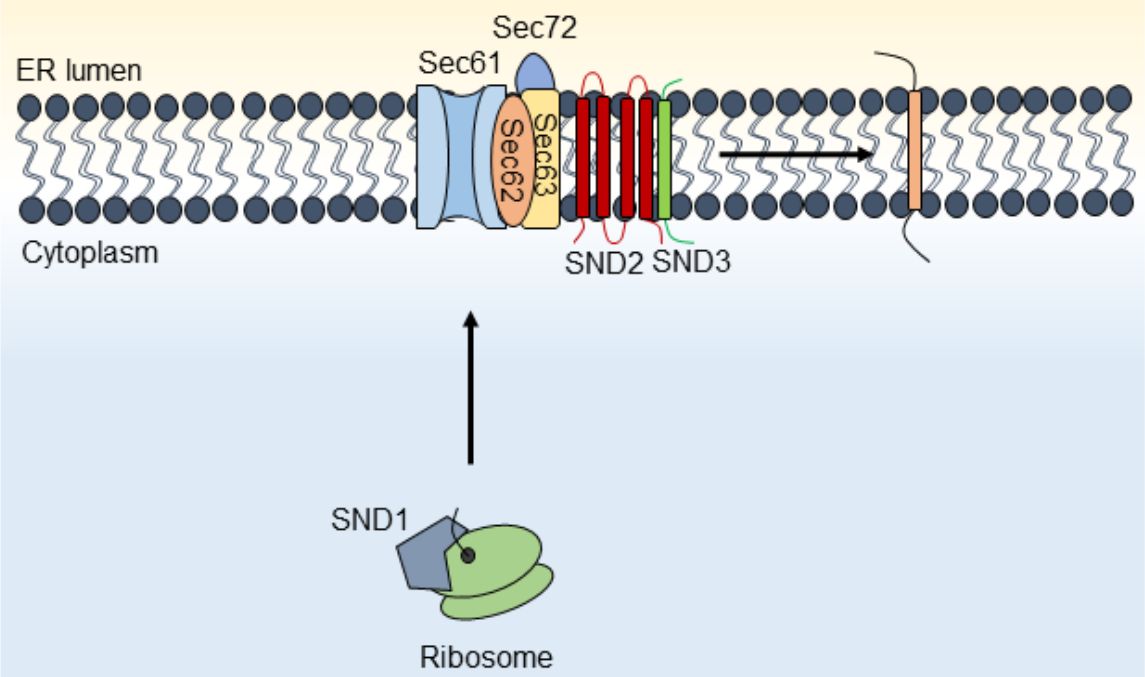

Figure 5: The SND pathway in yeast. The predicted peripheral ribosomal protein SND1 may deliver substrates to SND2 and SND3. Both proteins probably act as receptors and are associated with the Sec61 translocon as well as other auxiliary proteins. They may facilitate the insertion of substrates with preferably one central TMD yet overlap with substrates for both SRP- and GET-pathway.

Table 5: Overview of yeast, mammalian, and *Arabidopsis* SND orthologues.

SRP-independent (SND) pathway		
Yeast	*Mammalian*	*Arabidopsis (AGI Code)*
SND1	not found	not found
SND2	hSND2/TMEM208	*At*SND2a (At4g30500) [a] *At*SND2b (At2g23940) [a]
SND3	not found	not found

[a] see **Chapter 3**: "*Conservation of SND2 in plants*"

OBJECTIVES OF THE THESIS

In the last decades, studies on protein translocation to the endoplasmic reticulum mainly focused on Opisthokont models (Knight and High, 1998; Stefanovic and Hegde, 2007; Schuldiner et al., 2008) . Research on different insertion pathways has increased almost exponentially (Borgese et al., 2019; Shan, 2019). Recently, the Guided-Entry of Tail-anchored protein (GET) pathway was described for yeast and animals (Stefanovic and Hegde, 2007; Schuldiner et al., 2008) discussing the insertion of TA proteins in the ER membrane. In addition, an alternative pathway was discovered, the SRP-independent (SND) pathway (Aviram et al., 2016; Hassdenteufel et al., 2017). Although in *Arabidopsis thaliana* approximately 500 TA proteins are predicted (Kriechbaumer et al., 2009), knowledge of TA protein translocation and details on the relaying pathways in plants remains enigmatic.

This thesis aims at discovering and examining translocation pathways in *Arabidopsis thaliana*. Based on sequence comparison potential conservation of the GET- and SND-pathway will be addressed. For that purpose, interaction studies, *in vivo* localisation and biochemical approaches might help to characterize putative orthologues.

To elaborate the role of the GET pathway in plants, *loss-of-function* lines will be analysed phenotypically and their importance for the translocation of a model tail-anchored protein will be investigated.

Furthermore, two *At*GET1 interacting proteins with structural similarities to the yeast Get2 will be characterized. To this end, protein-protein interaction studies, subcellular localisation, and *in vitro* insertion assays will help to understand differences between these two proteins. The key question here is to understand whether they play a role as functional GET2 orthologues in *Arabidopsis*.

The dominant role of the GET pathway in TA protein translocation has been shown as well as the existence of backup pathways such as the SND pathway in yeast and mammals (Aviram et al., 2016; Hassdenteufel et al., 2017). As part of this work, two putative SND2 orthologues will be characterised in plants. General growth of single or double mutants also in consideration of potential crosstalk with other insertion pathways, especially the *Arabidopsis* GET-pathway, will be investigated. *In planta*

interaction analysis using immunoprecipitation-mass spectrometry (IP-MS) of SND2a-GFP and SND2b-GFP will provide an insight in protein function.

Additionally, as protein-protein interactions (PPIs) play a crucial role in many cellular processes, the aim was to show the improvement of three established interaction analysis methods by incorporation of the 2in1 Vector system. For that purpose, interactions among putative *Arabidopsis* SEC61 subunits will be investigated.

RESULTS

Chapter one: Loss of GET pathway orthologs in *Arabidopsis thaliana* causes root hair growth defects and affects SNARE abundance.

Xing, S., **Mehlhorn, D. G.**, Wallmeroth, N., Asseck, L.Y., Kar, R., Voss, A., Denninger, P., Schmidt, V. A., Schwarzländer, M., Stierhof, Y. D., Grossmann, G., Grefen, C., 2017, PNAS

Tail-anchored (TA) proteins are an important class within the type II oriented integral membrane proteins which makes up to ~3-5% of all IMPs in eukaryotic cells (Abell and Mullen, 2011). *In silico* prediction in *Arabidopsis thaliana* estimates around 500 TA proteins, approximately 10% of which encode SNARE (Soluble N-ethylmaleimide sensitive factor attachment protein receptor) family proteins, important for many physiological processes and vesicle trafficking (Kriechbaumer et al., 2009). The structure of TA proteins determined by a single C-terminal TMD and the lack of an N-terminal SS or TMD prohibits co-translational insertion by the SRP-dependent pathway (Shao and Hegde, 2011). To overcome this problem, TA proteins can be inserted post-translationally via the GET pathway (Hegde and Keenan, 2011). This pathway has originally been described in Opisthokonts (Stefanovic and Hegde, 2007; Schuldiner et al., 2008). A high degree of conservation in Archaeoplastida was often assumed, however, a dissection of the GET pathway in plants is missing.

Phylogenetic analysis of GET3 orthologues from 18 different species revealed two distinct GET3 clades present in Archaeplastida, termed clade GET3a and GET3bc (**Appendices I Fig. 1A**). While both clades maintain the GET3 characteristic ATPase domain, only GET3a candidates comprise binding sites for GET1 and a methionine rich GET3 motif. By contrast, transit peptides for mitochondrial or chloroplastic import were found in GET3bc (**Appendices I Fig. S1**). Consistent with these findings, subcellular localization of the three *Arabidopsis* GET3 orthologues using confocal laser scanning microscopy (CLSM) and transmission electron microscopy (TEM) analysis revealed *At*GET3a targeting to the cytosol whereas *At*GET3b localises to chloroplast stroma and *At*GET3c to the mitochondrial matrix (**Appendices I Fig. 1B-L, S2**).

Further *in silico* analysis identified *Arabidopsis* orthologues of GET1 and GET4 which were shown to localise to the ER membrane (*At*GET1) or the cytosol (*At*GET4) using confocal imaging (**Appendices I Fig. 2A-D, S7B**).

To elaborate whether physical interaction between the *Arabidopsis* GET orthologues exists, we used two different methods, the mating-based-split-ubiquitin system (mbSUS) and the ratiometric bimolecular fluorescence complementation (rBiFC). We observed homodimerization of *At*GET1 and *At*GET3a as well as interaction of these proteins with the other *Arabidopsis* GET pathway components except for *At*GET3b or *At*GET3c, not even in a truncated, cytosolic version (**Appendices I Fig. 2M, S3A-C**). Further interaction studies revealed several TA proteins as binding partners for *At*GET1 and *At*GET3a for example the Qa-SNARE SYP123 (**Appendices I Fig. 4A, S6**).

To address the issue if the *Arabidopsis* genes can functionally compensate the temperature-sensitive growth defect of yeast *Δget1* and *Δget3 loss-of function* strains, we explored heterologous complementation. Partial rescue of the growth defects in the corresponding yeast mutant strains was observed for *At*GET1 and *At*GET3a but not for *At*GET3b or *At*GET3c (**Appendices I Fig. S5**).

In contrast to the conditional lethal phenotype in yeast lacking GET pathway components or the embryo lethality seen in mice lacking the GET3 orthologue TRC40, we did not observe any obvious growth defects. However, T-DNA insertion lines for *At*GET1, *At*GET3a and *At*GET4, but not *At*GET3b or *At*GET3c, showed altered root hair growth. This decrease in root hair growth length was not further increased by multiple crosses between these T-DNA insertion lines. Reintroduction the corresponding genomic fragments allowed for a full recovery to wild type conditions (**Appendices I Fig. 3**).

The root hair growth defect coincides with a reduced abundance of transcript and protein levels of the root-hair specific Qa-SNARE SYP123 at the plasma membrane of *Atget1* and *Atget3a* lines which we observed using quantitative RT-PCR and immunoblot analysis of membrane fractions (**Appendices I Fig. 4B-D**).

To understand the physiological relevance of the GET pathway in *Arabidopsis*, *At*GET3a-GFP overexpression lines were assessed in the context of an *Atget1*

background. While overexpression of *At*GET3a-GFP in Col-0 did not reveal any obvious defect, abolishing the downstream capacity of the pathway results in dwarfed plants accompanied by altered root, silique, and seed development (**Appendices I Fig. 5A-C, S7A, C-F**). Further CLSM analysis revealed *At*GET3a-GFP clusters which probably remain in the vicinity of the ER. By contrast, *At*GET4-mCherry overexpression in *Atget1* lines did not show these clustered foci (**Appendices I Fig. 5D, S7B, Movie S1 and S2**).

Chapter two: Endoplasmic reticulum membrane receptors of the GET pathway are conserved throughout eukaryotes.

Asseck, L. Y., **Mehlhorn, D. G.**, Monroy, J. R., Ricardi, M. M., Breuninger, H., Wallmeroth, N., Berendzen, K. W., Nowrousian, M., Xing, S., Schwappach, B., Bayer, M., Grefen, C., 2021, PNAS

Comparing *in silico* sequence conservation of GET-pathway orthologues from yeast and mammals to plants has been led to the identification of most components of an *Arabidopsis thaliana* GET-pathway [**see Chapter one: Xing et al., 2017**]. However, one of the two ER membrane receptor proteins, namely GET2/CAML, required for TA protein insertion was not detected.

To address this issue, we performed an interaction screen in *Arabidopsis* using immunoprecipitation of *At*GET1-GFP with subsequent mass spectrometry (IP-MS). An unknown membrane protein, G1IP (*At*GET1 Interacting Protein), was identified (**Appendices II Table 1**). Despite its low sequence similarity to opisthokont GET2/CAML, it showed a strong structural conservation such as a positively charged cytosolic N-terminus and three transmembrane domains (**Appendices II Fig. 1A, S1A, S4, S6**). It was also detected in our previous published IP-MS as an interaction partner of *At*GET3a-GFP (Xing et al., 2017) substantiating the presumption that this protein may take part in the *At*GET-pathway. Additionally, a close homologue of G1IP was fished in the *At*GET1-GFP IP-MS which we named G1IP-*like* (**Appendices II Table 1**). In contrast to G1IP, G1IP-*like* was not found as an interaction partner of *At*GET3a-GFP (Xing et al., 2017).

GFP-G1IP and GFP-G1IP-*like* both co-localise with an ER marker, secRFP-HDEL in *A. thaliana*, as confirmed by CLSM (**Appendices II Fig. 1C-J**). To substantiate a relation between these proteins and *At*GET1 we investigated the expression pattern throughout different tissues and developmental stages. G1IP showed similar expression levels as *At*GET1. By contrast, G1IP-*like* is restricted to the inflorescence (**Appendices II Fig. 1B**). As the GET-pathway is an intricate system of proteins interacting with one another sequentially, we analysed interaction of G1IP and G1IP-*like* with the other *At*GET-pathway components. rBiFC assays in *Nicotiana benthamiana* leaf epidermal cells revealed that both proteins were able to interact with

*At*GET1 as seen in the IP-MS, but not with *At*GET3a or *At*GET4 (**Appendices II Fig. 1K-M, S2A-C**). Co-immunoprecipitation (Co-IP) analysis performed in *Arabidopsis thaliana* revealed that binding of G1IP to *At*GET3a is dependent on the presence of *At*GET1. However, interaction between G1IP-*like* and *At*GET3a was not detected even in presence of *At*GET1 (**Appendices II Fig. 1N-P**).

As previously reported, loss of *At*GET-pathway components compromises root hair growth (Xing et al., 2017). To test whether this is the case for G1IP or G1IP-*like*, we examined *loss-of-function* lines. We observed impaired root hair growth in *g1ip* mutants phenocopying the *Atget1* T-DNA insertion line. Expression of a genomic sequence of G1IP restores normal root hair growth. Additionally, the phenotype was not enhanced further in *Atget1/g1ip* double mutants. By contrast, *g1ip-like* mutants showed no significant difference to Col-0 in root hair length growth (**Appendices II Fig. 2A-B**).

To assess whether both genes are functionally conserved, we tried to complement the heat stress induced yeast phenotype of *Δget1get2* strains. Only coexpression of *At*GET1 and G1IP but not G1IP-*like* partially restored yeast viability. Additionally, we observed that receptor partners from the same species were more efficient than heterologous partner receptor combinations (**Appendices II Fig. 2C-D**).

To determine the association between the two receptor proteins, we used rBiFC and Co-IP. We demonstrated that G1IP is interacting with *At*GET1via its TMD and not its cytosolic domain (**Appendices II Fig. 3A-D, S2D-E**).

Finally, we assessed whether the conserved cluster of positively charged amino acids near the N-terminus of G1IP has an influence on TA protein insertion. To address this, we analysed the *in vitro* insertion of opsin-tagged human Syntaxin5 in pancreatic rough microsomes in the presence of recombinant cytosolic fragments of WRBcc (coiled coil), *At*GET1cc, CAMLcyt (cytosolic N-terminus), G1IPcyt, or its charge reversed version G1IP^{4E}cyt. Syntaxin5 insertion was disturbed by the positive controls (WRBcc, CAMLcyt) while *At*GET1cc had no effect. Similar to the mammalian CAMLcyt, insertion of the TA protein was diminished by G1IPcyt while mutation in the N-terminal conserved cluster (G1IP^{4E}cyt) reversed this effect to an almost normal insertion pattern (**Appendices II Fig. 3E-G**).

Chapter three: Conservation of SND2 in plants

Mehlhorn, D. G. and Grefen, C., unpublished manuscript

As described in **Chapters one and two**, loss of GET pathway function causes reduced root hair length, yet no pleiotropic phenotypes had been observed. Such mild phenotypes question if GET is indispensable in TA protein insertion in plants. Quite recently, a backup system for the GET pathway has been found in yeast and later mammals (Aviram et al., 2016; Hassdenteufel et al., 2017). The SRP-independent (SND) pathway was shown to facilitate insertion of moderately hydrophobic membrane proteins that lack an N-terminal SS and can compensate for the loss of SRP- and GET pathway (Aviram et al., 2016; Casson et al., 2017; Hassdenteufel et al., 2017). However, whether there is an SND pathway in plants possibly explaining the mild phenotype remains unknown.

For that reason, we investigated a possible conservation of the SND pathway using *in silico* sequence comparison and observed similar results as in mammals: no SND1 or SND3 orthologues. However, two SND2 orthologues, which we designated *At*SND2a and *At*SND2b can be found. Both proteins localize to the ER (**Appendices III Fig. 1C-M**), but comparison of expression patterns revealed that *At*SND2a is upregulated in siliques while *At*SND2b showed strong and almost ubiquitous distribution in most tissues (**Appendices III Fig. B**).

As the obvious interaction partners SND1 and SND3 were not found, we used ratiometric bimolecular fluorescence complementation (rBiFC) to investigate possible physical interaction partners of *At*SND2a and *At*SND2b such as translocon associated proteins and the GET pathway. We observed homo- and heterodimerisation among both SND2 proteins as well as interaction with translocon subunits and auxiliary proteins. Moreover, *At*GET1 was found to interact with *At*SND2a but not with *At*SND2b (**Appendices III Fig. 2**). Analysis of T-DNA insertion lines should provide further insights in the relationship with the *At*GET-pathway in regard to the root hair phenotype of *Atget1* mutants. Single *loss-of-function* lines do not display a discernible effect on plant growth despite slight reduction in root hair growth for *Atsnd2a*. In contrast to the synthetic lethal phenotype of Δget/snd yeast strains, we did not observe such an effect in *Arabidopsis Atget1/Atsnd2a* or *Atget1/Atsnd2b* double mutant lines. Instead, double

mutants between *Atsnd2a* or *Atsnd2b* and *At*get1 phenocopied the *Atget1* single mutant root hair growth defect (**Appendices III Fig. 3A**).

To investigate whether *At*SND2a and *At*SND2b can functionally substitute for the loss of each other, we analysed their transcript levels via qRT-PCR but did not detect a compensatory effect on the remaining homologue (**Appendices III Fig. S2C-D**). However, crossings of the single mutants displayed altered silique growth and decreased numbers of ovules (**Appendices III Fig. 5C-D**). In addition, segregation did not follow the Mendelian transmission ratio. A reduced amount of double homozygous progeny was observed, all dying at early seedling stages (**Appendices III Fig. 4A and Table 1**).

First insights on putative biochemical functions were provided by immunoprecipitation of *At*SND2a-GFP and *At*SND2b-GFP followed by mass spectrometry. Our results implicate both *At*SND2a and *At*SND2b as part of an intricate system for translocation processes (**Appendices III Fig. 6B and Table S1**).

In addition, *At*SND2a interacts with many proteins associated to stress response. To further study this finding, we treated plants with the drug Tunicamycin, blocking N-glycosylation, and found that *At*SND2a but not *At*SND2b transcription is increased upon ER-stress (**Appendices III Fig. 6C-D**).

Chapter four: 2in1 vectors improve in planta BiFC and FRET analyses

Mehlhorn, D. G., Wallmeroth, N., Berendzen, K. W., Grefen, C., 2018, Methods Mol Biol

Translocation of proteins rely on complex protein-protein interactions (PPIs). Chaperones need to bind clients and guide them to sophisticated translocon or insertase machineries which are composed of various proteins themselves. Therefore, analysis of these processes on a bio-molecular level requires the understanding of these interactions.

Here we demonstrated the interaction of three putative SEC61 translocon subunit homologues based on three different techniques to study PPIs improved by an incorporated 2in1-cloning approach. Three sets of homologues of the central pore Sec61α as well as the two subunits Sec61β and Sec61γ are encoded in the *Arabidopsis thaliana* genome. Implementing our improvements on ratiometric Bimolecular Fluorescence Complementation (rBiFC), FRET Acceptor Photobleaching (FRET-AB) and Fluorescence Lifetime Imaging (FET-FLIM) we showed physical interaction of *At*SEC61α1 with *At*SEC61β1 and *At*SEC61γ1, respectively (**Appendices IV Fig. 3, Fig. 4**).

DISCUSSION

Conservation and differences of the GET pathway in plants

Tail-anchored (TA) proteins encompass proteins with a variety of subcellular distributions and great importance in different cellular processes such as vesicle trafficking, protein translocation or regulation of transcription. In *Arabidopsis,* around 500 TA proteins were predicted (Kriechbaumer et al., 2009) with most of them translocating first to the ER before sorting to target membranes. A translocation machinery of ER-destined TA proteins called GET pathway was discovered in mammals and yeast (Stefanovic and Hegde, 2007; Schuldiner et al., 2008) yet an exact mechanism *in planta* remained to be determined. A high degree of evolutionary conservation was assumed, and only three research articles mentioned putative homologues of the human TRC40 or yeast Get3, respectively, in *Chlamydomonas reinhardtii* (Formighieri et al., 2013) and in *Arabidopsis thaliana* (Abell and Mullen, 2011; Duncan et al., 2013). In the research article "*Loss of GET pathway orthologs in Arabidopsis thaliana causes root hair growth defects and affects SNARE abundance*" (Xing et al., 2017), we discovered associated homologues of an *Arabidopsis* GET-pathway. However, intriguing differences among archaeplastidic GET components compared to Opisthokonts can be observed.

The Pretargeting complex

Based on sequence comparison, it is likely that *At*GET4 is a first constituent of a putative *Arabidopsis* TA protein pretargeting complex. This notion is further supported as it is an interaction partner of *At*GET3a and the *loss-of function* mutant displays the same phenotype as other *At*GET mutants suggesting it as part of the pathway (**Appendices I Fig. 2M, Fig. 3**).

In yeast, it was demonstrated that Get4 is strongly associated with Get5 (Chartron et al., 2010) and this complex mediates transfer of TA proteins from Sgt2 to Get3 (Wang et al., 2010). Interaction between Sgt2 and the Get4/Get5 complex is mediated by Get5 (Chartron et al., 2011) while Get4 interacts directly with an ATP-bound, closed dimer form of GET3 (Gristick et al., 2015). In plants, such a pretargeting system is still elusive

although putative orthologues for Get5 (UBQ12, At1g55060) and Sgt2 (TPR8, At4g08320) were suggested by Srivastava et al. (Srivastava et al., 2017). Nevertheless, the two assumed proteins were not characterized further. UBQ12 is thought to be a pseudogene, as it possesses three in-frame stop codons in the ubiquitin repeats (Bachmair et al., 2001), therefore its assumed role in the *At*GET-pathway is questionable given the lack of experimental evidence. Moreover, the ubiquitin-like domain present in Get5/UBL4A can be found in a wide range of proteins in *Arabidopsis*. Similarly, based on sequence comparison we observed not only TPR8 but multiple Sgt2/SGTA orthologues in *Arabidopsis*. This truly complicates determination of a plant pretargeting complex as many candidates need to be tested for their contribution, and they potentially act redundantly. It makes it also plausible that in plants, protein pretargeting requires various ubiquitin family proteins and not just a single candidate.

Mammalian pretargeting with the additional BAG6 is mechanistic distinguishable from yeast (Mariappan et al., 2010). Here, TRC35 (Get4) – UBL4A (Get5) interaction is not direct but mediated by BAG6 (Kuwabara et al., 2015; Mock et al., 2015). Furthermore, BAG6 is implicated as a hub for ubiquitin-mediated quality control. It recruits the BAG6-associated E3 ubiquitin ligase RNF126 (ring finger protein 126) which further ubiquitinates defective polypeptides for proteasomal degradation, thereby connecting SGTA to ER-associated degradation (ERAD) (Akahane et al., 2013; Kawahara et al., 2013; Leznicki et al., 2013). This process can be regulated by SGTA antagonizing ubiquitination and stabilising target proteins (Wunderley et al., 2014). Neither in yeast nor in plants such a mechanism has been reported. While an orthologue of BAG6 is lacking in yeast (Leznicki et al., 2013), the putative homologue At2g46240 in *Arabidopsis* is involved in responses to pathogen attacks by triggering autophagy (Li et al., 2016). However, knowledge about its role in a plant GET pathway is currently pending yet its existence suggests a link between quality control and translocation pathways in plants as well.

It has been shown that although there is a general mechanistic difference in yeast and mammal pretargeting complexes, the function in TA protein capturing appears to be conserved (Zhang et al., 2021). This leads to the hypothesis that a similar functional conservation may exist in plants.

Divergence of GET3 protein sequence

In *Arabidopsis thaliana*, three different GET3 proteins were identified (*At*GET3a, *At*GET3b and *At*GET3c). Comparing the sequences of these three paralogues revealed two distinct clades (GET3a and GET3bc) present in Archaeplastida and SAR supergroup but not in Opisthokonts and Amoebozoa indicating a duplication event in the evolution of eukaryotes (**Appendices I Fig. 1**)(Xing et al., 2017; Farkas et al., 2019; Mehlhorn et al., 2021). However, orthologues of *At*GET3c seem to be Brassicaceae-specific whereas several copies of *At*GET3b orthologues exist in other plant species as well (Bodensohn et al., 2019; Mehlhorn et al., 2021). GET3 of clade a are cytosolic proteins comprising a Get1 and Get4 binding motif as well as an ATPase motif. Consistent with this finding, *At*GET3a interacts with *At*GET4 and *At*GET1 (**Appendices I Fig. 2M**). The notion that *At*GET3a is a functional orthologue is further substantiated by its ability to interact with TA proteins and its depletion leads to reduced SYP123 (**Appendices I Fig. 4**) and SYP72 abundance within the plasma membrane (Srivastava et al., 2017; Xing et al., 2017).

The CxxC motif is necessary for the coordination of a zinc ion and dimer formation in mammals and yeast (Metz et al., 2006; Gunes Bozkurt and Karsten Rippe 2009; Mehlhorn et al., 2021). By contrast, it is missing in *At*GET3a. Still, *At*GET3a retains the ability to form dimers (**Appendices I Fig. 2M**). Instead, in plant GET3a proteins an ExxE motif and additional acidic residues adjacent to the site that usually bears the CxxC motif in other species' sequences may take over metal ion coordination and dimer stabilization. Moreover, an approximately 30 amino acid long, strongly charged extension was only found in the GET3a clade and is suggested to be involved in dimerization (Farkas et al., 2019; Mehlhorn et al., 2021). The cysteine arrangement within yeast Get3 was thought to be reminiscent of the bacterial ATP-independent chaperone Hsp33 (Voth et al., 2014). It has been demonstrated that Get3 indeed can act as an ATP-independent chaperone under oxidative stress conditions protecting unfolded proteins against aggregation (Powis et al., 2013; Voth et al., 2014).

Interestingly, the CxxC motif can be found in the clade bc. However, we did not observe complementation of the stress induced yeast *Δget3* phenotype by *At*GET3b or *At*GET3c not even in their truncated cytosolic variants (**Appendices I Fig. S5B**). This leads to the suggestion that both proteins might have another function. Partial rescue

was observed from *At*GET3a supporting the idea that despite lacking the CxxC motif it retained the chaperone function. It is likely that a difference in *At*GET3a structure, metal ion coordination or ability to interact with yeast co-chaperones is the reason for a partial rescue. Nevertheless, such a dual function of *At*GET3a in *Arabidopsis* has not been proven experimentally. Another indication for a dual function, probably as chaperone, might be provided by the overexpression experiment of *At*GET3a in the *Atget1* mutant background. Overexpression of *At*GET3a-GFP, but not *At*GET4-mCherry induced the formation of clusters in the absence of *At*GET1 (**Appendices I Fig. 5D, S7B, Movie S1 and S2**). A similar effect was observed for yeast Get3 overexpressed in the absence of its receptor (Schuldiner et al., 2008). This phenotype was shown to be connected to Get3 chaperone holdase function for even non-TA proteins (Schuldiner et al., 2008; Powis et al., 2013; Voth et al., 2014). Protection was enhanced by an at least fourfold molar excess of Get3 which is in line with our finding that in *Arabidopsis* the aggregate-like structures probably occurred dose dependently on *At*GET3a-GPF expression in *Atget1* background. We exclude that the clusters, which are localized in proximity to the ER, are *At*GET3a bound to the recently discovered G1IP receptor as we observed no interaction between *At*GET3a and G1IP in the absence of the co-receptor *At*GET1 (**Appendices II Fig. 1N-O**).

Up to date, the organellar function of *At*GET3b and *At*GET3c is not understood. A homologue of *At*GET3b is the arsenite transporter in *Chlamydomonas reinhardtii* (*Cr*ArsA1). It was shown that *Cr*ArsA1 supports the delivery of chloroplast destined TA proteins to the plastid outer envelope membrane (OEM) (Maestre-Reyna et al., 2017). Contradictory, it was proposed to be a cytoplasmic protein (Formighieri et al., 2013) although its N-terminal sequence clearly features an organellar transit peptide similar to other GET3bc clade homologues (Xing et al., 2017; Lin et al., 2019). *At*GET3b features an N-terminal transit peptide, and its subcellular localization is restricted to the stroma of chloroplasts (**Appendices I Fig. 1E-G**). This localization clearly precludes a possible involvement in TA protein delivery to the OEM. However, it is speculated that it might be involved in TA protein translocation to the inner envelope membrane or thylakoids (Anderson et al., 2019; Bodensohn et al., 2019). *At*GET3b does not bind *At*GET1 but it would be interesting to see if it associates with Alb3, a Get1 orthologue which is involved in membrane protein biogenesis in endosymbiotic organelles (Anghel et al., 2017; McDowell et al., 2021). In spite of

*At*GET3b lacking the Get1-binding motif, it might be plausible that *At*GET3b-Alb3 interaction requires a different binding motif, of currently unknown sequence.

*At*GET3c was proposed to localize to the mitochondrial outer membrane (MOM) (Duncan et al., 2011; Duncan et al., 2013), however we demonstrated a clear matrix localization which is in compliance with its transit peptide (**Appendices I Fig. 1H-L**). GET3c variants are *Brassicaceae*-specific while in *Fabidae* some GET3b homologues were predicted to localize to mitochondria as well (Bodensohn et al., 2019). An involvement in TA protein insertion into the inner membrane of mitochondria is currently unknown (Mehlhorn et al., 2021). However, *At*GET3c *loss-of-function* mutants displayed no discernible phenotype which contradicts a housekeeping role, as compromised mitochondrial protein biogenesis would lead to drastic phenotypes (Boos et al., 2019).

As in chloroplasts, another Get1 orthologue of the Oxa1/Alb3/YidC family of insertases is resident in the inner mitochondrial membrane (Oxa1) (Hennon et al., 2015) though the *At*GET3c sequence does not feature a Get1-binding motif it has not been tested to interact with Oxa1 so far (Anghel et al., 2017; Farkas et al., 2019). Its function remains to be determined.

The Arabidopsis thaliana GET1-G1IP receptor complex

In yeast, the TA protein/Get3 complex interacts with the ER-membrane via the receptors Get1/Get2 where the final step of translocation is initialized (Wang et al., 2014). The metazoan homologue of Get1 is WRB (Vilardi et al., 2011) while a direct homologue of *Sc*Get2 was not identified. Instead, CAML functionally replaces *Sc*Get2 in metazoans (Yamamoto and Sakisaka, 2012). Similarly, an evolutionary conserved *At*GET1 was found in *Arabidopsis thaliana* (Srivastava et al., 2017; Xing et al., 2017) yet no sequence homologue for Get2 or CAML. In the research article: "*Endoplasmic reticulum membrane receptors of the GET pathway are conserved throughout eukaryotes.*" (Asseck et al., 2021), we present a functional equivalent, termed G1IP.

G1IP does not have a high level of amino acid similarities but shares important features with *Sc*Get2 and CAML. It comprises three TMDs with a long cytosolic N-terminus and a luminal C-terminal region (Schuldiner et al., 2008; Yamamoto and Sakisaka, 2012;

Asseck et al., 2021). Furthermore, a basic N-terminal region supposedly representing the binding site for Get3/TRC40 (Stefer et al., 2011; Yamamoto and Sakisaka, 2012) can be found in G1IP which all together makes it plausible that it might be a remote homologue of ScGet2/CAML. This notion is further supported as *in silico* alignment with these features of CAML as query led to the discovery of a close sequence homologue of G1IP in *Arabidopsis lyrata* [Accession ID: EFH45527] (Borgese, 2020).

The motif conservation between G1IP and CAML/Get2 point to a co-selection, enabling its functional conservation and suggests that it shares a common evolutionary origin with CAML and *Sc*Get2. This thesis is further supported as phylogenetic analysis of G1IP points to early divergence of the Get2 proteins (**Appendices II Fig. 4**).

Besides its structural similarities, G1IP localises at the ER membrane and is constitutively co-expressed with *At*GET1 throughout plant development, consistent with its supposed role as a co-receptor of *At*GET1 (**Appendices II Fig. 1B-J**). This is further corroborated as *g1ip* lines display the same phenotype as other *get* mutants (**Appendices II Fig. 2B**) (Xing et al., 2017; Asseck et al., 2021). Additionally, G1IP physically interacts with *At*GET1 via its TMDs and not the cytosolic N-terminal domain which in turn might be important for interaction with *At*GET3a (**Appendices II Fig. 3A-D, S2D-E**).

In yeast, the Get2 cytosolic domain can bind Get3 (Stefer et al., 2011). Intriguingly, G1IP only binds to *At*GET3a in Col-0 but fails to interact in *Atget1* mutants indicating that *At*GET1 is needed to bridge or stabilise the physical interaction (Asseck et al., 2021). It might be possible that *At*GET1 leads to conformational changes in G1IP which favours *At*GET3a binding sites. In contrast, it has been reported in yeast that Get1 and Get2 can simultaneously bind Get3, despite some overlapping binding sites which compete for binding. It seems that Get1 displaces some Get2 interaction sites with Get3 (Stefer et al., 2011). In mammals, it was demonstrated that WRB and CAML compete for the interaction with TRC40 as well (Yamamoto and Sakisaka, 2012). Thus, we propose that the mechanism behind the interaction of the plant GET-receptor and *At*GET3a might differ from yeast and mammals.

Another difference can be observed in the coregulation between the two receptor subunits. Correct integration of the TMDs of CAML into the ER membrane is dependent on WRB in mammals. Depleted WRB causes incorrect incorporation of the second

TMD of CAML into the membrane. This leads to exposure of these domains to the ER lumen and triggers direct protein degradation (Carvalho et al., 2019; Inglis et al., 2020). It has also been noted that the coregulation of both receptor subunits might be partially occurring on transcriptional level (Colombo et al., 2016; Rivera-Monroy et al., 2016; Inglis et al., 2020). Our data do not support the strict coregulation on protein level, as we do not observe instability of G1IP in the absence of *At*GET1 indicating another mechanism of regulation compared to mammals (**Appendices II Fig. 1O**). However, we cannot exclude an alteration on transcriptional level as G1IP was ectopically expressed under the control of the RPS5a promoter (**Appendices II Fig. 1N**).

Conversely, whether the interaction of *At*GET3a with *At*GET1 depends on G1IP is currently not proven experimentally in *Arabidopsis thaliana*. Nevertheless, *At*GET3a interacts with *At*GET1 (**Appendices I Fig. 2M**) but not G1IP (**Appendices II Fig. 1L**) in *N. benthamiana* suggesting that the interaction might be independent.

It is noteworthy that in mammals, membrane integration of WRB is not directly related to CAML. In the absence of the co-receptor, accurate integration of WRB into the ER membrane still occurs. However, WRB is degraded afterwards as an unfunctional orphan subunit (Colombo et al., 2016; Carvalho et al., 2019; Inglis et al., 2020). This clearly has to be tested in plants.

CAML and *Sc*Get2 have been co-selected with a positively charged region within the N-terminus (Borgese, 2020) which is also present in G1IP comprising three arginines and one lysine (**Appendices II Fig. 3E**). In Opisthokonts, the basic residues are important for the interaction with *Sc*Get3 and TRC40 as reverse-charge mutagenesis abolishes binding and interferes with TA protein insertion (Stefer et al., 2011; Yamamoto and Sakisaka, 2012). It was also shown that the cytosolic N-terminus of CAML alters TA protein insertion (Yamamoto and Sakisaka, 2012). The native cytosolic domain of G1IP but not the site-directed substitution mutant version with a reversed charge in the basic region showed a similar inhibition of the mammalian TA protein translocation machinery (**Appendices II Fig. 3G**). Thus, we concluded a conserved role for this region in binding TRC40. We suggest that in G1IP the interaction is based on the positively charged clusters forming ionic interactions with conserved negatively charged regions in *At*GET3a as shown for the interaction between Get2 and Get3 (Mariappan et al., 2011; Stefer et al., 2011).

While the coiled-coil domain of WRB does interfere with TA protein insertion (Vilardi et al., 2011) in mammals, *Arabidopsis* GET1 coiled-coil domain has no effect on the mammalian insertion system (**Appendices II Fig. 3F**). We suggest that probably functional residues or binding sites for *At*GET3a in *At*GET1 differ from those of its mammalian orthologue. These divergences are noticable in complementation assays in yeast as well. Merely a partial rescue of the *Sc*Get1/*Sc*Get2 *loss-of-function* mutant phenotype was achieved by *At*GET1 and G1IP (**Appendices II Fig. 2C-D**) whereas WRB and CAML can fully restore the function of the yeast receptor complex *in vivo* (Vilardi et al., 2014). Inter-kingdom rescue combinations of *At*GET1 and *Sc*Get2 or *Sc*Get1 with G1IP are not as efficient as intra-kingdom combinations of the proteins (**Appendices II Fig. 2D**) indicating that no fully functional receptor complex can be established. It further indicates that functional domains might be conserved within the proteins of a species which cannot be surrogated by the inter-species proteins.

Complementation seems to be slightly stronger when *At*GET1 and *Sc*Get2 are co-expressed compared to *Sc*Get1 with G1IP (**Appendices II Fig. 2D**). This observation is in line with a similar experiment where heterologous receptor partners of WRB with *Sc*Get2 can rescue the yeast mutant growth defect while co-expression of *Sc*Get1 with CAML fails under most conditions (Vilardi et al., 2014). This suggests, that the eukaryotic Get2/CAML/G1IP is probably more strongly diverged during evolution becoming more specialized in their function compared to the more conserved Get1/WRB/*At*GET1.

The homologue G1IP-like

In our *At*GET1 interaction screen a protein similar in structure of G1IP was fished, hence termed G1IP-*like*. Just like G1IP, it localises at the ER membrane (**Appendices II Fig. 1G-J**) and shares a cluster of basic residues in its N-terminal region (**Appendices II Fig. S6**). However, the phenotype of *g1ip-like* does not reflect the short root hair phenotype of *Atget* mutants and it fails to complement the *Sc*Get1/*Sc*Get2 *loss-of-function* phenotype together with *At*GET1 (**Appendices II Fig. 2B-C**). Furthermore, its expression profile shows a non-ubiquitous pattern with distinct transcriptional activation in flowers (**Appendices II Fig. 1B**). Thus, we infer that G1IP but not G1IP-*like* is forming a GET-receptor complex with *At*GET1 in plants.

Nevertheless, G1IP-*like* expression in flowers and its similarities to G1IP make it likely that it adopts a similar function in flowers. At least in pollen this assumption can be rejected as the pollen specific SYP72 needs *At*GET3a for proper insertion into the ER membrane (Srivastava et al., 2017). However, G1IP-*like* does not interact with *At*GET3a despite its sequence similarity to G1IP, not even in the presence of *At*GET1 (**Appendices II Fig. 1M, S2C**). Therefore, we conclude that G1IP-*like* is most likely not involved in SYP72 translocation which also substantiates our conclusion that G1IP-*like* is not forming a GET-receptor for *At*GET3a.

Currently a functional analysis of G1IP-*like* is still missing. Interaction screens of G1IP-*like* in an *Atget1* background with Col-0 as control or in an irreversibly bound complex with *At*GET1 (utilizing split YFP) might hint on its functionality or substrates. Furthermore, characterization of *g1ip-like* mutants with focus on flower development might reveal specialized functions.

Is GET the dominant pathway in plants?

So far, the GET pathway is considered as the main route for post-translational insertion of TA proteins into the ER. Contrarily, there is evidence that challenged this suggestion. As TA proteins are numbered among approximately ~3-5% of all IMPs, maintaining vital cellular processes (Abell and Mullen, 2011), abolished translocation would certainly lead to very pronounced phenotypes. This suggestion is in line with observations made in mammals. An altered TRC (GET) – pathway interferes with TA protein translocation and knockouts of TRC40 leads to embryo lethality in mice (Mukhopadhyay et al., 2006; Favaloro et al., 2010) while severe organ defects in induced *trc40* or *wrb* mutants was shown (Lin et al., 2016; Norlin et al., 2016; Vogl et al., 2016). Contrary, yeast *get loss-of-function* strains are viable under non-stress conditions (Schuldiner et al., 2008). Lethality is only observed under applied oxidative stress but considered to be related to an additional function of Get3 as chaperone of unfolded soluble proteins (Voth et al., 2014). From this one could suppose an indispensability of the TRC-pathway in multicellular Opisthokonts for survival.

This conclusion must be rejected for other multicellular organisms such as plants. In *Arabidopsis thaliana*, despite elevated ER-stress levels (Srivastava et al., 2017) and

reduced root hair length (**Appendices I Fig. 3**) no discernible pleiotropic phenotype as for example seedling or embryo lethality was observed. However, strong phenotypes could be expected as seen in TA protein mutants such as the cytokinesis-specific SNARE KNOLLE (Lauber et al., 1997). Furthermore, merely two TA proteins have been experimentally demonstrated to be GET-pathway dependent in plants. In *Atget1* or *Atget3a* mutants, translocation of the root hair specific SNARE SYP123 is altered but not completely abolished (**Appendices I Fig. 4B-C**) suggesting that it is not solely dependent on *At*GET and alternative routes may exist. Similarly, the pollen specific SYP72 protein level is reduced but still detectable in microsomal fractions in *Atget3a* mutants and no pollen-related phenotype was observed (Srivastava et al., 2017).

Interaction analysis by rBiFC and mbSUS revealed that there are TA proteins in plants which do not interact with *At*GET3a or *At*GET1 such as SYP43 or the sucrase/ferredoxin-like family protein At5g40510 (**Appendices I Fig. 4A, S6**). Moreover, only 23 out of approximately 500 predicted TA proteins (Kriechbaumer et al., 2009) interacted in an IP-MS screen with *At*GET3a-GFP (**Appendices I Fig. S6B**) suggesting that in plants the GET-pathway might not play a major role in TA protein insertion and alternatives must exist. This is in line with analysis from yeast where only two out of 46 potential client TA proteins showed severe defects in *get loss-of-function* strains (Rivera-Monroy et al., 2016).

Alternative pathway(s) provide the possibility of secure, robust, and high-fidelity translocation of TA proteins. Consequently, strong defects could be avoided in case proteins are not inserted correctly or one path is disrupted. One example is presented by the yeast *SRP-independent* (SND) pathway. Its broad client spectrum allows for compensation of the function for both, SRP- and GET-pathway (Aviram et al., 2016). Furthermore, the GET pathway can lead mistargeted mitochondrial proteins through the ER for re-import into mitochondria via the ER- surface retrieval pathway (Hansen et al., 2018; Xiao et al., 2021). In plants, the distribution of TA proteins is even more challenging compared to other eukaryotic cells because of the additional endomembrane compartment. Therefore, the existence of various insertion pathways is plausible. Concluding from our data described in '*Conservation of SND2 in plants*' [Mehlhorn et al., manuscript: unpublished] it seems evident that alternative or redundant routes have evolved in plants as well.

Conservation of the SRP-independent (SND) pathway

The yeast SND pathway comprises three proteins, SND1-SND3. While no homologue for SND1 and SND3 was found in neither mammals nor plants, SND2 seems to be conserved in humans and *Arabidopsis* (hSND2/*At*SND2b) (Zhao et al., 2013; Hassdenteufel et al., 2017). The lack of SND1 and SND3 in other eukaryotic organisms raises the possibility that (i) there was an early divergence and only structural-functional conservation occurred as seen for the example with Get2/CAML/G1IP (Borgese, 2020), (ii) both proteins are functionally dispensable, or (iii) the mechanism changed and distinct proteins can carry out the function.

Surprisingly, in *Arabidopsi*s, we found a second SND2 protein (*At*SND2a) which seems to be Brassicaceae specific thus we infer that it might be a remnant of the last genome duplication event (Mabry et al., 2020; Walden et al., 2020) (**Appendices III Fig. 1A**). Both proteins probably have four transmembrane domains and are localising to the ER membrane (**Appendices III Fig. 1C-M, S1**) which is in line with data from *Sc*SND2 and hSND2 (Aviram and Schuldiner, 2017; Hassdenteufel et al., 2017). However, only *At*SND2b showed an almost ubiquitous expression pattern which would be expected for proteins involved in translocation. Contrarily, *At*SND2a is only highly expressed in siliques (**Appendices III Fig. 1B**). Therefore, it is plausible that *At*SND2b and not *At*SND2a is more important for general physiological processes. It further suggests functional specialization of *At*SND2a in siliques. Siliques are only found in Brassicaceae (Robles and Pelaz, 2005; Pabon-Mora et al., 2014) possibly explaining the duplication of *At*SND2.

We did not observe a compensation on transcriptional level in case one of both genes was missing (**Appendices III Fig. S2C-D**). This would speak against redundancy. However, we have evidence that supports the notion of at least partial functional redundancy. Data from an IP-MS analysis shows that both proteins share a large pool of interaction partners, suggesting overlapping function (**Appendices III Fig. 6A, Table S1**). Moreover, crosses of *loss-of-function* lines of *Atsnd2a* and *Atsnd2b* severely effect plant vitality when both proteins are missing while in single- or homozygous/heterozygous mutant lines no discernible phenotype can be detected (**Appendices III Fig. 4A**). Thus, we conclude that partial redundancy is most likely.

In yeast, the SND-pathway was reported to insert nascent proteins with a central TMD in the ER membrane and it compensates for the loss of SRP- and GET-pathway (Aviram et al., 2016). In humans, hSND2 provides a different, supposedly redundant targeting route to the ER (Aviram and Schuldiner, 2017; Casson et al., 2017; Hassdenteufel et al., 2017). It has been noted that depletion of hSND2 induces the upregulation of the transcript level of SRP-receptor subunits SRα and SRβ (Hassdenteufel et al., 2017). Although we do not see such an effect in plants (**Appendices III Fig. S3C-D**), we cannot rule out masking of the effect since partial redundancy of *At*SND2a and *At*SND2b in single knockout experiments. Nevertheless, we conclude that there is no upregulation of putative SRP-receptor homologues in single *At*snd2a or *At*snd2b mutants. Similarly, we do not see an up- or downregulation of GET-pathway components in those mutants or vice versa (**Appendices III Fig. 3B-E**). In humans a slight downregulation of hSND2 was detected on transcriptional level but an upregulation on protein level in a WRB depleted system (Hassdenteufel et al., 2017). So far, we did not test the *At*snd2a or *At*snd2b protein level in an *Atget* mutant background. In case *At*SND2 could compensate the loss of *Atget1* similar to mammals, upregulation on protein level would be expected as well. However, as there already is a difference on transcriptional level compared to mammals, unchanged protein level could be just as plausible. In that case, both pathways might not compensate each other in plants.

As both the *Sc*SND-pathway and hSND2 have been shown to provide an alternative targeting route to the ER (Aviram et al., 2016; Hassdenteufel et al., 2017), we propose a similar function of the *Arabidopsis* SND2 proteins. This notion is further supported through interaction partners of both proteins identified in our IP-MS analysis and their involvement in translocation (**Appendices III Fig. 6B and Table S1**). Similar interaction partners have been reported in humans (Hassdenteufel et al., 2017). Therefore, we propose that both proteins have a function in protein translocation.

As mentioned above, deletion of both SND and GET genes is lethal in yeast (Pan et al., 2006; Aviram et al., 2016). Contrarily, in *Arabidopsis*, deletion of *Atsnd2a/Atget1* or *Atsnd2b/Atget1* does not affect overall viability of the plants. The double mutants phenocopy the reduced root hair growth of single *Atget1* mutants (**Appendices III Fig. 3A**). Potential partial redundancy of *At*SND2a and *At*SND2b might conceal a possible effect though we suggest that SND and GET do not functionally compensate

each other. This is corroborated by our IP-MS analysis of *At*SND2 proteins which identified only a small number of TA proteins among the interacting proteins. Furthermore, compared to the IP-MS of our GET-proteins (**Appendices I and II**) (Xing et al., 2017; Asseck et al., 2021) there was little overlap of other interacting proteins. This indicates that in *Arabidopsis*, SND2a and SND2b have other substrate specificity determinants compared to GET.

Most striking is the pronounced phenotype of double mutants between *Atsnd2a* and *Atsnd2b* which seems to be seedling lethal (**Appendices III Fig. 4A**). While such a drastic defect is expected for improper protein translocation, it implies that the SND-pathway might be more important in plants than in yeast. Nevertheless, a substrate specificity analysis is still missing which would be necessary to determine which proteins take this possible route in plants. Based on the IP-MS data, appropriate candidates must be determined and tested for their membrane abundancy or mislocalisation in the *loss-of-function* lines. To circumvent the partial redundancy of *At*SND2a and *At*SND2b a heterologous system (*Δsnd2* yeast strains +/- *At*SND2) might be necessary. A more biased approach to search for homologue candidates from yeast or humans, known to be SND-dependent (Aviram and Schuldiner, 2017; Hassdenteufel et al., 2017), was not successful. One might speculate if in plants another substrate specificity exists.

AtSND2a possibly has an additional function

It is noteworthy that differences between *At*SND2a and *At*SND2b have been observed. Differences in expression pattern (**Appendices III Fig. 1B**), GET1 interaction (**Appendices III 2**), single mutant phenotype (**Appendices III Fig. 3A**) and divergence in the pool of potential interaction partners as identified in the IP-MS analysis (**Appendices III Fig. 6A-B**) lead to the hypothesis that *At*SND2a might have an additional function. In humans, hSND2 was reported to be involved in autophagy and ER-stress responses (Zhao et al., 2013) beside its role in ER targeting (Hassdenteufel et al., 2017). *At*SND2a but not *At*SND2b is induced upon Tunicamycin treatment and seems to interact with autophagy and ER-stress response related genes (**Appendices III Fig. 6B-D, Table S1**). This congruent observation leads to the conclusion that *At*SND2a might indeed have evolved a separate function distinct from *At*SND2b.

Consistently, hSND2 was quite recently shown to be transcriptionally regulated by cellular oxygen levels and hypoxia-inducible factor-1α (HIF-1 α) (Lei et al., 2020). hSND2 mRNA level was increased upon hypoxia condition (Lei et al., 2020). Again, this is in line with the findings of *At*SND2a induced by Tunicamycin since treatment with the ER stress agent leads to a changed redox state within the cell (Ozgur et al., 2014; Ozgur et al., 2015). Although a functional validation of hSND2 participation under different oxygen condition has not been tested so far, it is tempting to speculate that it might be related to an additional function in ER-stress response (Zhao et al., 2013) and that *At*SND2a but not *At*SND2b acquired this task. As a result of increased protein secretion activity and therefore elevated protein folding demand in the ER during pollen germination and/or pollen tube growth, reproductive cells experience enhanced ER stress (Sato and Maeshima, 2019). Although we did not obtain a pollen tube growth defect in our singe mutants and did not specifically test the mRNA level of both *At*SND2 proteins in pollen, it is tempting to speculate that *At*SND2a might be needed to cope with the increased ER stress in those cells.

An association of hSND2 with the cytoskeleton has been observed (Lei et al., 2020). hSND2 can interact with β-actin via an WH2 motif. Remarkably, *At*SND2a but not *At*SND2b coimmunoprecipitates with *At*ACT11, the closest homologue of β-actin (**Appendices III Table S1**) which further supports the hypothesis that *At*SND2a has adopted similar function as hSND2. Drastic remodelling of cytoskeletal structures is required during transitional developmental stages like gametogenesis, embryogenesis, or seed formation (Luptovciak et al., 2017). As *At*SND2a is expressed in siliques, an association with the cytoskeleton might be plausible.

Similarly, root hair development is strongly connected to cytoskeletal rearrangement (Bibikiva et al., 1999). Many actin isoform *loss-of-function* mutants display root hair growth defects (Cvrckova et al., 2010; Kandasamy et al., 2012). Matching, single *Atsnd2a* mutant displays a slight but significant reduction in root hair growth compared to wild type. This observation favours the thesis, that *At*SND2a is somehow connected to the cytoskeleton.

It should not be neglected that based on our rBiFC experiment, only *At*SND2a interacts with *At*GET1 (**Appendices III Fig. 2**). Although the exact implication of these

interaction is still elusive, it speaks again for an additional function in comparison to *At*SND2b.

Delivery of cargo to AtSND2

Targeting substrate to the putative SND2/SND3 receptor is supposed to be facilitated by SND1 in yeast (Aviram and Schuldiner, 2017). In humans and plants, the proteins involved in delivery of cargo to hSND2/*At*SND2 are not discovered so far. Nevertheless, several candidate genes can be proposed which may adopt this function.

Insights may again be gained from yeast translocation systems. For the yeast GET-pathway, Sgt2 is thought to be important for the translocation of TA proteins to the ER membrane. Quite recently, a mechanism distinctive from the pretargeting complex, involved in loading of Sgt2 with TA proteins has been discovered in yeast. The Hsp-70 like chaperone Ssa1 facilitates transfer of TA proteins from the ribosome to Sgt2 stimulated by the co-chaperone proteins Yfj1 and Sis1 [Cho et al., 2021; Cho and Shan, 2018].

Since no SND1 homologue has been discovered in plants, yet, its function may either be dispensable or other proteins may deliver preproteins to *At*SND2. We observed an interaction of both *At*SND2a and *At*SND2b with the putative Ssa1 homologue HSP70-2 (At5g02490) and the two putative Ydj1 homologues, ATJ2 (AT5g22060) and ATJ3 (At3g44110) in our IP-MS analysis (**Appendices III Table S1**). Furthermore, it was shown in mammals that the pretargeting proteins SGTA (homologue of Sgt2) or BAG6 are dispensable and TA protein targeting to the ER is still accomplished (Culver and Mariappan, 2021). This speaks for the idea that other chaperones may take over this function as it was seen for the EMC-pathway where chaperoning was preferably mediated by calmodulin [Guna et al. 2018]. Hypothetically, it may be conceivable that HSP70-2 and ATJ2/ATJ3 may play a role in delivery of cargo to *At*SND2.

Alternative pathways for TA proteins

Besides the GET- and SND-pathway, several other routes for TA proteins have been described in Opisthokonts (Aviram and Schuldiner, 2017; Casson et al., 2017; Shan, 2019). The ER membrane complex (EMC) is another post-translational insertase for TA proteins. Silencing EMC components alters successful integration of TA proteins in mammals (Guna et al., 2018; Volkmar et al., 2019). Orthologues of all mammalian EMC components can be found in *Arabidopsis* based on sequence homology (**see Introduction**) but its role in plants is currently uncertain. Nevertheless, we found some EMC homologues in the IP-MS interaction screen of *At*SND2a and *At*SND2b (**Appendices III Table S1**). Therefore, it is quite tempting to speculate that the *Arabidopsis* EMC homologues are likewise involved in translocation. As it was observed in mammals, some TA proteins are partially dependent on both EMC and TRC40 pathways suggesting functional redundancy between these two pathways (Guna et al., 2018; Volkmar et al., 2019). It might be possible that this overlap can also be found in plants which possibly explains the mild *Atget* mutant phenotype.

Another post-translational pathway is provided by the SEC61 translocon itself in cooperation with its auxiliary proteins SEC62/SEC63 (Abell et al., 2007; Wu et al., 2019). In *A. thaliana* it has been reported that *At*TRP7 together with *At*SEC62 and *At*Erdj2 (*At*SEC63) might act in post-translational translocation (Schweiger et al., 2012; Schweiger and Schwenkert, 2013). Again, *At*SEC62 and *At*SEC63 were shown to interact with *At*SND2a and *At*SND2b (**Appendices III Fig. 2, 6B**) indicating that there might be an overlap between these routes as well.

The chicken or the egg causality dilemma – or – which came first: translocon or translocation *

A rather philosophical question is the start of translocation itself. It has been shown that many translocon subunits of various translocation machineries are predicted TA proteins (Kriechbaumer et al., 2009; Pedrazzini, 2009) therefore post-translational insertion is required. A good example is the GET-pathway dependent model TA protein Sec61β (Stefanovic and Hegde, 2007; Hassdenteufel et al., 2017). However, other insertases for example those of the TA protein translocation machineries such as

GET1 or most EMC proteins are multi-spanning membrane proteins of Type I or III which implies they need the translocon (Martinez-Gil et al., 2011; Shao and Hegde, 2011; Denks et al., 2014; Wang et al., 2014; Aviram et al., 2016; Guna et al., 2018). Consequently, the question about the initial acquisition of minimal translocation machineries required to permit the insertion is justified.

Apparently, insertion machineries rely on themselves as seen in the co-regulation between Get1 and Get2 (Carvalho et al., 2019) or Sec61α (Knight and High, 1998). However, when not readily available, other mechanisms must ensure their insertion. *In vitro* analyses suggest that a minimal combination of cytosolic HSP40 and HSP70-8 is sufficient for ATP-dependent targeting and insertion of TA proteins in mammals (Abell et al., 2007; Rabu et al., 2008). Another plausible possibility is unassisted insertion as observed in mitochondria (Kemper et al., 2008) and in *in vitro* microsomal and liposomal systems (Brambillasca et al., 2006). Proteins with long domains (85 residues) were tested and could insert unassisted across protein-free bilayers (Brambillasca et al., 2006). Presumably, the unassisted translocation might be a valid answer to this conundrum.

Contrary, some proteins are incapable to utilize unassisted integration because of their tendency to aggregate in the cytosol before reaching the membrane (Brambillasca et al., 2006) and *in vivo* studies to demonstrate the above mentioned unassisted insertion are virtually impossible. It seems that our knowledge of insertion pathways is still too limited to finally solve such a fundamental question.

Nonetheless, eukaryotes have evolved many possibilities to facilitate proper insertion of membrane proteins not only to cope with the huge variety of proteins that must be translocated but also to compensate in case one pathway is altered. Thus, there is a lot to learn in terms of protein translocation and there might still be many targeting pathways waiting for discovery.

---

* Note from the author: This question was original raised by Prof. Dr. Christopher Grefen in my first practical course with him as supervisor and although I cannot give an appropriate answer, I hope after all those years in his group this is a better reply than I gave him first.

CONCLUSIONS AND PERSPECTIVES

Targeting and proper insertion of membrane proteins is crucial for maintaining cellular homeostasis. Within this work we provide insights in the *Arabidopsis* GET-pathway, a translocation machinery required for TA protein insertion. We could demonstrate that it is a conserved pathway although G1IP, a part of the GET-receptor complex is only a structurally conserved ortholog. We provided evidence that alternative routes for TA proteins must exist in plants aside from the GET-pathway due to the weak phenotype of corresponding loss of function lines. Therefore, we searched for homologues of the SND-pathway, an alternative route for TA proteins to the ER membrane recently described in yeast. Our data showed gene duplication of the SND2 homologue in Brassicaceae and the conclusion that both proteins are partially redundant and involved in translocation. Contrary to yeast, we did not observe a lethal phenotype when both SND and GET components are missing. Instead, double *loss-of-function* mutants between both *At*SND2 proteins lead to a severe impact on plant fertility. Here, a molecular dissection of the phenotype would help to discern the changes caused by the absence of both genes. An *in-situ* immunostaining in early seedlings or embryos, using a cytokinesis marker, a cell wall marker and a nucleus marker will aid to discern the subcellular effects of the phenotype.

This should be accompanied by an analysis on substrate specificity. As it was shown in yeast, the SND-pathway has a broad client spectrum (Aviram et al., 2016). It remains to be seen whether *Arabidopsis* SND2s can provide an alternative route for proteins to the ER and which cargos are dependent on a putative *At*SND pathway. Based on that, an elaborate bioinformatical analysis of the IP-MS data might show similarities on the topology of interacting proteins. Candidates identified could be tested in biochemical membrane insertion assays in the absence or presence of *At*SND2 proteins, possibly in a heterologous system as mentioned above (**see Discussion: Conservation of the SRP-independent (SND) pathway**).

Homologues of SND1 and SND3 are still elusive, and it would be of interest to experimentally demonstrate which proteins pair up with SND2 in plants. As discussed, HSP70-2 and ATJ2/ATJ3 seem to interact with *At*SND2 proteins. To test whether they are able to deliver cargo to *At*SND2, biochemical membrane insertion assays might be helpful as well given that shared substrates were identified.

To validate an additional function of *At*SND2a compared to *At*SND2b a focus on Tunicamycin induced ER stress might be essential. Co-localization studies of *At*SND2a with a known autophagy maker under different stress conditions as well as a detailed phenotypical analysis of the *Atsnd2a* single mutant compared to *Atsnd2b* mutants and Col-0 with focus on reproductive tissues or different oxygen level might reveal important findings.

Moreover, research on the *Arabidopsis* GET-pathway is still required as there are many open questions. Up to date, a pretargeting complex including *At*GET5 and *At*SGT2 are predicted yet not experimentally proven. The conserved *At*GET4 would provide a good basis to search for other components upstream of *At*GET1, G1IP and *At*GET3a. Either an IP-MS analysis using *At*GET4-GFP as bait or a more biased screen using the mating based Split Ubiquitin System (Grefen et al., 2009) to test sequence homologues of GET5 and Sgt2 found in *Arabidopsis* would help to identity possible candidates which then have to be further tested on their relation to the GET-pathway (e.g. root hair phenotype).

The question remains why Archeaplastida evolved organellar variants of the GET3 ATPase and what function they may have. Interaction studies or screens might answer this question. Additionally, a detailed analysis of the *Atget3b* and *Atget3c* mutants especially with a focus on organellar specific phenotypes can provide functional clues. Both proteins contain the CxxC motif (Xing et al., 2017) which is important for Get3 oxidative stress related chaperone function in yeast (Voth et al., 2014). Although both proteins did not rescue the yeast Get3 phenotype, investigation of a similar chaperone function within their compartments can be of great interest.

Furthermore, little is known on additional pathways for TA protein insertion in plants. Although the EMC homologues would provide a more biased basis to study the conservation of this pathway, interaction screens of different TA proteins to find recurring interaction partners could probably lead to the identification of novel pathways. We observed clear independency of the TA protein SYP43 from GET rendering it a suitable candidate to search for additional pathways while the GET dependent SYP72 or SYP123 could serve as control. Especially in a *get* mutant background boosting alternative routes, one might find interesting candidates even with SYP123 as it is not solely GET dependent.

A big conundrum is the proper targeting and distribution of TA proteins to their various destinations as they can be found in almost all cellular membranes (Abell and Mullen, 2011). Although huge progress in this area has been achieved in the past few years (Maggio et al., 2007; Stefanovic and Hegde, 2007; Abell and Mullen, 2011; Rao et al., 2016; Chio et al., 2017; Costello et al., 2017) the exact properties which define the localisation are still enigmatic. Especially precise answers for multi-targeted TA proteins are still missing. Localisation experiments on multi-targeting TA proteins with changes in hydrophobicity, length of the C-terminal element and position of the transmembrane domain might be interesting. These features are predicted to be crucial to determine subcellular distribution (Chio et al., 2017; Costello et al., 2017) and those changes or domain swaps with other TA proteins may force multi-spanning TA proteins to mislocate to one/another organelle. These modifications might provide evidence of the underlying mechanisms or information on other targeting properties. Such domain swap studies recently revealed the importance of a C-terminal RK/ST motif in the import of the plant TA protein OEP7.2 into the plastid outer envelope membrane (Teresinski et al., 2019). Notwithstanding, such an unambiguous amino acid motif for TA protein distribution has not been found so far in Opisthokonts.

There are many open questions on protein translocation pathways in plants that require addressing in future research. Despite many similarities of the Archaeplastida pathways compared to Opisthokonts, our research revealed significant differences confirming the relevance of research of such fundamental homeostatic pathways in plants.

REFERENCES

Abell BM, Mullen RT (2011) Tail-anchored membrane proteins: exploring the complex diversity of tail-anchored-protein targeting in plant cells. Plant Cell Rep **30:** 137-151

Abell BM, Pool MR, Schlenker O, Sinning I, High S (2004) Signal recognition particle mediates post-translational targeting in eukaryotes. EMBO J **23:** 2755-2764

Abell BM, Rabu C, Leznicki P, Young JC, High S (2007) Post-translational integration of tail-anchored proteins is facilitated by defined molecular chaperones. J Cell Sci **120:** 1743-1751

Akahane T, Sahara K, Yashiroda H, Tanaka K, Murata S (2013) Involvement of Bag6 and the TRC pathway in proteasome assembly. Nat Commun **4:** 2234

Anderson SA, Singhal R, Fernandez DE (2019) Membrane-Specific Targeting of Tail-Anchored Proteins SECE1 and SECE2 Within Chloroplasts. Front Plant Sci **10:** 1401

Anghel SA, McGilvray PT, Hegde RS, Keenan RJ (2017) Identification of Oxa1 Homologs Operating in the Eukaryotic Endoplasmic Reticulum. Cell Rep **21:** 3708-3716

Asseck LY, Mehlhorn DG, Monroy JR, Ricardi MM, Breuninger H, Wallmeroth N, Berendzen KW, Nowrousian M, Xing S, Schwappach B, Bayer M, Grefen C (2021) Endoplasmic reticulum membrane receptors of the GET pathway are conserved throughout eukaryotes. Proc Natl Acad Sci U S A **118**

Ast T, Schuldiner M (2013) All roads lead to Rome (but some may be harder to travel): SRP-independent translocation into the endoplasmic reticulum. Crit Rev Biochem Mol Biol **48:** 273-288

Asvin K.K. Lakkaraju, Camille Mary, Anne Scherrer, Arthut E. Johnson KS (2008) SRP maintains nascent chains translocation-competent by slowing translation rates to match limiting numbers of targeting sites. Cell **133:** 400-451

Aviram N, Ast T, Costa EA, Arakel EC, Chuartzman SG, Jan CH, Hassdenteufel S, Dudek J, Jung M, Schorr S, Zimmermann R, Schwappach B, Weissman JS, Schuldiner M (2016) The SND proteins constitute an alternative targeting route to the endoplasmic reticulum. Nature **540:** 134-138

Aviram N, Schuldiner M (2017) Targeting and translocation of proteins to the endoplasmic reticulum at a glance. J Cell Sci **130:** 4079-4085

Bachmair A, Novatchkova M, Potuschak T, Eisenhaber F (2001) Ubiquitylation in plants a post-genomic look at a post-translational modification. TRENDS in Plant Science **6:** 463-470

Bibikiva TN, Blancaflor EB, Gilroy S (1999) Microtubules regulate tip growth and orientation in root hairs ofArabidopsis thaliana. The Plant Journal **17:** 657-665

Blacker TS, Duchen MR (2016) Investigating mitochondrial redox state using NADH and NADPH autofluorescence. Free Radic Biol Med **100:** 53-65

Bodensohn US, Simm S, Fischer K, Jaschke M, Gross LE, Kramer K, Ehmann C, Rensing SA, Ladig R, Schleiff E (2019) The intracellular distribution of the components of the GET system in vascular plants. Biochim Biophys Acta Mol Cell Res **1866:** 1650-1662

Boos F, Kramer L, Groh C, Jung F, Haberkant P, Stein F, Wollweber F, Gackstatter A, Zoller E, van der Laan M, Savitski MM, Benes V, Herrmann JM (2019) Mitochondrial protein-induced stress triggers a global adaptive transcriptional programme. Nat Cell Biol **21:** 442-451

Borgese N (2020) Searching for remote homologs of CAML among eukaryotes. Traffic **21:** 647-658

Borgese N, Colombo S, Pedrazzini E (2003) The tale of tail-anchored proteins: coming from the cytosol and looking for a membrane. J Cell Biol **161:** 1013-1019

Borgese N, Coy-Vergara J, Colombo SF, Schwappach B (2019) The Ways of Tails: the GET Pathway and more. Protein J **38:** 289-305

Borgese N, Fasana E (2011) Targeting pathways of C-tail-anchored proteins. Biochim Biophys Acta **1808:** 937-946

Brambillasca S, Yabal M, Makarow M, Borgese N (2006) Unassisted translocation of large polypeptide domains across phospholipid bilayers. J Cell Biol **175:** 767-777

Buchana BB, Gruissem W, Jones RL (2015) Biochemistry and Molecular Biology of Plants 2nd Edition. John Wiley & Sons, Ltd.

Carvalho HJF, Del Bondio A, Maltecca F, Colombo SF, Borgese N (2019) The WRB Subunit of the Get3 Receptor is Required for the Correct Integration of its Partner CAML into the ER. Sci Rep **9:** 11887

Casson J, McKenna M, Hassdenteufel S, Aviram N, Zimmerman R, High S (2017) Multiple pathways facilitate the biogenesis of mammalian tail-anchored proteins. J Cell Sci **130:** 3851-3861

Chang YW, Chuang YC, Ho YC, Cheng MY, Sun YJ, Hsiao CD, Wang C (2010) Crystal structure of Get4-Get5 complex and its interactions with Sgt2, Get3, and Ydj1. J Biol Chem **285:** 9962-9970

Chartron JW, Gonzalez GM, Clemons WM, Jr. (2011) A structural model of the Sgt2 protein and its interactions with chaperones and the Get4/Get5 complex. J Biol Chem **286:** 34325-34334

Chartron JW, Suloway CJ, Zaslaver M, Clemons WM, Jr. (2010) Structural characterization of the Get4/Get5 complex and its interaction with Get3. Proc Natl Acad Sci U S A **107:** 12127-12132

Chio US, Cho H, Shan SO (2017) Mechanisms of Tail-Anchored Membrane Protein Targeting and Insertion. Annu Rev Cell Dev Biol **33:** 417-438

Chitwood PJ, Juszkiewicz S, Guna A, Shao S, Hegde RS (2018) EMC Is Required to Initiate Accurate Membrane Protein Topogenesis. Cell **175:** 1507-1519 e1516

Colombo SF, Cardani S, Maroli A, Vitiello A, Soffientini P, Crespi A, Bram RF, Benfante R, Borgese N (2016) Tail-anchored Protein Insertion in Mammals: Function nd Reciprocal Interactions of the Two Subunits of the TRC40 Receptor. J Biol Chem **291:** 15292-15306

Costello JL, Castro IG, Camoes F, Schrader TA, McNeall D, Yang J, Giannopoulou EA, Gomes S, Pogenberg V, Bonekamp NA, Ribeiro D, Wilmanns M, Jedd G, Islinger M, Schrader M (2017) Predicting the targeting of tail-anchored proteins to subcellular compartments in mammalian cells. J Cell Sci **130:** 1675-1687

Cournia Z, Allen TW, Andricioaei I, Antonny B, Baum D, Brannigan G, Buchete NV, Deckman JT, Delemotte L, Del Val C, Friedman R, Gkeka P, Hege HC, Henin J, Kasimova MA, Kolocouris A, Klein ML, Khalid S, Lemieux MJ, Lindow N, Roy M, Selent J, Tarek M, Tofoleanu F, Vanni S, Urban S, Wales DJ, Smith JC, Bondar AN (2015) Membrane Protein Structure, Function, and Dynamics: a Perspective from Experiments and Theory. J Membr Biol **248:** 611-640

Culver J, Mariappan M (2021) Deubiquitinases USP20/33 promote the biogenesis of tail-anchored membrane proteins. J Cell Biol.

Cvrckova F, Bezvoda R, Zarsky V (2010) Computational identification of root hair-specific genes in Arabidopsis. Plant Signal Behav **5:** 1407-1418

Dahl JU, Gray MJ, Jakob U (2015) Protein quality control under oxidative stress conditions. J Mol Biol **427:** 1549-1563

David J. Anderson, Peter Walter, Blobel G (1982) Signal recognition protein is required for the integration of acetylcholine receptor delta subunit, a transmembrane glycoprotein, into the endoplasmic reticulum membrane. J Cell Biol **93:** 501-506

Denic V, Dotsch V, Sinning I (2013) Endoplasmic reticulum targeting and insertion of tail-anchored membrane proteins by the GET pathway. Cold Spring Harb Perspect Biol **5:** a013334

Denks K, Vogt A, Sachelaru I, Petriman NA, Kudva R, Koch HG (2014) The Sec translocon mediated protein transport in prokaryotes and eukaryotes. Mol Membr Biol **31:** 58-84

Deshaies RJ, Sanders SL, Feldheim DA, Scheckman R (1991) Assembly of yeast Sec proteins involved in translocation into the endoplasmic reticulum into a membrane-bound multisubunit complex. Nature **349**

Duncan O, Taylor NL, Carrie C, Eubel H, Kubiszewski-Jakubiak S, Zhang B, Narsai R, Millar AH, Whelan J (2011) Multiple lines of evidence localize signaling, morphology, and lipid biosynthesis machinery to the mitochondrial outer membrane of Arabidopsis. Plant Physiol **157:** 1093-1113

Duncan O, van der Merwe MJ, Daley DO, Whelan J (2013) The outer mitochondrial membrane in higher plants. Trends Plant Sci **18:** 207-217

Farkas A, De Laurentiis EI, Schwappach B (2019) The natural history of Get3-like chaperones. Traffic **20:** 311-324

Favaloro V, Vilardi F, Schlecht R, Mayer MP, Dobberstein B (2010) Asna1/TRC40-mediated membrane insertion of tail-anchored proteins. J Cell Sci **123:** 1522-1530

Formighieri C, Cazzaniga S, Kuras R, Bassi R (2013) Biogenesis of photosynthetic complexes in the chloroplast of Chlamydomonas reinhardtii requires ARSA1, a homolog of prokaryotic arsenite transporter and eukaryotic TRC40 for guided entry of tail-anchored proteins. Plant J **73:** 850-861

Gilmore R, Blobel G, Walter P (1982) Protein translocation across the endoplasmic reticulum. I. Detection in the microsomal membrane of a receptor for the signal recognition particle. The Journal of cell biology **95:** 463-469

Gilmore R, Walter P, Blobel G (1982) Protein translocation across the endoplasmic reticulum. II. Isolation and characterization of the signal recognition particle receptor. The Journal of cell biology **95:** 470-477

Goder V, Spiess M (2001) Topogenesis of membrane proteins: determinants and dynamics. FEBS Lett **504:** 87-93

Grefen C, Obrdlik P, Harter K (2009) The determination of protein-protein interactions by the mating-based split-ubiquitin system (mbSUS). Methods Mol Biol **479:** 217-233

Gristick HB, Rao M, Chartron JW, Rome ME, Shan SO, Clemons WM, Jr. (2014) Crystal structure of ATP-bound Get3-Get4-Get5 complex reveals regulation of Get3 by Get4. Nat Struct Mol Biol **21:** 437-442

Gristick HB, Rome ME, Chartron JW, Rao M, Hess S, Shan SO, Clemons WM, Jr. (2015) Mechanism of Assembly of a Substrate Transfer Complex during Tail-anchored Protein Targeting. J Biol Chem **290:** 30006-30017

Guna A, Volkmar N, Christianson JC, Hegde RS (2018) The ER membrane protein complex is a transmembrane domain insertase. Science **359:** 470-473

Gunes Bozkurt GS, Fabio Vilardi, Stefan Amlacher, Klemens Wild, Gert Bange, Vincenzo Favaloro,, Karsten Rippe EH, Bernhard Dobberstein, Irmgard Sinning (2009) Structural insights into tail-anchored protein binding and membrane insertion by Get3. PNAS **106:** 21131-21136

Hansen KG, Aviram N, Laborenz J, Bibi C, Meyer M, Spang A, Schuldiner M, Herrmann JM (2018) An ER surface retrieval pathway safeguards the import of mitochondrial membrane proteins in yeast. Science **361:** 1118-1122

Harada Y, Li H, Wall JS, Li H, Lennarz WJ (2011) Structural studies and the assembly of the heptameric post-translational translocon complex. J Biol Chem **286:** 2956-2965

Hassdenteufel S, Sicking M, Schorr S, Aviram N, Fecher-Trost C, Schuldiner M, Jung M, Zimmermann R, Lang S (2017) hSnd2 protein represents an alternative targeting factor to the endoplasmic reticulum in human cells. FEBS Lett **591:** 3211-3224

Hegde RS, Keenan RJ (2011) Tail-anchored membrane protein insertion into the endoplasmic reticulum. Nat Rev Mol Cell Biol **12:** 787-798

Hennon SW, Soman R, Zhu L, Dalbey RE (2015) YidC/Alb3/Oxa1 Family of Insertases. J Biol Chem **290:** 14866-14874

Higy M, Junne T, Spiess M (2004) Topogenesis of membrane proteins at the endoplasmic reticulum. Biochemistry **43:** 12716-12722

Hu S, Ye H, Cui Y, Jiang L (2020) AtSec62 is critical for plant development and is involved in ER-phagy in Arabidopsis thaliana. J Integr Plant Biol **62:** 181-200

Inglis AJ, Page KR, Guna A, Voorhees RM (2020) Differential Modes of Orphan Subunit Recognition for the WRB/CAML Complex. Cell Reports **30:** 3691-3698.e3695

Johnson N, Powis K, High S (2013) Post-translational translocation into the endoplasmic reticulum. Biochim Biophys Acta **1833:** 2403-2409

Jonikas MC, Collins SR, Vladimir D, Oh E, Quan EM, Schmid V, Weibezahn J, Schwappach B, Walter P, Weissman JS, Schuldiner M (2009) Comprehensive Characterization of Genes Required for Protein Folding in the Endoplasmic Reticulum. Science **323:** 1693-1697

Kandasamy MK, McKinney EC, Roy E, Meagher RB (2012) Plant vegetative and animal cytoplasmic actins share functional competence for spatial development with protists. Plant Cell **24:** 2041-2057

Kawahara H, Minami R, Yokota N (2013) BAG6/BAT3: emerging roles in quality control for nascent polypeptides. J Biochem **153:** 147-160

Kemper C, Habib SJ, Engl G, Heckmeyer P, Dimmer KS, Rapaport D (2008) Integration of tail-anchored proteins into the mitochondrial outer membrane does not require any known import components. J Cell Sci **121:** 1990-1998

Knight BC, High S (1998) Membrane integration of Sec61alpha: a core component of the endoplasmic reticulum translocation complex. Biochem. J **331:** 161-167

Kriechbaumer V, Shaw R, Mukherjee J, Bowsher CG, Harrison AM, Abell BM (2009) Subcellular distribution of tail-anchored proteins in Arabidopsis. Traffic **10:** 1753-1764

Kuwabara N, Minami R, Yokota N, Matsumoto H, Senda T, Kawahara H, Kato R (2015) Structure of a BAG6 (Bcl-2-associated athanogene 6)-Ubl4a (ubiquitin-like protein 4a) complex reveals a novel binding interface that functions in tail-anchored protein biogenesis. J Biol Chem **290:** 9387-9398

Lakkaraju AK, Thankappan R, Mary C, Garrison JL, Taunton J, Strub K (2012) Efficient secretion of small proteins in mammalian cells relies on Sec62-dependent posttranslational translocation. Mol Biol Cell **23:** 2712-2722

Lang S, Benedix J, Fedeles SV, Schorr S, Schirra C, Schauble N, Jalal C, Greiner M, Hassdenteufel S, Tatzelt J, Kreutzer B, Edelmann L, Krause E, Rettig J, Somlo S, Zimmermann R, Dudek J (2012) Different effects of Sec61alpha, Sec62 and Sec63 depletion on transport of polypeptides into the endoplasmic reticulum of mammalian cells. J Cell Sci **125:** 1958-1969

Lauber MH, Waizenegger I, Steinmann T, Schwarz H, Mayer U, Hwang I, Lukowitz W, Jürgens G (1997) The *Arabidopsis* KNOLLE Protein Is a Cytokinesis-specific Syntaxin. J Cell Biol **139:** 1485-1493

Lei P, Xiao Y, Li P, Xie P, Wang H, Huang S, Song P, Zhao Y (2020) hSnd2/TMEM208 is an HIF-1alpha-targeted gene and contains a WH2 motif. Acta Biochim Biophys Sin (Shanghai) **52:** 328-331

Leznicki P, Roebuck QP, Wunderley L, Clancy A, Krysztofinska EM, Isaacson RL, Warwicker J, Schwappach B, High S (2013) The association of BAG6 with SGTA and tail-anchored proteins. PLoS One **8:** e59590

Li Y, Kabbage M, Liu W, Dickman MB (2016) Aspartyl Protease-Mediated Cleavage of BAG6 Is Necessary for Autophagy and Fungal Resistance in Plants. Plant Cell **28:** 233-247

Lin SY, Vollrath MA, Mangosing S, Shen J, Cardenas E, Corey DP (2016) The zebrafish pinball wizard gene encodes WRB, a tail-anchored-protein receptor essential for inner-ear hair cells and retinal photoreceptors. J Physiol **594:** 895-914

Lin TW, Chen CC, Wu SM, Chang YC, Li YC, Su YW, Hsiao CD, Chang HY (2019) Structural analysis of chloroplast tail-anchored membrane protein recognition by ArsA1. Plant J **99:** 128-143

Luptovciak I, Samakovli D, Komis G, Samaj J (2017) KATANIN 1 Is Essential for Embryogenesis and Seed Formation in Arabidopsis. Front Plant Sci **8:** 728

Lyman SK, Schekman R (1997) Binding of Secretory Precursor Polypeptides to a Translocon Subcomplex Is Regulated by BiP. Cell **88:** 85-96

Mabry ME, Brose JM, Blischak PD, Sutherland B, Dismukes WT, Bottoms CA, Edger PP, Washburn JD, An H, Hall JC, McKain MR, Al-Shehbaz I, Barker MS, Schranz ME, Conant GC, Pires JC (2020) Phylogeny and multiple independent whole-genome duplication events in the Brassicales. Am J Bot **107:** 1148-1164

Maestre-Reyna M, Wu SM, Chang YC, Chen CC, Maestre-Reyna A, Wang AH, Chang HY (2017) In search of tail-anchored protein machinery in plants: reevaluating the role of arsenite transporters. Sci Rep **7:** 46022

Maggio C, Barbante A, Ferro F, Frigerio L, Pedrazzini E (2007) Intracellular sorting of the tail-anchored protein cytochrome b5 in plants: a comparative study using different isoforms from rabbit and Arabidopsis. J Exp Bot **58:** 1365-1379

Mariappan M, Li X, Stefanovic S, Sharma A, Mateja A, Keenan RJ, Hegde RS (2010) A ribosome-associating factor chaperones tail-anchored membrane proteins. Nature **466:** 1120-1124

Mariappan M, Mateja A, Dobosz M, Bove E, Hegde RS, Keenan RJ (2011) The mechanism of membrane-associated steps in tail-anchored protein insertion. Nature **477:** 61-66

Martinez-Gil L, Sauri A, Marti-Renom MA, Mingarro I (2011) Membrane protein integration into the endoplasmic reticulum. FEBS J **278:** 3846-3858

Mateja A, Paduch M, Chang HY, Szydlowska A, Kossiakoff AA, Hegde RS, Keenan RJ (2015) Protein targeting. Structure of the Get3 targeting factor in complex with its membrane protein cargo. Science **347:** 1152-1155

Mateja A, Szlachcic A, Downing ME, Dobosz M, Mariappan M, Hegde RS, Keenan RJ (2009) The structural basis of tail-anchored membrane protein recognition by Get3. Nature **461:** 361-366

Matlack KES, Misselwitz B, Plath K, Rapoport TA (1999) BiP Acts as a Molecular Ratchet during Posttranslational Transport of Prepro-α Factor across the ER Membrane. Cell **97:** 553-564

McClellan AJ, Brodsky JL (2000) Mutation of the ATP-Binding Pocket ofSSA1Indicates That a FunctionalInteraction Between Ssa1p and Ydj1p Is Required for Post-translationalTranslocation Into the Yeast Endoplasmic Reticulum. Genetics **156:** 501-512

McDowell MA, Heimes M, Fiorentino F, Mehmood S, Farkas A, Coy-Vergara J, Wu D, Bolla JR, Schmid V, Heinze R, Wild K, Flemming D, Pfeffer S, Schwappach B, Robinson CV, Sinning I (2020) Structural Basis of Tail-Anchored Membrane Protein Biogenesis by the GET Insertase Complex. Mol Cell **80:** 72-86 e77

McDowell MA, Heimes M, Sinning I (2021) Structural and molecular mechanisms for membrane protein biogenesis by the Oxa1 superfamily. Nat Struct Mol Biol **28:** 234-239

Mehlhorn DG, Asseck LY, Grefen C (2021) Looking for a Safe Haven: Tail-anchored Proteins and their Membrane Insertion Pathways. Plant Physiology

Mehlhorn DG, Wallmeroth N, Berendzen KW, Grefen C (2018) 2in1 Vectors Improve In Planta BiFC and FRET Analyses. Methods Mol Biol **1691:** 139-158

Metz J, Wachter A, Schmidt B, Bujnicki JM, Schwappach B (2006) The yeast Arr4p ATPase binds the chloride transporter Gef1p when copper is available in the cytosol. J Biol Chem **281:** 410-417

Mitterreiter MJ, Bosch FA, Brylok T, Schwenkert S (2019) The ER luminal C-terminus of AtSec62 is critical for male fertility and plant growth in Arabidopsis thaliana. Plant J

Mock JY, Chartron JW, Zaslaver M, Xu Y, Ye Y, Clemons WM, Jr. (2015) Bag6 complex contains a minimal tail-anchor-targeting module and a mock BAG domain. Proc Natl Acad Sci U S A **112:** 106-111

Mukhopadhyay R, Ho YS, Swiatek PJ, Rosen BP, Bhattacharjee H (2006) Targeted disruption of the mouse Asna1 gene results in embryonic lethality. FEBS Lett **580:** 3889-3894

Müller L, de Escauriaza MD, Lajoie P, Theis M, Jung M, Muller A, Burgard C, Greiner M, Snapp EL, Dudek J, Zimmermann R (2010) Evolutionary gain of function for the ER membrane protein Sec62 from yeast to humans. Mol Biol Cell **21:** 691-703

Neveu E, Khalifeh D, Salamin N, Fasshauer D (2020) Prototypic SNARE Proteins Are Encoded in the Genomes of Heimdallarchaeota, Potentially Bridging the Gap between the Prokaryotes and Eukaryotes. Curr Biol **30:** 2468-2480 e2465

Nicolson GL (2014) The Fluid-Mosaic Model of Membrane Structure: still relevant to understanding the structure, function and dynamics of biological membranes after more than 40 years. Biochim Biophys Acta **1838:** 1451-1466

Noh S-J, Kwon CS, Oh D-H, Moon JS, Chung W-I (2003) Expression of an evolutionarily distinct novel BiP gene during the unfolded protein response in Arabidopsis thaliana. Gene **311:** 81-91

Norlin S, Parekh VS, Naredi P, Edlund H (2016) Asna1/TRC40 Controls beta-Cell Function and Endoplasmic Reticulum Homeostasis by Ensuring Retrograde Transport. Diabetes **65:** 110-119

Novick P, Field C, Scheckman R (1980) Identification of 23 Complementation Groups required for post-translational events in the yeast secretory pathway. Cell **21:** 205-215

Nyathi Y, Wilkinson BM, Pool MR (2013) Co-translational targeting and translocation of proteins to the endoplasmic reticulum. Biochim Biophys Acta **1833:** 2392-2402

Ozgur R, Turkan I, Uzilday B, Sekmen AH (2014) Endoplasmic reticulum stress triggers ROS signalling, changes the redox state, and regulates the antioxidant defence of Arabidopsis thaliana. J Exp Bot **65:** 1377-1390

Ozgur R, Uzilday B, Sekmen AH, Turkan I (2015) The effects of induced production of reactive oxygen species in organelles on endoplasmic reticulum stress and on the unfolded protein response in arabidopsis. Ann Bot **116:** 541-553

Pabon-Mora N, Wong GK, Ambrose BA (2014) Evolution of fruit development genes in flowering plants. Front Plant Sci **5:** 300

Pan X, Ye P, Yuan DS, Wang X, Bader JS, Boeke JD (2006) A DNA integrity network in the yeast Saccharomyces cerevisiae. Cell **124:** 1069-1081

Panzner S, Dreier L, Hartmann E, Kostka S, Rapoport TA (1995) Posttranslational protein transport in yeast reconstituted with a purified complex of Sec proteins and Kar2p. Cell **81:** 561-570

Park E, Rapoport TA (2012) Mechanisms of Sec61/SecY-mediated protein translocation across membranes. Annu Rev Biophys **41:** 21-40

Paul P, Simm S, Blaumeiser A, Scharf KD, Fragkostefanakis S, Mirus O, Schleiff E (2013) The protein translocation systems in plants - composition and variability on the example of Solanum lycopersicum. BMC Genomics **14:** 189

Pedrazzini E (2009) Tail-Anchored Proteins in Plants. Journal of Plant Biology **52:** 88-101

Pobre KFR, Poet GJ, Hendershot LM (2019) The endoplasmic reticulum (ER) chaperone BiP is a master regulator of ER functions: Getting by with a little help from ERdj friends. J Biol Chem **294:** 2098-2108

Powis K, Schrul B, Tienson H, Gostimskaya I, Breker M, High S, Schuldiner M, Jakob U, Schwappach B (2013) Get3 is a holdase chaperone and moves to deposition sites for aggregated proteins when membrane targeting is blocked. J Cell Sci **126:** 473-483

Rabu C, Wipf P, Brodsky JL, High S (2008) A precursor-specific role for Hsp40/Hsc70 during tail-anchored protein integration at the endoplasmic reticulum. J Biol Chem **283:** 27504-27513

Rao M, Okreglak V, Chio US, Cho H, Walter P, Shan SO (2016) Multiple selection filters ensure accurate tail-anchored membrane protein targeting. Elife **5**

Reithinger JH, Kim JE, Kim H (2013) Sec62 protein mediates membrane insertion and orientation of moderately hydrophobic signal anchor proteins in the endoplasmic reticulum (ER). J Biol Chem **288:** 18058-18067

Richter JD, Coller J (2015) Pausing on Polyribosomes: Make Way for Elongation in Translational Control. Cell **163:** 292-300

Rivera-Monroy J, Musiol L, Unthan-Fechner K, Farkas A, Clancy A, Coy-Vergara J, Weill U, Gockel S, Lin SY, Corey DP, Kohl T, Strobel P, Schuldiner M, Schwappach B, Vilardi F (2016) Mice lacking WRB reveal differential biogenesis requirements of tail-anchored proteins in vivo. Sci Rep **6:** 39464

Robles P, Pelaz S (2005) Flower and fruit development in Arabidopsis thaliana. Int J Dev Biol **49:** 633-643

Sato R, Maeshima M (2019) The ER-localized aquaporin SIP2;1 is involved in pollen germination and pollen tube elongation in Arabidopsis thaliana. Plant Mol Biol **100:** 335-349

Schuldiner M, Metz J, Schmid V, Denic V, Rakwalska M, Schmitt HD, Schwappach B, Weissman JS (2008) The GET complex mediates insertion of tail-anchored proteins into the ER membrane. Cell **134:** 634-645

Schweiger R, Muller NC, Schmitt MJ, Soll J, Schwenkert S (2012) AtTPR7 is a chaperone-docking protein of the Sec translocon in Arabidopsis. J Cell Sci **125:** 5196-5207

Schweiger R, Schwenkert S (2013) AtTPR7 as part of the Arabidopsis Sec post-translocon. Plant Signaling and Behaviour

Shan SO (2019) Guiding Tail-anchored Membrane Proteins to the ER In a Chaperone Cascade. J Biol Chem

Shao S, Hegde RS (2011) Membrane protein insertion at the endoplasmic reticulum. Annu Rev Cell Dev Biol **27:** 25-56

Shen J, Zeng Y, Zhuang X, Sun L, Yao X, Pimpl P, Jiang L (2013) Organelle pH in the Arabidopsis endomembrane system. Mol Plant **6:** 1419-1437

Simpson PJ, Schwappach B, Dohlman HG, Isaacson RL (2010) Structures of Get3, Get4, and Get5 provide new models for TA membrane protein targeting. Structure **18:** 897-902

Singer SJ, Nicolson GL (1972) The fluid mosaic model of the structure of cell membranes. Science **175:** 720-731

Srivastava R, Zalisko BE, Keenan RJ, Howell SH (2017) The GET System Inserts the Tail-Anchored Protein, SYP72, into Endoplasmic Reticulum Membranes. Plant Physiol **173:** 1137-1145

Stefanovic S, Hegde RS (2007) Identification of a targeting factor for posttranslational membrane protein insertion into the ER. Cell **128:** 1147-1159

Stefer S, Reitz S, Wang F, Wild K, Pang YY, Schwarz D, Bomke J, Hein C, Lohr F, Bernhard F, Denic V, Dotsch V, Sinning I (2011) Structural basis for tail-anchored membrane protein biogenesis by the Get3-receptor complex. Science **333:** 758-762

Steinbeck J, Fuchs P, Negroni YL, Elsasser M, Lichtenauer S, Stockdreher Y, Feitosa-Araujo E, Kroll JB, Niemeier JO, Humberg C, Smith EN, Mai M, Nunes-Nesi A, Meyer AJ, Zottini M, Morgan B, Wagner S, Schwarzlander M (2020) In Vivo NADH/NAD(+) Biosensing Reveals the Dynamics of Cytosolic Redox Metabolism in Plants. Plant Cell **32:** 3324-3345

Suloway CJ, Chartron JW, Zaslaver M, Clemons WM, Jr. (2009) Model for eukaryotic tail-anchored protein binding based on the structure of Get3. Proc Natl Acad Sci U S A **106:** 14849-14854

Suloway CJ, Rome ME, Clemons WM, Jr. (2012) Tail-anchor targeting by a Get3 tetramer: the structure of an archaeal homologue. EMBO J **31:** 707-719

Teresinski HJ, Gidda SK, Nguyen TND, Howard NJM, Porter BK, Grimberg N, Smith MD, Andrews DW, Dyer JM, Mullen RT (2019) An RK/ST C-Terminal Motif is Required for Targeting of OEP7.2 and a Subset of Other Arabidopsis Tail-Anchored Proteins to the Plastid Outer Envelope Membrane. Plant Cell Physiol **60:** 516-537

Vilardi F, Lorenz H, Dobberstein B (2011) WRB is the receptor for TRC40/Asna1-mediated insertion of tail-anchored proteins into the ER membrane. J Cell Sci **124:** 1301-1307

Vilardi F, Stephan M, Clancy A, Janshoff A, Schwappach B (2014) WRB and CAML are necessary and sufficient to mediate tail-anchored protein targeting to the ER membrane. PLoS One **9:** e85033

Vogl C, Panou I, Yamanbaeva G, Wichmann C, Mangosing SJ, Vilardi F, Indzhykulian AA, Pangrsic T, Santarelli R, Rodriguez-Ballesteros M, Weber T, Jung S, Cardenas E, Wu X, Wojcik SM, Kwan KY, Del Castillo I, Schwappach B, Strenzke N, Corey DP, Lin SY, Moser T (2016) Tryptophan-rich basic protein (WRB) mediates insertion of the tail-anchored protein otoferlin and is required for hair cell exocytosis and hearing. EMBO J

Volkmar N, Thezenas ML, Louie SM, Juszkiewicz S, Nomura DK, Hegde RS, Kessler BM, Christianson JC (2019) The ER membrane protein complex promotes biogenesis of sterol-related enzymes maintaining cholesterol homeostasis. J Cell Sci **132**

Voss NR, Gerstein M, Steitz TA, Moore PB (2006) The geometry of the ribosomal polypeptide exit tunnel. J Mol Biol **360:** 893-906

Voth W, Schick M, Gates S, Li S, Vilardi F, Gostimskaya I, Southworth DR, Schwappach B, Jakob U (2014) The protein targeting factor Get3 functions as ATP-independent chaperone under oxidative stress conditions. Mol Cell **56:** 116-127

Walden N, German DA, Wolf EM, Kiefer M, Rigault P, Huang XC, Kiefer C, Schmickl R, Franzke A, Neuffer B, Mummenhoff K, Koch MA (2020) Nested whole-genome duplications coincide with diversification and high morphological disparity in Brassicaceae. Nat Commun **11:** 3795

Wang F, Brown EC, Mak G, Zhuang J, Denic V (2010) A chaperone cascade sorts proteins for posttranslational membrane insertion into the endoplasmic reticulum. Mol Cell **40:** 159-171

Wang F, Chan C, Weir NR, Denic V (2014) The Get1/2 transmembrane complex is an endoplasmic-reticulum membrane protein insertase. Nature **512:** 441-444

Wang F, Whynot A, Tung M, Denic V (2011) The mechanism of tail-anchored protein insertion into the ER membrane. Mol Cell **43:** 738-750

Weiqun Song, David Raden, Elisabet C. Mandon, Gilmore R (2000) Role of Sec61α in the Regulated Transfer of the Ribosome–Nascent Chain Complex from the Signal Recognition Particle to the Translocation Channel. Cell **100:** 333-343

Wereszczynski J, McCammon JA (2012) Nucleotide-dependent mechanism of Get3 as elucidated from free energy calculations. Proc Natl Acad Sci U S A **109:** 7759-7764

Whitley P, Mingarro I (2014) Stitching proteins into membranes, not sew simple. Biol Chem **395:** 1417-1424

Wideman JG (2015) The ubiquitous and ancient ER membrane protein complex (EMC): tether or not? F1000Res **4:** 624

Wu X, Cabanos C, Rapoport TA (2019) Structure of the post-translational protein translocation machinery of the ER membrane. Nature **566:** 136-139

Wunderley L, Leznicki P, Payapilly A, High S (2014) SGTA regulates the cytosolic quality control of hydrophobic substrates. J Cell Sci **127:** 4728-4739

Xiao T, Shakya VP, Hughes AL (2021) ER targeting of non-imported mitochondrial carrier proteins is dependent on the GET pathway. Life Sci Alliance **4**

Xing S, Mehlhorn DG, Wallmeroth N, Asseck LY, Kar R, Voss A, Denninger P, Schmidt VA, Schwarzlander M, Stierhof YD, Grossmann G, Grefen C (2017) Loss of GET pathway orthologs in Arabidopsis thaliana causes root hair growth defects and affects SNARE abundance. Proc Natl Acad Sci U S A **114:** E1544-E1553

Yamamoto M, Maruyama D, Endo T, Nishikawa S (2008) Arabidopsis thaliana has a set of J proteins in the endoplasmic reticulum that are conserved from yeast to animals and plants. Plant Cell Physiol **49:** 1547-1562

Yamamoto Y, Sakisaka T (2012) Molecular machinery for insertion of tail-anchored membrane proteins into the endoplasmic reticulum membrane in mammalian cells. Mol Cell **48:** 387-397

Zalisko BE, Chan C, Denic V, Rock RS, Keenan RJ (2017) Tail-Anchored Protein Insertion by a Single Get1/2 Heterodimer. Cell Rep **20:** 2287-2293

Zhang Y, De Laurentiis E, Bohnsack KE, Wahlig M, Ranjan N, Gruseck S, Hackert P, Wolfle T, Rodnina MV, Schwappach B, Rospert S (2021) Ribosome-bound Get4/5 facilitates the capture of tail-anchored proteins by Sgt2 in yeast. Nat Commun **12:** 782

Zhao Y, Hu J, Miao G, Qu L, Wang Z, Li G, Lv P, Ma D, Chen Y (2013) Transmembrane protein 208: a novel ER-localized protein that regulates autophagy and ER stress. PLoS One **8:** e64228

Ziehe D, Dunschede B, Schunemann D (2017) From bacteria to chloroplasts: evolution of the chloroplast SRP system. Biol Chem **398:** 653-661

APPENDICES

I. Xing et al., 2017:

Loss of GET pathway orthologs in Arabidopsis thaliana causes root hair growth defects and affects SNARE abundance

Loss of GET pathway orthologs in *Arabidopsis thaliana* causes root hair growth defects and affects SNARE abundance

Shuping Xing[a], Dietmar Gerald Mehlhorn[a], Niklas Wallmeroth[a], Lisa Yasmin Asseck[a], Ritwika Kar[a], Alessa Voss[a], Philipp Denninger[b], Vanessa Aphaia Fiona Schmidt[b], Markus Schwarzländer[c], York-Dieter Stierhof[d], Guido Grossmann[b], and Christopher Grefen[a,1]

[a]Centre for Plant Molecular Biology, Developmental Genetics, University of Tübingen, 72076 Tuebingen, Germany; [b]Centre for Organismal Studies, CellNetworks Excellence Cluster, University of Heidelberg, 69120 Heidelberg, Germany; [c]Institute of Crop Science and Resource Conservation, University of Bonn, 53113 Bonn, Germany; and [d]Centre for Plant Molecular Biology, Microscopy, University of Tübingen, 72076 Tuebingen, Germany

Edited by Natasha V. Raikhel, Center for Plant Cell Biology, Riverside, CA, and approved December 19, 2016 (received for review November 28, 2016)

Soluble *N*-ethylmaleimide–sensitive factor attachment protein receptor (SNARE) proteins are key players in cellular trafficking and coordinate vital cellular processes, such as cytokinesis, pathogen defense, and ion transport regulation. With few exceptions, SNAREs are tail-anchored (TA) proteins, bearing a C-terminal hydrophobic domain that is essential for their membrane integration. Recently, the Guided Entry of Tail-anchored proteins (GET) pathway was described in mammalian and yeast cells that serve as a blueprint of TA protein insertion [Schuldiner M, et al. (2008) *Cell* 134(4):634–645; Stefanovic S, Hegde RS (2007) *Cell* 128(6):1147–1159]. This pathway consists of six proteins, with the cytosolic ATPase GET3 chaperoning the newly synthesized TA protein posttranslationally from the ribosome to the endoplasmic reticulum (ER) membrane. Structural and biochemical insights confirmed the potential of pathway components to facilitate membrane insertion, but the physiological significance in multicellular organisms remains to be resolved. Our phylogenetic analysis of 37 GET3 orthologs from 18 different species revealed the presence of two different GET3 clades. We identified and analyzed GET pathway components in *Arabidopsis thaliana* and found reduced root hair elongation in *Atget* lines, possibly as a result of reduced SNARE biogenesis. Overexpression of *At*GET3a in a receptor knockout (KO) results in severe growth defects, suggesting presence of alternative insertion pathways while highlighting an intricate involvement for the GET pathway in cellular homeostasis of plants.

GET pathway | TA proteins | SNAREs | ER membrane | root hairs

Plants show remarkable acclimation and resilience to a broad spectrum of environmental influences as a consequence of their sedentary lifestyle. On the cellular level, such flexibility requires genetic buffering capacity as well as fine-tuned signaling and response systems. Soluble *N*-ethylmaleimide–sensitive factor attachment protein receptor (SNARE) proteins make a critical contribution toward acclimation (1, 2). Their canonical function facilitates membrane fusion through tight interaction of cognate SNARE partners at vesicle and target membranes (3). This vital process guarantees cellular expansion through addition of membrane material, cell plate formation, and cargo delivery (4, 5). SNARE proteins are also involved in regulating potassium channels and aquaporins (6–8).

Most SNARE proteins are Type II oriented and referred to as tail-anchored (TA) proteins with a cytosolic N terminus and a single C-terminal transmembrane domain (TMD) (9). TA proteins are involved in vital cellular processes in all domains of life, such as chaperoning, ubiquitination, signaling, trafficking, and transcript regulation (10–13). The nascent protein is almost fully translated when the hydrophobic TMD emerges from the ribosome, requiring shielding from the aqueous cytosol to guarantee protein stability, efficient folding, and function (14). One way of facilitating this posttranslational insertion is by proteinaceous components of a Guided Entry of Tail-anchored proteins (GET) pathway that was identified in yeast and mammals (15, 16).

In yeast, recognition of nascent TA proteins is accomplished through a tripartite pretargeting complex at the ribosome consisting of SGT2, GET5, and GET4. This complex binds to the TMD and delivers the TA protein to the cytosolic ATPase GET3 (17, 18). GET3 arranges as zinc-coordinating homodimer and shuttles the client protein to the endoplasmic reticulum (ER) membrane receptors GET1 and GET2, which finalize insertion of the TA protein (15, 19, 20).

This GET pathway is thought to be the main route for TA protein insertion into the ER, but surprisingly, its loss in yeast is only conditionally lethal (15). Conversely, lack of the mammalian GET3 orthologs TRC40 (transmembrane domain recognition complex of 40 kDa) leads to embryo lethality in mice, complicating global physiological analyses (21). Nevertheless, a handful of recent studies have started to analyze individual physiological consequences of the GET pathway in vivo using tissue-specific knockout (KO) approaches and observed that its function is required for a diverse range of physiological processes, such as insulin secretion, auditory perception, and photoreceptor function, in animals (22–24). A high degree of evolutionary conservation is often assumed, and it has been recognized that some components of the GET pathway are present in *Arabidopsis thaliana* (25, 26). However, considering the specific physiological roles of the GET pathway observed in yeast and mammals, its significance cannot

Significance

Root hairs are unicellular extensions of the rhizodermis, providing anchorage and an increase in surface area for nutrient and water uptake. Their fast, tip-focused growth showcases root hairs as an excellent genetic model to study physiological and developmental processes on the cellular level. We uncovered a root hair phenotype that is dependent on putative *Arabidopsis* orthologs of the Guided Entry of Tail-anchored (TA) proteins (GET) pathway, which facilitates membrane insertion of TA proteins in yeast and mammals. We found that plants have evolved multiple paralogs of specific GET pathway components, albeit in a compartment-specific manner. In addition, we show that differential expression of pathway components causes pleiotropic growth defects, suggesting alternative pathways for TA insertion and additional functions of GET in plants.

Author contributions: S.X. and C.G. designed research; S.X., D.G.M., N.W., L.Y.A., R.K., A.V., P.D., V.A.F.S., M.S., Y.-D.S., G.G., and C.G. performed research; S.X., D.G.M., M.S., Y.-D.S., G.G., and C.G. analyzed data; and C.G. wrote the paper with input from M.S.

The authors declare no conflict of interest.

This article is a PNAS Direct Submission.

Freely available online through the PNAS open access option.

See Commentary on page 1762.

[1]To whom correspondence should be addressed. Email: christopher.grefen@zmbp.uni-tuebingen.de.

This article contains supporting information online at www.pnas.org/lookup/suppl/doi:10.1073/pnas.1619525114/-/DCSupplemental.

be straightforwardly extrapolated across eukaryotes. A global genetic dissection of the pathway in a multicellular organism, let alone in plants, is currently lacking.

GET3/TRC40 are distant paralogs of the prokaryotic ArsA (arsenite-translocating ATPase), a protein that is part of the arsenic detoxification pathway in bacteria (27). Evidence points toward the GET pathway—albeit at a simpler scale—that exists already in Archaebacteria (10, 28). Because yeast and mammals are closely related in the supergroup of Opisthokonts (29), limiting any comparative power, we aimed to investigate pathway conservation in other eukaryotes. We also wanted to understand the impact that lack of GET pathway function has on plant development, considering that it started entering the textbooks as a default route for TA protein insertion.

Our results show that loss of GET pathway function in *A. thaliana* impacts on root hair length. This phenotype coincides with reduced protein levels at the plasma membrane of an important root hair-specific SNARE, conforming to the role of the GET pathway in TA protein insertion. However, similarly to yeast, no global pleiotropic phenotypes were observed, pointing to the existence of functional backup. However, ectopic overexpression of the cytosolic ATPase *At*GET3a in the putative receptor KO *Atget1* leads to severe growth defects, underscoring pathway conservation while implying an intricate role of the GET pathway in cellular homeostasis of plants.

Results

GET3 Paralogs Might Have Evolved as Early as Archaea. To identify potential orthologs of GET candidates, we used in silico sequence comparison (BLASTp and National Center for Biotechnology Information) of yeast and human GET proteins against the proteome of 16 different species from 13 phyla (Tables 1 and 2). Candidate sequences were assembled in a phylogenetic tree that, surprisingly, reveals that two distinct GET3 clades, which we

Table 1. Accession numbers of GET3/TRC40/ArsA orthologs of clade a used for the phylogenetic tree in Fig. 1 and their putative GET1/WRB and GET4/TRC40 orthologs identified via BLASTp search

	GET3/TRC40 orthologs		Up-/downstream orthologs	
Phylum and species	Accession no.	Length (aa)	GET1/WRB	GET4/TRC35
Eubacteria				
Proteobacteria				
Escherichia coli	KZO75668	583*	Not found	Not found
Proteoarchaeota				
Lokiarchaeota				
Lokiarchaeum sp.	KKK44956	338	Not found	Not found
Opisthokonta				
Chordata				
Homo sapiens	NP_004308	348	NP_004618	NP_057033
Ascomycota				
Saccharomyces cerevisiae	AAT93183	354	NP_011495	NP_014807
Amoebozoa				
Discosea				
Acanthamoeba castellanii	XP_004368068	330	XP_004353131	XP_004367722
Mycetozoa				
Dictyostelium purpureum	XP_003289495	330	Not found	XP_003283186
Archaeplastida				
Angiospermae				
Arabidopsis thaliana	NP_563640	353	NP_567498	NP_201127
Medicago truncatula	XP_013444959	358	XP_003629131	XP_003591984
Brachypodium distachyon	XP_003578462	363	XP_003564144	XP_003569076
Amborella trichopoda	XP_006857946	353	XP_006855737	ERM96291
Lycopodiophyta				
Selaginella moellendorffii	XP_002973461	360	Not found	XP_002969945 XP_002981415
Marchantiophyta				
Marchantia polymorpha	OAE26618	370	OAE20217	OAE20690
Bryophyta				
Physcomitrella patens	XP_001758936	365	XP_001760426	XP_001760372
	XP_001774198	365		XP_001758146
Chlorophyta				
Chlamydomonas reinhardtii	XP_001693332	319	XP_001695038	XP_001695333
Rhodophyta				
Galdieria sulphuraria	XP_005708637	706*	XP_005707118	XP_005704684
SAR				
Chromerida				
Vitrella brassicaformis	CEM03518	412	Not found	CEL97893
Heterokontophyta				
Nannochloropsis gaditana	EWM27451	370	EWM21897	EWM27335
Chromalveolata				
Cryptophyta				
Guillardia theta	XP_005837457	310	XP_005829401	XP_005841994

*Tandem GET3.

termed GET3a and GET3bc, respectively, exist in Archaeplastida and SAR (supergroup of stramenopiles, alveolates, and Rhizaria) but do not exist in Opisthokonts (yeast and animals) and Amoebozoa. The deep branching of the tree implies that duplication events must have occurred early in the evolution of eukaryotes (Fig. 1*A*). Interestingly, the recently identified phylum of *Lokiarchaeota*, which is thought to form a monophyletic group with eukaryotes (30), expresses two distinct GET3 orthologs, one of which aligns within the GET3bc clade while lacking some of the important sequence features of eukaryotic GET3 (Fig. S1*A*). This observation suggests that the last eukaryotic common ancestor had already acquired two copies of GET3.

In Rhodophytes and higher Angiospermae, a third GET3bc paralog branched off. Interestingly, the tandem ATPase motif—likely a consequence of gene duplication in the prokaryotic ArsA and suggested to be a key difference between ArsA and GET3/TRC40 homologs (28)—is not found in either of two *Lokiarchaeota* GET3; conversely, in Rhodophytes and SAR species, GET3 paralogs exist that contain duplications (Tables 1 and 2). Importantly, such repeats are not restricted to the GET3bc clade but also, are found among red algae GET3a orthologs (e.g., XP_005708637). Comparing sequence conservation of GET3 orthologs reveals that residues important for ATPase function are maintained in all candidates (Fig. S1 *A* and *B*). However, the sites for GET1 binding and the methionine-rich GET3 motif (31, 32) are only conserved in GET3a candidates of eukaryotes, concurring with the presence of GET1 and GET4 orthologs in most of these species (Table 1).

Strikingly, in silico analysis of the N termini of the identified GET3 orthologs predicts for almost all GET3bc—but not for GET3a candidates—the presence of a transit peptide for mitochondrial or chloroplastic import (Table 2). This observation is also in line with the fact that GET3bc proteins are, on average, larger than their GET3a paralogs (Tables 1 and 2), matching the length range of targeting sequences for the bioenergetic organelles.

Distinct Differences in Subcellular Localization of AtGET3 Paralogs. The three GET3 paralogs of *A. thaliana* were in silico-predicted to localize to the cytosol (*At*GET3a; At1g01910), chloroplast (*At*GET3b; At3g10350), and mitochondria (*At*GET3c; At5g60730), respectively (Tables 1 and 2). To corroborate these predictions, stably transformed, *A. thaliana Ubiquitin10* promoter (P_{UBQ10})-driven GFP fusions were generated (33). Confocal laser scanning microscopy (CLSM) and transmission electron microscopy (TEM)

Table 2. Accession numbers of GET3/TRC40/ArsA orthologs of clade bc used for the phylogenetic tree in Fig. 1 and their in silico prediction of an N-terminal signal/transit peptide using three different prediction tools (TargetP 1.1, ChloroP 1.1, and Predotar v1.03)

	GET3/TRC40 orthologs		Signal/transit peptide prediction		
Phylum and species	Accession no.	Length (aa)	TargetP 1.1	ChloroP 1.1	Predotar v1.03
Eubacteria					
Proteobacteria					
Escherichia coli	KZO75668	583*		Non-Eukaryote	
Proteoarchaeota					
Lokiarchaeota					
Lokiarchaeum sp.	KKK42590	329		Non-Eukaryote	
Archaeplastida					
Angiospermae					
A. thaliana	NP_187646	433	C	C	C
	NP_200881	391	M	C	M
Medicago truncatula	XP_003591867	406	C	C	Possibly C
	XP_013455984	381	C	C	C
Brachypodium distachyon	XP_003570659	403	M	C	M
	XP_010239988	371	M	—	M
Amborella trichopoda	XP_006827440	407	C	C	C
Lycopodiophyta					
Selaginella moellendorffii	XP_002974288	432	C	C	Possibly M
Marchantiophyta					
Marchantia polymorpha	OAE21403	432	C	—	C
Bryophyta					
Physcomitrella patens	XP_001781368	331	M	C	Possibly M
	XP_001764873	359		N terminus incomplete	
Chlorophyta					
Chlamydomonas reinhardtii	XP_001702275	513†	M	C	C
Rhodophyta					
Galdieria sulphuraria	XP_005705663	481	—	—	Possibly ER
	XP_005703923	757*	M	C	Possibly C
SAR					
Heterokontophyta					
Nannochloropsis gaditana	EWM30283	817*	M	—	Possibly C
Chromerida					
Vitrella brassicaformis	CEM11669	809*	M	—	Possibly ER
Chromalveolata					
Cryptophyta					
Guillardia theta	XP_005822752	418	S	C	ER

C, chloroplast; M, mitochondrion; S, signal peptide.
*Tandem GET3.
†Second P-loop motif at C terminus of protein.

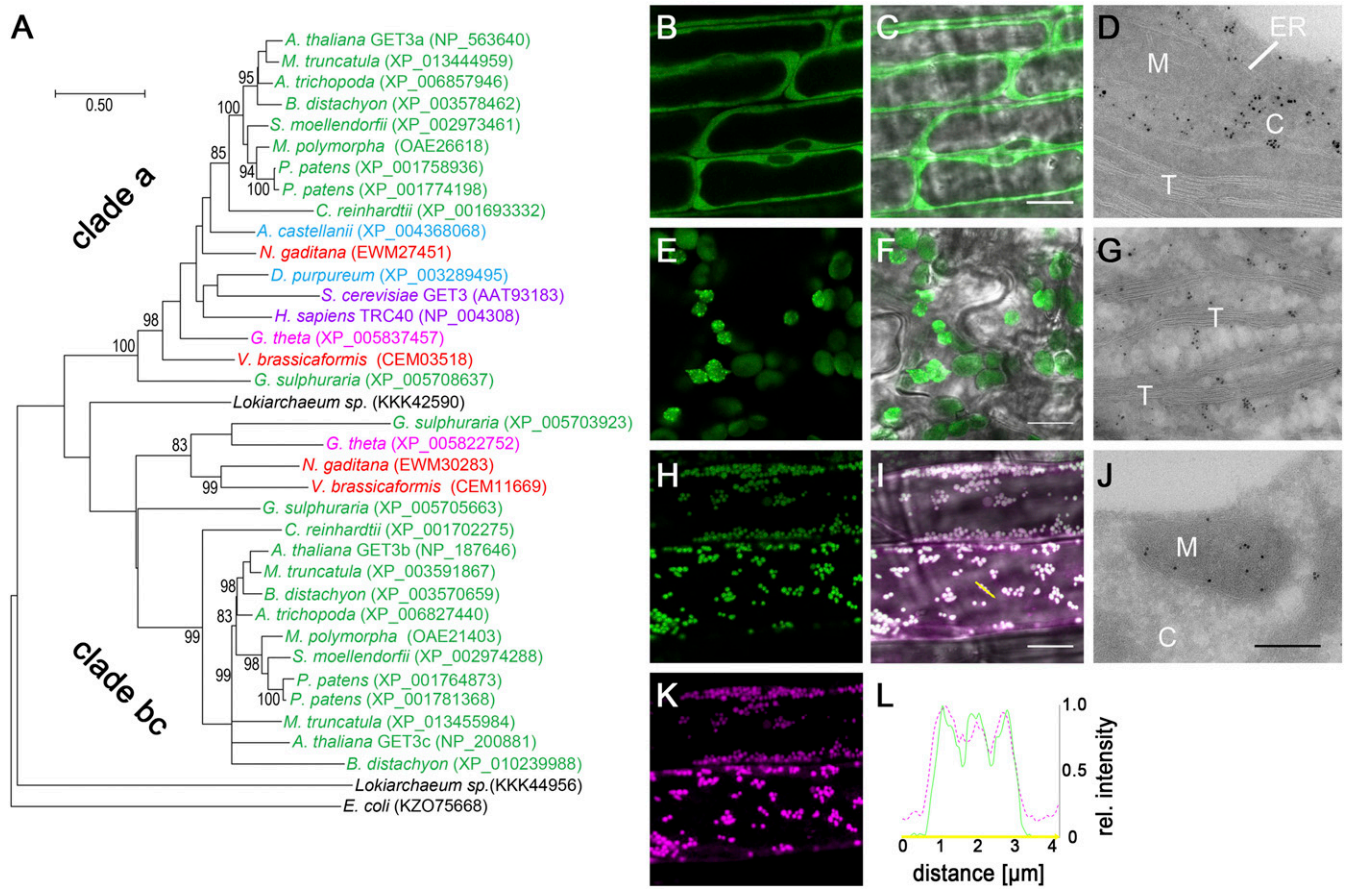

Fig. 1. Analysis of GET3 orthologs of different species. (*A*) Maximum likelihood rooted phylogenetic tree of GET3 orthologs revealing two major GET3 branches; 1,000 bootstraps were applied, and confidence ratios above 70 are included at nodes. Species color code: black, Eubacteria/Proteoarchaeota; purple, Opisthokonta; light blue, Amoebozoa; green, Archaeplastida; red, SAR; magenta, Chromalveolata. (Scale bar: changes per residue.) (*B–L*) Subcellular localization of (*B–D*) *At*GET3a, (*E–G*) *At*GET3b, and (*H–L*) *At*GET3c in stably transformed *A. thaliana* using CLSM and TEM analysis (controls in Fig. S2). (*K*) *At*GET3c-GFP–expressing specimens were treated with MitoTracker Orange to counterstain mitochondria. (*L*) Line histogram in (*I*) merged image along the yellow arrow confirms colocalization. C, cytosol; M, mitochondrion; T, thylakoid. (Scale bars: *B*, *C*, *E*, *F*, *H*, *I*, and *K*, 10 μm; *D*, *G*, and *J*, 300 nm.)

analyses reveal distinct subcellular localization patterns for three *At*GET3 paralogs (Fig. 1 *B–L* and Fig. S2): *At*GET3a is detected in the cytosol, *At*GET3b localizes to chloroplasts, and *At*GET3c localizes to mitochondria.

To resolve subplastidic localization of *At*GET3b-GFP and *At*GET3c-GFP, we used TEM analysis. Immunogold labeling indicates that *At*GET3b localizes to the stroma of chloroplasts (Fig. 1*G* and Fig. S2 *C* and *D*) and that *At*GET3c localizes to the matrix of mitochondria (Fig. 1*J* and Fig. S2 *E–G*). The mitochondrial localization of *At*GET3c had previously been reported in transiently transformed *A. thaliana* cell culture to localize to the outer mitochondrial membrane (26). By contrast, the immunogold data and high-resolution CLSM colocalization analysis of stably transformed *A. thaliana* seedlings using MitoTracker Orange consistently suggest a matrix localization for *At*GET3c (Fig. 1 *H–L*). These results are also in compliance with the presence of a transit peptide, a hallmark of organellar import (34).

Identifying the Membrane Receptor for *At*GET3a. Previous analyses have indicated that the *Sc*GET1 ortholog is missing in plants (26). Refining search parameters and using *Hs*WRB (tryptophan-rich basic protein) as template, we identified At4g16444 of *A. thaliana*. Sequence conservation of GET1 orthologs seems weaker than among GET3 candidates, but comparing TMD prediction using TMHMM (www.cbs.dtu.dk/services/TMHMM/) reveals striking structural similarity between the orthologs of different species (Fig. S1*C*). All GET1 candidates that we identified are predicted to have the typical three TMD structures of GET1/WRB with a luminal N terminus and a cytosolic C terminus as well as a cytosolic coiled coil domain between first and second TMDs (35). Additionally, publicly available microarray data confirm constitutive and well-correlated expression pattern for the putative *At*GET1 and *At*GET3a in accordance with a potential housekeeping function of the candidates (Fig. S3*D*).

To experimentally validate At4g16444 as *At*GET1, we devised localization and interaction studies. CLSM analysis of *A. thaliana* leaves that stably coexpress an ER marker protein [secreted red fluorescent protein (secRFP-HDEL)] and P_{UBQ10}-driven, C-terminally GFP-tagged *At*GET1 showed a high degree of colocalization (Fig. 2 *A–D*). Because both *Sc*GET1 and *Hs*WRB also localize to the ER membrane, this lends further support for At4g16444 being the *A. thaliana* GET1 ortholog (20, 35). Additionally, direct in planta interaction analysis using coimmunoprecipitation mass spectrometry (CoIP-MS) of *At*GET3a-GFP–expressing lines identified At4g16444 with high confidence consistently in two biological replicates among the interactors (Dataset S1).

To test interaction between *At*GET1 and all three different *At*GET3 paralogs, we used the mating-based Split-Ubiquitin System (SUS) (36). The putative *At*GET1 forms homodimers with a C-terminally tagged NubA fusion and interacts with *At*GET3a (tagged at either termini) but does not interact with the organellar localized *At*GET3b or *At*GET3c (Fig. S3*C*). Even when an N-terminal NubG tag presumably masks the transit peptides, which

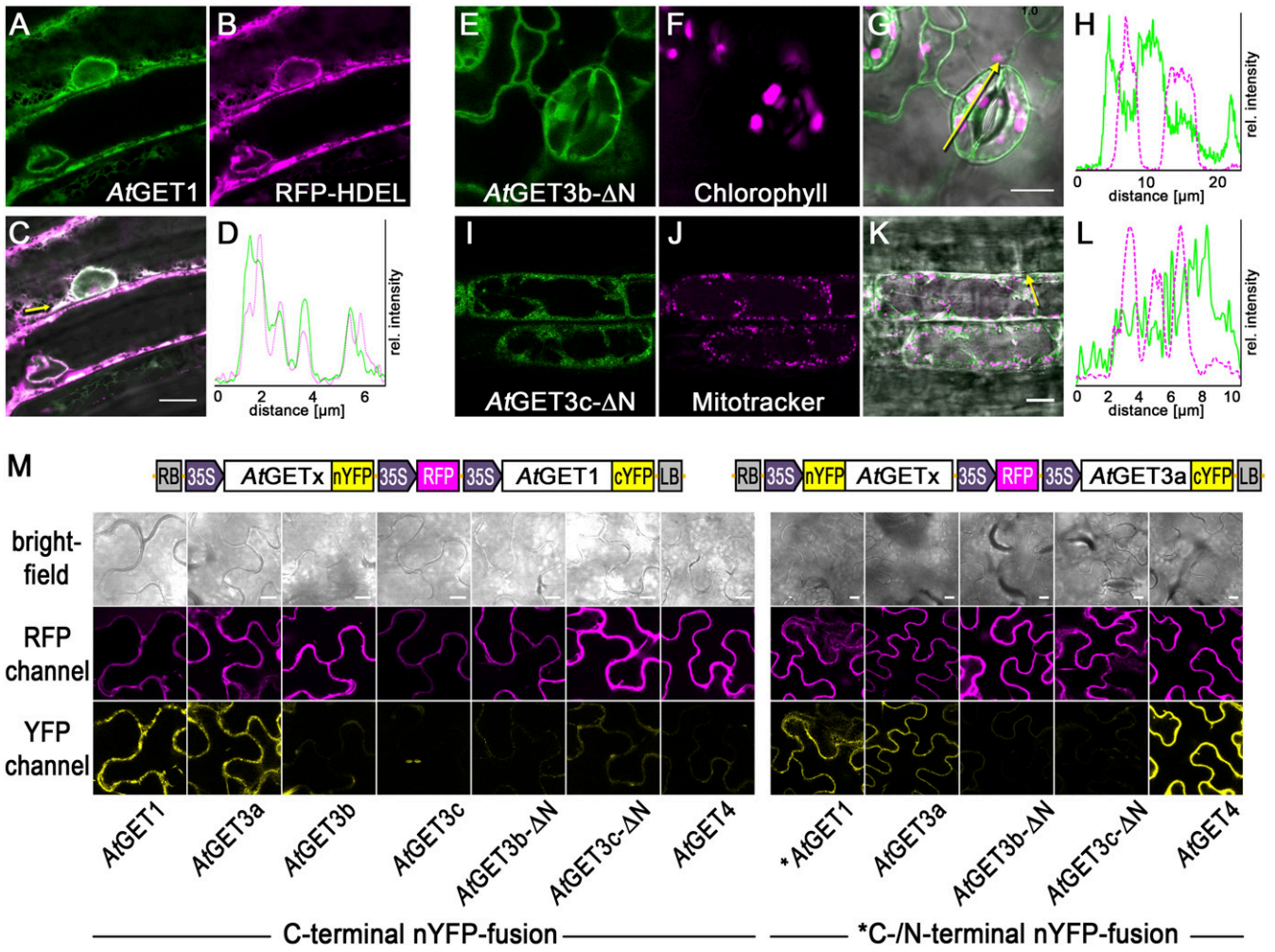

Fig. 2. Interaction analysis among *A. thaliana* GET pathway orthologs. (*A–D*) At4g16444, the putative *At*GET1, C-terminally tagged with GFP in stably transformed *A. thaliana* coexpressing the ER marker RFP-HDEL. (*D*) Line histograms along yellow arrows in *C* confirm colocalization. (*E–L*) CLSM analysis of N-terminally truncated *At*GET3b and *At*GET3c candidates. Counterimaging using autofluorescence of (*F*) chlorophyll or (*J*) MitoTracker Orange allows (*H* and *L*) line histograms in (*G* and *K*) merged images along yellow arrows that corroborate cytosolic retention. (*M*) Exemplary confocal images of rBiFC analysis of (*Left*) *At*GET1 and (*Right*) *At*GET3a with GET pathway orthologs and truncated constructs. Boxed cartoons show construct design above exemplary images of transiently transformed *Nicotiana benthamiana* leaves. A statistical analysis of the data is in Fig. S3. (Scale bars: 10 µm.)

might prevent organellar import and cause their cytosolic retention, an interaction with *At*GET1 cannot be observed.

To understand whether the physical separation of *At*GET3b/c prevents interaction with *At*GET1, we truncated the first 68 aa of *At*GET3b and 50 aa of *At*GET3c, which lead to their cytosolic localization (Fig. 2 *E–L*). We applied ratiometric bimolecular fluorescence complementation (rBiFC) (37) to assess whether such artificial mislocalization renders *At*GET3b/c susceptible to interaction with *At*GET1. Clearly, *At*GET1 homodimerizes and interacts with the cytosolic *At*GET3a but does not homodimerize or interact with the plastidic *At*GET3 paralogs or their transit peptide deletion versions (Fig. 2*M* and Fig. S3 *A* and *B*), confirming that a change in localization does not alter binding behavior. This absence of interaction seems consistent with the lack of a GET1-binding motif (32, 38) in the sequences of *At*GET3b/c, further indicating that these likely lack functional redundancy with *At*GET3a.

To test this hypothesis before phenotypic complementation, we assessed heterodimerization with *At*GET3a. Here, we also included the putative upstream binding partner of *At*GET3a, *At*GET4 (At5g63220), which we identified through in silico analysis. The expression pattern of *At*GET4 resembles that of *At*GET3a (Fig. S3*E*), and the protein localizes to the cytosol (see Fig. S7*B*). rBiFC analysis substantiates that *At*GET3a interacts with *At*GET1, itself, and *At*GET4 but fails to heterodimerize with *At*GET3b/c. Both proteins were expressed in their truncated, cytosolic form; hence, the lack of interaction cannot be attributed to compartmentalization (Fig. 2*M* and Fig. S3 *A* and *B*). Because dimerization of *Sc*GET3 is a prerequisite for function (31), this result also negates functional redundancy between GET3 paralogs.

Functional Analyses of *A. thaliana* GET Orthologs. Loss of function of TRC40, the GET3 ortholog in mammals, causes embryonic lethality befitting of the vital function of TA protein insertion (21). How would loss of GET pathway orthologs impact on survival, growth, and development in plants?

Unexpectedly, multiple different alleles of T-DNA (transfer DNA) insertion lines of each of the five *At*GET orthologs identified (Fig. S4 *A* and *B*) did not reveal any obvious growth defects. Seeds germinated, and seedlings developed indistinguishable from wild-type (WT) plants. However, a more detailed phenotypic inspection revealed that seedlings of *Atget1*, *Atget3a*, and *Atget4* lines had significantly shorter root hairs compared with Columbia-0 (Col-0) WT plants, whereas *Atget3b* and *Atget3c* did not (Fig. 3 *A* and *B* and Fig. S4*C*). Expressing genomic versions of the GET genes restores near WT-like root hair growth. By contrast, a point

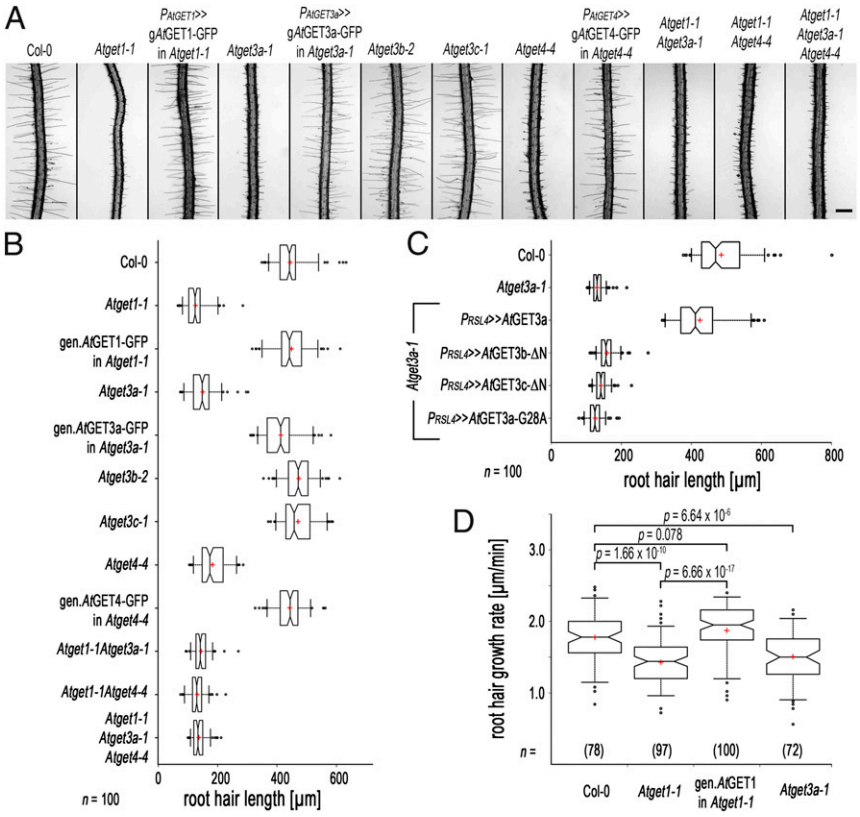

Fig. 3. Loss of function of some *A. thaliana* GET orthologs causes root hair growth defects. (*A*) Exemplary images of root elongation zones of 10-d-old T-DNA insertion lines of *A. thaliana* GET orthologs and genomic complementation. *Atget1-1*, *Atge3a-1*, and *Atget4-4* but not *Atget3b-2* and *Atget3c-1* lines show reduced growth of root hairs compared with WT Col-0 and can be complemented by their respective genomic constructs. Double or triple KOs phenocopy single T-DNA insertion lines. Transcript analysis and additional alleles can be found in Fig. S4. (*B*) Boxplot depicting length of the 10 longest root hairs of 10 individual roots ($n = 100$). Center lines of boxes represent median with outer limits at 25th and 75th percentiles. Notches indicate 95% confidence intervals; Altman whiskers extend to 5th and 95th percentiles, outliers are depicted as black dots, and red crosses mark sample means. (Scale bars: 500 µm.) (*C*) Boxplot as before, showing root hair length of Col-0 and *Atget3a-1* and complementation thereof using a root hair-specific promoter (RSL4; At1g27740) and N-terminally 3xHA-tagged coding sequences of *At*GET3a, *At*GET3b-ΔN, *At*GET3c-ΔN, and *At*GET3a-G28Ay. (*D*) Boxplot as before, showing root hair growth rates of exemplary T-DNA insertion lines and complemented *Atget1-1* line in micrometers per minute.

mutant of the P loop of the ATPase motif (*At*GET3a-G28A) expressed under a root hair-specific promoter (*RSL4*) (39) prevents rescue in *Atget3a*, suggesting that ATPase activity of *At*GET3a is essential for normal root hair growth (Fig. 3*C*). To substantiate our analysis of the *At*GET3b/c paralogs, we expressed the transit peptide deletion variants in the *Atget3a* background. The mislocalized *At*GET3b/c constructs failed to rescue the growth defects, suggesting evolution of alternative functions in the bioenergetic organelles (Fig. 3*C*).

Multiple crosses between individual T-DNA insertion lines of *At*GET1, *At*GET3a, and *At*GET4 did not yield an enhanced phenotype (i.e., further reduction of root hair length compared with their corresponding parental single-KO lines) (Fig. 3 *A* and *B*), indicating interdependent functionality of all three proteins within a joint pathway. A more detailed kinetic analysis on roots grown in RootChips (40) revealed that the shorter overall root hair length in *Atget1* and *Atget3a* correlates with slowed down growth speed (Fig. 3*D*).

Root hairs together with pollen tubes are the fastest growing cells in plants and rely on efficient delivery of membrane material to the tip (41). Although we had not observed aberrant segregation ratios of T-DNA insertion lines, which could indicate compromised fertility, we analyzed pollen tube growth in vivo and in vitro but found growth speed as well as final length unaffected in the GET pathway mutants (Fig. S4 *D* and *E*).

The genetic evidence for function of *At*GET1 and *At*GET3a in a joint pathway allowing effective root hair growth in *A. thaliana* prompted us to assess their functional conservation. In yeast, *Sc*GET1 and *Sc*GET3 are not essential; however, their absence leads to lethality under a range of different abiotic stress conditions (15). We, therefore, tested *A. thaliana* GET orthologs in BY4741 WT and corresponding KO strains for their ability to rescue yeast survival under restrictive conditions. *At*GET1 (Fig. S5*A*) and to a much lesser extent, *At*GET3a (Fig. S5*B*) hardly rescue growth in corresponding KOs, and all other *At*GET3 orthologs—full length or truncated—failed to rescue at all. This result provides strong evidence that the functions of *AtGET1* and *AtGET3a* may have diverged from yeast, more strongly so for *At*GET3a.

Loss of the GET Pathway Leads to Reduced Protein Levels of SYP123 in Root Hairs. We compared the predicted "TA-proteome" of *A. thaliana* (13) with the list of interaction partners of *At*GET3a-GFP from CoIP-MS analysis (Dataset S1). Only 23 TA proteins were detected that coprecipitated with *At*GET3a-GFP but not GFP alone (Fig. S6*B*). However, in SUS and rBiFC analysis, *At*GET3a interacts with a number of candidate TA proteins that we did not find in our CoIP-MS. Among others, the SNARE syntaxin of plants 123 (SYP123) as well as its R-SNARE partner VAMP721 and the TA protein SEC61β, subunit of the SEC61 translocon, interact with both *At*GET1 and *At*GET3a (Fig. 4*A* and Fig. S6 *A* and *C*). The SNARE SYP43 as well as the non-TA SNARE protein SNAP33 failed to interact. SYP123 is a plasma membrane-localized Qa-SNARE that specifically expresses in root hair cells, and its loss results in short root hairs (42). We crossed GFP-SYP123 under its own promoter (42) with our *Atget1-1* and *Atget3a-1* lines to analyze for misinsertion, mislocalization, or cytosolic retention.

CLSM analysis of root hairs expressing SYP123 in WT and mutant backgrounds showed normal distribution of SYP123 in bulge formation and developed root hairs (Fig. S7*A*). No cytosolic aggregates or increased fluorescence foci were visible in the cytoplasm, which was reminiscent of findings in yeast *get* pathway KOs (15, 43). However, we repeatedly observed differences in GFP signal under identical conditions and settings. GFP fluorescence intensity of root hairs is consistently stronger in the WT than in *Atget1* and *Atget3a* lines (Fig. 4*B*), suggestive of lower SYP123 protein levels in the plasma membrane of *Atget* lines.

To substantiate this finding, we performed membrane fractionation of protein extracts from roughly 250 roots per line (Fig. 4*C*). Immunoblot analysis revealed that GFP-SYP123 levels in the membrane fraction of *Atget1* and *Atget3a* lines were strikingly lower than in WT background, suggesting that loss of GET pathway functionality reduces SYP123 abundance

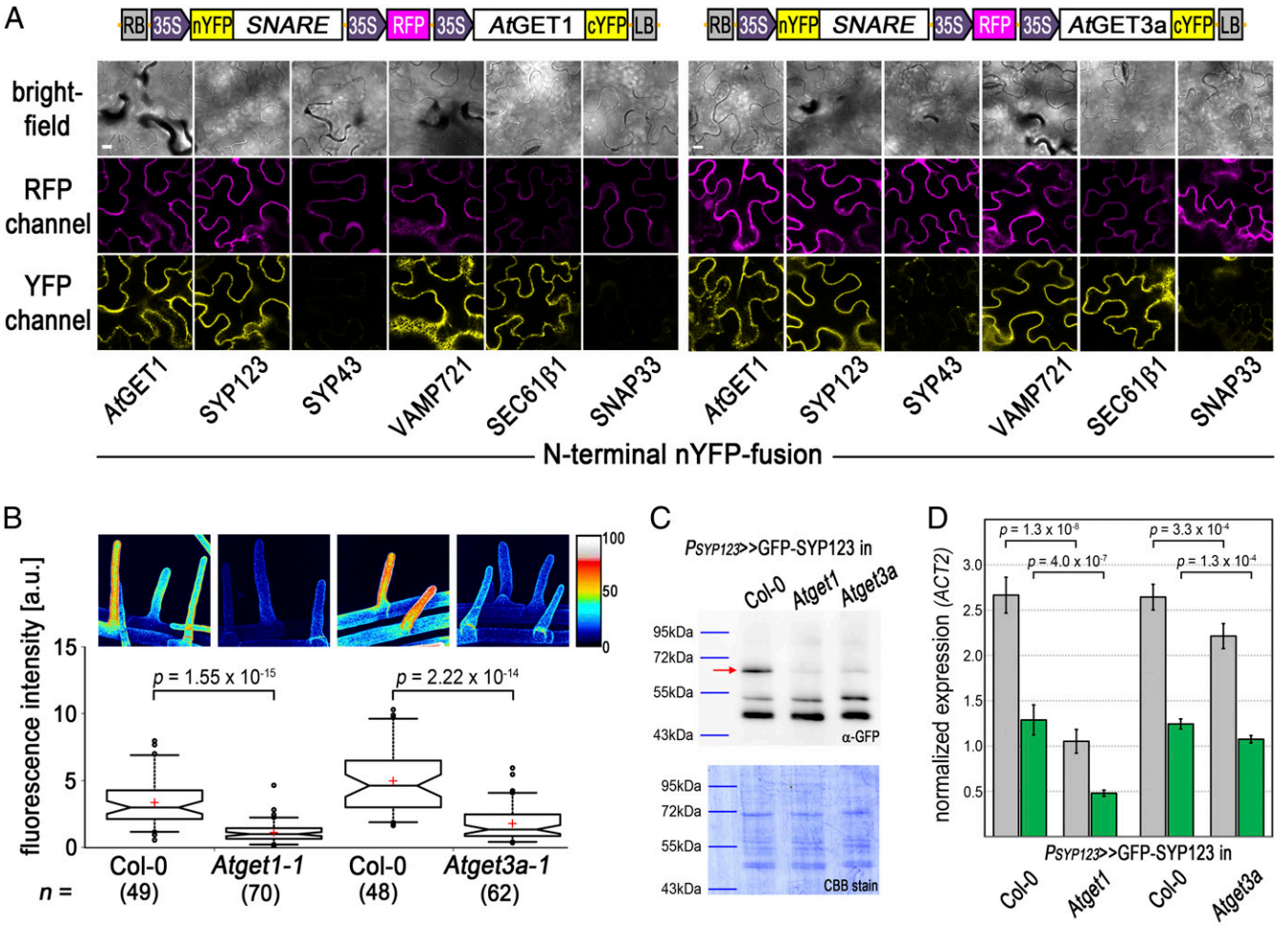

Fig. 4. The root hair-specific Qa-SNARE SYP123 shows reduced protein levels in *Atget* lines. (*A*) rBiFC analysis of (*Left*) AtGET1 and (*Right*) AtGET3a with candidate SNARE/TA proteins. Boxed cartoons show construct design above representative images of epidermal cells from transiently transformed *N. benthamiana* leaves. The statistical analysis of the data is presented in Fig. S6C. (Scale bars: 10 μm.) (*B* and *C*) Analysis of root hairs expressing P_{SYP123} >> GFP-SYP123 in *Atget1*-1, *Atget3a*-1, or corresponding Col-0 WT. (*B*) Boxplot of root hair fluorescence intensities of average-intensity *z* projections (number in parentheses below the *x* axis). Boxplot as in Fig. 3; *P* values confirm a significant difference in fluorescence intensity between GFP-SYP123 expression in WT (stronger) vs. T-DNA insertion lines (weaker). Heat maps of exemplary *z* projections are in *Upper*. (*C*) Anti-GFP immunoblots of membrane fractions from the marker lines detect a strong GFP-SYP123 band at 62.8 kDa, which is significantly and visibly weaker in *Atget3a* and *Atget1* lines than in WT Col-0. Bands below are likely the result of unspecific cross-reaction of antibody and plant extract. Coomassie brilliant blue staining (CBB stain) of blot confirms equal loading of protein. (*D*) qRT-PCR analysis of SYP123 transcript levels was performed using either SYP123- (gray) or GFP-specific (green) primers to resolve differences in mRNA levels on Col-0, *Atget1*, or *Atget3a* background. Expression levels were normalized to the Actin2 control. Error bars: SD ($n = 6$).

in the membrane. Quantitative RT-PCR (qRT-PCR) analyses further indicated that SYP123 transcript levels are also reduced in both mutants compared with the WT, with a milder transcript reduction in the *Atget3a* than in the *Atget1* background (Fig. 4*D*). Notably, the differences between endogenous and transgenic levels of transcript remain equal in all lines at roughly 50%, which confirms native expression of the marker construct (44) and suggests regulation of SYP123 in *get* lines also at transcript level.

Overexpression of *At*GET3a in *Atget1* Reveals Severe Growth Defects. The general viability of *Atget* mutants and the fact that at least part of SYP123 finds its way to the plasma membrane in root hairs of mutants question the role of the GET pathway as the sole route for TA protein insertion in *A. thaliana*. To further understand the physiological importance of the pathway in planta, we crossed the overexpressing *At*GET3a-GFP with the *Atget1-1* line. The rationale was to synthetically increase the activity of an upstream player, while limiting downstream capacity of the pathway to enhance phenotypes associated with dysfunction of the pathway. Such overexpression of the cytosolic *At*GET3a in its receptor KO leads to dwarfed plants. Main inflorescence, root, silique, and seed development are severely compromised compared with the parental lines (Fig. 5 *A–C* and Fig. S7 *C–F*). In addition to the obvious aboveground phenotype, the growth of root hairs is impaired more strongly compared with the individual loss of function *Atget1-1* lines (Fig. S7*F*). Such stronger phenotype might be a consequence of short-circuiting alternative insertion pathways, further depleting vital TA proteins from reaching their site of action.

CLSM analysis of the subcellular expression of *At*GET3-GFP in the leaf epidermis of homozygous *Atget1* lines reveals cells with increased GFP fluorescence in foci among cells that resemble the normal cytoplasmic distribution of *At*GET3a-GFP (Fig. 5*D*, *Right* and Movie S1). Conversely, no cells with GFP foci are present in leaf samples of heterozygous *Atget1*$^{(+/-)}$ lines expressing the same construct, and an even cytoplasmic distribution of *At*GET3a-GFP is observable instead (Fig. 5*D*, *Left* and Movie S2). Foci may be a result of clustering of uninserted TA proteins with multimers of *At*GET3a, similar to effects observed in yeast *Δget1* KOs (43, 45). We have also analyzed expression of

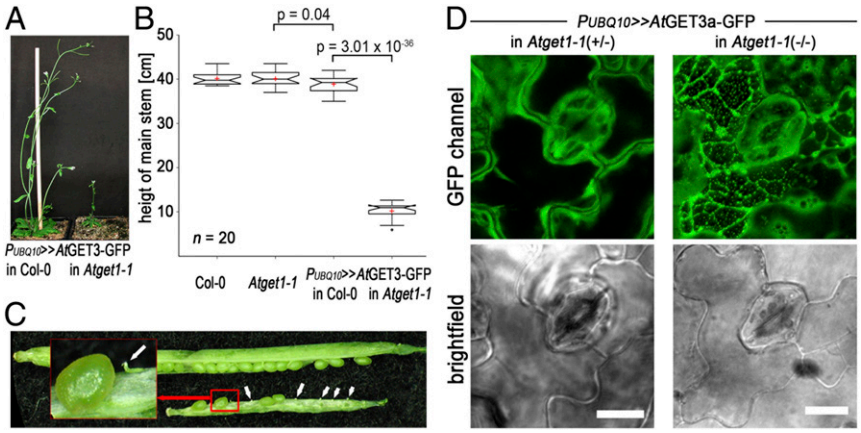

Fig. 5. Ectopic overexpression of *At*GET3a in *Atget1* causes severe growth defects. (*A*) Exemplary images of 6-wk-old *A. thaliana* plants expressing *At*GET3a-GFP in either Col-0 WT or *Atget1* showing significant differences in growth. (*B*) Boxplot summarizing the height of the main inflorescences of 20 individual 6-wk-old *A. thaliana* lines as labeled below the *x* axis. Boxplot as in Fig. 3 but with Tukey whiskers that extend to 1.5× interquartile range. (*C*) Siliques of mutant plants [*At*GET3a-GFP in *Atget1* (silique below)] show a high number of aborted embryos in contrast to single *Atget1* lines (silique above). The statistical analysis can be found in Fig. S7C. (*D*) Maximum projection *z* stacks of 20 images at 1.1-μm optical slices at 63× magnification showing subcellular localization of *At*GET3a-GFP in (*Left*) heterozygous or (*Right*) homozygous *Atget1-1* lines. Bright-field images below are taken from the 10th image in each stack. The full *z* stacks are shown in Movies S1 and S2. (Scale bars: 10 μm.)

*At*GET4-mCherry in an *Atget1-1* background but did not detect similar aggregate-like structures (Fig. S7*B*).

Discussion

Numerous biochemical and structural insights from yeast and in vitro systems have convincingly established the ability of the GET pathway to facilitate membrane insertion of TA proteins (reviewed in ref. 46). However, because TRC40 KO mice are embryonic lethal, physiological consequences of GET loss of function in an in vivo context remain insufficiently understood, and those that are available are typically specific to mammalian features. Such findings are in contrast to the high degree of conservation that GET homologs show across the eukaryotic domain, a situation where the model plant *A. thaliana* provides a highly suitable system for additional study.

Phylogenetic analysis of GET pathway components reveals an alternative GET3 clade, which must have evolved before the last eukaryotic ancestor. This hypothesis becomes apparent from the deeply branching phylogenetic tree (Fig. 1*A*) but also, by the presence of a second distinct GET3 homolog in the recently discovered *Lokiarchaeum* sp., which forms a monophyletic group with eukaryotes (30). One of the *Ls*GET3 copies aligns within the GET3bc clade, with sequences that seem to only exist in Archaeplastida and SAR, whereas Opisthokonts and Amoebozoa may have lost this paralog. GET3bc branched off once more in some red algae and higher plants to evolve another plastidic GET3 paralog. It is unlikely that this third paralog is the result of endosymbiosis, because its sequence homology is too closely related to the other organellar candidate.

Neither root hair nor general growth in *A. thaliana* seem affected by lack of *At*GET3b/c, and their biological function will require dedicated study in the future. Their localization in the plastid stroma and the mitochondrial matrix; failure to interact with *At*GET1, *At*GET3a, or *At*GET4; absence of obvious downstream candidates to facilitate membrane insertion; lack of conserved sequence motifs for TA binding (Fig. S1); and failure to complement the *At*GET3a-related growth defects (Fig. 3*C*) deem it unlikely that *At*GET3b/c function is related to TA protein insertion.

A previous structural analysis of an archaeal (*Methanocaldococcus jannaschii*) GET3 ortholog inferred some key features that would distinguish GET3 from its prokaryotic ArsA ancestor sequence (28), namely the tandem repeat (exclusive to ArsA) and a conserved CxxC motif (specific for GET3). By contrast, our phylogenetic analysis uncovered the tandem repeat in candidate sequences of both eukaryotic GET3 clades, disproving it as a decisive feature solely of ArsA. Such sequence repeats may explain the presence of a third closely related GET3 paralog in higher plants and red algae as a consequence of an earlier tandem duplication, but this hypothesis requires in-depth analysis of more sequences from different species.

The CxxC motif, which is found in both Metazoa and Fungi GET3 orthologs, also exists in the Amoebozoan and *Lokiarchaeota* GET3 orthologs and seemingly plays a role in zinc binding/coordination (19). However, this motif is absent in the Archaeplastida and SAR GET3a orthologs, where other invariant cysteines—CVC—some 40 aa upstream of the presumed CxxC motif are present. In contrast to the CxxC motif, the CVC motif can be found in all eukaryotic GET3a orthologs that we analyzed. Nevertheless, the CxxC motif is required for *Sc*GET3 to act as a general chaperone under oxidative stress conditions, binding unfolded proteins and preventing their aggregation (43, 45). Hence, it is conceivable that GET3bc paralogs—that feature CxxC (Fig. S1*B*)—have evolved as organellar chaperones with putative thiol-disulfide oxidoreductase function and lost (or never had) the TA insertion capability, whereas GET3a orthologs maintained (or acquired) both functions. Notably, the chaperone function of *Sc*GET3 is ATP-independent, whereas TA-insertase activity depends on ATP (43). A version of *At*GET3a, where the ATPase motif is mutated (G28A), fails to rescue the root hair growth phenotype (Fig. 3*C*), suggesting that it is caused by the TA insertion function of *At*GET3a, which is dependent on ATPase function (15).

Generally, T-DNA insertion in *AtGET1*, *AtGET3a*, or *AtGET4* leads to a reduction in root hair growth. Complementation with tagged or genomic constructs of the corresponding genes rescues normal growth connecting phenotype with genotype. Interestingly, multiple crosses between loss of function lines of three key players of an *A. thaliana* GET pathway do not lead to a more severe phenotype (i.e., even shorter root hairs than the single T-DNA insertion lines as measured, e.g., in plants overexpressing *At*GET3a-GFP in *Atget1*) (Fig. S7*F*). This observation indicates that the three genes act in a linear pathway in *A. thaliana*, which is in agreement with findings in other species (15, 16). Nevertheless, it seems difficult to reconcile our findings with a putative GET pathway as the sole and global route responsible for insertion of TA proteins in plants similar to its proposed role in yeast or mammals (46). Of the estimated 500 TA proteins in *A. thaliana* (13), many are vital for development and survival of the plant. Especially SNARE proteins, which facilitate vesicle fusion to drive processes, such as cytokinesis, pathogen defense, and ion homeostasis (4, 7, 47), require correct and efficient membrane insertion. Inability of the plant to insert TA proteins should yield severe growth defects at least similar to if not stronger than—for example—the *knolle* phenotype caused by an *syp111* loss of function allele (coding for the Qa-SNARE KNOLLE). *Knolle* plants fail to grow beyond early seedling stage because of incomplete cell plate formation (48).

Absence of the root hair-specific Qa-SNARE SYP123 was shown to cause defects in root hair growth (42) as a result of reduced vesicle trafficking. Although lack of *At*GET pathway components in planta did not lead to complete absence or mislocalization of SYP123 within the plasma membrane of root hairs, a significant reduction of protein levels was observed in vivo. Although this result was also confirmed biochemically, levels of SYP123 mRNA in *Atget1* as well as *Atget3a* lines are also

reduced (Fig. 4*D*), albeit not as strongly as the reduction of protein detected in the membrane fraction of mutants (Fig. 4*C*). Taken together, our findings indicate feedback control, where loss of *At*GET function and the resulting failure of SYP123 protein insertion activate inhibition at the transcript level to decrease steady-state levels of both mRNA and protein. Functional cross-talk between the GET pathway and its impact on transcript regulation had been shown previously in other eukaryotes (23, 49).

The fact that lack of GET function can phenotypically only be detected in root hairs might be associated with these requiring fast and efficient trafficking of cargo and membrane material to the tip (42). Hence, slight imbalances in protein biogenesis owing to the absence of one major insertion pathway might strain alternative but unknown insertion systems, at which point lack of the GET pathway becomes rate-limiting. This effect is not reoccurring in the other fast-growing plant cells—pollen tubes—not only suggesting presence of an alternative pathway but also, questioning the monopoly of TA protein insertion of the GET pathway. Nevertheless, our SYP123 case study supports a role of the GET pathway in planta for regulating SNARE abundance. Interaction of *At*GET1 and *At*GET3a with a wide range of different TA proteins was also shown, but we identified two TA proteins that failed to interact (SYP43 and At5g40510). Also, CoIP-MS analysis of *At*GET3a-GFP detected only about 23 TA proteins, less than 5% of all TA proteins predicted to be present in *A. thaliana* (13) (Fig. S6*B*). Although the latter might be attributed to weak or transient binding of the TMD with *At*GET3a or premature dissolution of binding through experimental conditions, it nevertheless raises questions as to the GET pathway being exclusively engaged in TA protein insertion into the ER. Among the many proteins that were detected in CoIP-MS analysis with *At*GET3a-GFP, a lot of non-TA proteins but proteins related to trafficking or proteostasis were detected (Dataset S1). If some of these interactions can be confirmed in future studies, functional analyses might uncover alternative roles for *At*GET3a.

Our findings are summarized in a working model of a presumed GET pathway in plants (Fig. 6). While under normal growth conditions, the GET pathway acts as main route for TA protein insertion into the ER membrane (Fig. 6*A*), and loss of either component or a combination thereof brings alternative pathways into play (Fig. 6*B*). The existence of alternative insertion mechanisms is indicated by not only the relatively mild phenotype but also, the limited number of TA proteins that we found to interact with *At*GET3a, raising the question of how TA proteins that do not interact with GET pathway components get inserted into membranes. In yeast, it has been shown that some TA proteins can insert unassisted and that chaperoning in the cytosol is facilitated by heatshock proteins (50); however, any alternative receptor remains elusive. Presence of an alternative insertion pathway in *A. thaliana* is also supported by the overexpression of the cytosolic *At*GET3a in its receptor KO, which has severe phenotypic consequences (Figs. 5 and 6*C*). This observation corroborates a hierarchical connection of *At*GET3a and *At*GET1, because presence of the latter can rescue the growth defects. It further suggests the existence of an alternative pathway for TA insertion with weaker affinity toward pretargeting factors, such as *At*GET4, at the ribosome, because the aberrant amounts of *At*GET3a seem to deplete the alternative pathway. Lastly, the *At*GET3a foci that can occur in cells of mutant plants (but never in the WT background) (Fig. 5*D*) and that are similar to aggregates observed in stressed yeast cells (43) suggest additional functions of *At*GET3a that nonetheless depend on *At*GET1. The aggregate-like structures were not found in all cells of mutant plants, suggesting a dosage-dependent effect (i.e., if levels of *At*GET3a-GFP exceed a certain threshold, clustering occurs). Clusters may consist of multimers of *At*GET3a, complexes of *At*GET3a bound to TA proteins, or *At*GET3a/TA proteins bound to the elusive *At*GET2 receptor. In yeast, *Sc*GET2 is the first contact point at receptor level for the *Sc*GET3-TA protein complex before the TA protein is delivered to *Sc*GET1 (20); hence, lack of *At*GET1 could keep a putative *At*GET3a/TA protein aggregate stably in the vicinity of the ER.

Future work on this mutant in particular will help to resolve functions of GET components in *A. thaliana*. A current debate about potential cross-talk between GET components in TA protein insertion and protein quality control in yeast and animal cells (51) may be further underpinned by our findings in plants, which provide the fundament to broad comparative investigations in the near future.

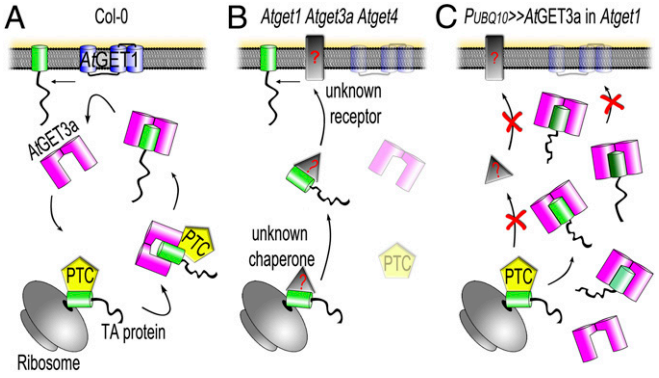

Fig. 6. Model hypothesizing the subcellular mechanism of *A. thaliana* GET orthologs. (*A*) In WT Col-0, a pretargeting complex (PTC) likely comprising *A. thaliana* SGT2 and GET5 (both of which revealed many potential orthologs through in silico analyses) as well as the in silico-identified *At*GET4, which interacts with *At*GET3a in vivo, might receive nascent TA proteins from the ribosome and deliver these to the homodimer of *At*GET3a, in turn shuttling the client TA protein to the ER receptor *At*GET1 (an *At*GET2 could not be identified through extensive BLASTp analysis and was left out of the figure). (*B*) The hypothetical situation in a single *Atget1*, *Atget3a*, or *Atget4* or crosses thereof. In the absence of a functional GET pathway, most TA proteins are delivered by an unknown alternative pathway (depicted as a gray triangle or rectangle with red question marks). (*C*) Overexpression of *At*GET3a in absence of a docking station to unload client TA proteins might lead to cytosolic aggregates and block of TA insertion. The affinity between the PTC and *At*GET3a might be a decisive factor here, because the unknown alternative pathway does not seem to compensate for the aberrant presence of *At*GET3a.

Materials and Methods

Plant Growth Conditions. Seeds were grown on 1/2 Murashige and Skoog medium including 1% sugar and 0.9% plant agar, pH 5.7. Plants were cultivated in a 16-h light/8-h dark cycle at 18 °C or 23 °C in the growth chamber (*SI Materials and Methods*).

Construct Design. Most constructs were designed by Gateway Recombination Reaction; vectors used for localization analyses can be found in ref. 33. A full list of oligonucleotides and constructs can be found in Tables S1 and S2 (*SI Materials and Methods*).

Interaction Analyses. We performed rBiFC in transiently transformed tobacco according to the work in ref. 37 (*SI Materials and Methods*).

Microscopy. CLSM microscopy was performed using a Leica SP8 at the following laser settings: GFP at 488-nm excitation (ex) and 490- to 520-nm emission (em); YFP at 514-nm ex and 520- to 560-nm em; and RFP/Mitotracker at 561-nm ex and 565- to 620-nm em. Chlorophyll autofluorescence was measured using the 488-nm laser line and em at 600–630 nm. TEM analysis and more details are in *SI Materials and Methods*.

T-DNA Lines. The following T-DNA lines were characterized (Fig. S4 *A* and *B*): Sail_1210_E07 (*Atget1-1*), GK_246D06 (*Atget1-2*), SALK_033189 (*Atget3a-1*), SALK_100424 (*Atget3a-2*), SALK_012980 (*Atget3a-3*), SALK_017702 (*Atget3b-2*), SALK_091152 (*Atget3c-1*), SALK_069782 (*Atget4-1*), and SALK_121195 (*Atget4-4*). This work suggests new names for *Arabidopsis thaliana* genes previously termed "unknown": *At*GET1 (At4g16444), *At*GET3a (At1g01910), *At*GET3b (At3g10350), *At*GET3c (At5g60730), and *At*GET4 (At5g63220).

More details and other methods are in *SI Materials and Methods*.

Note Added in Proof. During revision of this article, an analysis of conditional *wrb* KO mice demonstrated that the GET pathway is required for only a subset—but not all—TA proteins in vivo (67). Also, an alternative ER insertion pathway was described in yeast (68) and another study reported an ER-stress and early flowering phenotype of the *Atget1-1* and *Atget3a-1* lines (69).

ACKNOWLEDGMENTS. We thank Masa H. Sato for sharing the GFP-SYP123 marker line and Gabriel Schaaf for vector pDRf1-GW and yeast strains. MS analysis was done at the Proteomics Centre, University of Tübingen, and we thank Mirita Franz-Wachtel for her help in interpreting the data. We also thank Gerd Jürgens and Marja Timmermans for critical discussions and comments on the manuscript, Antje Feller and Jaquelynn Mateluna for help with the quantitative PCR analysis, and Eva Schwörzer and Laure Grefen for technical support. This work was supported by an Emmy Noether Fellowship SCHW 1719/1-1 from the Deutsche Forschungsgemeinschaft (DFG; to M.S.), CellNetworks Research Group funds (to G.G.), seed funding through the Collaborative Research Council 1101 (SFB1101; to C.G.), and an Emmy Noether Fellowship GR 4251/1-1 from the DFG (to C.G.).

1. Lipka V, Kwon C, Panstruga R (2007) SNARE-ware: The role of SNARE-domain proteins in plant biology. *Annu Rev Cell Dev Biol* 23:147–174.
2. Grefen C, Blatt MR (2008) SNAREs–molecular governors in signalling and development. *Curr Opin Plant Biol* 11(6):600–609.
3. Rizo J, Südhof TC (2012) The membrane fusion enigma: SNAREs, Sec1/Munc18 proteins, and their accomplices–guilty as charged? *Annu Rev Cell Dev Biol* 28:279–308.
4. Jürgens G, et al. (2015) Plant cytokinesis: A tale of membrane traffic and fusion. *Biochem Soc Trans* 43(1):73–78.
5. Surpin M, et al. (2003) The VTI family of SNARE proteins is necessary for plant viability and mediates different protein transport pathways. *Plant Cell* 15(12):2885–2899.
6. Hachez C, et al. (2014) Arabidopsis SNAREs SYP61 and SYP121 coordinate the trafficking of plasma membrane aquaporin PIP2;7 to modulate the cell membrane water permeability. *Plant Cell* 26(7):3132–3147.
7. Grefen C, et al. (2015) A vesicle-trafficking protein commandeers Kv channel voltage sensors for voltage-dependent secretion. *Nat Plants* 1:15108.
8. Zhang B, et al. (2015) The Arabidopsis R-SNARE VAMP721 interacts with KAT1 and KC1 K+ channels to moderate K+ current at the plasma membrane. *Plant Cell* 27(6):1697–1717.
9. Borgese N, Colombo S, Pedrazzini E (2003) The tale of tail-anchored proteins: Coming from the cytosol and looking for a membrane. *J Cell Biol* 161(6):1013–1019.
10. Borgese N, Fasana E (2011) Targeting pathways of C-tail-anchored proteins. *Biochim Biophys Acta* 1808(3):937–946.
11. Beilharz T, Egan B, Silver PA, Hofmann K, Lithgow T (2003) Bipartite signals mediate subcellular targeting of tail-anchored membrane proteins in Saccharomyces cerevisiae. *J Biol Chem* 278(10):8219–8223.
12. Kalbfleisch T, Cambon A, Wattenberg BW (2007) A bioinformatics approach to identifying tail-anchored proteins in the human genome. *Traffic* 8(12):1687–1694.
13. Kriechbaumer V, et al. (2009) Subcellular distribution of tail-anchored proteins in Arabidopsis. *Traffic* 10(12):1753–1764.
14. Hegde RS, Keenan RJ (2011) Tail-anchored membrane protein insertion into the endoplasmic reticulum. *Nat Rev Mol Cell Biol* 12(12):787–798.
15. Schuldiner M, et al. (2008) The GET complex mediates insertion of tail-anchored proteins into the ER membrane. *Cell* 134(4):634–645.
16. Stefanovic S, Hegde RS (2007) Identification of a targeting factor for posttranslational membrane protein insertion into the ER. *Cell* 128(6):1147–1159.
17. Chang YW, et al. (2010) Crystal structure of Get4-Get5 complex and its interactions with Sgt2, Get3, and Ydj1. *J Biol Chem* 285(13):9962–9970.
18. Simpson PJ, Schwappach B, Dohlman HG, Isaacson RL (2010) Structures of Get3, Get4, and Get5 provide new models for TA membrane protein targeting. *Structure* 18(8):897–902.
19. Metz J, Wächter A, Schmidt B, Bujnicki JM, Schwappach B (2006) The yeast Arr4p ATPase binds the chloride transporter Gef1p when copper is available in the cytosol. *J Biol Chem* 281(1):410–417.
20. Wang F, Chan C, Weir NR, Denic V (2014) The Get1/2 transmembrane complex is an endoplasmic-reticulum membrane protein insertase. *Nature* 512(7515):441–444.
21. Mukhopadhyay R, Ho YS, Swiatek PJ, Rosen BP, Bhattacharjee H (2006) Targeted disruption of the mouse Asna1 gene results in embryonic lethality. *FEBS Lett* 580(16):3889–3894.
22. Daniele LL, Emran F, Lobo GP, Gaivin RJ, Perkins BD (2016) Mutation of wrb, a component of the guided entry of tail-anchored protein pathway, disrupts photoreceptor synapse structure and function. *Invest Ophthalmol Vis Sci* 57(7):2942–2954.
23. Norlin S, Parekh VS, Naredi P, Edlund H (2016) Asna1/TRC40 controls β-cell function and endoplasmic reticulum homeostasis by ensuring retrograde transport. *Diabetes* 65(1):110–119.
24. Vogl C, et al. (2016) Tryptophan-rich basic protein (WRB) mediates insertion of the tail-anchored protein otoferlin and is required for hair cell exocytosis and hearing. *EMBO J* 35(23):2536–2552.
25. Abell BM, Mullen RT (2011) Tail-anchored membrane proteins: Exploring the complex diversity of tail-anchored-protein targeting in plant cells. *Plant Cell Rep* 30(2):137–151.
26. Duncan O, van der Merwe MJ, Daley DO, Whelan J (2013) The outer mitochondrial membrane in higher plants. *Trends Plant Sci* 18(4):207–217.
27. Zhou T, Radaev S, Rosen BP, Gatti DL (2000) Structure of the ArsA ATPase: The catalytic subunit of a heavy metal resistance pump. *EMBO J* 19(17):4838–4845.
28. Suloway CJ, Rome ME, Clemons WM, Jr (2012) Tail-anchor targeting by a Get3 tetramer: The structure of an archaeal homologue. *EMBO J* 31(3):707–719.
29. Adl SM, et al. (2012) The revised classification of eukaryotes. *J Eukaryot Microbiol* 59(5):429–493.
30. Spang A, et al. (2015) Complex archaea that bridge the gap between prokaryotes and eukaryotes. *Nature* 521(7551):173–179.
31. Mateja A, et al. (2009) The structural basis of tail-anchored membrane protein recognition by Get3. *Nature* 461(7262):361–366.
32. Stefer S, et al. (2011) Structural basis for tail-anchored membrane protein biogenesis by the Get3-receptor complex. *Science* 333(6043):758–762.
33. Grefen C, et al. (2010) A ubiquitin-10 promoter-based vector set for fluorescent protein tagging facilitates temporal stability and native protein distribution in transient and stable expression studies. *Plant J* 64(2):355–365.
34. Garg SG, Gould SB (2016) The role of charge in protein targeting evolution. *Trends Cell Biol* 26(12):894–905.
35. Vilardi F, Lorenz H, Dobberstein B (2011) WRB is the receptor for TRC40/Asna1-mediated insertion of tail-anchored proteins into the ER membrane. *J Cell Sci* 124(Pt 8):1301–1307.
36. Grefen C, Obrdlik P, Harter K (2009) The determination of protein-protein interactions by the mating-based split-ubiquitin system (mbSUS). *Methods Mol Biol* 479:217–233.
37. Grefen C, Blatt MR (2012) A 2in1 cloning system enables ratiometric bimolecular fluorescence complementation (rBiFC). *Biotechniques* 53(5):311–314.
38. Mariappan M, et al. (2011) The mechanism of membrane-associated steps in tail-anchored protein insertion. *Nature* 477(7362):61–66.
39. Datta S, Prescott H, Dolan L (2015) Intensity of a pulse of RSL4 transcription factor synthesis determines Arabidopsis root hair cell size. *Nat Plants* 1:15138.
40. Grossmann G, et al. (2011) The RootChip: An integrated microfluidic chip for plant science. *Plant Cell* 23(12):4234–4240.
41. Grierson C, Nielsen E, Ketelaarc T, Schiefelbein J (2014) Root hairs. *Arabidopsis Book* 12:e0172.
42. Ichikawa M, et al. (2014) Syntaxin of plant proteins SYP123 and SYP132 mediate root hair tip growth in Arabidopsis thaliana. *Plant Cell Physiol* 55(4):790–800.
43. Voth W, et al. (2014) The protein targeting factor Get3 functions as ATP-independent chaperone under oxidative stress conditions. *Mol Cell* 56(1):116–127.
44. Enami K, et al. (2009) Differential expression control and polarized distribution of plasma membrane-resident SYP1 SNAREs in Arabidopsis thaliana. *Plant Cell Physiol* 50(2):280–289.
45. Powis K, et al. (2013) Get3 is a holdase chaperone and moves to deposition sites for aggregated proteins when membrane targeting is blocked. *J Cell Sci* 126(Pt 2):473–483.
46. Denic V, Dötsch V, Sinning I (2013) Endoplasmic reticulum targeting and insertion of tail-anchored membrane proteins by the GET pathway. *Cold Spring Harb Perspect Biol* 5(8):a013334.
47. Kwon C, et al. (2008) Co-option of a default secretory pathway for plant immune responses. *Nature* 451(7180):835–840.
48. Lukowitz W, Mayer U, Jürgens G (1996) Cytokinesis in the Arabidopsis embryo involves the syntaxin-related KNOLLE gene product. *Cell* 84(1):61–71.
49. Jonikas MC, et al. (2009) Comprehensive characterization of genes required for protein folding in the endoplasmic reticulum. *Science* 323(5922):1693–1697.
50. Johnson N, Powis K, High S (2013) Post-translational translocation into the endoplasmic reticulum. *Biochim Biophys Acta* 1833(11):2403–2409.
51. Casson J, McKenna M, High S (2016) On the road to nowhere: Cross-talk between post-translational protein targeting and cytosolic quality control. *Biochem Soc Trans* 44(3):796–801.
52. Kumar S, Stecher G, Tamura K (2016) MEGA7: Molecular Evolutionary Genetics Analysis Version 7.0 for Bigger Datasets. *Mol Biol Evol* 33(7):1870–1874.
53. Karnik A, Karnik R, Grefen C (2013) SDM-Assist software to design site-directed mutagenesis primers introducing "silent" restriction sites. *BMC Bioinformatics* 14:105.
54. Xing S, Wallmeroth N, Berendzen KW, Grefen C (2016) Techniques for the analysis of protein-protein interactions in vivo. *Plant Physiol* 171(2):727–758.
55. Grefen C (2014) The split-ubiquitin system for the analysis of three-component interactions. *Methods Mol Biol* 1062:659–678.
56. Hecker A, et al. (2015) Binary 2in1 vectors improve in planta (co)localization and dynamic protein interaction studies. *Plant Physiol* 168(3):776–787.
57. Spitzer M, Wildenhain J, Rappsilber J, Tyers M (2014) BoxPlotR: A web tool for generation of box plots. *Nat Methods* 11(2):121–122.
58. Grossmann G, et al. (2012) Time-lapse fluorescence imaging of Arabidopsis root growth with rapid manipulation of the root environment using the RootChip. *J Vis Exp* 65:pii:4290.
59. Schindelin J, et al. (2012) Fiji: An open-source platform for biological-image analysis. *Nat Methods* 9(7):676–682.
60. Jiang L, et al. (2005) VANGUARD1 encodes a pectin methylesterase that enhances pollen tube growth in the Arabidopsis style and transmitting tract. *Plant Cell* 17(2):584–596.
61. Boavida LC, McCormick S (2007) Temperature as a determinant factor for increased and reproducible in vitro pollen germination in Arabidopsis thaliana. *Plant J* 52(3):570–582.
62. Roppolo D, et al. (2011) A novel protein family mediates Casparian strip formation in the endodermis. *Nature* 473(7347):380–383.
63. Tokuyasu KT (1989) Use of poly(vinylpyrrolidone) and poly(vinyl alcohol) for cryoultramicrotomy. *Histochem J* 21(3):163–171.
64. Park M, Touihri S, Müller I, Mayer U, Jürgens G (2012) Sec1/Munc18 protein stabilizes fusion-competent syntaxin for membrane fusion in Arabidopsis cytokinesis. *Dev Cell* 22(5):989–1000.
65. Husbands AY, Benkovics AH, Nogueira FT, Lodha M, Timmermans MC (2015) The ASYMMETRIC LEAVES complex employs multiple modes of regulation to affect adaxial-abaxial patterning and leaf complexity. *Plant Cell* 27(12):3321–3335.
66. Loqué D, Lalonde S, Looger LL, von Wirén N, Frommer WB (2007) A cytosolic trans-activation domain essential for ammonium uptake. *Nature* 446(7132):195–198.
67. Rivera-Monroy J, et al. (2016) Mice lacking WRB reveal differential biogenesis requirements of tail-anchored proteins in vivo. *Sci Rep* 6:39464.
68. Aviram N, et al. (2016) The SND proteins constitute an alternative targeting route to the endoplasmic reticulum. *Nature* 540(7631):134–138.
69. Srivistava R, Zalisko BE, Keenan RJ, Howell SH (December 6, 2016) The GET system inserts the tail-anchored SYP72 protein into endoplasmic reticulum membranes. *Plant Physiol*, 10.1104/pp.16.00928.

Supporting Information

Xing et al. 10.1073/pnas.1619525114

SI Materials and Methods

In Silico and Phylogenetic Analysis. GET pathway orthologs were identified through BLASTp search (National Center for Biotechnology Information) against proteomes of candidate species and using default settings. Multiple sequence alignments were computed using the MUSCLE algorithm with default settings of MEGA7 (52). Evolutionary history was inferred by using the maximum likelihood method based on the Whelan and Goldman + frequency mode, applying 1,000 bootstraps to validate branching. The tree with the highest log likelihood (−12,793.272) is shown. Percentages of trees above 70 in which the associated taxa clustered together are shown next to the branches. Initial trees for the heuristic search were obtained automatically by applying Neighbor-Join and BioNJ algorithms to a matrix of pairwise distances estimated using a JTT model and then, selecting the topology with superior log-likelihood value. A discrete Gamma distribution was used to model evolutionary rate differences among sites [five categories (+G; parameter = 1.377)]. The rate variation model allowed for some sites to be evolutionarily invariable ([+I]; 4.147% sites). The tree is drawn to scale, with branch lengths measured in the number of substitutions per site. The analysis involved 37 amino acid sequences. All positions with less than 95% site coverage were eliminated. That is, fewer than 5% alignment gaps, missing data, and ambiguous bases were allowed at any position. There were a total of 279 positions in the final dataset.

Construct Generation and Plant Transformation. All P_{UBQ10} promoter-driven constructs were generated using Gateway technology as described previously (33). Full-length coding sequences of each gene were PCR-amplified; inserted into pDONR207, pDONR221-P1P4, or pDONR221-P3P2 via BP (ThermoFisher) reaction; and confirmed by sequencing (37). A point mutation of *At*GET3a (G28A) was introduced through site-directed mutagenesis as described by ref. 53. Generation of $P_{AtGET3a}$ >> *At*GET3a-GFP-3xHA, P_{AtGET1} >> *At*GET1-GFP-3xHA, and P_{AtGET4} >> *At*GET4-GFP-3xHA was done by conventional cloning from genomic DNA. The genomic fragment from start to stop codon was amplified and inserted into the binary vector P_{UBQ10} >> GFP-3xHA 5′ of GFP. The 3′ UTR of the respective gene was amplified as well and inserted 3′ of the 3xHA tag. After verification through sequencing, the promoter region of the gene was amplified and inserted to replace the *UBQ10* promoter. These constructs were first transformed into *Agrobacterium tumefaciens* GV3101 and then, dipped with WT (Col-0) plants. Oligonucleotides are listed in Table S1, and all constructs used are in Table S2.

Interaction Assays. The mating-based SUS was applied for the detection of protein–protein interactions in yeast (36). Application of methionine decreases Cub/bait-fusion expression. The lower affinity of C-terminal NubA compared with N-terminal NubG fusions was compensated for through the use of low-methionine levels (54). All interaction assays were performed as described previously (55).

The rBiFC (37) was applied to test in planta protein–protein interaction as described previously (56). All boxplots were generated using BoxPlotR (57).

Plant Growth Conditions. All mutant (Fig. S4 *A* and *B*) and transgenic lines are in Columbia (Col-0) background and were obtained from the Nottingham *Arabidopsis* Stock Centre (arabidopsis.info/). Seeds were imbibed on wet paper and stratified for 2–4 d in the dark at 4 °C before sowing on soil or surface-sterilized with chlorine gas and plated on 1/2-strength solid Murashige and Skoog medium including 1% sugar and 0.9% plant agar, pH 5.7. Plants were cultivated in a 16-h light/8-h dark cycle at 18 °C or 23 °C in the growth chamber.

Analysis of Root Hair Growth Kinetics. Root hair growth kinetics and in part, SYP123 localization were determined on roots grown in RootChips, polydimethylsiloxane-based microfluidic perfusion devices for *Arabidopsis thaliana* root imaging (40). Plant cultivation on RootChips was performed as described elsewhere (58).

Image analysis of root hair growth rate was performed on bright-field time stacks in FIJI (59) as follows; time stacks of *n* time points were duplicated and truncated by three time points at the beginning and the end. The absolute difference between the two stacks was calculated using the FIJI image calculator tool. The resulting stack now highlighted the tip of every growing root hair as particle-like signal. The velocity of this tip representation was subsequently analyzed using the FIJI TrackMate plugin.

Root Hair, Pollen Tube Growth, and CLSM Analysis. The roots from 10-d-old seedlings grown on 1/2 Murashige and Skoog medium plates were imaged under a light microscope (ZEISS; Axiophot) using 2.5× objective. Root hair length was measured using ImageJ. The 10 longest root hairs from 10 individual roots were examined per WT, T-DNA insertion, or complemented line.

Pollination experiments and aniline blue staining for pollen tube growth in pistils were performed as previously described (60). In vitro pollen germination was performed as reported previously (61). Pollen tubes were imaged 7 h after pollen germination on solid medium, and pollen tube length was quantified using ImageJ.

For subcellular localization of the *At*GETx-GFP fusions and GFP-SYP123 in root hairs, roots of 7-d-old seedlings grown on plates or leaves from 2-wk-old plants grown in soil were observed. CLSM images were taken using a Leica SP8 CLSM. To exclude quantitative effects of the genetic background in our GFP fluorescence intensity analysis (Fig. 4*B*), we analyzed descendants of individual heterozygous lines. Macroscopic detection of the root hair phenotype allowed identification of homozygous *get* mutants, which were analyzed for mean fluorescence in root hairs as well as a similar number of randomly picked segregated lines. From at least 15 analyzed roots per line, the 5 with the strongest GFP signals were chosen for fluorescence intensity analysis. Laser settings used are given. GFP signals were measured at 488-nm ex and 490- to 520-nm em, YFP signals were measured at 514-nm ex and 520- to 560-nm em, and RFP/Mitotracker signals were measured at 561-nm ex and 565- to 620-nm em. Chlorophyll autofluorescence was measured using the 488-nm laser line and em at 600–630 nm.

Immuno-TEM. Immunogold labeling of ultrathin thawed cryosections was performed as described previously (62). Cotyledons were fixed with 4% (vol/vol) formaldehyde followed by 8% (vol/vol) formaldehyde for 30 and 120 min, respectively. Fixed cotyledons were infiltrated with a mixture of 20% (wt/vol) polyvinylpyrrolidone and 1.8 M sucrose (63) and frozen in liquid nitrogen. Ultrathin cryosections (80–100 nm) were cut with a cryoultramicrotome (UC7/FC7; Leica) at −110 °C. Thawed cryosections mounted on TEM grids were blocked with 0.2% milk powder/0.2% BSA in PBS and incubated with rabbit anti-GFP serum (1:200) for 60 min followed by several washing

steps using blocking buffer. Thereafter, sections were incubated with goat anti-rabbit coupled to ultrasmall gold (Fig. 1 *D* and *G*) (1:50; Aurion) or coupled to 6-nm gold (Fig. 1*J*) (1:30; Dianova) for 60 min. Gold particles were silver-enhanced using R-Gent (Aurion) for 45 and 35 min. Labeled cryosections were stained with 1% aqueous uranyl acetate and embedded in methyl cellulose containing 0.45% uranyl acetate. Sections were viewed in a JEM-1400plus TEM (Jeol) at 120 kV accelerating voltage, and micrographs were recorded with a TemCam-F416 CMOS Camera (Tietz).

CoIP-MS Analysis. Protein extracts of P_{UBQ10} >> AtGET3a-GFP and as control, P_{UBQ10} >> GFP seedlings grown under continuous light were harvested after 5 d. Three grams plant tissue was taken for the immunoprecipitation according to the work in ref. 64 with slight modifications. Only the second washing buffer (50 mM Tris·HCl, pH 7.5, 150 mM NaCl, 0.1% Triton X-100) was used, but it was used four times; 60-μL GFP-Trap Beads (ChromoTek) were added to each sample. The final precipitate in 2× Laemmli buffer was analyzed by MS at the University of Tübingen Proteome Center. Two individual biological replicates were performed, and candidates that interacted with GFP only were omitted from the final list of interaction partners (Dataset S1).

Membrane Fractionation. Root samples (0.2–1 g) of 3-wk-old seedlings grown on 1/2 Murashige and Skoog plates (+1% sucrose + 25 μg/ml Hygromycin) were harvested and ground on ice. Samples were treated in a ratio of 1:2 with extraction buffer [1 M Tris·HCl, pH 7.5, 1 M $MgCl_2$, 1 M DTT, 1/2 tablet protease inhibitor (cOmplete, EDTA-free; ROCHE), 0.5 M sucrose] and homogenized. Separation of membrane and cytosol was achieved through sequential centrifugation: 10 min at 10,000 × *g* and 4 °C to purify samples from cell debris followed by 1 h at 100,000 × *g* and 4 °C. Membrane pellets were resuspended in 50 μL fresh extraction buffer and sonicated for 5 s at 60% power, and protein concentration was measured using Bradford reagent prior immunoblotting. Protein samples were adjusted to equal concentration using Laemmli buffer [+3.5% (vol/vol) β-Mercaptoethanol] and boiled for 20 min at 65 °C.

qRT-PCR Analysis. Total RNAs were isolated from 100 mg 5-d-old seedlings grown on 1/2 Murashige and Skoog medium by using the Isolate II RNA Plant Kit (Bioline). For cDNA synthesis, ProtoScript II–First Strand cDNA Synthesis Kit (NEB; 1 μg RNA) was used. qRT-PCR was performed using oligonucleotides (Table S1) specific to SYP123, GFP, and ACT2 as internal control. iQ SYBR Green Supermix (Bio-Rad) was used and performed on the CFX96 Real-Time PCR System (Bio-Rad). Relative quantification values were calculated using the $2^{-\Delta Ct}$ method, with the ΔCt of ACT2 as normalization control (65).

Yeast Complementation Analysis. *A. thaliana* genes for the yeast complementation analysis were expressed from a 2μ origin plasmid (pYOX1-Dest) under the strong constitutive yeast PMA1 promoter, which was based on the Gateway-compatible pDRf1-GW vector (66). *Get1p* and *get3p* KO and corresponding BY4741 WT strains were originally created by the *Saccharomyces* Genome Deletion Project, Stanford. Yeast was grown and transformed as described for the SUS analysis but using Uracil as selection marker. Yeast was dropped in 10 times OD dilutions on selection media and grown under different temperatures for 3 d.

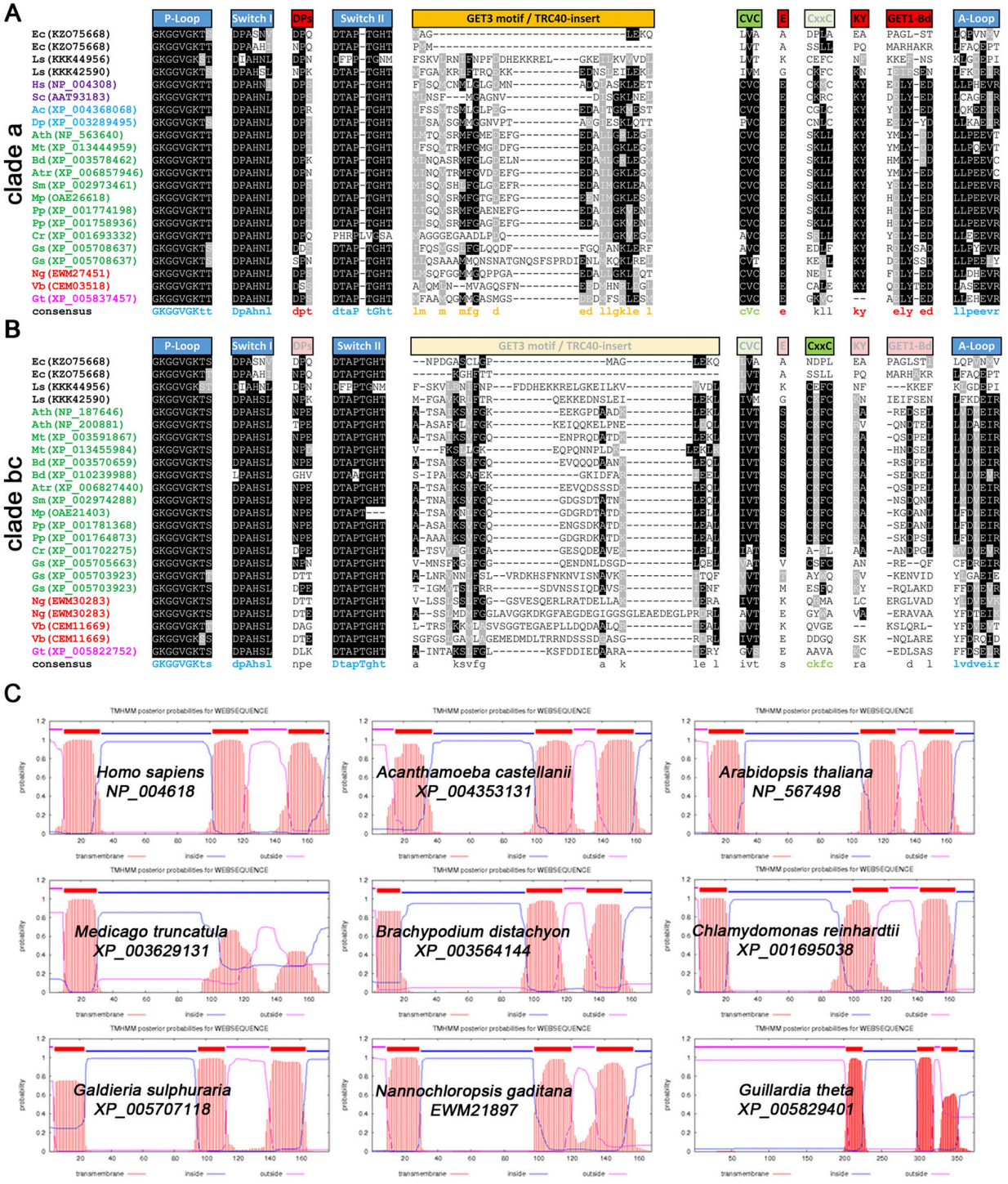

Fig. S1. Sequence and structural evaluation of GET orthologs. Excerpts of multiple sequence alignments of (*A*) clade a and (*B*) clade bc GET3 orthologs showing conserved motives. ATPase motifs are in blue (P loop and Switches I and II), and GET1 binding motifs are in red (conserved only in clade a). Cysteine residues (CVC and CxxC motives) important for metal binding/dimerization are in light green. Absence or partial conservation of motives is depicted through opaqueness of boxes above the sequences. Tandem sequences were split and treated as two individual GET3 orthologs for accessions: KZO75668, XP_005708637, XP_005703923, EWM30283, and CEM11669. Ac, *Acanthamoeba castellanii*; Ath, *A. thaliana*; Atr, *Amborella trichopoda*; Bd, *Brachypodium distachyon*; Cr, *Chlamydomonas reinhardtii*; Dp, *Dictyostelium purpureum*; Ec, *Escherichia coli*; Gs, *Galdieria sulphuraria*; Gt, *Guillardia theta*; Hs, *Homo sapiens*; Ls, *Lokiarchaeum* sp.; Mp, *Marchantia polymorpha*; Mt, *Medicago truncatula*; Ng, *Nannochloropsis gaditana*; Pp, *Physcomitrella patens*; Sc, *Saccharomyces cerevisiae*; Sm, *Selaginella moellendorffii*; Vb, *Vitrella brassicaformis*. (*C*) Exemplary TMD prediction of membrane domains of ScGET1, HsWRB, and putative orthologs in different eukaryotic species (www.cbs.dtu.dk/services/TMHMM/).

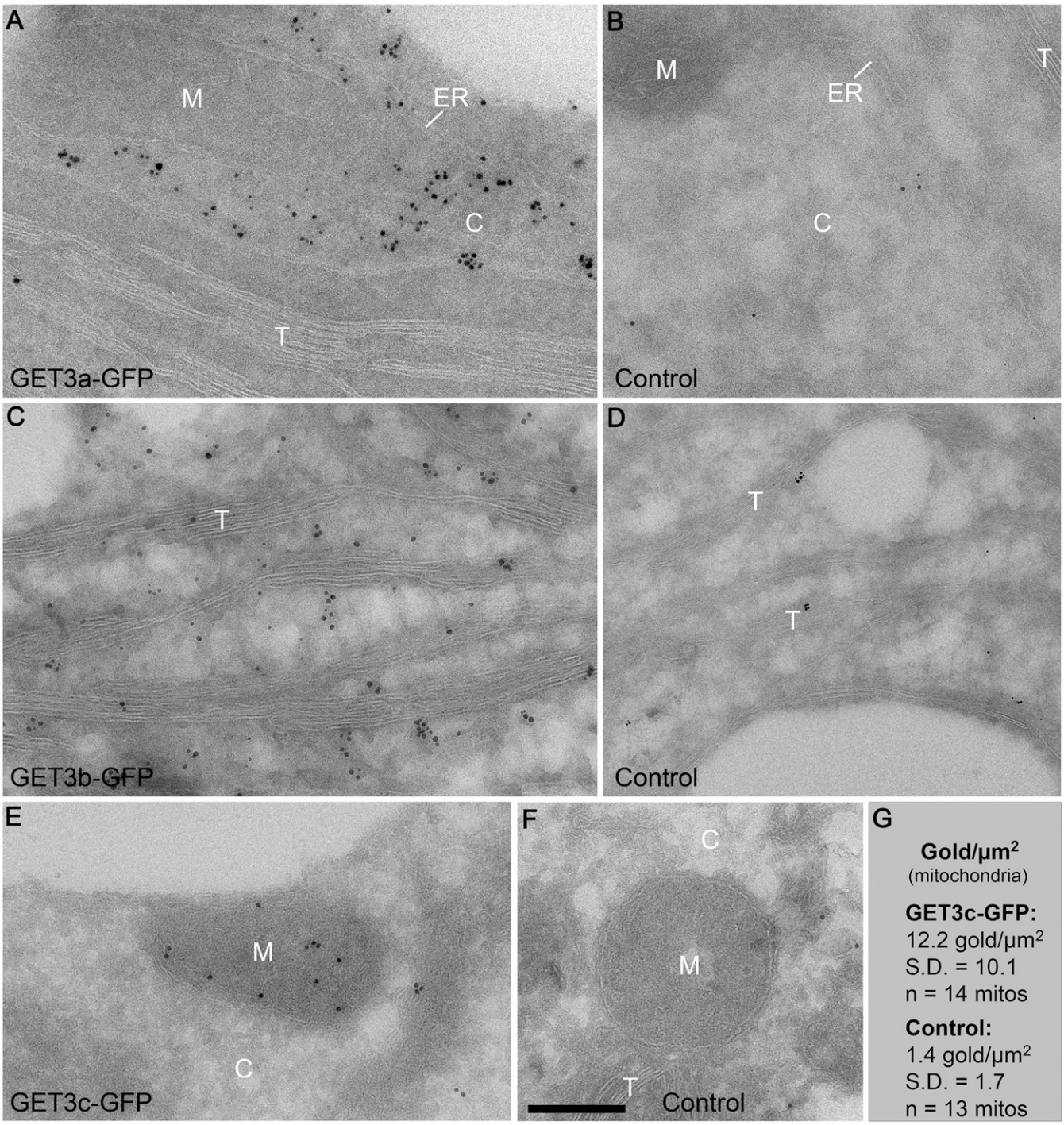

Fig. S2. Expanded view of localization analysis of AtGET orthologs (original TEM images shown in Fig. 1 *D*, *G*, and *J*). High-resolution images and controls of TEM analysis shown in parts in Fig. 1 *D*, *G*, and *J*. TEM immunogold labeling of GFP in (*A*) *At*GET3a-GFP (cytoplasm), (*C*) *At*GET3b-GFP (chloroplasts), and (*E*) *At*GET3c-GFP (mitochondria) expressing seedlings using ultrathin thawed cryosections of cotyledons. Control experiments using seedlings missing the corresponding fusion protein are shown in *B*, *D*, and *F*. *G* shows a statistical analysis of the relatively weak but specific mitochondrial gold labeling in *At*GET3c-GFP seedlings. C, cytoplasm; M, mitochondrion; T, thylakoid. (Scale bar: *A*–*F*, 300 nm.)

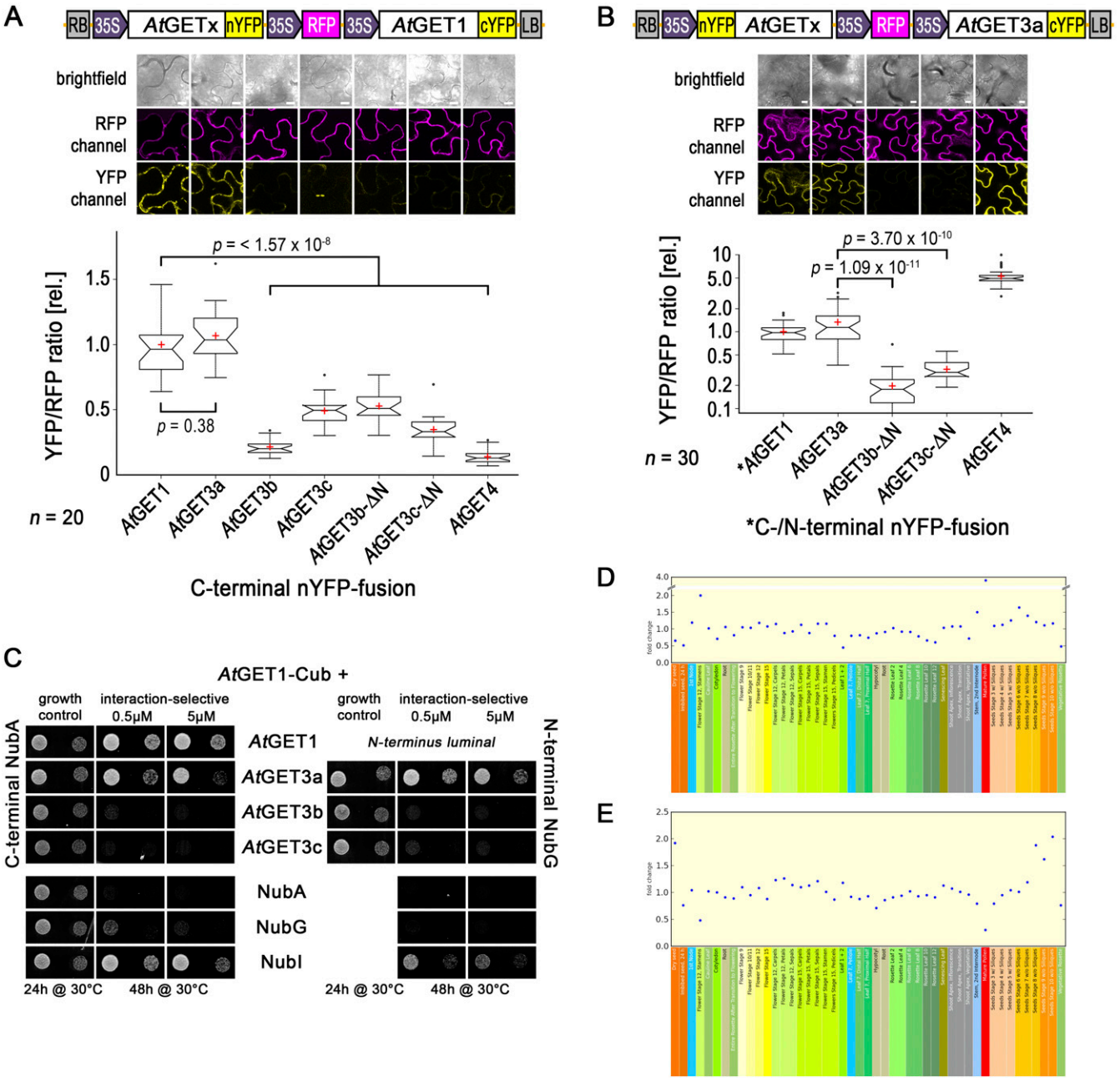

Fig. S3. Interaction analysis of *At*GET pathway orthologs. (*A* and *B*) Complete rBiFC analysis of (*A*) *At*GET1 and (*B*) *At*GET3a with GET pathway orthologs and truncated constructs. Boxed cartoons show construct design above representative images of epidermal cells from transiently transformed *Nicotiana benthamiana* leaves. Larger versions of confocal images are presented in Fig. 2*M*. YFP/RFP mean fluorescence intensities from 20 different leaf sections were calculated and ratioed against the average YFP/RFP ratio of *At*GET1 homodimerization or *At*GET3a–*At*GET1 interaction. Center lines of boxes represent medians, with outer limits at 25th and 75th percentiles. Notches indicate 95% confidence intervals; Tukey whiskers extend to 1.5× interquartile range, outliers are depicted as black dots, and red crosses mark sample means. (Scale bars: 10 μm.) (*C*) Split Ubiquitin interaction analysis in yeast. (*Left*) C-terminally NubA- or (*Right*) N-terminally NubG-tagged *At*GET3 orthologs were coexpressed with *At*GET1-Cub in yeast. Untagged NubA, NubG, or NubI were used as negative (NubG or NubA) or positive (NubI) controls, respectively. Growth on interaction-selective media was detected for yeast coexpressing *At*GET1-Cub and *At*GET1-NubA as well as *At*GET3a-Nub fusion. The plastidic *At*GET3 paralogs do not interact with *At*GET1 in yeast in either tag orientation complementing the rBiFC analysis. (*D* and *E*) eFP browser screenshots showing fold changes in expression ratios of (*D*) *At*GET1 with *At*GET3a and (*E*) *At*GET3a with *At*GET4 over different developmental stages from publicly available microarray data (bar.utoronto.ca/efp_arabidopsis/cgi-bin/efpWeb.cgi).

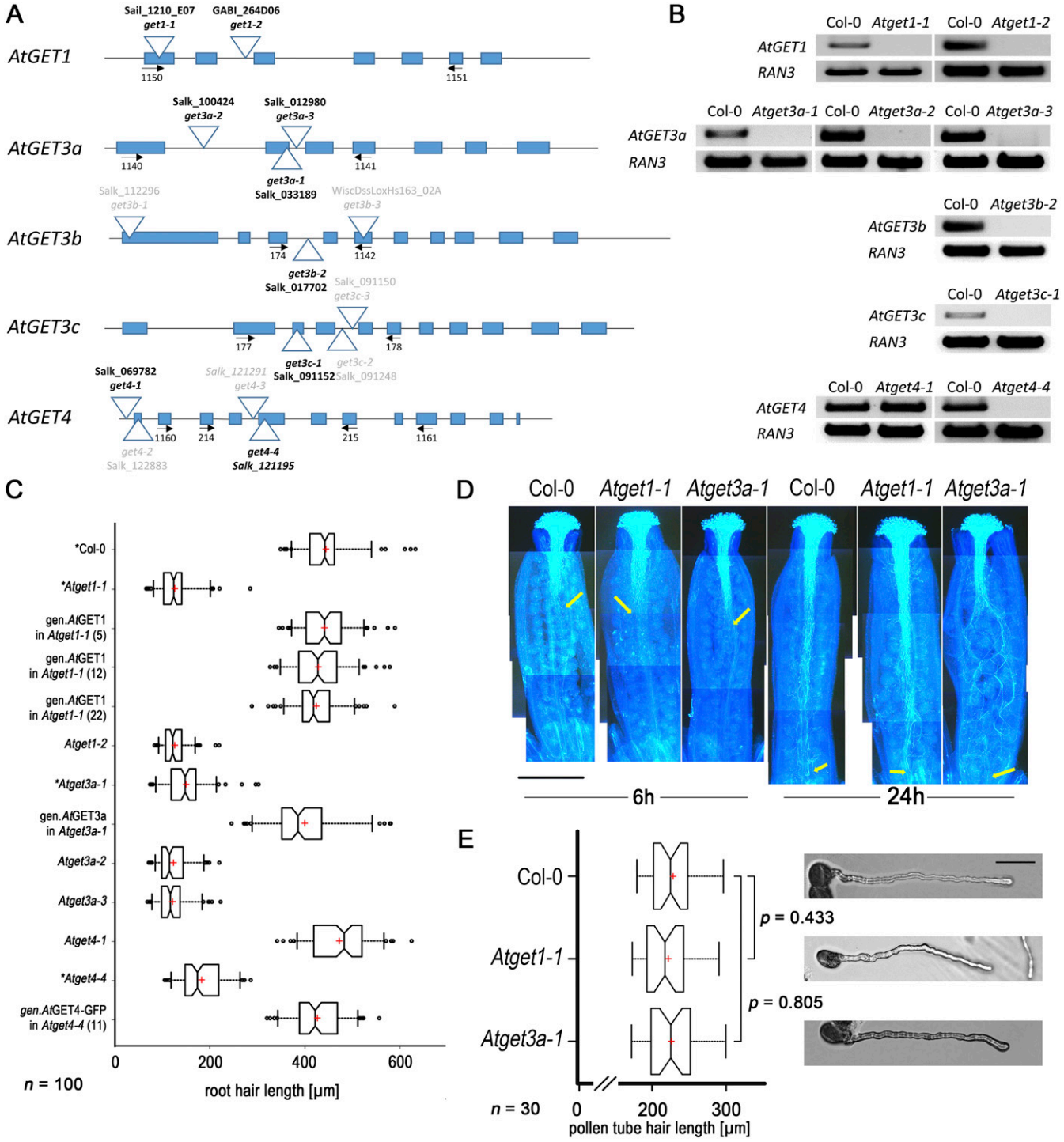

Fig. S4. Functional analysis of AtGET orthologs in planta and yeast. (*A*) Cartoon depicting the sequence-verified position of each T-DNA analyzed in this work (in black type font). (*B*) DNA gels of semi–qRT-PCR corroborate lack of transcript in all mutant lines except *Atget4-1* in line with this being a T-DNA insertion in the 5′ UTR. RAN3 (At5g55190) transcript was used as control. (*C*) Expanded root hair growth analysis showing additional alleles and complementation thereof. Note that the 5′ UTR-inserted *Atget4-1* line that still transcribes *At*GET4 shows WT-like root hair growth. *Values that are also in Fig. 3. (*D*) Aniline blue staining of pollen tubes (the WT and *Atget* mutants) grown for 6 or 24 h, respectively, after pollination of Col-0 pistils. Yellow arrows point to exemplary pollen tubes termini that have reached ovules. Pictures are composites of individual images along the pistil, and exposure was enhanced to visualize the bright blue pollen tubes against the darker blue background. (*E*) Growth of pollen tubes was measured in vitro from 30 individual pollen grains 7 h postgermination (representative images in *Right*). Center lines of boxes represent medians, with outer limits at 25th and 75th percentiles. Notches indicate 95% confidence intervals; Tukey whiskers extend to 1.5× interquartile range, and red crosses mark sample means. (Scale bar: 50 μm.)

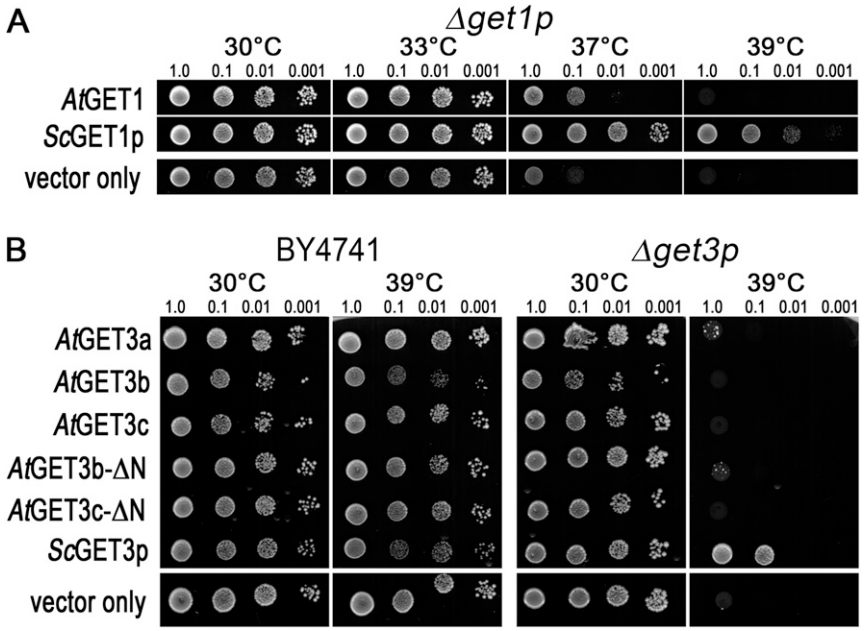

Fig. S5. Complementation assays of yeast KO strains with *A. thaliana* orthologs. (*A*) The yeast *get1* KOs are partially rescued by the *A. thaliana* GET1/WRB ortholog *At*GET1 (At4g16444). Yeast growth was monitored after 3 d in different growth temperatures (33 °C to 39 °C). A genomic fragment of yeast *Sc*GET1p was used as a positive control, and an empty vector was used as a negative control. (*B*) Yeast WT (BY4741) or *get3* KO expressing different *At*GET3 orthologs and truncations thereof and grown under different temperatures. Expression of *Sc*GET3p in the KO rescues growth under heat stress, whereas the *A. thaliana* ortholog *At*GET3a can only partially complement the phenotype. The plastidic-localized *At*GET3b and *At*GET3c and their N-terminal deletion versions fail to complement.

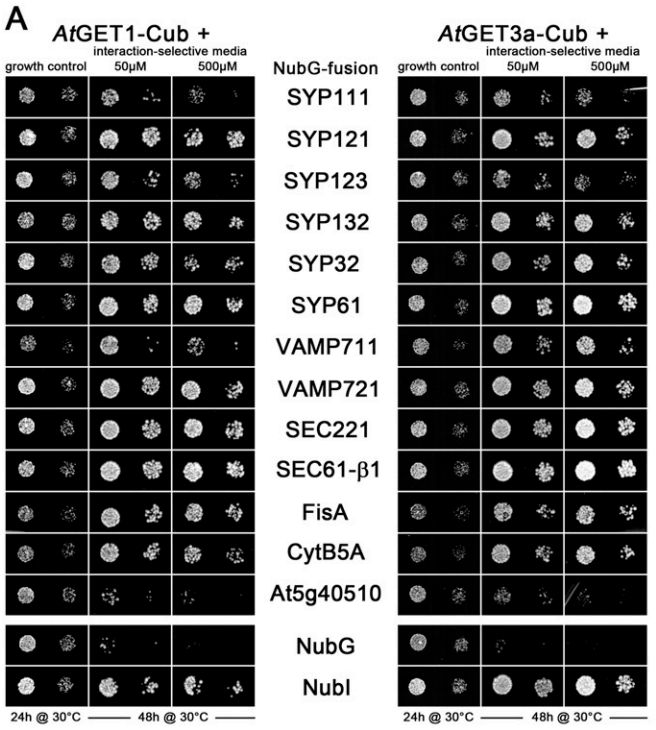

B *At*GET3a-GFP-interacting TA proteins (CoIP-MS)

AGI code	name	description (TAIR10)	aa	location*
At1g06530	PMD2	Peroxisomal and Mitochondrial Division factor 2	323	mitochondrion
At1g54780	TLP18.3	Thylakoid lumen 18.3 kDa protein	285	chloroplast
At1g79040	PSBR	Photosystem II subunit R	140	chloroplast
At2g27730		copper ion binding protein, unknown protein	113	mitochondrion
At3g10860		Cytochrome b-c1 complex, subunit 8 protein	72	mitochondrion
At3g27240		Cytochrome C1 family - electron carrier activity	307	mitochondrion
At3g27820	MDAR4	Monodehydroascorbate Reductase 4	488	peroxisome
At3g63150	MIRO2	MIRO-related GTPase 2	643	mitochondrion
At3g63410	APG1	Albino or Pale Green mutant 1	338	chloroplast
At4g24920		secE/sec61-gamma protein	69	ER membrane
At4g32150	VAMP711	R-SNARE	219	tonoplast
At5g17170	ENH1	Enhancer of sos3-1	271	chloroplast
At5g21430	NdhU	NADH Dehydrogenase-like complex U	218	chloroplast
At5g27540	MIRO1	MIRO-related GTPase 1	648	mitochondrion
At5g43970	TOM22-V	Translocase of Outer Membrane 22-V	99	mitochondrion
At5g51010		Rubredoxin-like superfamily protein	154	chloroplast
At5g64940	ATH13	ATP-binding cassette (ABC) 2 homolog 13	761	chloroplast
At2g40765		unknown transmembrane protein	57	PM
At3g52730		Ubiquinol-cytochrome C reductase	72	mitochondrion
At3g63160	OEP6	Outer Envelope Protein 6, unknown protein	69	chloroplast
At5g02160		unknown transmembrane protein	129	chloroplast
At5g13430		Ubiquinol-cytochrome C reductase	272	mitochondrion
At5g47990	CYP705A5	Cytochrome P450, family 705	511	ER membrane

* predicted by SUBA (http://suba.plantenergy.uwa.edu.au/) or TAIR10 (https://www.arabidopsis.org)

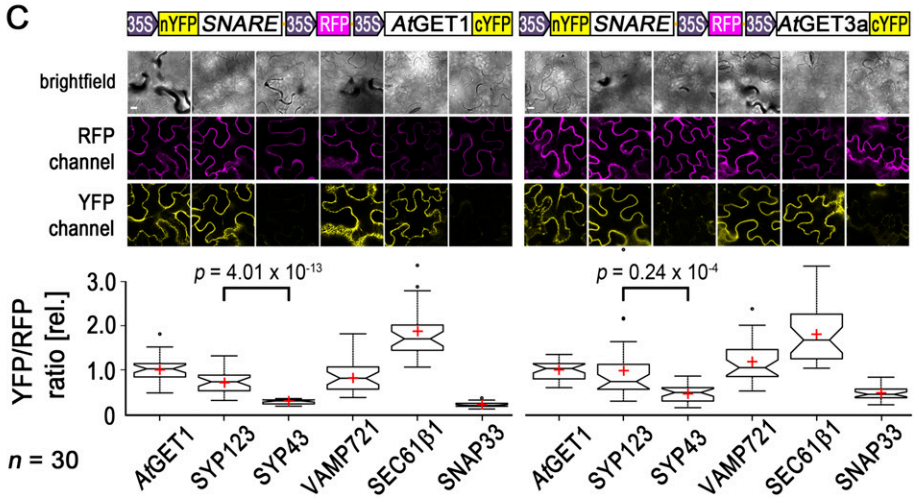

Fig. S6. Expanded information on TA–protein interactions. (*A*) SUS interaction analyses of candidate SNARE/TA proteins with *At*GET1 and *At*GET3a as Cub/bait fusion. Growth on interaction-selective media (-Ade and -His) was monitored after 2 d, and control plates were monitored after 24 h. OD_{600} 1.0 and 0.1 dilutions were dropped, with NubG serving as negative control and NubI (WT version) serving as positive control, respectively. (*B*) TA proteins that were identified via CoIP-MS of AtGET3a-GFP–expressing plants that were not detected in GFP-only expressing plants. (*C*) Complete rBiFC analysis of (*Left*) *At*GET1 and (*Right*) *At*GET3a with candidate SNARE/TA proteins. Boxed cartoons show construct design above exemplary images of transiently transformed *N. benthamiana* leaves. Larger versions of these confocal images are in Fig. 4*A*. YFP/RFP mean fluorescence intensities from 30 different leaf sections were calculated and ratioed against the average YFP/RFP ratio of *At*GET1 homodimerization or *At*GET3a-*At*GET1 interaction. Center lines of boxes represent medians, with outer limits at 25th and 75th percentiles. Notches indicate 95% confidence intervals; Tukey whiskers extend to 1.5× interquartile range, outliers are depicted as black dots, and red crosses mark sample means. (Scale bars: 10 μm.)

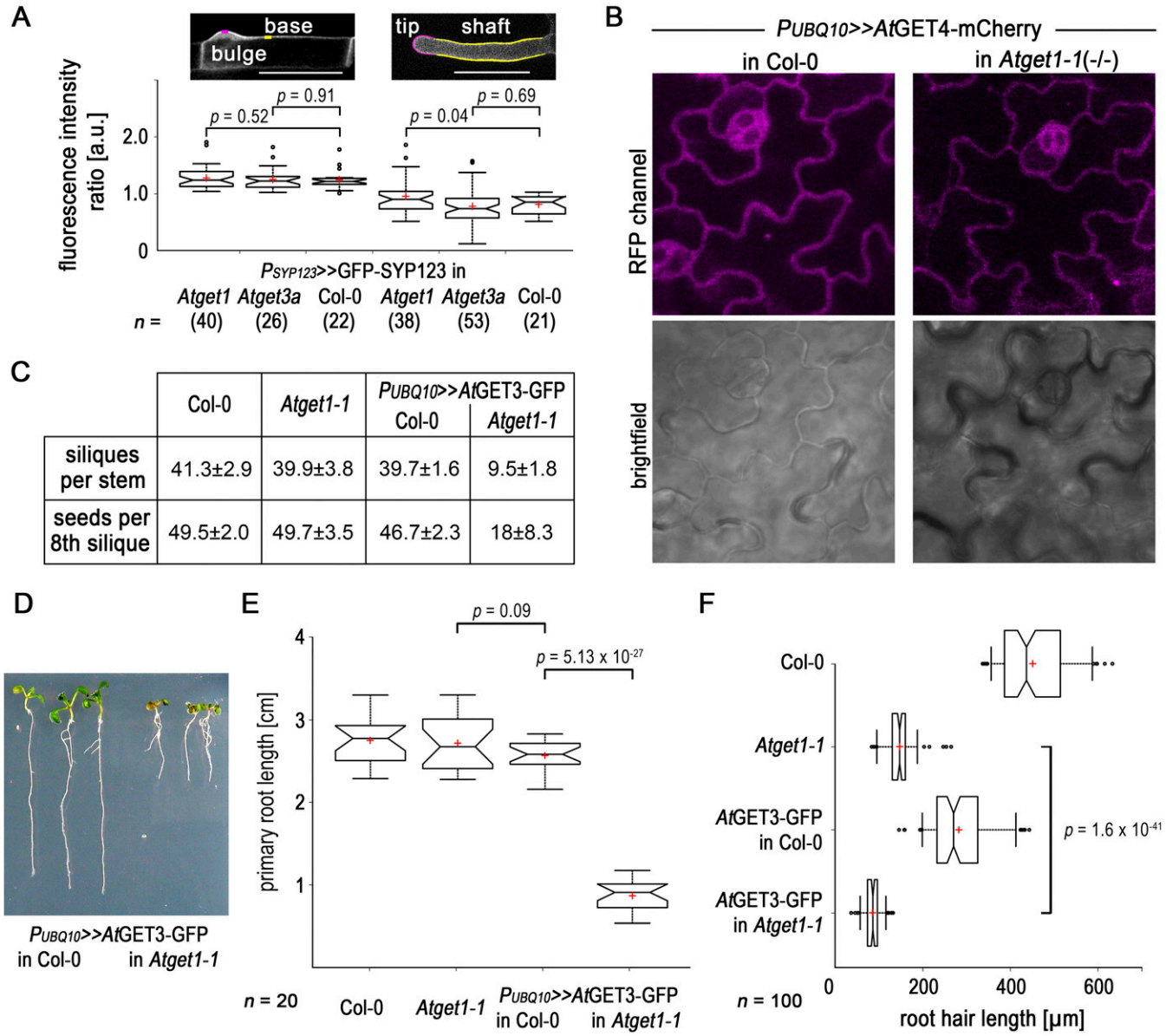

Fig. S7. Global effects of GET pathway mutants in *Arabidopsis*. (*A*) Polarity of SYP123 expression in (*Left*) bulges and (*Right*) outgrown root hairs is not altered in WT and T-DNA insertion lines. (*Inset*) Microscopy pictures depict measurement of polarity ratios: mean fluorescence intensities were ratioed along the newly forming bulges (magenta) against the basal plasma membrane (yellow) or tip vs. shaft. Boxplot as in Fig. 4. Number of analyzed root hairs is in parentheses below the *x* axis. (Scale bars: 50 µm.) (*B*) Subcellular analysis of *At*GET4-mCherry expressed in (*Left*) Col-0 and (*Right*) *Atget1-1* revealing even cytosolic localization. (*C*) Siliques of main inflorescences of 20 individual lines were counted, and the eighth silique of each stem was opened and scored for aberrant seed development. The mutant plant (*At*GET3a-GFP in *Atget1*) has significantly fewer siliques and fewer developed seeds per silique. Values are mean ± SD. An exemplary image can be found in Fig. 5C. (*D–F*) Additional, root growth-related phenotypes of the *At*GET3a-GFP in *Atget1-1*–expressing plants in Fig. 5. (*D*) Exemplary primary roots of plants expressing *At*GET3a-GFP in either (*Left*) WT Col-0 or (*Right*) *Atget1-1*. (*E*) Boxplot as in Fig. 5 showing the root length of 20 individual seedlings for each line. (*F*) Root hair length of the longest root hairs of 10 individual lines.

Table S1. Oligonucleotides used for cloning and RT-PCR

No.	5′–3′ Sequence	Purpose
83	GGGGACAAGTTTGTACAAAAAAGCAGGCTTAATGGCGGCGGATTTGCCGGAGG	pDONR207-AtGET3a
85	GGGGACCACTTTGTACAAGAAAGCTGGGTGGCCACTCTTGACCCGTTCGAGTTC	pDONR207-AtGET3a
104	GGGGACAAGTTTGTACAAAAAAGCAGGCTGCATGGCGACTCTGTCTTCCTATCTG	pDONR207-AtGET3b
106	GGGGACCACTTTGTACAAGAAAGCTGGGTGTTTCCAAATGATATCGCCCAAGAAG	pDONR207-AtGET3b
107	GGGGACAAGTTTGTACAAAAAAGCAGGCTGCATGGCGGCTTTACTTCTCCTCAATC	pDONR207-AtGET3c
109	GGGGACCACTTTGTACAAGAAAGCTGGGTGTTTCCAAATGAGATCACCCATGAAC	pDONR207-AtGET3c
89	GGGGACAAGTTTGTACAAAAAAGCAGGCTTAATGGAAGGAGAGAAGCTTATAGAAG	pDONR207-AtGET1
91	GGGGACCACTTTGTACAAGAAAGCTGGGTGGAACTCCACGAACCTACACAC	pDONR207-AtGET1
86	GGGGACAAGTTTGTACAAAAAAGCAGGCTTAATGTCGAGAGAGAGGATCAAACGTG	pDONR207-AtGET4
88	GGGGACCACTTTGTACAAGAAAGCTGGGTGGCCCATCATCTTGAAGATGTCTCC	pDONR207-AtGET4
261	TCGGAGGTAAAGCAGGTGTTGGGAAG	Introducing G28A in AtGET3a
262	TCTTCCCAACACCTGCTTTACCTCCG	Introducing G28A in AtGET3a
631	GCGGATTTAAATAGATAAGGCTCTGTTCTTCCC	3′ End fragment of AtGET3a
632	TGCAGATTATAACGCTTGTCACAGATACCCTTCAAC	3′ End fragment of AtGET3a
633	TGACTGGAGCTCTTAATTAAAGGCCTATGGCGGCGGATTTGCCGGAGGCGAC	Genomic fragment of AtGET3a
634	GCACTAGTGCCACTCTTGACCCGTTCGAGTTC	A genomic fragment of AtGET3a
554	TAGTCGTTAATTAATCAGAGGAGAGAGCTAAGTGAAGGG	AtGET3a promoter
553	TTAGCCCGGGTGCTAATTCCTTGCTCGTCTCTCTTC	AtGET3a promoter
625	GCGGATTTAAATATCGCATCCCTGAAAAGAGTGAAG	3′ End fragment of AtGET1
626	TGCAGATTATAATAAGTACACGCGTCTTTAGAATC	3′ End fragment of AtGET1
627	TGACTGGAGCTCAGGCCTATGGAAGGAGAGAAGCTTATAGAAG	Genomic fragment of AtGET1
628	GCACTAGTGAACTCCACGAACCTACACACATATTTG	Genomic fragment of AtGET1
629	TGACTGGAGCTCGGCGCGCCTTAATTAAAGTTGGCCAAAGTAGAAAATGGTTG	AtGET1 promoter
630	GAAGGCCTTAACCCTTTTGCTGATTACTGATTC	AtGET1 promoter
635	GCGGATTTAAATGGAAGGAGTTTGAAGAGTGAGTTC	3′ End fragment of *At*GET4
636	TGCAGATTATAAGCTCTGTAATACTTCTTGTTTCG	3′ End fragment of *At*GET4
657	TGACTGGAGCTCAGGCCTATGTCGAGAGAGAGGATCAAACGTG	Genomic fragment of *At*GET4
658	TGCAGCTAGCGCCCATCATCTACACAGTTTCAATGG	Genomic fragment of *At*GET4
659	TGACTGGAGCTCGGCGCGCCTTAATTAACCTCTAACTATCTCTCCCTAGCTAG	AtGET4 promoter
660	GAAGGCCTGGATCTCAAGGATTTGTTGTTTTC	AtGET4 promoter
442	GTAGGCCTATTGTAAATTAACGATCTCATATTG	RSL4 promoter
443	TCACTAGTCGCTCTAACTGATCAACTCTTGCC	RSL4 promoter
761	GGGGACAAGTTTGTACAAAAAAGCAGGCTTAATGGCTAGCCCAACGGAGACGATTTC	AtGET3b ΔN68
762	GGGGACAAGTTTGTACAAAAAAGCAGGCTTAATGGCTACTCTTGCTGAAGGAGCTTC	AtGET3c ΔN50
1140	ATGGCGGCGGATTTGCCGGAGGCG	RT-PCR for *At*GET3a
1141	TCACATCTTTCAAGCCCTCAAGTC	RT-PCR for *At*GET3a
174	ATAAACCCTGAGAAGGCTAGGGAAGAG	RT-PCR for *At*GET3b
1142	TCAAGATTTTACCAATGGATGCATC	RT-PCR for *At*GET3b
177	TGAGATCATTAGCTACTCTTGCTGAAG	RT-PCR for *At*GET3c
178	TGGGAGCAGTATCAAAAACTATACGAG	RT-PCR for *At*GET3c
214	TCACCGCTCAAAGATTCTCTGAAGC	RT-PCR for *At*GET4
215	TCTCGGGGTCCTCAGCTCTAACAAAATG	RT-PCR for *At*GET4
1160	AGGCAATTACTATGGAGCTTTGC	RT-PCR for *At*GET4
1161	TCTCATCCATCATAAAGTTTGCATC	RT-PCR for *At*GET4
1150	GTTAATGGAAGGAGAGAAGCTTATAG	RT-PCR for *At*GET1
1151	TACATGGCCTGTCATGTGACCTCC	RT-PCR for *At*GET1
1408	ATTGGTTTCCTCTTTTCCTCGCTCCG	RT-PCR for *At*GET2
1410	AGTGCATCCATTATCTTCTTCACC	RT-PCR for *At*GET2
1546	ATGAACGATCTTATCTCAAGCTCATTC	RT-PCR for SYP123
547	TCAAGGTCGAAGTAGAGTGTTAAAG	RT-PCR for SYP123
	AGAACACCCCCATCGGCGAC	RT-PCR for GFP
	TGATCGCGCTTCTCGTTGGGGTC	RT-PCR for GFP
	GCCATCCAAGCTGTTCTCTC	RT-PCR for ACT2
	CAGTAAGGTCACGTCCAGCA	RT-PCR for ACT2

Table S2. Entry and destination constructs used

Int. no.	Name	Vector	Insert	Purpose
e002	pDONR207-Syp111-ST	pDONR207	At1g08560	Entry clone
e004	pDONR207-Syp121-ST	pDONR207	At3g11820	Entry clone
e080	pDONR207-VAMP711-ST	pDONR207	At4g32150	Entry clone
e081	pDONR207-VAMP721-ST	pDONR207	At1g04750	Entry clone
e190	pDONR221-L3L2-VAMP721-ST	pDONR221-P3P2	At1g04750	Entry clone
e192	pDONR221-L3L2-SNAP33-ST	pDONR221-P3P2	At5g61210	Entry clone
E006	pDONR207-SYP61-ST	pDONR207	At1g28490	Entry clone
E008	pDONR207-*At*GET3a-ST	pDONR207	At1g01910	Entry clone
E009	pDONR207-*At*GET3a-wo	pDONR207	At1g01910	Entry clone
E011	pDONR207-*At*GET4-wo	pDONR207	At5g63220	Entry clone
E012	pDONR207-*At*GET1-ST	pDONR207	At4g16444	Entry clone
E013	pDONR207-*At*GET1-wo	pDONR207	At4g16444	Entry clone
E014	pDONR207-SEC221-ST	pDONR207	At1g11890	Entry clone
E101	pDONR207-*At*GET3b-ST	pDONR207	At3g10350	Entry clone
E102	pDONR207-*At*GET3b-wo	pDONR207	At3g10350	Entry clone
E103	pDONR207-*At*GET3c-ST	pDONR207	At5g60730	Entry clone
E104	pDONR207-*At*GET3c-wo	pDONR207	At5g60730	Entry clone
E105	pDONR207-SYP32-ST	pDONR207	At3g24350	Entry clone
E107	pDONR221-L3L2-AtSEC221-ST	pDONR221-P3P2	At1g11890	Entry clone
E108	pDONR221-L1L4-GET3a-wo	pDONR221-P1P4	At1g01910	Entry clone
E109	pDONR221-L1L4-GET4-wo	pDONR221-P1P4	At5g63220	Entry clone
E120	pDONR221-L3L2-AtSYP43-ST	pDONR221-P3P2	At3g05710	Entry clone
E124	pDONR207-*Sc*GET3p-ST	pDONR207	YDL100C	Entry clone
E126	pDONR207-SYP123-ST	pDONR207	At4g03330	Entry clone
E128	pDONR207-SYP132-ST	pDONR207	At5g08080	Entry clone
E143	pDONR207-At5g40510-ST	pDONR207	At5g40510	Entry clone
E154	pDONR221-L3L2-SYP123-ST	pDONR221-P3P2	At4g03330	Entry clone
E157	pDONR221-L3L2-*At*GET4-ST	pDONR221-P3P2	At5g63220	Entry clone
E195	pDONR221-L3L2-*At*GET1-wo	pDONR221-P3P2	At4g16444	Entry clone
E196	pDONR221-L1L4-*At*GET1-wo	pDONR221-P1P4	At4g16444	Entry clone
E198	pDONR221-L1L4-*At*GET3b-wo	pDONR221-P1P4	At3g10350	Entry clone
E199	pDONR221-L1L4-*At*GET3c-wo	pDONR221-P1P4	At5g60730	Entry clone
E221	pDONR207-*At*GET3bΔ*N*-ST	pDONR207	At3g10350	Entry clone
E222	pDONR207-*At*GET3bΔ*N*-wo	pDONR207	At3g10350	Entry clone
E223	pDONR207-*At*GET3cΔ*N*-ST	pDONR207	At5g60730	Entry clone
E224	pDONR207-*At*GET3cΔ*N*-wo	pDONR207	At5g60730	Entry clone
E243	pDONR221-L3L2-SEC61β-ST	pDONR221-P3P2	At2g45070	Entry clone
E252	pDONR221-L1L4-AtGET3bΔ*N*-wo	pDONR221-P1P4	At3g10350	Entry clone
E254	pDONR221-L1L4-AtGET3cΔ*N*-wo	pDONR221-P1P4	At5g60730	Entry clone
E265	pDONR221-L3L2-*At*GET3a-wo	pDONR221-P3P2	At1g01910	Entry clone
E289	pDONR207-FisA-ST	pDONR207	At3g57090	Entry clone
E374	pDONR207-CYTb5A-ST	pDONR207	At5g53560	Entry clone
D0116	pDRf1-*At*GET1	pDRf1-GW	E012	Complementation
D0584	pZU-LC-*Sc*GET1p	pZU-LC	Genomic DNA	Complementation
D0512	pYOX1-*At*GET3a	pYOX1-Dest	E008	Complementation
D0513	pYOX1-*At*GET3b	pYOX1-Dest	E101	Complementation
D0514	pYOX1-*At*GET3bΔN	pYOX1-Dest	E221	Complementation
D0515	pYOX1-*At*GET3cΔN	pYOX1-Dest	E223	Complementation
D0516	pYOX1-*Sc*GET3	pYOX1-Dest	E124	Complementation
D0520	pYOX1-*At*GET3c	pYOX1-Dest	E103	Complementation
D0296	pMetYC-*At*GET1	pMetYC-Dest	E013	SUS
D0076	pMetOYC-*At*GET3a	pMetOYC-Dest	E009	SUS
D0078	pNX35-*At*GET3a	pNX35-Dest	E008	SUS
D0086	pNX35-*At*GET3b	pNX35-Dest	E101	SUS
D0088	pNX35-*At*GET3c	pNX35-Dest	E103	SUS
D0298	pXNubA22-*At*GET3a	pXNubA22-Dest	E009	SUS
D0299	pXNubA22-*At*GET3b	pXNubA22-Dest	E102	SUS
D0300	pXNubA22-*At*GET3c	pXNubA22-Dest	E104	SUS
D0297	pXNubA22-*At*GET1	pXNubA22-Dest	E013	SUS
D0081	pNX35-SEC221	pNX35-Dest	E014	SUS
D0098	pNX35-SYP32	pNX35-Dest	E105	SUS
d517	pNX35-SYP121	pNX35-Dest	e004	SUS
d537	pNX35-VAMP711	pNX35-Dest	e080	SUS

Table S2. Cont.

Int. no.	Name	Vector	Insert	Purpose
d538	pNX35-VAMP721	pNX35-Dest	e081	SUS
D0754	pNX35-Syp111	pNX35-Dest	e002	SUS
D0756	pNX35-Syp61	pNX35-Dest	E006	SUS
D0786	pNX35-SYP123	pNX35-Dest	E126	SUS
D0787	pNX35-SYP132	pNX35-Dest	E128	SUS
D0788	pNX35-At5g40510	pNX35-Dest	E143	SUS
D0789	pNX35-SEC61-β1	pNX35-Dest	E228	SUS
D0790	pNX35-CYTb5A	pNX35-Dest	E374	SUS
D0791	pNX35-FisA	pNX35-Dest	E289	SUS
D0273	pBiFCt-nYFP-*At*GET4-*At*GET3a-cYFP	pBiFCt-2in1-NC	E108 + E157	rBiFC
D0356	pBiFCt-*At*GET1-nYFP-*At*GET1-cYFP	pBiFCt-2in1-CC	E196 + E195	rBiFC
D0355	pBiFCt-*At*GET1-nYFP-*At*GET4-cYFP	pBiFCt-2in1-CC	E109 + E195	rBiFC
D0354	pBiFCt-*At*GET1-nYFP-*At*GET3a-cYFP	pBiFCt-2in1-CC	E108 + E195	rBiFC
D0545	pBiFCt-*At*GET1-nYFP-*At*GET3bΔ*N*-cYFP	pBiFCt-2in1-CC	E252 + E195	rBiFC
D0546	pBiFCt-*At*GET1-nYFP-*At*GET3cΔ*N*-cYFP	pBiFCt-2in1-CC	E254 + E195	rBiFC
D0361	pBiFCt-*At*GET1-nYFP-*At*GET3b-cYFP	pBiFCt-2in1-CC	E198 + E195	rBiFC
D0362	pBiFCt-*At*GET1-nYFP-*At*GET3c-cYFP	pBiFCt-2in1-CC	E199 + E195	rBiFC
D0965	pBiFCt-*At*GET3a-nYFP-*At*GET3a-cYFP	pBiFCt-2in1-NC	E108 + E265	rBiFC
D0966	pBiFCt-*At*GET3a-nYFP-*At*GET3bΔ*N*-cYFP	pBiFCt-2in1-NC	E252 + E265	rBiFC
D0973	pBiFCt-*At*GET3a-nYFP-*At*GET3cΔ*N*-cYFP	pBiFCt-2in1-NC	E254 + E265	rBiFC
D0123	pBiFCt-nYFP-SYP43-*At*GET3a-cYFP	pBiFCt-2in1-NC	E108 + E120	rBiFC
D0395	pBiFCt-NC-nYFP-SYP43-ST-*At*GET1-cYFP	pBiFCt-2in1-NC	E196 + E107	rBiFC
D0980	pBiFCt-NC-nYFP-SYP123-*At*GET1-cYFP	pBiFCt-2in1-NC	E196 + E154	rBiFC
D0267	pBiFCt-nYFP-SYP123-*At*GET3a-cYFP	pBiFCt-2in1-NC	E108 + E154	rBiFC
D0371	pBiFCt-NC-nYFP-VAMP721-*At*GET1-cYFP	pBiFCt-2in1-NC	E196 + e190	rBiFC
D0588	pBiFCt-NC-nYFP-SNAP33-ST-*At*GET3a-cYFP	pBiFCt-2in1-NC	E108 + e192	rBiFC
D0589	pBiFCt-NC-nYFP-Vamp721-ST-*At*GET3a-cYFP	pBiFCt-2in1-NC	E108 + e190	rBiFC
D0418	pBiFCt-NC-nYFP-Ssß1-ST-*At*GET1-cYFP	pBiFCt-2in1-NC	E196 + E243	rBiFC
D0590	pBiFCt-NC-nYFP-Ssß1-ST-*At*GET3a-cYFP	pBiFCt-2in1-NC	E108 + E243	rBiFC
D0090	pUBQ10::*At*GET3a-GFP	pUBQ10-GW-GFP	E009	Localization
D0091	pUBQ10::*At*GET3b-GFP	pUBQ10-GW-GFP	E102	Localization
D0092	pUBQ10::*At*GET3c-GFP	pUBQ10-GW-GFP	E104	Localization
D0160	pUBQ10::*At*GET1-GFP	pUBQ10-GW-GFP	E013	Localization
D0504	pUBQ10::*At*GET4-mCherry	pUBQ10-GW-mCherry	E011	Localization
D0399	pUBQ10::*At*GET3bΔ*N*-GFP	pUBQ10-GW-GFP	E222	Localization
D0405	pUBQ10::*At*GET3cΔ*N*-GFP	pUBQ10-GW-GFP	E224	Localization

ST, native stop codon; wo, without stop codon.

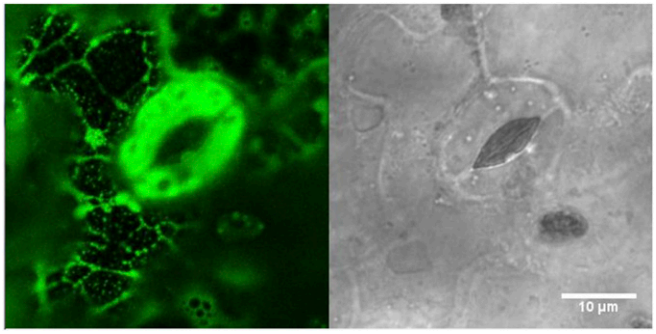

Movie S1. CLSM *z* stack of *At*GET3a-GFP in homozygous *Atget1*$^{(-/-)}$.

Movie S1

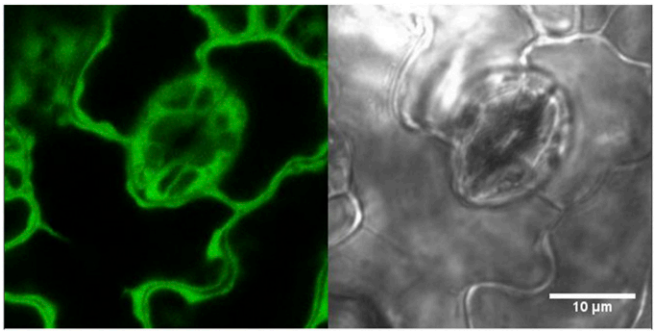

Movie S2. CLSM *z* stack of *At*GET3a-GFP in heterozygous *Atget1*$^{(-/+)}$.

Movie S2

Dataset S1. CoIP-MS raw data of P_{UBQ10} >> GET3-GFP interaction partners in WT Col-0 plants from two individual biological replicates (R1 and R2)

Dataset S1

II. Asseck et al., 2020:

Endoplasmic reticulum membrane receptors of the GET pathway are conserved throughout eukaryote

Endoplasmic reticulum membrane receptors of the GET pathway are conserved throughout eukaryotes

Lisa Yasmin Asseck[a,b], Dietmar Gerald Mehlhorn[a,b], Jhon Rivera Monroy[c,d], Martiniano Maria Ricardi[b], Holger Breuninger[a], Niklas Wallmeroth[a], Kenneth Wayne Berendzen[a], Minou Nowrousian[b], Shuping Xing[a], Blanche Schwappach[c], Martin Bayer[e], and Christopher Grefen[a,b,1]

[a]Developmental Genetics, Centre for Plant Molecular Biology, University of Tübingen, 72076 Tübingen, Germany; [b]Department of Molecular and Cellular Botany, Ruhr-University Bochum, 44780 Bochum, Germany; [c]Department of Molecular Biology, University Medical Center Göttingen, 37073 Göttingen, Germany; [d]High-Complexity Instrument Laboratory, Universidad de La Salle, 110231 Bogotá, Colombia; and [e]Department of Cell Biology, Max Planck Institute for Developmental Biology, 72076 Tübingen, Germany

Edited by Natasha V. Raikhel, Center for Plant Cell Biology, Riverside, CA, and approved November 14, 2020 (received for review August 20, 2020)

Type II tail-anchored (TA) membrane proteins are involved in diverse cellular processes, including protein translocation, vesicle trafficking, and apoptosis. They are characterized by a single C-terminal transmembrane domain that mediates posttranslational targeting and insertion into the endoplasmic reticulum (ER) via the Guided-Entry of TA proteins (GET) pathway. The GET system was originally described in mammals and yeast but was recently shown to be partially conserved in other eukaryotes, such as higher plants. A newly synthesized TA protein is shielded from the cytosol by a pretargeting complex and an ATPase that delivers the protein to the ER, where membrane receptors (Get1/WRB and Get2/CAML) facilitate insertion. In the model plant *Arabidopsis thaliana*, most components of the pathway were identified through *in silico* sequence comparison, however, a functional homolog of the coreceptor Get2/CAML remained elusive. We performed immunoprecipitation-mass spectrometry analysis to detect in vivo interactors of *At*GET1 and identified a membrane protein of unknown function with low sequence homology but high structural homology to both yeast Get2 and mammalian CAML. The protein localizes to the ER membrane, coexpresses with *At*GET1, and binds to *Arabidopsis* GET pathway components. While loss-of-function lines phenocopy the stunted root hair phenotype of other *Atget* lines, its heterologous expression together with the coreceptor *At*GET1 rescues growth defects of *Δget1get2* yeast. Ectopic expression of the cytosolic, positively charged N terminus is sufficient to block TA protein insertion in vitro. Our results collectively confirm that we have identified a plant-specific GET2 in *Arabidopsis*, and its sequence allows the analysis of cross-kingdom pathway conservation.

GET pathway | tail-anchored proteins | SNAREs | ER membrane | root hairs

Membrane proteins are ubiquitous in all domains of life. In eukaryotes, approximately one-third of all open reading frames are identified or predicted to integrate with at least one transmembrane domain (TMD) into the lipid bilayer (1). Most membrane proteins are recognized as such at the ribosome during translation and are immediately inserted into the ER membrane via a pathway known as cotranslational insertion. Recognition of these membrane proteins is based on an N-terminal signal sequence or the first TMD and its isochronal detection by the signal recognition particle (SRP) on emergence from the ribosome.

A number of membrane proteins are neither recognized by the SRP nor cotranslationally inserted, however. Among these are the tail-anchored (TA) proteins, which feature a single C-terminal TMD that inserts into the ER membrane in a type II orientation; that is, the N-terminal part of the protein faces the cytosol. Important members of this membrane protein family are *N*-ethylmaleimide–sensitive factor attachment protein receptors (SNAREs) that catalyze membrane fusion events in eukaryotes (2–4). However, the absence of an N-terminal signal sequence in TA proteins dictates their insertion to be posttranslational and requires chaperoning of the mature protein through the cytosol to the membrane. The Guided-Entry of TA proteins (GET) pathway was found to perform the steps necessary for the task of receiving the nascent TA proteins, chaperoning these to the membrane and insert via dedicated receptors (5).

A pretargeting complex comprising Sgt2, Get4, and Get5 (metazoa: SGTA, TRC35, UBL4A, and BAG6) receives the TA protein from the ribosome (6, 7) and hands it over to the homodimer ATPase Get3 (TRC40) (6–9). Transfer of the TA protein to Get3 requires the hydrolysis of ATP (10, 11). The terminal insertion step is initiated through interaction of the Get3-TA complex first with the ER membrane receptor Get2 (CAML), followed by release of ADP and subsequent disassembly of the complex facilitated by interaction with Get1 (WRB) (12, 13). A stretch of positively charged amino acids within the cytosolic N terminus of Get2/CAML is required for Get3/TRC40 binding (14, 15).

The ER receptors of the GET pathway form an intricate relationship (16). Knockout of WRB in cardiomyocytes results in reduced protein levels of CAML. Interestingly, this difference is caused posttranslationally, as mRNA levels are not altered (17). Rather, the lack of sufficient protein level of WRB within the membrane leads to incomplete integration of CAML and its subsequent proteasomal degradation (18).

Significance

The GET pathway is required for the insertion of tail-anchored (TA) membrane proteins in the endoplasmic reticulum (ER) of yeast and mammals. Some orthologous genes had also been identified in higher plants with the exception of one of the two ER membrane receptors required for membrane insertion. Get2/CAML is required for the pathway's cytosolic chaperone to dock and release its TA protein cargo. Here we report the identification of the elusive plant GET pathway receptor through an interaction screen in *Arabidopsis*. The candidate allows detection of further Get2/CAML orthologs in higher plants, revealing conservation and function of structural features across kingdoms. Additionally, our results demonstrate that these features, rather than sequence conservation, determine functionality of the candidate within the pathway.

Author contributions: S.X., B.S., and C.G. designed research; L.Y.A., D.G.M., J.R.M., M.M.R., N.W., S.X., M.B., and C.G. performed research; K.W.B., M.N., and M.B. contributed new reagents/analytic tools; L.Y.A., H.B., K.W.B., M.N., B.S., M.B., and C.G. analyzed data; and L.Y.A. and C.G. wrote the paper.

The authors declare no competing interest.

This article is a PNAS Direct Submission.

This open access article is distributed under Creative Commons Attribution-NonCommercial-NoDerivatives License 4.0 (CC BY-NC-ND).

[1]To whom correspondence may be addressed. Email: christopher.grefen@rub.de.

This article contains supporting information online at https://www.pnas.org/lookup/suppl/doi:10.1073/pnas.2017636118/-/DCSupplemental.

Published December 21, 2020.

Downloaded by guest on December 23, 2020

While the GET pathway was originally described in opisthokonts (19, 20), it was recently shown to be partially conserved in other eukaryotes, such as Archaeplastida (21, 22). The main GET pathway components were identified through in silico analysis of protein sequence conservation (21, 22). In this way, orthologs for Get1/WRB, Get3/TRC40, Get4/TRC35, Get5, and Sgt2 were identified in *Arabidopsis thaliana*. Similar to the initial mystery around the existence of a functional Get2 ortholog in animals (15), our sequence analysis alone did not reveal potential candidates in higher plants.

Here we now report the identification and functional characterization of an archaeplastidic ortholog of the opisthokont Get2/CAML through an immunoprecipitation-mass spectrometry (IP-MS) approach. Using *At*GET1-GFP–expressing *Arabidopsis* plants, we detected an unknown membrane protein, At4g32680, which we temporarily assigned as G1IP (*At*GET1-interacting protein). The protein shows low sequence similarity to the opisthokont Get2/CAML but apparent conservation of structural features: a positively charged, cytosolic N terminus followed by three TMDs. T-DNA insertion and CRISPR loss-of-function lines phenocopy other *Atget* lines, while double-receptor knockouts do not show exacerbated effects, suggesting pathway conservation. G1IP together with *At*GET1 can complement the growth defects of the yeast receptor knockout, and expression of the charged stretch at the N terminus is sufficient to interrupt TA protein import in dog reticulocytes. Extensive interaction analyses revealed that G1IP interacts with other pathway components. Collectively, our results suggest that G1IP codes for a plant-specific GET2 that is functionally equivalent to its yeast and mammalian counterparts, although only TMDs and small sequence motifs are conserved across eukaryotes.

The protein sequence of *Arabidopsis* GET2 serves as an important puzzle piece in understanding cross-kingdom evolution of the GET pathway. It seems likely that the plant GET2 orthologs, fungi Get2, and mammalian CAML derived from a common ancestor, and that the evolutionary pressure was maintained on the structural features of a cytosolic, positively charged stretch at the N terminus and three TMDs at the C terminus.

Results and Discussion

An Unknown Transmembrane Protein Interacts with *At*GET1 and *At*GET3a In Planta. Both GET receptor-forming protein pairs Get1 and Get2 in yeast (19, 23), as well as WRB and CAML (15) in mammalian cells, have been shown to copurify. Thus, we chose affinity purification as a promising strategy to identify the elusive coreceptor of *At*GET1. We performed immunoprecipitation of *At*GET1-GFP stably expressed in *A. thaliana* wild-type (WT), Col-0, followed by mass spectrometry analysis. Two biological replicates were executed, and candidates that came up in both experiments and predicted to contain TMDs were considered high-confidence targets (Table 1).

Since both Get2 and CAML contain a C-terminal membrane-anchoring domain with three transmembrane helices, we focused on candidates with such a structure. We identified an unknown membrane protein, G1IP (*At*GET1-interacting protein; At4g32680), which appeared to match these preferences (Fig. 1*A*). Interestingly, G1IP was also detected in our previously published IP-MS results using *At*GET3a-GFP (22), substantiating that this protein may indeed be part of the *Arabidopsis* GET pathway. In addition, a close homolog of G1IP exists in *Arabidopsis* (At1g52343) that we termed G1IP-*like*. This protein was identified in both IP-MS analyses of *At*GET1, but not when using *At*GET3a-GFP as a target (22) (Table 1).

Multiple sequence alignment using MegaX showed only low overall similarity between G1IP and yeast Get2 or mammalian CAML, respectively (*SI Appendix*, Fig. S1*A*). However, structural comparison revealed that the predicted membrane topology of G1IP suggests a type II orientation with a long cytosolic N terminus, three transmembrane helices, and a luminal C-terminal region (TMHMM, Tmpred, and Protter version 1.0) (24) closely resembling the structure of yeast Get2 and mammalian CAML (Fig. 1*A*). Moreover, Phyre2 and HHpred analyses of the sequence maps part of the N terminus of G1IP (amino acids 6 to 27) with the crystal structure of cytosolic *Sc*Get2 bound to *Sc*Get3 (structures 3ZS9_D and 3SJD_E, respectively).

The predicted orientation of G1IP was experimentally verified using ratiometric bimolecular fluorescence complementation (rBiFC) (25) with the coreceptor *At*GET1 (*SI Appendix*, Fig. S1*B*). The putative structure of G1IP-*like* is similar to that of G1IP with a relatively large N-terminal cytosolic region and two or three transmembrane helices in the C-terminal domain, predicted via TMHMM or TMpred, respectively.

G1IP and *At*GET1 Share the Same Expression Profile and Subcellular Localization. To determine a functional relationship between G1IP and *At*GET1, we assessed the expression patterns by quantitative PCR (qPCR). Consistent with expression data of publicly available microarray and proteomics data (26), qPCR analysis revealed constitutive coexpression of G1IP and *At*GET1 at almost identical levels across all tissues and developmental stages, supporting the notion of a shared molecular pathway (Fig. 1*B*). In contrast, G1IP-*like* exhibited flower-specific gene expression in both qPCR and in silico analysis (eFP Browser), indicating functional divergence of the two homologs. Such an organ-specific expression pattern of G1IP-*like* most likely contradicts a putative housekeeping function that the *At*GET1 coreceptor needs to fulfill within the GET pathway. Instead, G1IP-*like* may have acquired novel, flower-specific functions independent of *At*GET1.

The *At*GET1 receptor was previously described as an ER-localized protein (22). However, in silico prediction suggests a nuclear localization for G1IP (suba.live/factsheet.html?id=AT4G32680.1), which would contradict a potential ER import function of a GET pathway coreceptor. To investigate the subcellular localization of G1IP in *A. thaliana*, we created stable transgenic plants that coexpress N-terminally GFP-tagged G1IP with the ER marker secRFP-HDEL. Using confocal laser scanning microscopy (CLSM), we were able to confirm a subcellular ER localization for G1IP (Fig. 1 *C*–*F*), as was demonstrated previously for *At*GET1 (22). Similar to its homolog, G1IP-*like* also localizes to the ER membrane (Fig. 1 *G*–*J*).

G1IP Binds *At*GET3a Only in the Presence of *At*GET1. To corroborate and expand the analyses of physical interaction of G1IP and G1IP-*like* with *Arabidopsis* GET pathway components, we performed rBiFC (25, 27, 28) and coimmunoprecipitation (co-IP) analyses. Complementation of the YFP signal, a cue for physical interaction, was detected only in samples in which *At*GET1 was coexpressed with G1IP or G1IP-*like* (Fig. 1 *K*–*M* and *SI Appendix*, Fig. S2 *A*–*C*). The residual YFP signal in samples with *At*GET3a was comparable to the biological negative control of *At*GET4, a protein found further upstream of the pathway that is unable to interact on its own with the receptors in yeast and mammals (7, 29). Given our identification of G1IP as a binding partner of *At*GET3a in our previously published IP-MS analyses (22), this lack of an interaction in rBiFC was somewhat surprising.

Therefore, we generated a new set of Gateway-compatible 2in1 co-IP vectors allowing for high constitutive gene coexpression in *Arabidopsis* (Fig. 1*N*). Interestingly, interaction was detected only in WT (Fig. 1*O*) and not in the *Atget1-2* mutant background (Fig. 1*P*), suggesting that the interaction of *At*GET3a and G1IP is highly sensitive to the presence or absence of *At*GET1 (see Fig. 4*C*). It was recently demonstrated that the human Get1 ortholog WRB is required for protein stability and correct insertion of CAML, the Get2 receptor in metazoa (18); however, we did not observe instability of ectopically expressed G1IP in *Atget1-2* mutants (Fig. 1*P*).

Downloaded by guest on December 23, 2020

Table 1. AGI codes and identifiers of candidates identified in both replicates of *At*GET1-GFP IP-MS analyses and predicted to contain TMDs

			Prediction tool			
			Localization,	Number of TMDs		
AGI	Gene name	Description	SUBA	TMHMM	TMpred	Also detected via *At*GET3a-GFP (22)
AT4G32680	*G1IP*	Unknown transmembrane protein	Nuc	3	4 or 3	Yes
AT1G52343	*G1IP-like*	Unknown transmembrane protein	Cyt/Mito	2	3	No
AT5G13490	*AAC2*	ADP/ATP carrier 2	Mito	3	5 or 4	Yes
AT5G13430		Ubiquinol-cytochrome C reductase FeS subunit	Mito	0	2	Yes
AT1G50200	*ALATS*	Alanyl-tRNA synthetase	Mito	0	1	Yes
AT4G01100	*ADNT1*	Adenine nucleotide transporter 1	Mito	0	4	Yes
AT5G41670		6-phosphogluconate dehydrogenase family protein	Mito/Chp	0	2	Yes
AT2G38040	*CAC3*	Carboxyltransferase alpha subunit	Chp	0	3	Yes
AT1G64190		6-phosphogluconate dehydrogenase family protein	Chp	0	2	Yes
AT1G29900	*CARB*	Carbamoyl phosphate synthetase B	Chp	0	2 or 1	Yes
AT5G30510	*RPS1*	Ribosomal protein S1	Chp	0	1	No
AT5G53480		ARM repeat superfamily protein	Cyt/Nuc/Chp	0	3	No
AT2G20580	*RPN1A*	26S proteasome regulatory subunit S2 1A	Cyt/Nuc	0	5 or 4	Yes
AT4G24820		26S proteasome regulatory subunit Rpn7	Cyt/Nuc	0	1	Yes
AT2G30490	*C4H*	Cinnamate-4-hydroxylase	ER	0	2	Yes
AT5G47990	*CYP705A5*	Cytochrome P450 705A5	ER	0	4	Yes
AT1G07810	*ECA1*	ER-type Ca2 -ATPase 1	ER	8	9	Yes
AT3G51460	*RHD4*	Phosphoinositide phosphatase family protein	ER	2	3	Yes
AT1G70770		Protein of unknown function DUF2359	ER	0	2 or 1	Yes
AT4G21150	*HAP6*	Ribophorin II (RPN2) family protein	ER	4	4	Yes
AT1G29310		SecY protein transport family protein	Golgi	10	10 or 9	Yes
AT4G25820	*XTH14*	Xyloglucan endotransglucosylase/hydrolase 14	CW	1	1	Yes

Nuc, nucleus; Cyt, cytosol; Mito, mitochondria; Chp, chloroplast; CW, cell wall.

G1IP Phenocopies GET Pathway Mutants. We have previously shown that loss of some GET pathway components in *A. thaliana* leads to reduced root hair elongation under standard growth conditions (22). To investigate whether G1IP belongs to the same pathway, we analyzed the root hair growth of putative loss-of-function lines (Fig. 2*A* and *SI Appendix*, Fig. S3). The T-DNA insertion line *g1ip-3* showed significantly shorter root hairs at seedling level compared with WT Col-0 and similar to the *A. thaliana* GET pathway mutant *get1-1* (22) (Fig. 2*B*). Expression of a genomic version of the *G1IP* gene under the constitutively active VAMP721 promoter (*g1ip-3* compl.) restored WT-like root hair growth.

G1IP in Concert with *At*GET1 Can Complement Yeast GET Receptor Mutants. It had been demonstrated that the loss of GET pathway components in yeast results in a lack of (heat) stress tolerance (30). Therefore, we tested whether G1IP or G1IP-*like* are able to complement yeast growth under increasing temperatures (Fig. 2 *C* and *D*). The simultaneous expression of *At*GET1 and G1IP is able to weakly recover the viability of the *Δget1get2* strain (31), indicating at least some functional conservation between the *Arabidopsis* and yeast genes (Fig. 2*C*). However, coexpression of the *Arabidopsis* homolog G1IP-*like* together with *At*GET1 in *Δget1get2* is not able to rescue the lethality at higher temperatures, comparable to the vector-only control. The lack of a noticeable phenotype in *g1ip-like* lines, along with the different expression profile and lack of rescue of *Δget1get2* yeast, strongly suggest that G1IP-*like* has acquired a novel function independent of the GET pathway.

In another approach, we tested the importance of a heterologous or homologous partner receptor for yeast rescue (Fig. 2*D*). Mixing the corresponding receptors of the different species did not rescue as efficiently as the homologous combinations of *At*GET1/G1IP or *Sc*GET1/*Sc*GET2; however, the combination of *Sc*GET1 with G1IP appears to perform even weaker than the opposite combination with *At*GET1 and *Sc*GET2, mirroring an earlier observation with the mammalian GET2 ortholog CAML (30). This result implies that the eukaryotic Get2/CAML in general may have undergone more structural changes during evolution, making it more specialized as opposed to the more conserved GET1/WRB.

G1IP Interacts with the *At*GET1 Receptor via Its TMDs. Mammalian WRB and CAML have been previously shown to associate via interactions between their TMDs, thereby forming a functional receptor complex (15). Therefore, we examined the importance of the transmembrane region of G1IP in binding to *At*GET1 using rBiFC and co-IP. We separated the cytosolic tail (amino acids 1 to 173) of G1IP from its TMD region (amino acids 174 to 282) and tested both domains individually for *At*GET1 interaction (Fig. 3 *A* and *B* and *SI Appendix*, Fig. S2 *D* and *E*). Interaction of full-length G1IP with *At*GET1 in rBiFC resulted in strong YFP complementation, with a YFP:RFP ratio above the positive control *At*GET1 with *At*GET3a. While the ratio was lower using the truncated construct G1IP-TMDs, it nonetheless gave a strong signal of YFP complementation; however, the cytosolic part of G1IP showed an almost complete absence of signal comparable to the biological negative control of *At*GET1 and *At*GET4.

The rBiFC result was corroborated via co-IP by leveraging a 2in1 Förster resonance energy transfer (FRET) construct (35) transiently transformed in *Nicotiana benthamiana* (Fig. 3*C*). Fusion proteins of *At*GET1-EGFP coexpressed with mCherry-G1IP, mCherry-G1IPcyt, or mCherry-G1IP-TMDs were purified from tobacco leaf extracts via the RFP-trap antibody. After complex elution, immunoblotting against GFP revealed the presence of *At*GET1-GFP in eluates of G1IP and G1IP-TMDs but not of G1IPcyt (Fig. 3*D*). Our results indicate that G1IP acts as binding partner of *At*GET1 via its TMDs.

Downloaded by guest on December 23, 2020

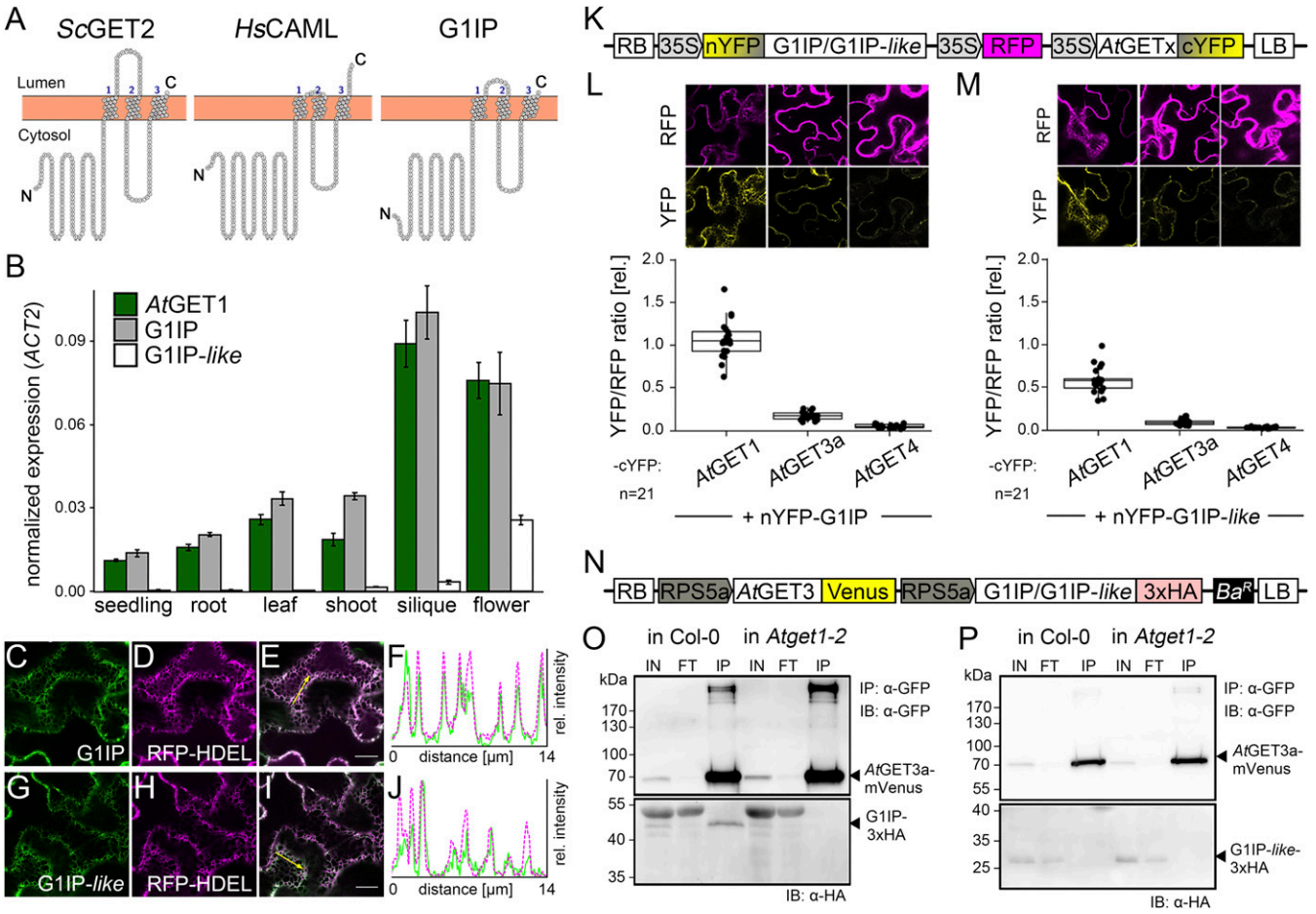

Fig. 1. G1IP coexpresses with *At*GET1, localizes to the ER, and interacts with *At*GET1 and *At*GET3a. (*A*) Transmembrane topology prediction of *Sc*GET2, *Hs*CAML, and G1IP using Protter. (*B*) Relative transcript levels of *At*GET1, G1IP, and G1IP-*like* in different organs of *A. thaliana* Col-0 plants measured by qPCR analysis. ACT2 was used as a reference gene. Error bars indicate SD. $n = 3$. (*C*–*J*) CLSM analysis of the subcellular localization of p35S::GFP-G1IP (*C*–*F*) and p35S::GFP-G1IP-*like* (*G*–*J*) in leaves of stably transformed *A. thaliana* lines coexpressing the ER marker RFP-HDEL. Line histograms (*F* and *J*) along yellow arrows in *E* and *I* confirm colocalization. (Scale bars: 10 μm.) (*K*) Schematic of the 2in1 rBiFC constructs used in *L* and *M*. (*L* and *M*) rBiFC analysis of G1IP (*L*) and G1IP-*like* (*M*) with *Arabidopsis* GET pathway components. Exemplary CLSM images of transiently transfected *N. benthamiana* leaves are depicted. Mean fluorescence levels of 21 areas were measured in YFP and RFP channels, ratioed, and plotted to show YFP complementation. The center lines of boxes represent the median with outer limits at the 25th and 75th percentiles. Tukey whiskers extend to 1.5 times the IQR. All values are depicted as black dots. (*N*) Schematic of the 2in1 co-IP constructs used in *O* and *P*. (*O* and *P*) Co-IP of *At*GET3a with G1IP (*O*) or G1IP-*like* (*P*) in Col-0 and *Atget1-2* mutant background. Protein extracts of *Arabidopsis* seedlings overexpressing *At*GET3a-mVenus and G1IP-3xHA or G1IP-*like*-3xHA were immunoprecipitated with anti-GFP beads. Protein–protein interaction was detected by immunoblotting using anti-GFP and anti-HA antibodies. IN, input; FT, flow-through; IP, immunoprecipitate.

Interference of the Cytosolic G1IP N Terminus in TA Protein Insertion. Despite the low level of sequence similarity between G1IP and yeast Get2 or mammalian CAML, multiple protein sequence alignment showed that a cluster of positively charged amino acids near the N terminus is conserved among the proteomes of vertebrates, plants, and fungal lineages (Fig. 3*E* and *SI Appendix*, Fig. S4). This motif is proposed to be crucial for binding of *Sc*Get3 (14) and its mammalian homolog TRC40 (15) and has been shown to segregate with the membrane-anchoring domain of Get2/CAML-*like* proteins in a position-specific iterative (PSI)-BLAST analysis (32). To determine the functional effect of this cluster in G1IP, we performed site-directed substitution mutagenesis to reverse the charge of four amino acid residues: R9E, R10E, R11E, and K12E = G1IP^{4E} (Fig. 3*E*).

We then in vitro expressed/translated the human Syntaxin5 (Stx5) fused to a C-terminal opsin-tag (Stx5-op) in TNT reticulocyte lysate and added recombinant cytosolic fragments of MBP-WRBcc, GST-CAMLcyt, GST-*At*GET1cc, GST-G1IPcyt, and GST-G1IP^{4E}cyt together with pancreatic rough microsomes (RMs) to the reaction mix (here "cc" refers to the cytosolic coiled-coil domain in WRB or *At*GET1, and "cyt" refers to the cytosolic N terminus of CAML or G1IP). If the C terminus of Stx5 is exposed to the ER lumen, the opsin-tag becomes glycosylated, confirming successful membrane insertion. This assay had been used previously to demonstrate that the cytosolic coiled-coil domain of WRB and the cytosolic N terminus of CAML are capable of interfering with TA protein insertion (15, 33). The ratio of glycosylated and nonglycosylated Stx5-op, determined via the band shift in immunoblot analyses, revealed that the native cytosolic domain of G1IP, but not the reverse-charged mutant version (G1IP^{4E}cyt), prevents insertion of the in vitro translated TA protein Stx5 into ER-derived microsomes (Fig. 3 *F* and *G*). The interference of the native G1IP N terminus with the mammalian machinery for TA protein insertion suggests a conserved role for this domain in binding of TRC40/GET3. However, the coiled-coil motif of *At*GET1 does not inhibit membrane insertion, indicating that the binding sites or functional residues may have diverged from those of its ortholog in mammals. These functional differences are also evident from the yeast complementation assays (Fig. 2 *C* and *D*) and underpin the

Downloaded by guest on December 23, 2020

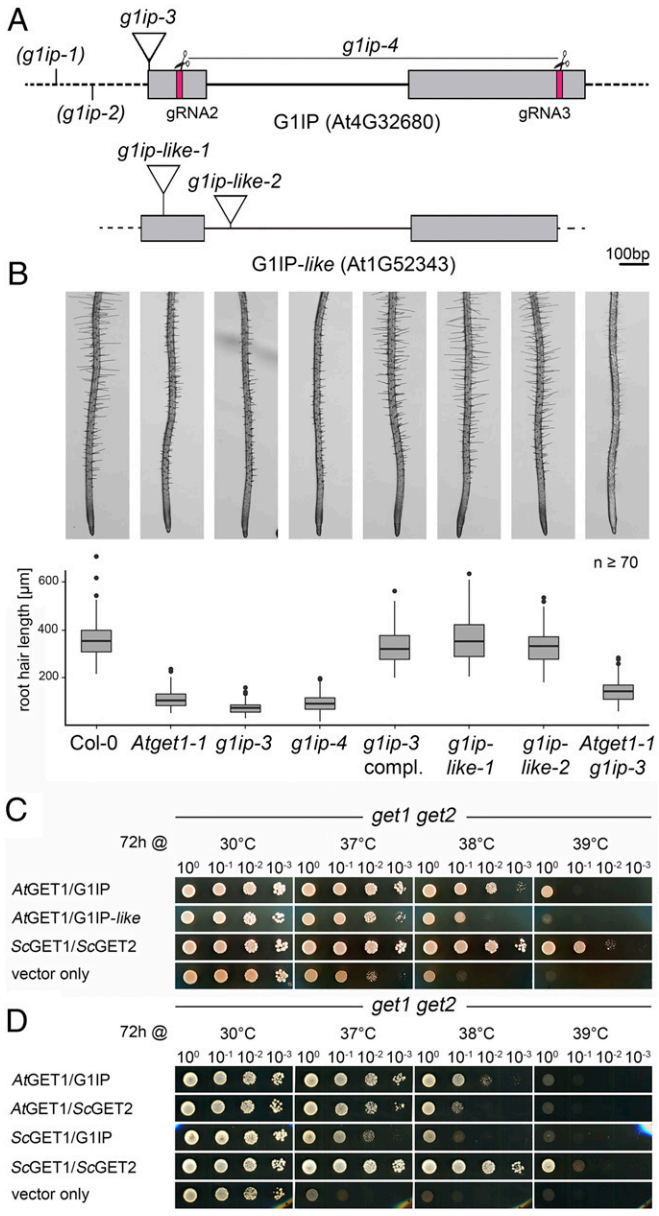

Fig. 2. G1IP phenocopies GET pathway mutants in *Arabidopsis* and partially complements a yeast GET receptor mutant in combination with *At*GET1. (*A*) Schematic illustration of the G1IP gene structure. The T-DNA in *g1ip-3* is inserted 5 bp downstream of the ATG with an additional insertion of AGTT. In *g1ip-1* and *g1ip-2*, the T-DNA insertion is within the 5′ UTR (dotted line), 333 bp and 201 bp upstream of the ATG, respectively. The *g1ip-4* line lacks the part between the CRISPR target sites indicated in red and symbolized by the scissors above. (*B*) Representative images of roots of 10-d-old mutant seedlings or complemented lines. Boxplots show quantification of root hair length of the 10 longest root hairs from at least seven seedlings per genotype. Center lines of boxes represent the median, with outer limits at the 25th and 75th percentiles. Tukey whiskers extend to 1.5 times the IQR. Outliers are depicted as black dots. (*C* and *D*) Yeast complementation analyses of the yeast *Δget1get2* double-deletion strain with different combinations of *A. thaliana* and *S. cerevisiae* proteins. Growth was monitored after 3 d in different temperatures. Genomic fragments of yeast GET1 and GET2 were used as positive controls, and empty vectors were used as negative controls. Since the T-DNA insertion in *g1ip-3* is located close to the ATG, and to confirm that the observed phenotype is a result of the insertion mutation in *G1IP*, we also performed CRISPR/Cas9 genome editing to generate a *g1ip* complete deletion mutant (*g1ip*-4). Root hair growth in this line was reduced, phenocopying the T-DNA line *g1ip-3* and thereby confirming that loss of G1IP leads to the reduced root hair growth. Simultaneous homozygous knockout of *At*GET1 and G1IP did not exacerbate the short root hair phenotype, indicating that both genes may be part of the same pathway (Fig. 2*B*). In contrast, *g1ip-like* T-DNA insertion lines exhibited WT-like root hair growth without any significant growth defects at later stages.

importance of the positively charged motif common to yeast Get2, mammalian CAML, and *Arabidopsis* G1IP. In summary, the experimental evidence presented here builds a strong case that G1IP is indeed *At*GET2, the *Arabidopsis* ortholog of yeast Get2 and mammalian CAML.

The GET Receptor Complex Shows Low Evolutionary Conservation. While interaction data and the root hair phenotype seem to confirm that *At*GET1 and G1IP/*At*GET2 act in the same pathway, sequence conservation of the two receptors is poor compared with opisthokont candidates (*SI Appendix*, Fig. S1*A*). Similarly, sequence conservation between fungal Get2 and mammalian CAML is equally poor, leading the authors who identified the connection to postulate that "mammalian cells have no genes homologous to Get2" (15).

Our finding of G1IP/*At*GET2, however, gave us an amino acid sequence with which we were able to identify numerous archaeplastidic homologs to compare with both fungal GET2 and metazoan CAML sequences (Fig. 4 and *SI Appendix*, Fig. S5). The structural similarities of the cross-kingdom proteins are striking regarding the putative number of TMDs (three), the topology of the proteins (cytosolic N terminus, luminal C terminus), and, most importantly, the positively charged N terminus (at least four arginine or lysine residues in a row; see motifs in Fig. 4). A recently published independent analysis using PSI-BLAST showed that the N-terminal Get3 interaction motif and the C-terminal membrane anchoring domain coevolve and allow the identification of candidate GET2 homologs from distantly related groups, including plants (32).

Our phylogenetic analysis of (putative) GET2 homologs from different eukaryotic groups clearly separates homologs from high-level groups (animals, fungi, and plants) (Fig. 4). Somewhat surprisingly, the Brassicales GET2 homologs are clustered separately at the bases of the eudicots. The G1IP-*like* proteins—which we now term GET2-*like*—are only found in the Rosids, clustering as a separate branch. The most striking difference within the N-terminal Get3 interaction motif is a conserved alanine residue in *At*GET2 and GET2 orthologs (*SI Appendix*, Fig. S6). *At*GET2-*like* instead features an additional glutamic acid residue, with the exception of the GET2-*like* protein from *Vitis vinifera*, which clusters at the base of the GET2-*like* proteins. The positions of the Brassicales GET2 and the GET2-*like* proteins might be explained by two whole-genome duplication events in the core Brassicales and the rosid lineages, respectively (34). These events might have led to differential loss of one copy in the Brassicales and evolution of GET2 in the rosids, although other possible explanations involving gene duplications and losses cannot be excluded.

Taken together, the structural similarities of *At*GET2 with either fungal GET2 or metazoan CAML, the network of physical interactions with other components of the *Arabidopsis* GET pathway, complementation of yeast knockouts, and the phenocopying of the loss-of-function *Arabidopsis* mutants strongly suggest that we have indeed identified the functional ortholog of GET2 in *Arabidopsis*. This discovery is consistent with a recent independent bioinformatic analysis (32) presenting candidate Get2/CAML homologs based on PSI-BLAST and allows recognition of GET2/CAML orthologs in other higher plant species or even basal Archaeplastida (*SI Appendix*, Table S1). In addition, we have identified a rosid lineage-specific homolog GET2-*like* that seems nonfunctional in the context of a plant GET pathway. This identification of the missing GET receptor in plants paves

Downloaded by guest on December 23, 2020

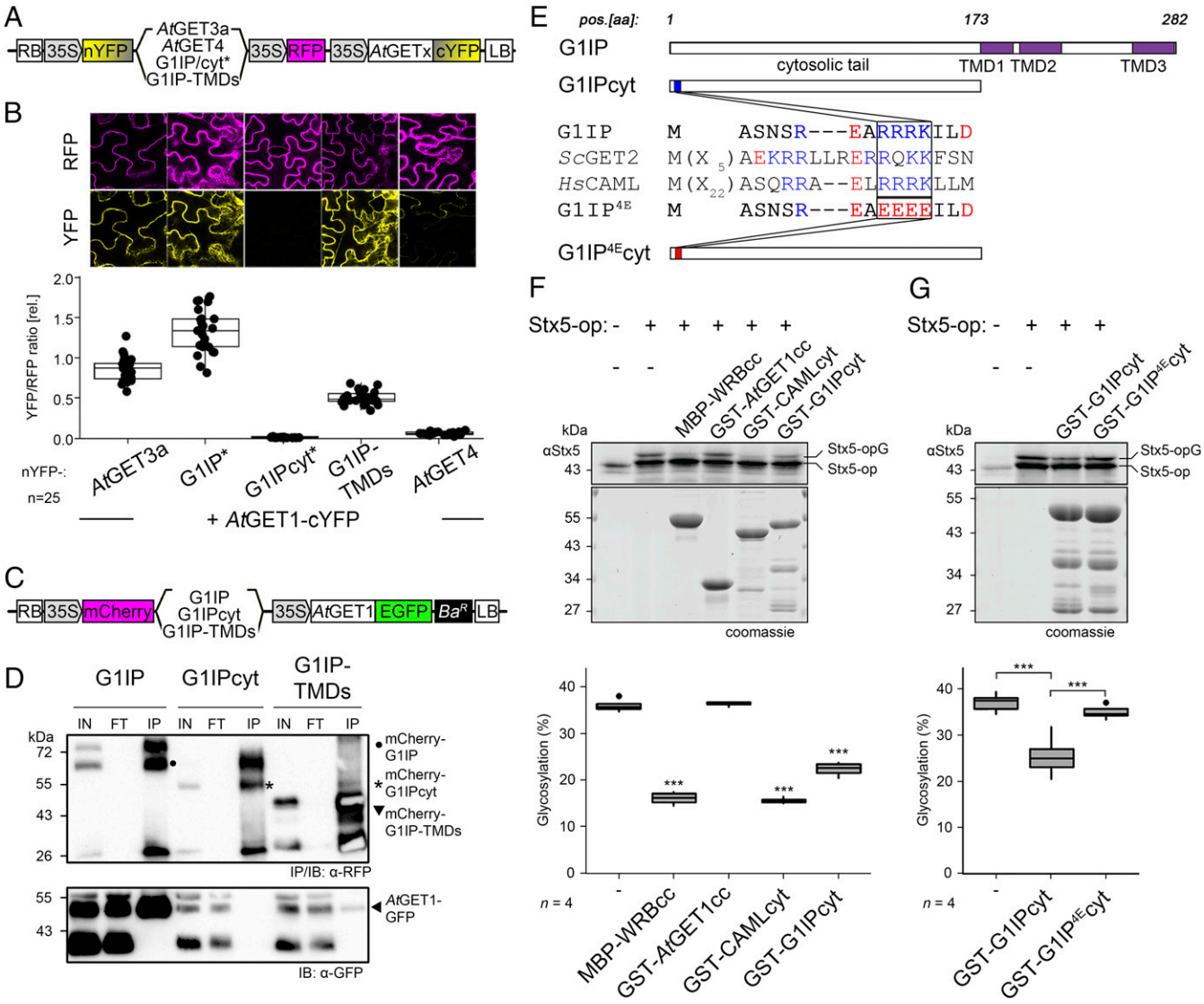

Fig. 3. The TMD region of G1IP mediates interaction with *At*GET1, and its cytosolic N terminus can interfere with the mammalian insertion system. (*A*) Schematic of the 2in1 rBiFC constructs used in *B*. G1IP and G1IPcyt were tagged C-terminally to avoid masking the N-terminal motif, marked with an asterisk. (*B*) rBiFC analysis using full-length and truncated versions of G1IP to test for interaction with *At*GET1. Exemplary CLSM images of transiently transfected *N. benthamiana* leaves are depicted. Mean fluorescence of at least 25 areas was measured in YFP and RFP channels, ratioed, and plotted to show YFP complementation. Center lines of boxes represent the median, with outer limits at the 25th and 75th percentiles. Tukey whiskers extend to 1.5 times the IQR. All values are depicted as black dots. (*C*) Schematic of the 2in1 FRET constructs used for co-IP in *D*. (*D*) Co-IP of full-length and truncated G1IP with *At*GET1, transiently expressed in *N. benthamiana* leaves. Protein extracts were immunoprecipitated with anti-RFP beads, and protein–protein interaction was detected by immunoblotting using anti-RFP and anti-GFP antibodies. IN, input; FT, flow-through; IP, immunoprecipitate. (*E*) Schematic representation of full-length, truncated, and mutated G1IP. The small alignment highlights a conserved cluster of positively charged amino acids and its charge-reversal mutation in the G1IP^{4E}cyt mutant, respectively. (*F* and *G*) Insertion assays into microsomal membranes. Stx5-op was translated in vitro in rabbit reticulocyte lysate and incubated with recombinant cytosolic fragments and pancreatic rough microsomes. Protein extracts were immunoblotted with anti-Stx5 antibody, and ER insertion was monitored via band shift reporting glycosylation. Boxplots show quantification of the immunoblots from four independent experiments. The center lines of boxes represent the median, with outer limits at the 25th and 75th percentiles. Tukey whiskers extend to 1.5 times the IQR. Outliers are depicted as black dots. ***$P < 0.001$, Student's *t* test.

the way for future research into pathway function and conservation in the eukaryotic domain of life. The absence of a more severe growth defect in GET pathway mutants of *Arabidopsis* remains puzzling and suggests the presence of additional membrane-targeting pathways and/or alternative functions of GET in plants.

Materials and Methods

Construct Generation and Plant Transformation. Most constructs were designed using Gateway technology or the Gateway-compatible cloning system 2in1 (25, 28, 35). For generation of the reverse-charged mutation of G1IP, three arginine and one lysine residue at positions 9 to 12 were exchanged with glutamic acid residues by site-directed mutagenesis as described previously (36).

PVAMP721>>GFP-myc-gG1IP was generated by classical cloning. The genomic fragment of G1IP from start codon to 261 bp downstream of the stop codon was PCR-amplified and inserted into the binary vector PVAMP721>>GFP-myc 3′ of myc.

Constructs were transformed into *Agrobacterium tumefaciens* GV3101 and used to transform Col-0 or respective mutant plants or infiltrated into *N. benthamiana* leaves (28). For the CRISPR construct, annealed oligos (forward: 5′-ATTG + protospacer; reverse: 5′-AAAC + rev-com protospacer) were

Downloaded by guest on December 23, 2020

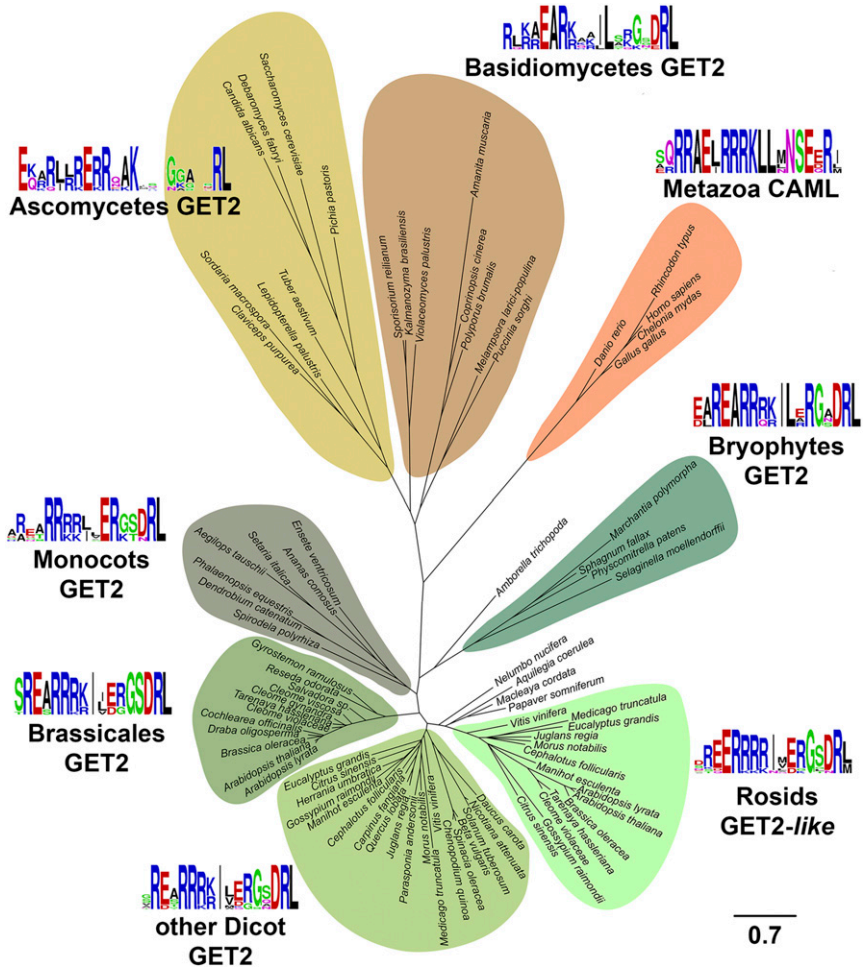

Fig. 4. Phylogenetic tree of GET2, CAML, and plant-specific GET2/GET2-like homologous proteins. A multiple alignment was generated with Muscle, and the phylogenetic tree was generated with MrBayes. The scale bar indicates expected substitutions per site. Bayesian probabilities of the branching pattern as well as accession numbers of the sequences used are provided in the corresponding cladogram in *SI Appendix*, Fig. S5.

sequentially ligated into pEn-2xChimera (37) via BbsI and Esp3I, respectively, followed by Gateway cloning into pEC-CAS9. Target sites (3′-AAGAAGTAG AATCGGAAGG-5′ and 5′-GATGATGGTGAAGAAGATAA-3′) were selected using CRISPR-P 2.0 (38). Constructs were transformed into Col-0 through floral dipping, and T1 plants were selected by red fluorescence.

Cloning of pEC-CAS9. A modified version of pDe-CAS9 (39) containing pOLE-OLE-tagRFP was digested using EcoRI. The EC promoter (40) and Cas9-attR1 fragment (39) were PCR-amplified separately with overlapping ends and combined with the vector backbone by In-Fusion cloning. The resulting vector, pEC-CAS9, was verified by restriction digest and sequencing.

Plant Material and Growth Conditions. All mutant and transgenic lines used in this work were in the Columbia (Col-0) background. T-DNA insertion lines were obtained from the Nottingham *Arabidopsis* Stock Centre (arabidopsis.info/), and insertion sites were verified by sequencing: Atget1-1 (SAIL_1210_E07) (22), Atget1-2 (GK_264D06), g1ip-1 (SALK_100089), g1ip-2 (SALK_119358), g1ip-3 (SALK_034959), g1ip-like-1 (SAIL_760_H02), and g1ip-like-2 (SALK_045533).

The CRISPR-based mutant line was generated with a dual sgRNA approach and screened using a visual selection marker (FAST-Red). Expression of Cas9 was driven by the egg cell-specific promoter EC1. Large-fragment deletion mutants were identified by PCR-based genotyping and verified by sequencing. The primer sets used for genotyping are listed in *SI Appendix*, Table S2.

Plants were grown at 22 °C under long-day conditions (16-h light/8-h dark) in soil or on half-strength Murashige and Skoog agar plates (1%; pH 5.7). Seeds were surface-sterilized with chlorine gas and stratified at 4 °C for 2 to 3 d in darkness to equalize germination.

rBiFC. Coding sequences were cloned into binary 2in1 rBiFC vectors (25) and transformed into *N. benthamiana* through syringe-mediated infiltration as described previously (28). Fluorescence intensities were measured at 3 d postinfiltration using a Leica SP8 confocal laser scanning microscope (YFP at 514 nm excitation (ex) and 520–560 nm emission (em); RFP at 561 nm ex and 565–620 nm em). YFP/RFP ratios were calculated from at least 21 different leaf regions and plotted using BoxPlotR (shiny.chemgrid.org/boxplotr/).

Subcellular Localization Analysis. Coding sequences were cloned into the Gateway vector pH7WGF2 (41) and cotransformed with an ER membrane marker (CD3-959 or CD3-960) into Col-0 through floral dipping. T1 plants were selected on hygromycin and leaves were imaged using a Leica SP8 confocal laser scanning microscope (GFP at 488 nm ex and 490–520 nm em; RFP at 561 nm ex and 565–620 nm em).

Root Hair Imaging and Measurements. Roots from 10-d-old seedlings grown on half-strength Murashige and Skoog agar plates were imaged with a Zeiss Axio Zoom V16 light microscope, and the length of the 10 longest root hairs from at least seven seedlings per genotype were measured using ImageJ ($n \geq 70$).

qPCR and RT-PCR Analysis. Total RNA was isolated from various plant tissues (100 mg) using the GeneMATRIX Universal RNA Purification Kit (Roboklon). Then 1 μg of each sample was converted into cDNA using the Protoscript II-First-Strand cDNA Synthesis Kit (New England BioLabs). cDNA was diluted 1:5 and quantified on the CFX96 Real-Time PCR System (Bio-Rad) using GoTag qPCR Master Mix (Promega) with SYBR Green. Transcript levels were calculated by the 2-ΔCt method and normalized to ACT2 expression. For

Downloaded by guest on December 23, 2020

semiquantitative RT-PCR, first-strand cDNA was amplified for 30 cycles and verified by agarose gel electrophoresis. Primer sets used for qPCR and RT-PCR are listed in *SI Appendix*, Table S2.

Yeast Complementation Assay. *Saccharomyces cerevisiae* genes with part of the 5′ and 3′ flanking regions (~0.5 kb) were cloned into low-copy number ARS/CEN vectors. *A. thaliana* genes (full-length CDS) were constitutively expressed from 2μ origin plasmids using the yeast PMA1 promoter. The *Δget1get2* double-deletion mutant (MATa his3Δ1 leu2Δ0 met15Δ0 ura3Δ0 ygl020c::KanR yer083c::NatR) (19) was cotransformed as described previously (42) and dropped in 10-fold serial dilutions in vector-selective medium (complete supplement medium [CSM] L-, U-) and grown at different temperatures for 3 d.

Creation of 2in1 Co-IP Vectors (mVenus/3xHA). The new set of Gateway-compatible 2in1 co-IP vectors (pCoIP-2in1-NN, -NC, -CN, -CC) was generated by classical cloning. RPS5a driven N- and C-terminally 3xHA-tagged R3R2 expression cassettes were generated by replacing the 35S promoter in pUC57-Tec-*N*-HA and pUC35S-R3R2-3xHA (NarI/HpaI) with the RPS5a promoter (1,684 bp), which was PCR-amplified and flanked by NarI-StuI/NaeI (blunt end, like HpaI) restriction sites (pUC-RPS-HA-lacZ and pUC-RPS-lacZ-HA). The resulting expression cassettes were excised via StuI and inserted into pBBb (35) via EcoICRI (blunt end, like StuI) to yield the intermediate vectors pCoIP-intA and pCoIP-intB. Another pUC helper vector, pUC-RPS5a::R1R4, was created by introducing the RPS5a promoter via NarI/NaeI into pUC57-Tec-*N*-myc. mVenus was PCR- amplified (NaeI/SpeI) and inserted via NaeI/HpaI 5′ of the R1R4 expression cassette (pUC-RPS5-Ven-R1R4). To introduce mVenus at the C terminus, PCR-amplified mVenus-TGA (NaeI/PsiI) was inserted into pUC-RPS5a::R1R4 via PsiI (pUC-RPS5-R1R4-Ven). For the final 2in1 vector assembly, the intermediate vectors pCoIP-intA and pCoIP-intB were linearized via AfeI, and the R3R2 and R1R4 expression cassettes were inserted (StuI/FspI). All vectors were verified by restriction digest and sequencing.

Co-IP Analysis: Stable Gene Expression in *Arabidopsis*. Here 3 g of *Arabidopsis* seedlings were harvested after 10 d under continuous light. Cells were lysed by mortar grinding in liquid nitrogen and thawed in lysis buffer (50 mM Tris pH 7.5, 150 mM NaCl, 1% Triton X-100; 1.43 mL/g) supplemented with protease inhibitor mixture (cOmplete EDTA-free; Roche). Cell debris was removed by centrifugation and filtration through two layers of Miracloth. Then 2.5 mL of supernatant was mixed with 2 mL of lysis buffer and incubated with anti-GFP beads (25 μL, GFP-trap; Chromotek) for 2 h at 4 °C under mild rotation. Beads were collected by centrifugation, transferred onto spin columns, and washed six times with washing buffer (50 mM Tris pH 7.5, 150 mM NaCl, and 0.5% Triton X-100) supplemented with protease inhibitor mixture. (Co-) Immunoprecipitated proteins were eluted with 2× Laemmli buffer (+ 3% β-mercaptoethanol) at 80 °C for 5 min, separated by sodium dodecyl sulfate polyacrylamide gel electrophoresis (SDS-PAGE), and detected by Western blot analysis (anti-HA peroxidase from rat IgG1 [Roche, 1:1,000], anti-GFP from mouse IgG1κ [Roche, 1:1,000], and anti-mouse IgG [Fc-specific] produced in goat [Sigma-Aldrich, 1:10,000]).

Co-IP Analysis: Transient Gene Expression in *N. Benthamiana*. FRET 2in1 destination vectors containing monomeric enhanced green fluorescent protein (mEGFP) and mCherry (pFRETgc-2in1) were used to transiently express recombinant proteins in *N. benthamiana* for co-IP analysis (28, 35). Leaf material (150 to 600 mg) was harvested at 3 d postinfiltration and homogenized after freezing in liquid nitrogen. Lysis buffer (25 mM Tris pH 8.0, 150 mM NaCl, 1% Nonidet P-40, and 0.5% Na-deoxycholate) supplemented with protease inhibitor mixture and 2 mM DTT was added and incubated for 1 h at 4 °C with mild rotation. After centrifugation, the supernatant was mixed with 20 to 25 μL of RFP beads (RFP-trap; Chromotek) and then incubated for 1 h at 4 °C with mild rotation. Beads were collected by centrifugation, transferred onto spin columns, and rinsed twice with lysis buffer, followed by six washes with wash buffer (25 mM Tris pH 8.0 and 150 mM NaCl). (Co-) Immunoprecipitated proteins were eluted with 2× Laemmli buffer (+ 3.5% β-mercaptoethanol) and then heated at 65 °C for 15 min (membrane proteins) or at 95 °C for 5 min (soluble proteins). Proteins were separated by SDS-PAGE and detected by Western blot analysis (anti-RFP from mouse [Chromotek, 1:2,500], anti-GFP from mouse IgG1κ [Roche, 1:1,000], and anti-mouse IgG [Fc-specific] produced in goat [Sigma-Aldrich, 1:10,000]).

Protein Purification. *Escherichia coli* BL21 DE3 cells were transformed with GST-tagged versions of the cytosolic portions of *At*GET1 and G1IP. Expression was induced with 200 μM isopropyl β-d-1-thiogalactopyranoside in 1 L of 2YT-3% glycerol cultures at an OD_{600} of 0.5. The cell pellet was collected after 3 h at 30 °C and lysed by sonification in ice-cold purification buffer (20 mM Hepes, 2% glycerol, 150 mM potassium acetate, 5 mM magnesium acetate, 1 mM EDTA, 1 mM DTT, and 1 mM PMSF, pH 7.4). The lysate was cleared by centrifugation at 100.000 × *g* for 30 min and then incubated with glutathione Sepharose resin (GE Healthcare). After 1 h of binding, the resin was washed sequentially with purification buffer, purification buffer containing 5 mM ATP, and purification buffer for 10 min. GST-tagged protein was eluted with purification buffer containing 20 mM glutathione.

Expression of the N-terminal domain of CAML (GST-CAMLcyt) and the WRB coiled-coil domain (MBP-WRBcc) was carried out as described previously (15, 33).

Stx5-op In Vitro Transcription/Translation and Insertion Assay into Microsomes. Reactions were performed in the TnT Quick Coupled Transcription/Translation System (Promega) as described previously (17, 43) with some modifications. Stx5-op synthesis was induced with 100 ng of pGem3z-Stx5-op in 4.5 μL of TNT reticulocyte lysate for 90 min at 30 °C. Where indicated, equimolar amounts (5 μM) of recombinant cytosolic fragments (MBP-WRBcc, GST-CAMLcyt, GST-*At*GET1, GST-G1Ipcyt, and GST-G1IP4Ecyt) and pancreatic RMs were added to the reaction mix after Stx5 translation was completed. After 90 min of incubation at 30 °C with the RMs, the reaction was stopped with SDS loading buffer, followed by analysis by Western blot with rabbit anti-Stx5 antibody (Synaptic Systems; 110053).

Multiple Alignments and Construction of Phylogenetic Trees. Multiple alignments were generated with Muscle in MEGA6.06 (44, 45). Phylogenetic analyses were performed with MrBayes 3.2.7a, with 500,000 generations (46).

Data Availability. All study data are included in the main text and *SI Appendix*.

ACKNOWLEDGMENTS. We thank Simon Klesen for cloning and providing the pEC-CAS9 vector and Eva Schwörzer and Laure Grefen for excellent technical assistance. The IP-MS analysis was performed at the Proteomics facility of the University of Tübingen; we are grateful to Mirita Franz for helpful advice during data analyses. This project was supported through a Carl Zeiss doctoral fellowship to D.G.M. and funding from the German Research Foundation to M.N. (NO 407/7-1), B.S. (SFB1190-P04), M.B. (SFB1101-B01) and C.G. (Emmy Noether fellowship GR 4251/1-1, GR 4251/1-2, and SFB1101-A06).

1. S. Shao, R. S. Hegde, Membrane protein insertion at the endoplasmic reticulum. *Annu. Rev. Cell Dev. Biol.* **27**, 25–56 (2011).
2. V. Lipka, C. Kwon, R. Panstruga, SNARE-ware: The role of SNARE-domain proteins in plant biology. *Annu. Rev. Cell Dev. Biol.* **23**, 147–174 (2007).
3. G. Jürgens *et al*., Plant cytokinesis: A tale of membrane traffic and fusion. *Biochem. Soc. Trans.* **43**, 73–78 (2015).
4. R. Jahn, R. H. Scheller, SNAREs—Engines for membrane fusion. *Nat. Rev. Mol. Cell Biol.* **7**, 631–643 (2006).
5. U. S. Chio, H. Cho, S. O. Shan, Mechanisms of tail-anchored membrane protein targeting and insertion. *Annu. Rev. Cell Dev. Biol.* **33**, 417–438 (2017).
6. J. W. Chartron, C. J. Suloway, M. Zaslaver, W. M. Clemons Jr, Structural characterization of the Get4/Get5 complex and its interaction with Get3. *Proc. Natl. Acad. Sci. U.S.A.* **107**, 12127–12132 (2010).
7. Y. W. Chang *et al*., Crystal structure of Get4-Get5 complex and its interactions with Sgt2, Get3, and Ydj1. *J. Biol. Chem.* **285**, 9962–9970 (2010).
8. G. Bozkurt *et al*., Structural insights into tail-anchored protein binding and membrane insertion by Get3. *Proc. Natl. Acad. Sci. U.S.A.* **106**, 21131–21136 (2009).
9. A. Mateja *et al*., The structural basis of tail-anchored membrane protein recognition by Get3. *Nature* **461**, 361–366 (2009).
10. M. E. Rome, M. Rao, W. M. Clemons, S. O. Shan, Precise timing of ATPase activation drives targeting of tail-anchored proteins. *Proc. Natl. Acad. Sci. U.S.A.* **110**, 7666–7671 (2013).
11. H. B. Gristick *et al*., Crystal structure of ATP-bound Get3-Get4-Get5 complex reveals regulation of Get3 by Get4. *Nat. Struct. Mol. Biol.* **21**, 437–442 (2014).
12. K. Kubota, A. Yamagata, Y. Sato, S. Goto-Ito, S. Fukai, Get1 stabilizes an open dimer conformation of get3 ATPase by binding two distinct interfaces. *J. Mol. Biol.* **422**, 366–375 (2012).
13. F. Wang, C. Chan, N. R. Weir, V. Denic, The Get1/2 transmembrane complex is an endoplasmic-reticulum membrane protein insertase. *Nature* **512**, 441–444 (2014).
14. S. Stefer *et al*., Structural basis for tail-anchored membrane protein biogenesis by the Get3-receptor complex. *Science* **333**, 758–762 (2011).
15. Y. Yamamoto, T. Sakisaka, Molecular machinery for insertion of tail-anchored membrane proteins into the endoplasmic reticulum membrane in mammalian cells. *Mol. Cell* **48**, 387–397 (2012).

Downloaded by guest on December 23, 2020

16. S. F. Colombo *et al*., Tail-anchored protein insertion in mammals: Function and reciprocal interactions OF the two subunits of the TRC40 receptor. *J. Biol. Chem.* **291**, 15292–15306 (2016).
17. J. Rivera-Monroy *et al*., Mice lacking WRB reveal differential biogenesis requirements of tail-anchored proteins in vivo. *Sci. Rep.* **6**, 39464 (2016).
18. H. J. F. Carvalho, A. Del Bondio, F. Maltecca, S. F. Colombo, N. Borgese, The WRB subunit of the Get3 receptor is required for the correct integration of its partner CAML into the ER. *Sci. Rep.* **9**, 11887 (2019).
19. M. Schuldiner *et al*., The GET complex mediates insertion of tail-anchored proteins into the ER membrane. *Cell* **134**, 634–645 (2008).
20. S. Stefanovic, R. S. Hegde, Identification of a targeting factor for posttranslational membrane protein insertion into the ER. *Cell* **128**, 1147–1159 (2007).
21. R. Srivastava, B. E. Zalisko, R. J. Keenan, S. H. Howell, The GET system inserts the tail-anchored protein, SYP72, into endoplasmic reticulum membranes. *Plant Physiol.* **173**, 1137–1145 (2017).
22. S. Xing *et al*., Loss of GET pathway orthologs in Arabidopsis thaliana causes root hair growth defects and affects SNARE abundance. *Proc. Natl. Acad. Sci. U.S.A.* **114**, E1544–E1553 (2017).
23. K. L. Auld *et al*., The conserved ATPase Get3/Arr4 modulates the activity of membrane-associated proteins in Saccharomyces cerevisiae. *Genetics* **174**, 215–227 (2006).
24. U. Omasits, C. H. Ahrens, S. Müller, B. Wollscheid, Protter: Interactive protein feature visualization and integration with experimental proteomic data. *Bioinformatics* **30**, 884–886 (2014).
25. C. Grefen, M. R. Blatt, A 2in1 cloning system enables ratiometric bimolecular fluorescence complementation (rBiFC). *Biotechniques* **53**, 311–314 (2012).
26. J. Mergner *et al*., Mass-spectrometry-based draft of the Arabidopsis proteome. *Nature* **579**, 409–414 (2020).
27. S. Xing, N. Wallmeroth, K. W. Berendzen, C. Grefen, Techniques for the analysis of protein-protein interactions in vivo. *Plant Physiol.* **171**, 727–758 (2016).
28. D. G. Mehlhorn, N. Wallmeroth, K. W. Berendzen, C. Grefen, 2in1 vectors improve in planta BiFC and FRET analyses. *Methods Mol. Biol.* **1691**, 139–158 (2018).
29. Y. W. Chang *et al*., Interaction surface and topology of Get3-Get4-Get5 protein complex, involved in targeting tail-anchored proteins to endoplasmic reticulum. *J. Biol. Chem.* **287**, 4783–4789 (2012).
30. F. Vilardi, M. Stephan, A. Clancy, A. Janshoff, B. Schwappach, WRB and CAML are necessary and sufficient to mediate tail-anchored protein targeting to the ER membrane. *PLoS One* **9**, e85033 (2014).
31. K. Powis *et al*., Get3 is a holdase chaperone and moves to deposition sites for aggregated proteins when membrane targeting is blocked. *J. Cell Sci.* **126**, 473–483 (2013).
32. N. Borgese, Searching for remote homologs of CAML among eukaryotes. *Traffic* **21**, 647–658 (2020).
33. F. Vilardi, H. Lorenz, B. Dobberstein, WRB is the receptor for TRC40/Asna1-mediated insertion of tail-anchored proteins into the ER membrane. *J. Cell Sci.* **124**, 1301–1307 (2011).
34. M. S. Barker, H. Vogel, M. E. Schranz, Paleopolyploidy in the Brassicales: Analyses of the Cleome transcriptome elucidate the history of genome duplications in Arabidopsis and other Brassicales. *Genome Biol. Evol.* **1**, 391–399 (2009).
35. A. Hecker *et al*., Binary 2in1 vectors improve in planta (co-) localisation and dynamic protein interaction studies. *Plant Physiol.* **168**, 776–787 (2015).
36. A. Karnik, R. Karnik, C. Grefen, SDM-Assist software to design site-directed mutagenesis primers introducing "silent" restriction sites. *BMC Bioinformatics* **14**, 105 (2013).
37. J. Durr, R. Papareddy, K. Nakajima, J. Gutierrez-Marcos, Highly efficient heritable targeted deletions of gene clusters and non-coding regulatory regions in Arabidopsis using CRISPR/Cas9. *Sci. Rep.* **8**, 4443 (2018).
38. H. Liu *et al*., CRISPR-P 2.0: An improved CRISPR-Cas9 tool for genome editing in plants. *Mol. Plant* **10**, 530–532 (2017).
39. F. Fauser, S. Schiml, H. Puchta, Both CRISPR/Cas-based nucleases and nickases can be used efficiently for genome engineering in Arabidopsis thaliana. *Plant J. Cell Mol. Biol.* **79**, 348–359 (2014).
40. Z. P. Wang *et al*., Egg cell-specific promoter-controlled CRISPR/Cas9 efficiently generates homozygous mutants for multiple target genes in Arabidopsis in a single generation. *Genome Biol.* **16**, 144 (2015).
41. M. Karimi, A. Depicker, P. Hilson, Recombinational cloning with plant gateway vectors. *Plant Physiol.* **145**, 1144–1154 (2007).
42. L. Y. Asseck, N. Wallmeroth, C. Grefen, ER membrane protein interactions using the split-ubiquitin system (SUS). *Methods Mol. Biol.* **1691**, 191–203 (2018).
43. J. Pfaff *et al*., Emery-Dreifuss muscular dystrophy mutations impair TRC40-mediated targeting of emerin to the inner nuclear membrane. *J. Cell Sci.* **129**, 502–516 (2016).
44. K. Tamura, G. Stecher, D. Peterson, A. Filipski, S. Kumar, MEGA6: Molecular evolutionary genetics analysis version 6.0. *Mol. Biol. Evol.* **30**, 2725–2729 (2013).
45. R. C. Edgar, MUSCLE: Multiple sequence alignment with high accuracy and high throughput. *Nucleic Acids Res.* **32**, 1792–1797 (2004).
46. F. Ronquist, J. P. Huelsenbeck, MrBayes 3: Bayesian phylogenetic inference under mixed models. *Bioinformatics* **19**, 1572–1574 (2003).

Downloaded by guest on December 23, 2020

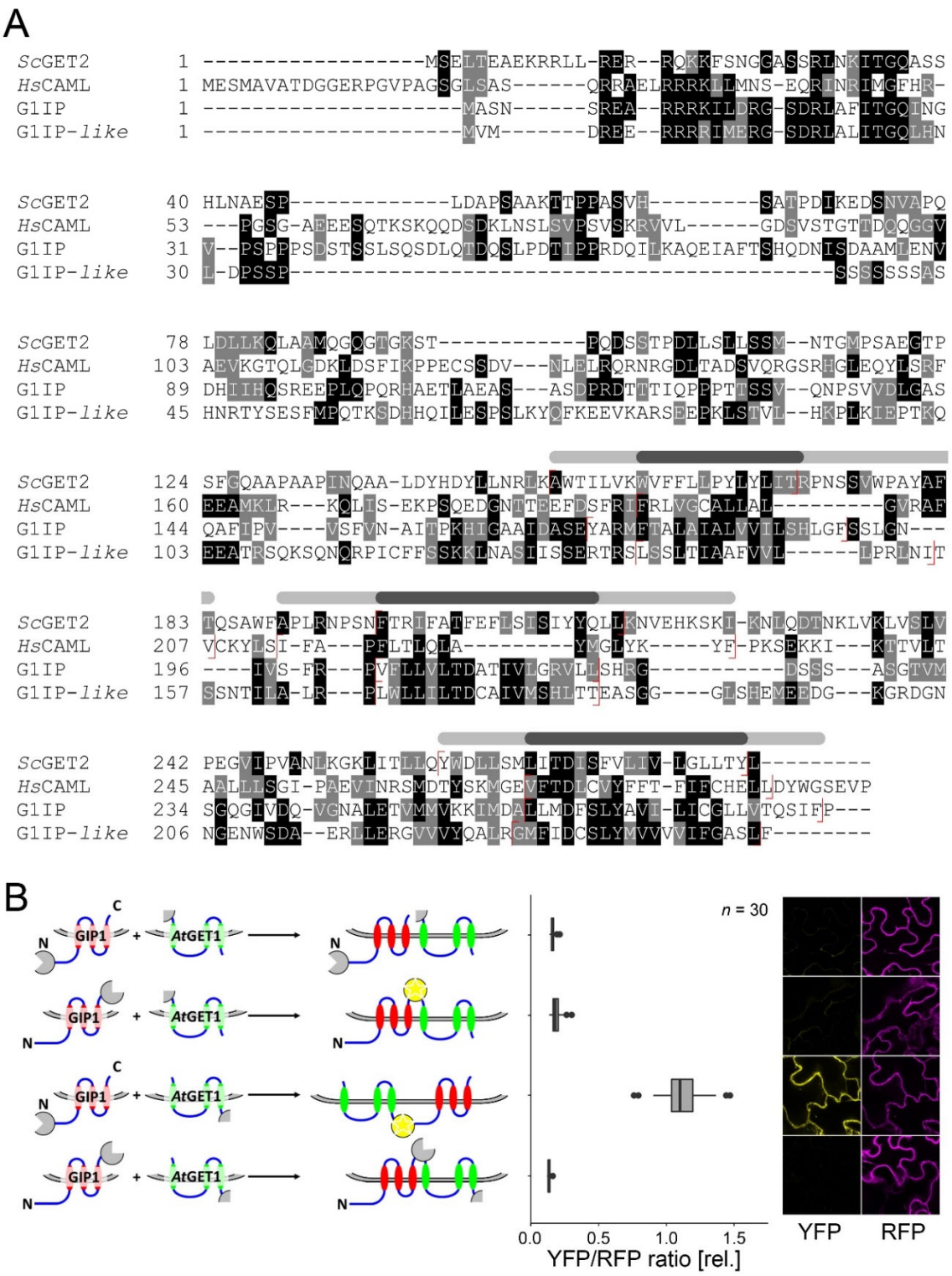

Supplemental Figure S1: (A) Multiple sequence alignment of *Hs*Caml, *Sc*GET2, *Arabidopsis* G1IP and G1IP-*like*. Background color within the aligned sequences indicates identical (black) or similar (gray) amino acids. The grey bars above the aligned sequences represent the predicted transmembrane domain helices (Protter). Red horizontal lines within each sequence mark beginning and end of the predicted helices. (B) Topological analysis of the putative receptor pair *At*GET1 and G1IP. Four different orientations for N-terminal or C-terminal tagging of YFP halves were fused to either *At*GET1 or G1IP and analysed via rBiFC for complementation of signal to verify presence of both termini in either cytosolic or luminal side of the ER membrane. In principle, two combinations should show fluorescence, however, only N-terminally tagged G1IP and C-terminally tagged *At*GET1 yielded significant YFP complementation. Failure of fluorescence complementation in the reciprocal interaction pair may be due to a different pH or redox state in the ER lumen or masking of the AtGET1 N-terminus may lead to incomplete or aberrant membrane insertion.

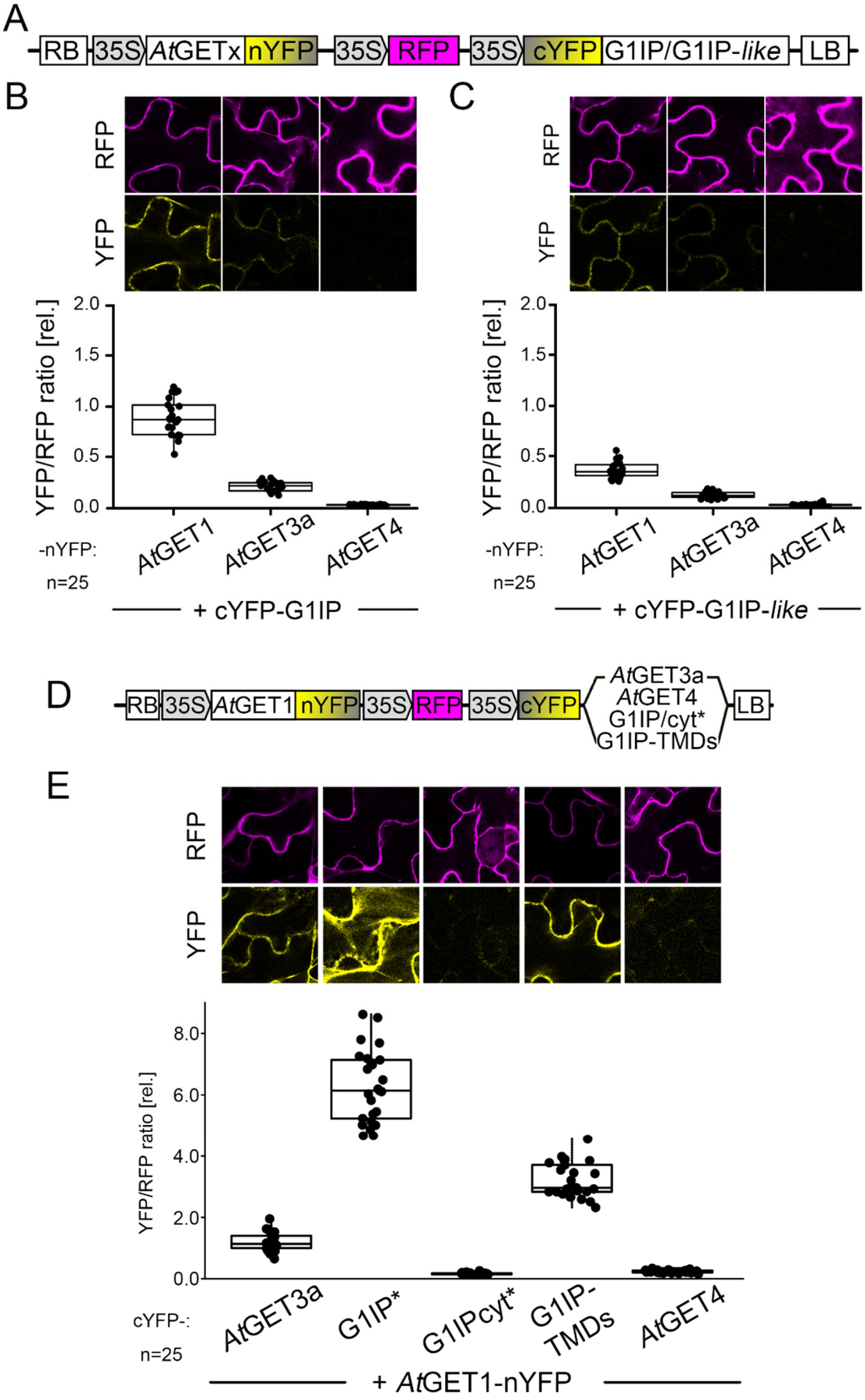

Supplemental Figure S2: (A-C) ratiometric Bimolecular Fluorescence analyses with reciprocal fusion of probes (fluorescent split-fragments) corresponding to Figure 1L, M. (D, E) Reciprocal fusion of probes corresponding to Figure 3B.

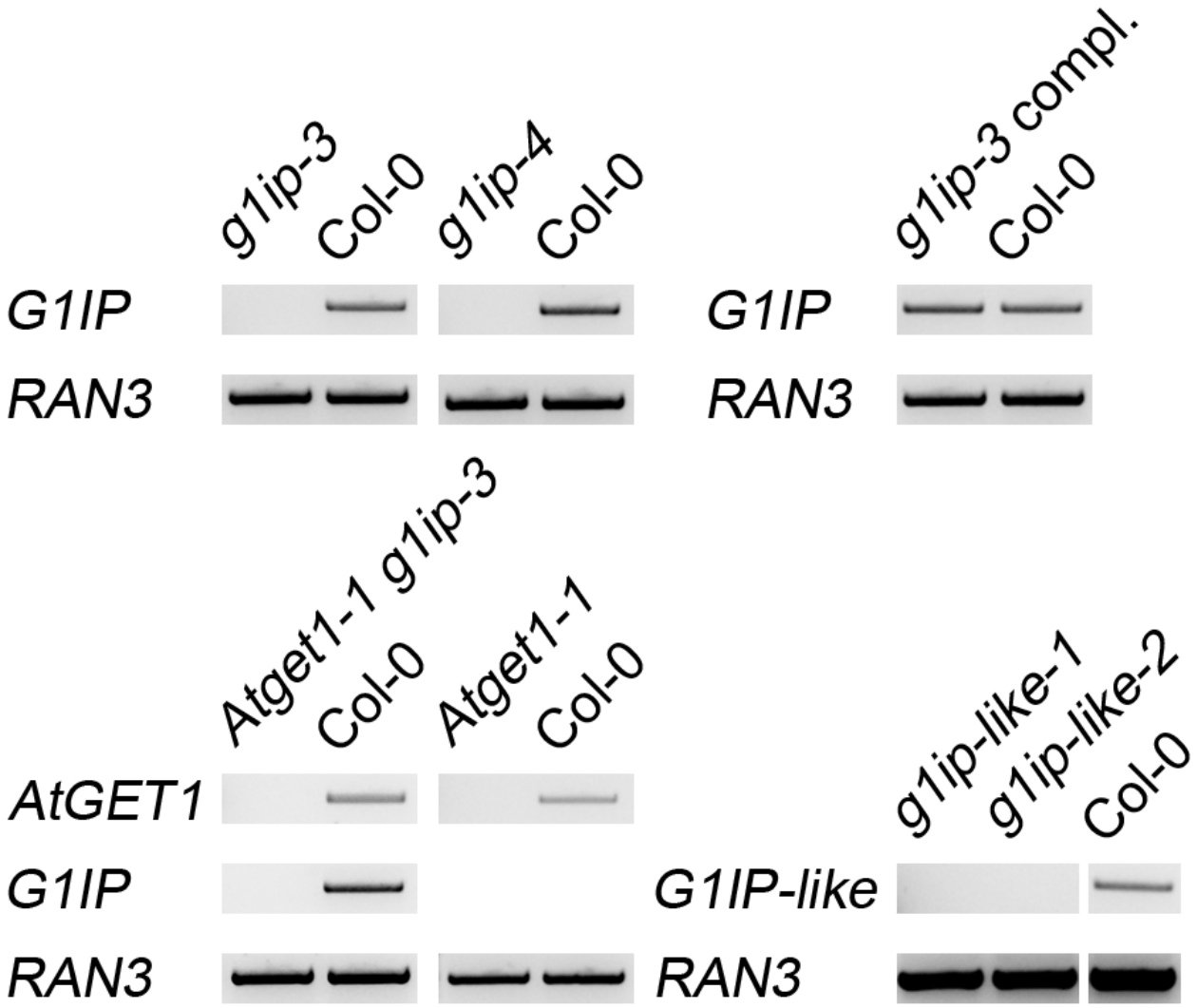

Supplemental Figure S3: RT-PCR analysis of transcript levels in plant lines used for analysis of root hair growth (Figure 2B). RAN3 was used as control. Note: the cDNA for *g1ip-like* lines was generated from flower tissue as G1IP-*like* cannot be detected in cDNA samples acquired from Col-0 whole seedlings.

Supplemental Figure S4: Multiple sequence alignment of the conserved N-terminal motif of Archaeplastida and homologous fungal GET2 and metazoan CAML proteins

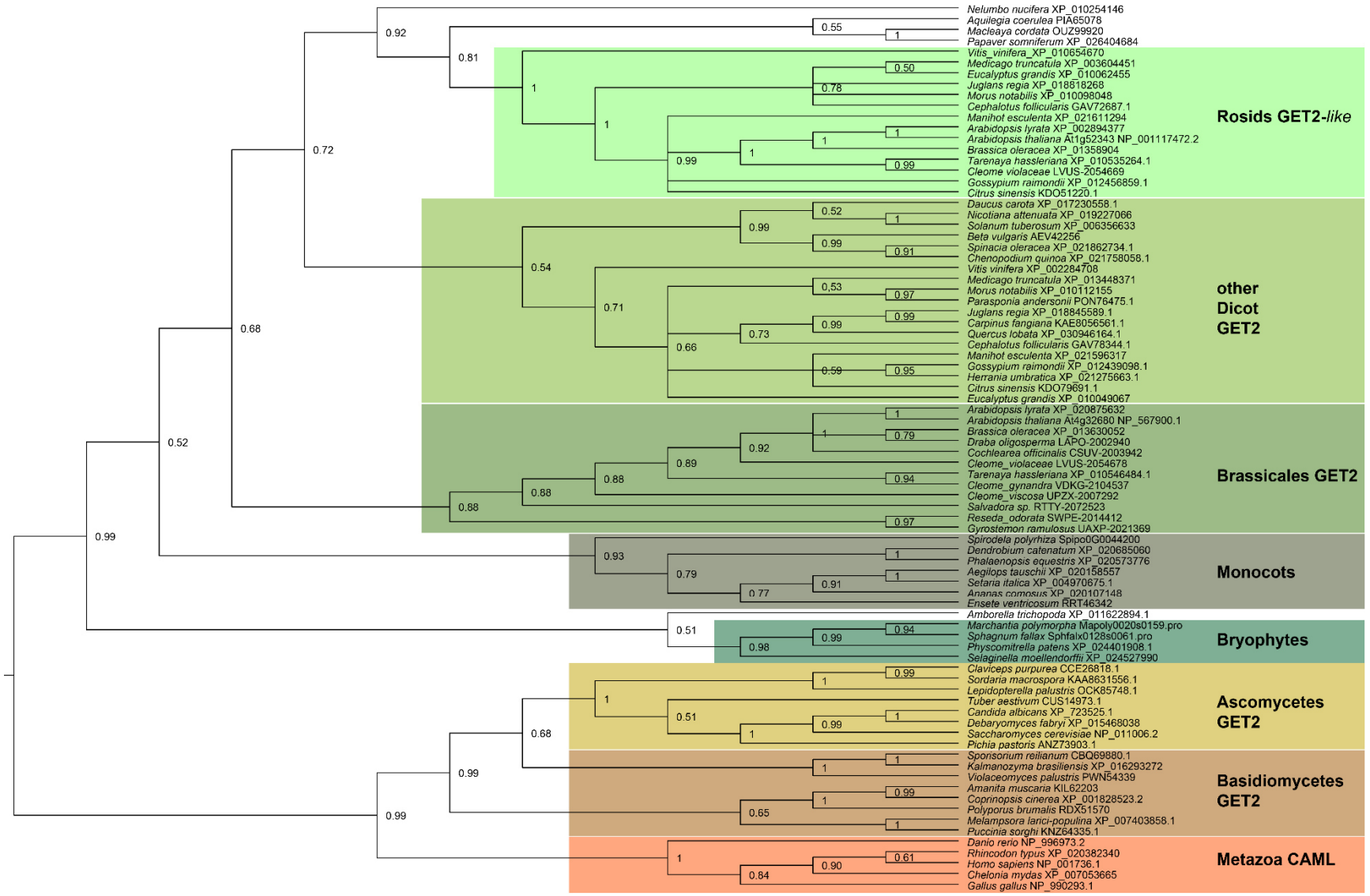

Supplemental Figure S5: Phylogenetic tree of GET2 and G1IP-*like* homologous proteins. A multiple alignment was generated with Muscle and the phylogenetic tree generated with MrBayes. Bayesian probabilities are given at the branches.
The tree was rooted with the branch leading to the animal/fungal (ascomycota and basidiomycota) lineages. Accession numbers or locus tag numbers or sequence numbers from the 1000 plant transcriptomes initiative [1] are given after the species names.

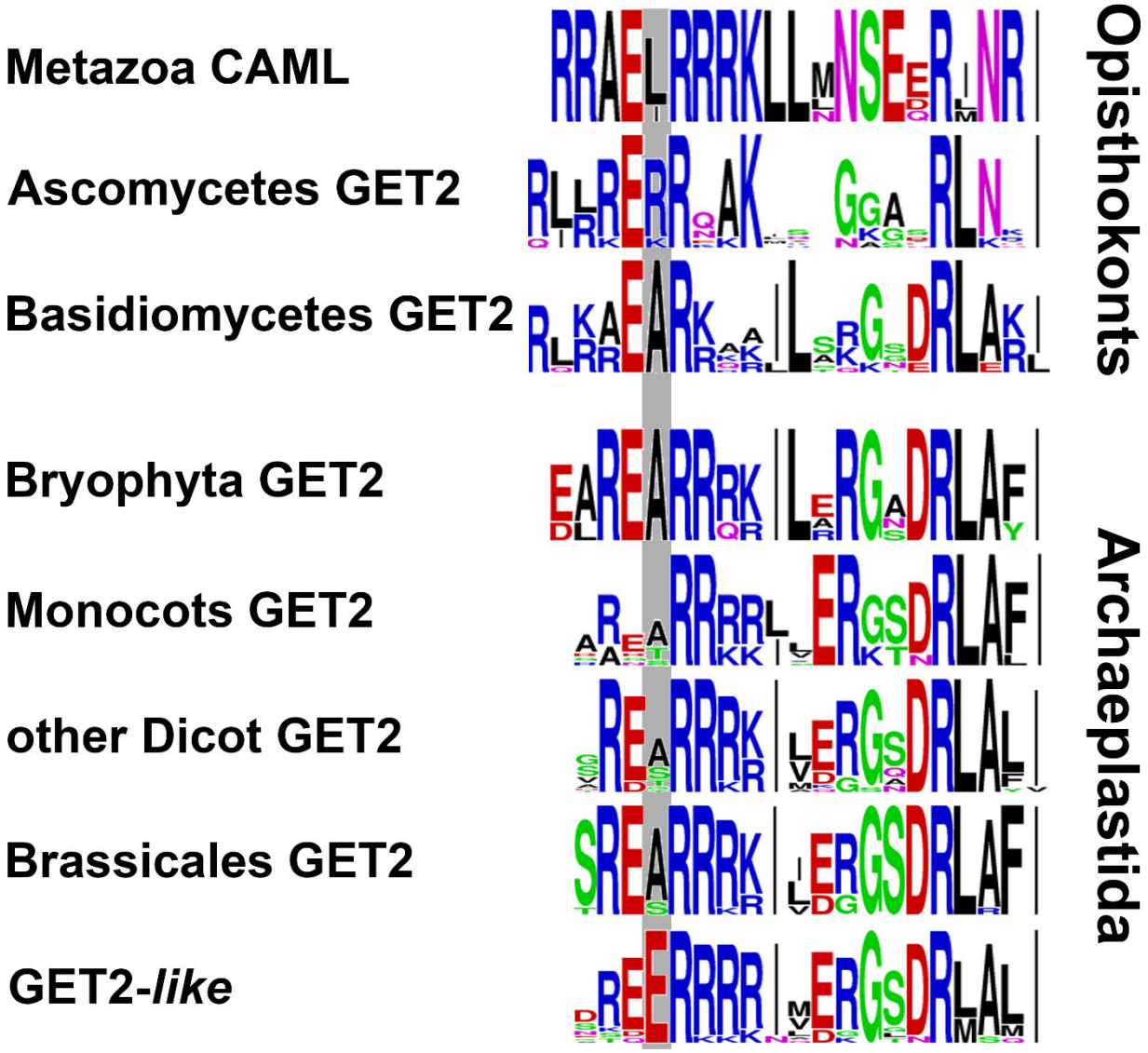

Supplemental Figure S6: N-terminal sequence motifs of GET2, CAML and GET2-like homologs assembled from the alignment in Figure S4 and visualised using Weblogo (https://weblogo.berkeley.edu/logo.cgi). The grey vertical bar underneath the motifs highlights the conserved Glutamic acid residue in G1IP-*like* sequences opposed to all other eukaryotic homologs.

Table S1. Accession numbers of sequences used for multiple alignments and phylogenetic analyses of GET2/CAML orthologs of Archaeplastida and Opisthokonts.

Group	Species	Accession number or locus tag number
Rosida GET2-*like*	*Arabidopsis lyrata*	XP_002894377
	Arabidopsis thaliana	NP_001117472.2
	Brassica oleracea	XP_01358904
	Cephalotus follicularis	GAV72687.1
	Citrus sinensis	KDO51220.1
	Cleome violaceae	LVUS-2054669[1]
	Eucalyptus grandis	XP_010062455
	Gossypium raimondii	XP_012456859.1
	Juglans regia	XP_018818268
	Manihot esculenta	XP_021611294
	Medicago truncatula	XP_003604451
	Morus notabilis	XP_010098048
	Tarenaya hassleriana	XP_010535264.1
	Vitis_vinifera	XP_010654670
Brassicales GET2	*Arabidopsis lyrata*	XP_020875632
	Arabidopsis thaliana	NP_567900.1
	Brassica oleracea	XP_013630052
	Cleome_gynandra	VDKG-2104537[1]
	Cleome_violaceae	LVUS-2054678[1]
	Cleome_viscosa	UPZX-2007292[1]
	Cochlearea officinalis	CSUV-2003942[1]
	Draba oligosperma	LAPO-2002940[1]
	Gyrostemon ramulosus	UAXP-2021369[1]
	Reseda_odorata	SWPE-2014412[1]
	Salvadora sp.	RTTY-2072523[1]
	Tarenaya hassleriana	XP_010546484.1
other Dicot GET2	*Beta vulgaris*	AEV42256
	Carpinus fangiana	KAE8056561.1
	Cephalotus follicularis	GAV78344.1
	Chenopodium quinoa	XP_021758058.1
	Citrus sinensis	KDO79691.1
	Daucus carota	XP_017230558.1
	Eucalyptus grandis	XP_010049067
	Gossypium raimondii	XP_012439098.1
	Herrania umbratica	XP_021275663.1
	Juglans regia	XP_018845589.1
	Manihot esculenta	XP_021596317
	Medicago truncatula	XP_013448371
	Morus notabilis	XP_010112155
	Nicotiana attenuata	XP_019227066
	Parasponia andersonii	PON76475.1
	Quercus lobata	XP_030946164.1
	Spinacia oleracea	XP_021862734.1
	Solanum tuberosum	XP_006356633
	Vitis vinifera	XP_002284708
	Aquilegia coerulea	PIA65078
	Macleaya cordata	OUZ99920
	Nelumbo nucifera	XP_010254146
	Papaver somniferum	XP_026404684
Monocots	*Aegilops tauschii*	XP_020158557
	Ananas comosus	XP_020107148
	Dendrobium catenatum	XP_020685060
	Ensete ventricosum	RRT46342
	Phalaenopsis equestris	XP_020573776
	Setaria italica	XP_004970675.1
	Spirodela polyrhiza	Spipo0G0044200
	Ginkgo biloba	SGTW-2038521[1]

Gymnosperms etc.	*Metasequoia glyptostroboides*	NRXL-2062375[1]
	Picea engelmanii	AWQB-2010070[1]
	Amborella trichopoda	XP_011622894.1
Bryophyta	*Marchantia polymorpha*	Mapoly0020s0159
	Physcomitrella patens	XP_024401908.1
	Sphagnum fallax	Sphfalx0128s0061
	Selaginella moellendorffii	XP_024527990
Ascomycetes	*Candida albicans*	XP_723525.1
	Claviceps purpurea	CCE26818.1
	Debaryomyces fabryi	XP_015468038
	Lepidopterella palustris	OCK85748.1
	Pichia pastoris	ANZ73903.1
	Saccharomyces cerevisiae	NP_011006.2
	Sordaria macrospora	KAA8631556.1
	Tuber aestivum	CUS14973.1
Basidiomycetes	*Amanita muscaria*	KIL62203
	Coprinopsis cinerea	XP_001828523.2
	Kalmanozyma brasiliensis	XP_016293272
	Melampsora larici-populina	XP_007403858.1
	Polyporus brumalis	RDX51570
	Puccinia sorghi	KNZ64335.1
	Sporisorium reilianum	CBQ69880.1
	Violaceomyces palustris	PWN54339
Metazoa	*Chelonia mydas*	XP_007053665
	Danio rerio	NP_996973.2
	Gallus gallus	NP_990293.1
	Homo sapiens	NP_001736.1
	Rhincodon typus	XP_020382340

[1]Sequence from the 1000 plant transcriptomes initiative [1]

Table S2: List of primers used in this study

#	5'-3' Sequence	Purpose
439	ATGGAAGGAGAGAAGCTTATAGAAG	qRT-PCR for *At*GET1
134	AGCCTCTCTCAAAAGCTGCTTAATTTC	qRT-PCR for *At*GET1
1408	ATTGGTTTCCTCTTTTCCTCGCTCCG	qRT-PCR for G1IP
1799	GCCGTTGATCTGACCAGTGATA	qRT-PCR for G1IP
1781	ATGGTGATGGATAGAGAAGAAAGG	qRT-PCR for G1IP-*like*
1953	GAGAAGCCGATGATGAGGAAGA	qRT-PCR for G1IP-*like*
1672	GCCATCCAAGCTGTTCTCTC	qRT-PCR for ACT2
1673	CAGTAAGGTCACGTCCAGCA	qRT-PCR for ACT2
98	ACCAGCAAACCGTGGATTACCCTAGC	RT-PCR for *At*RAN3
99	ATTCCACAAAGTGAAGATTAGCGTCC	RT-PCR for *At*RAN3
1150	GTTAATGGAAGGAGAGAAGCTTATAG	RT-PCR for *At*GET1
1151	TACATGGCCTGTCATGTGACCTCC	RT-PCR for *At*GET1
1408	ATTGGTTTCCTCTTTTCCTCGCTCCG	RT-PCR for G1IP
1410	AGTGCATCCATTATCTTCTTCACC	RT-PCR for G1IP
1800	ATGGCGTCGAACAGCAGA	RT-PCR for G1IP
2351	GCAAAACACAAATCTACCGAGCACA	RT-PCR for G1IP
1781	ATGGTGATGGATAGAGAAGAAAGG	RT-PCR for G1IP-like
1782	TTAAAAAAGAGAGGCTCCAAAAATAACA	RT-PCR for G1IP-like
2316	ATTGAAGAAGTAGAATCGGAAGG	CRISPR of G1IP (gRNA2)
2317	AAACCCTTCCGATTCTACTTCTT	CRISPR of G1IP (gRNA2)
2318	ATTGATGATGGTGAAGAAGATAA	CRISPR of G1IP (gRNA3)
2319	AAACTTATCTTCTTCACCATCAT	CRISPR of G1IP (gRNA3)
1249	TACTGGGCCCATGGCGTCGAACAGCAGAGAAGCC	Genomic fragment of G1IP
1250	GGACTAGTAATCTCAAAACAAGAAAAAATACAC	Genomic fragment of G1IP
133	TGAAGGCTTCAAATTTCTGTGAATCC	Genotyping of *get1-1*
134	AGCCTCTCTCAAAAGCTGCTTAATTTC	Genotyping of *get1-1*
1093	TTGCAGCGATTGCATCTCCCTCTC	Genotyping of *g1ip-3*
1094	CGATTTCTTGAGCTTTAAGAATCTG	Genotyping of *g1ip-3*
2350	ACACTTGAATTGGCCCGTTAAGAAG	Genotyping of *g1ip-4*
2351	GCAAAACACAAATCTACCGAGCACA	Genotyping of *g1ip-4*
1434	TTCTTCCCTGCTTTGATGGATG	Genotyping of *g1ip-4*
1496	GAACATAGGGAAGAATTCATCTTTC	Genotyping of *g1ip-like1/2*
1497	TGAAGAACAGTCGAGAGTTTTGGTTC	Genotyping of *g1ip-like1/2*
1888	CAGAGAAGCCGAGGAGGAGGAGATTCTAGATAGAGGATCTG	SDM on G1IP
1889	CTATCTAGAATCTCCTCCTCCTCGGCTTCTCTGCTG	SDM on G1IP
1056	GGGGACAAGTTTGTACAAAAAAGCAGGCTTAATGGCGTCGAA CAGCAGAG	pDONR207-G1IP
1134	GGGGACCACTTTGTACAAGAAAGCTGGGTCTAAGGAAAGAT GCTTTGGGTGAC	pDONR207-G1IP

1594	GGGGACCACTTTGTACAAGAAAGCTGGGTCTCGAGTTACATCCGTGCGTATTCCGAAG	pDONR207-G1IPcyt
2043	GGGGACAAGTTTGTACAAAAAAGCAGGCTCTATGTTCACAGCTCTTGCGATTG	pDONR207-G1IP-TMDs
1582	GGGGACAAGTTTGTACAAAAAAGCAGGCTTAATGGTGATGGATAGAGAAGAAAGGA	pDONR207-G1IP-*like*
1583	GGGGACCACTTTGTACAAGAAAGCTGGGTTTAAAAAAGAGAGGCTCCAAAAATAACA	pDONR207-G1IP-*like*

References

1. One Thousand Plant Transcriptomes, I. (2019). One thousand plant transcriptomes and the phylogenomics of green plants. Nature *574*, 679-685.

III. Mehlhorn et al., unpublished manuscript:

Conservation of SND2 in plants

Manuscript

Conservation of SND2 in plants

Dietmar G. Mehlhorn, & Christopher Grefen

Faculty of Biology & Biotechnology, Molecular & Cellular Botany, University of Bochum, Universitätsstraße 150, 44780 Bochum, Germany

Working Title: Conservation of SND2 in plants

Short Summary: tail-anchored proteins, SND Pathway, GET pathway, *Arabidopsis thaliana*, plants, ER membrane translocation, SRP independent

Abstract:

Translocation of intact proteins into the endoplasmic reticulum (ER) membrane is a crucial step in protein biosynthesis. Different pathways for co- and post-translational insertion evolved in eukaryotes to deal with this challenge. One such system - recently discovered in yeast - is the SRP independent (SND) pathway comprising of three proteins that facilitate insertion of moderately hydrophobic membrane proteins that lack an N-terminal signal peptide. Here, we report evidence to support pathway conservation in plants. At least one functional ortholog in *Arabidopsis thaliana* existing as two paralogs, *At*SND2a and *At*SND2b was found. In comparison to the potentially related Guided Entry of Tail-anchored (GET) pathway mutants, individual T-DNA insertion lines of *Atsnd2a* but not *Atsnd2b* reveal a mild root hair growth phenotype in otherwise normally growing plants. Combinations with the GET pathway receptor loss of function line *Atget1-1* phenocopy the root hair growth defects of *Atget1-1* indicating that both SND2 genes do not serve as backup for the GET pathway in root hairs. Crossing both mutant alleles, however, leads to transmission defects and seedling lethality. Interaction studies implicate both *At*SND2a and *At*SND2b as part of an intricate system for translocation processes and/or stress response which is reminiscent of *h*SND2 function in mammalian cells. Our work indicates, despite probable partial redundancy, diversification of these two tasks in *Arabidopsis*.

Introduction

Membrane proteins play crucial roles for membrane integrity and ultimately cellular function in all domains of life. Roughly one third of the average eukaryotic proteome comprises integral membrane proteins (1). To maintain functionality, proper translocation of the nascent protein must be guaranteed during biogenesis. The endoplasmic reticulum (ER) serves as interface for the insertion and maturation of most membrane proteins as well as their redirection to target membrane. Correct integration of nascent proteins in the ER membrane, however, is a challenging task. The hydrophobic transmembrane domain(s) (TMD) must be shielded from the aqueous cytosol, followed by guidance to the ER and insertion while maintaining the correct topology of individual TMDs.

To overcome these difficulties, chaperones and their receptors – translocon and insertase complexes - orchestrate protein shuttling and insertion. Two different temporal modes of action exist, *co*-translational and *post*-translational insertion. Co-translational insertion requires interaction of the signal recognition particle (SRP) pathway with the emerging N-terminal signal sequence (SS) or a first TMD of a nascent secretory or membrane protein (2). Translation is then arrested until docking of the SRP/ribosome nascent chain (RNC) complex to the ER membrane via the SRP-receptor (SR), resulting in a transfer of RNC from SRP to the SEC61 translocon where protein translation is resumed (3, 4).

Up to ~3-5% of all integral membrane proteins, however, require post-translational delivery and insertion. The '*reverse'* type II orientation of the so-called tail-anchored (TA) proteins is represented by a cytosolic N-terminal stretch and a single C-terminal TMD, followed by an approximately 30 residue long polar region (5). The absence of an N-terminal SS or TMD prevents SRP recognition necessitating *post*-translational insertion (1). The Guided Entry of Tail-anchored (GET) pathway was shown to mediate translocation of this type of proteins in yeast and mammals (6, 7). Recognition of fully translated TA proteins occurs via a complex comprising Sgt2, Get4 and Get5 (metazoan: SGTA, TRC35, UBL4A and BAG6) at the ribosome (8, 9). Transfer of the TA protein to the homodimeric ATPase Get3 (TRC40) requires ATP (10-12). After shuttling of the client to the ER membrane, insertion is initiated through interaction of the GET3a-TA-complex with the receptors GET1 (WRB) and GET2 (CAML) (13, 14).

The GET pathway's involvement in post-translational membrane insertion of TA proteins has been well established. There are, however, considerable clues that challenge GET being solely responsible for this task. From the earliest studies in yeast it was clear that survival rates of *loss-of-function* strains are not affected under normal growth conditions (7). Later, dissection of the yeast phenotype revealed an additional function of GET3 as holdase chaperone under cytotoxic stress (15, 16). While mice embryo lacking GET proteins are aborted (17), tissue-specific knockdowns are viable but highlight an involvement in crucial functions (18-21). In *Archaeplastida* a high degree of conservation was observed leading to the discovery of orthologues for most of the components in *Arabidopsis thaliana* (22-24). Similar to their fungal/metazoan orthologs, *loss-of function* lines in *Arabidopsis* are not lethal leading to mild phenotypes such as an increased ER-stress level (22) and reduced root hair growth (23, 24). *In vivo* studies identified only a limited number of TA proteins dependent on the GET system (19, 20) and only few were found to bind GET components in *Arabidopsis* (23). This leads to the conclusion that alternative pathways must exist.

In the past few years such pathways in yeast and mammals have indeed been discovered (25-27). In an *in vitro* cell system, TA proteins were shown to be post-translationally inserted by the SRP-dependent pathway (26, 28). Furthermore, yeast TA proteins with low hydrophobicity utilized the ER membrane protein complex (EMC) pathway (29). More recently, an insertion pathway for proteins with a central TMD was described in yeast which can also compensate for the loss of the SRP – and GET-pathway (25). This SRP-independent (SND) pathway comprises three components SND1-3 (25). While the cytosolic SND1 is proposed to coordinate co-translational capturing of nascent proteins at the ribosome, SND2 and SND3 are membrane-bound and associate with the SEC61 translocon and auxiliary proteins as SEC63, potentially acting as receptors. Although main targets are proteins with a central TMD, double knockout of SND and Get components in yeast lead to lethality suggesting its role as a backup system for TA proteins (25). Partial pathway conservation was shown in mammals where at least one component, hSND2 (also named TMEM208) exists (30, 31).

Here, we report the identification of two putative SND2 orthologues (*At*SND2a and *At*SND2b) encoded in the *Arabidopsis* genome. Both seem to be linked to the translocation machinery at the ER membrane. We demonstrate that unlike in yeast,

104 double knockouts of *At*SND2a or *At*SND2b with *At*GET1 are not lethal but phenocopy
105 the *Atget1* root hair phenotype.

106 While single *Atsnd2a* and *Atsnd2b loss-of-function* lines display no obvious phenotype,
107 crosses between these lines seem to lead to transmission defects and seedling
108 lethality which can be complemented by reintroduction of one of the genomic
109 sequences showing at least partial redundancy of both genes. Interaction partners
110 identified with an immunoprecipitation-mass spectrometry (IP-MS) approach showed
111 that both proteins are in an environment where it is likely that they assist in the
112 translocation of precursor polypeptides, however differences in expression pattern,
113 induction upon stress response and individual interaction partners are pointing to a
114 possible neofunctionalization of *At*SND2a.

Results

SND2 is conserved in Archaeplastida

The rather mild root hair growth defects in *At*GET *loss-of-function* lines question the GET pathways sole responsibility for TA protein translocation into the ER membrane of plants. As recently shown in yeast and mammals, the SRP-independent (SND) pathway can facilitate insertion of type II membrane proteins such as TA Proteins (25, 32). Similar to findings in mammals, *in silico* comparison of yeast SND1-3 failed to predict orthologs among *A. thaliana* reference protein sequences (https://www.ncbi.nlm.nih.gov/) for SND1 or SND3. However, sequence orthologs of *Sc*SND2 can be found in mammals (hSND2) (30, 32) and in plants (*Arabidopsis thaliana* At2g23940). Surprisingly, a second SND2 orthologue (At4g30500) can be identified in *Arabidopsis* with approximately 77% sequence identity (BlastP) to the homologous *At*SND2. We designated the two genes SND2a (At4g30500) and SND2b (At2g23940). The second paralog of SND2 (SND2a) is specific to Brassicaceae (**Fig. 1A**), most likely a remnant of the last genome duplication event (33, 34). The coding sequences of both proteins are 522 base pairs long and encode proteins with 173 amino acid residues of 19,3 kDa or 19,6 kDa predicted molecular mass, respectively. The predicted membrane topology of SND2a and SND2b suggests a type II polytopic orientation with two transmembrane helices (TMHMM) (**Fig. S1 A**), however, alignment analysis reveals four transmembrane domains as observed in *Sc*SND2 with minor amino acid changes in the conserved region (**Fig. S1 B**). The C-terminus contains either KTRS (SND2a) or KTRT (SND2b) amino acid sequences which is reminiscent of a KKxx-*like* motifs in mammals, important for ER-membrane retention signalling (predicted by https://psort.hgc.jp/form2.html) (35) yet nothing is known in plants about such a motif.

SND2a and SND2b share the same subcellular localisation but differ in expression pattern

In silico analyses predict an ER localisation for both proteins. To corroborate this subcellular localisation, we co-transfected tobacco leaf cells with SND2a-YFP or SND2b-YFP and ER-marker sec-RFP-HDEL. Analyses by confocal laser scanning

microscopy (CSLM) demonstrate that both SND2a-YFP (**Fig. 1C-F**) and SND2b-YFP (**Fig. 1G-J**) localise to the ER. These results were confirmed in stably transformed *A. thaliana* plants expressing either SND2a-GFP or SND2b-GFP (**Fig 1K-N**). Thus, we conclude that both proteins are ER-membrane proteins. Translocation is a major challenge throughout all developmental stages of all organisms requiring sufficient amounts of involved proteins. Therefore, high expression levels of the two *Arabidopsis* SND2 orthologues across all tissues and developmental stages would be expected and reflect such a universal task. To test this hypothesis, we assessed the expression pattern by quantitative real time PCR (qRT-PCR). The results confirmed that SND2b is almost ubiquitously expressed with reduced levels in flowers (**Fig 1B**). Expression of SND2a was quite low in most of the tested tissues or in seedlings compared to SND2b yet there was a strong induction in siliques (**Fig. 1B**).

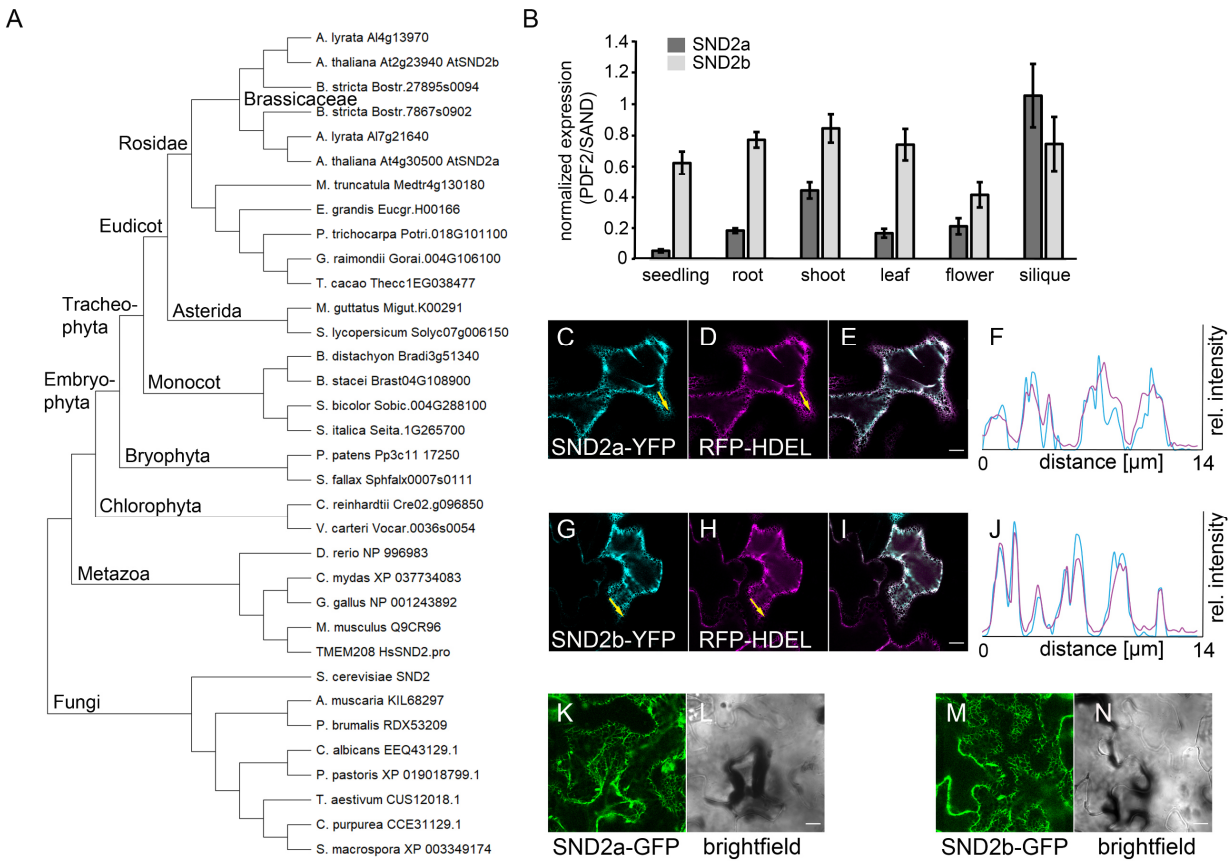

Figure 1: Analysis of SND2 orthologs of different species.
(A) Maximum likelihood tree of SND2 orthologs reveals branching of SND2 in Brassicaceae. (B) Relative transcript levels of SND2a and SND2b in different tissues of *A. thaliana* Col-0 plants measured by qRT-PCR analysis. PDF2 and SAND were used as reference genes. Error bars indicate SD of technical replicates. (n=3). (C-J) CLSM analysis of the subcellular localization of p35S::SND2a-mVenus (C-F) and p35S::SND2b-mVenus (G-J) transiently

expressed in tobacco leaves coexpressing the ER marker sec-RFP-HDEL. Line histograms (F, J) along yellow arrows measured in C, D, G and H confirmed colocalization (Scale bar: 10µm). (K-N) CLSM analysis of the subcellular localization of pUBQ10::SND2a-GFP (K-J) and pUBQ10::SND2b-GFP (M-N) in leaves of stably transformed *A. thaliana* lines (Scale bar: 10µm).

SND2a and SND2b share binding partners in the translocation machinery with minor differences

Since orthologues of *Sc*SND1 and *Sc*SND3 have not yet been found in plants, these obvious interaction partners in a potential translocation machinery are currently missing. To test whether SND2a and SND2b physically interact with partners of translocon associated proteins that were determined through sequence comparison or published previously (23, 36, 37), we performed ratiometric Bimolecular Fluorescence Complementation (rBiFC) analysis (36, 38, 39). We found that SND2a and SND2b homo- and heterodimerise (**Fig. 2**) Moreover, interaction of SND2a with the translocon subunit and tail-anchored protein *At*SEC61β1 and the translocon auxiliary protein *At*SEC62, recently described in Mitterreiter et al. 2019 and Hu et al. 2020 (37, 40) was detected. Reduced YFP/RFP ratio was observed when interaction of SND2a and the translocon subunit *At*SEC61α1 were tested. *At*GET1 was found to interact with SND2a, however, the YFP signal in the interaction assay with *At*GET3a was comparable to the negative control (**Fig. 2A**). Similar results were observed when using SND2b as binding partner with the major difference being that the YFP signal in samples testing the interaction with *At*GET1 was not distinguishable to the negative control (**Fig. 2B**). In both cases, the TA protein SYP123 was used as negative control as it is a known substrate of the *At*GET-pathway (23). These results indicate that both SND2 orthologues are capable of physical association with predicted translocon components yet differ in their relationship with the GET-pathway.

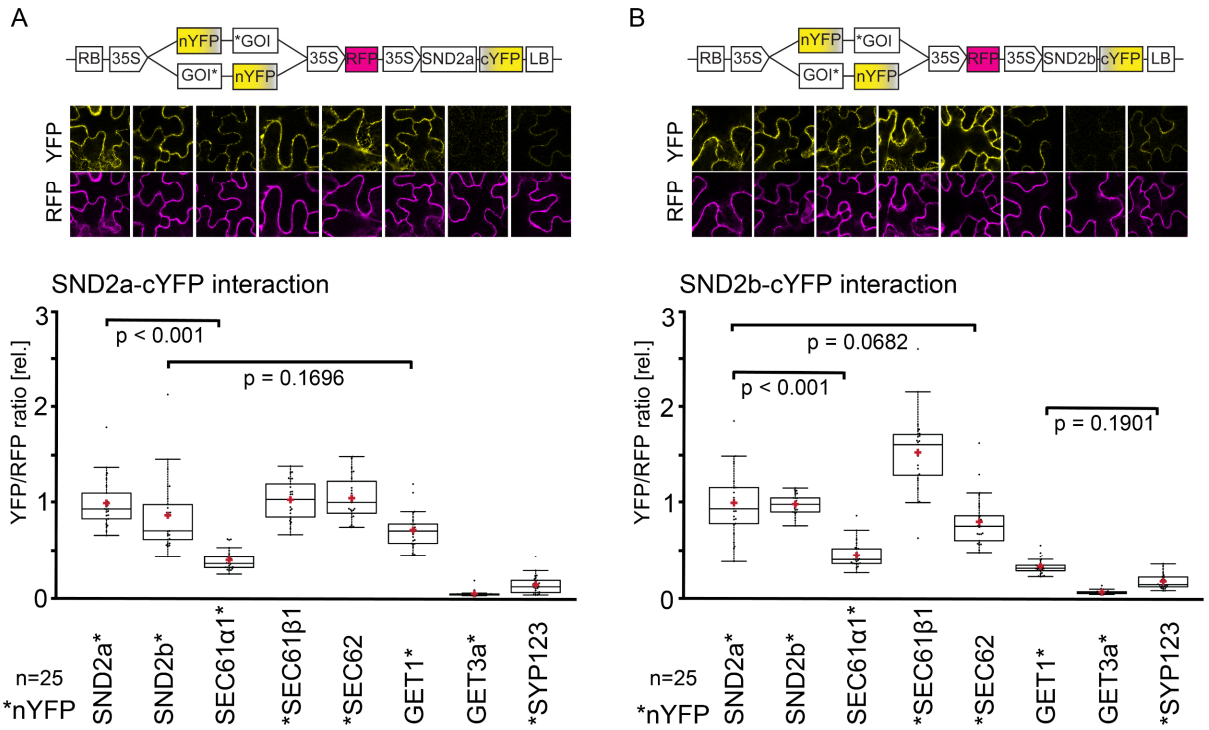

Figure 2: SND2a and SND2b homo- and heterodimerize and interact with translocon and GET-pathway components. (A-B) Schematic of the 2in1 rBiFC constructs used for the analysis of SND2a-cYFP (A) or SND2b-cYFP (B) interaction with nYFP-tagged proteins are shown in the upper panel. Exemplary CLSM images of transiently transfected *N. benthamiana* leaves are depicted in the middle panel. Ratios of mean fluorescence levels of 25 areas measured in YFP and RFP channels were normalized against a positive control before blotting to demonstrate YFP complementation. The central line of boxes represents the median with outer limits at the 25th and 75th percentils. Tukey whiskers extend to 1.5 times the interquartile range. The red crosses mark the mean while black dots show the individual values. Asterisks indicate tag orientation of nYFP. P – values were obtained from a Tukey HSD all pairs test.

Individual knockout of snd2a or snd2b has only minor effects on the phenotype

To assess the genetic impact of the interaction differences regarding *At*GET1 (**Fig. 2**) we analysed *snd2a* and *snd2b* T-DNA insertion lines and double mutants with *Atget1*. Confirmed *loss-of-function* lines of *snd2a* and *snd2b* (**Fig. S2 A-D**) did not reveal any obvious growth defects. Seedling development as well as fertilization or seed germination was indistinguishable from Col-0 plants. As previously shown, loss of *At*GET1 in *A. thaliana* leads to a reduced root hair elongation (23). Therefore, we performed a root hair growth assay of single mutants and double mutants of *snd2a* or *snd2b* with *Atget1*. Only s*nd2a* showed slightly but significantly shorter root hairs compared to wildtype which can be complemented by expression of genomic SND2a under the control of the UBQ10 promoter (**Fig. 3A**). Double homozygous T-DNA insertion lines of *snd2a* or *snd2b* with *Atget1* phenocopy the root hair length of the

Atget1 single *loss-of-function* line (**Fig. 3A**). To exclude a compensatory effect of the GET- or putative SND-pathway, we performed qRT-PCR analysis. However, expression of neither SND2a nor SND2b was altered in *get1* mutants compared to wild type (**Fig. 3B-C**). Similar results were obtained for *At*GET1 and *At*GET3a expression patterns in *snd2a* or *snd2b* mutants (**Fig. 3D-E**).

As the single mutants did not display a severe phenotypic defect, we investigated potential redundancy between *snd2a* and *snd2b*.

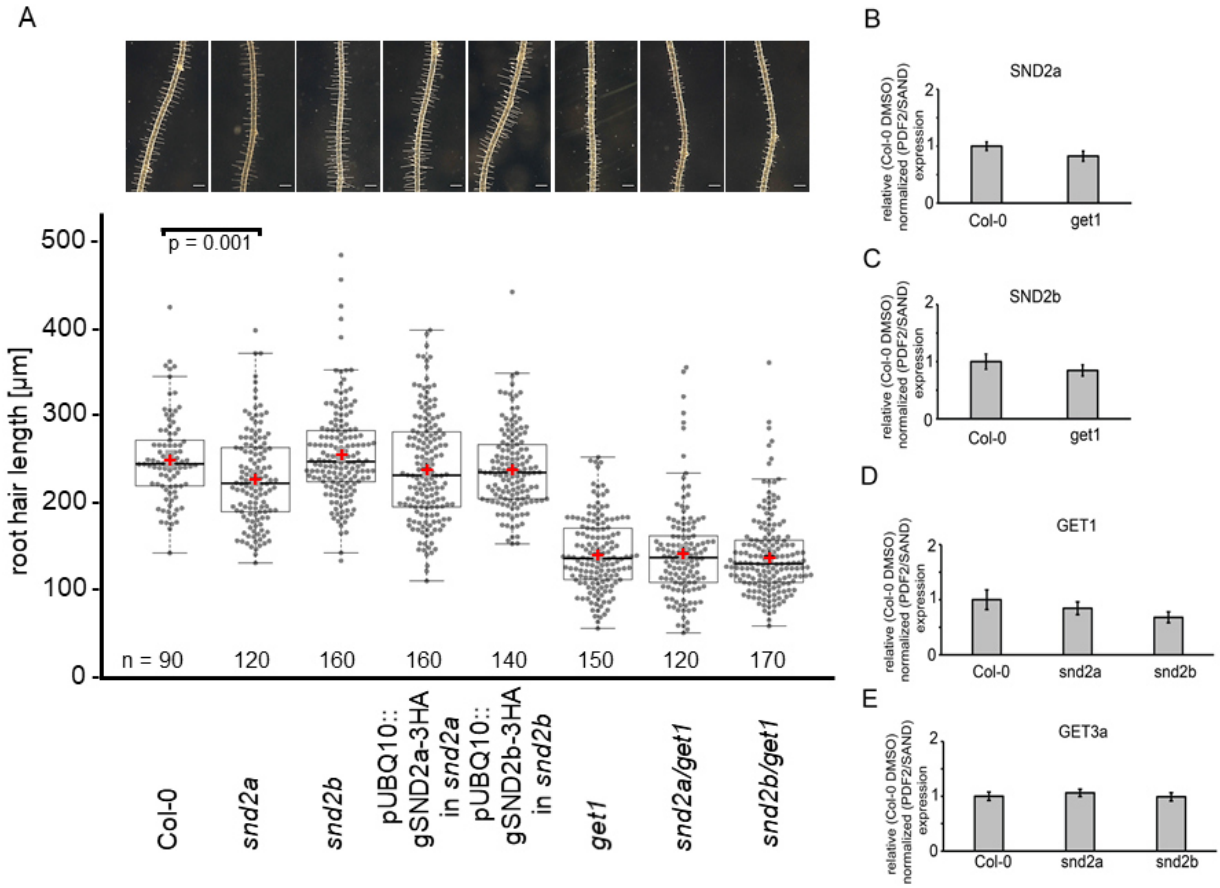

Figure 3: *Loss-of-function analysis* of SND2a and SND2 in single mutants and in combination with get1 mutants. (A) Exemplary images of root hair phenotypes. Scale bar = 300µm. In the lower panel, measurements of the 10 longest root hairs of individual roots from Col-0, single mutants, complementation lines and crosses with a *get1* background are blotted. (n = 90-170, individual values indicated in the box plot). The central line of boxes represents the median with outer limits at the 25th and 75th percentils. Tukey whiskers extend to 1.5 times the interquartile range. The red crosses mark the mean while black dots show the individual values. P – values were obtained from a Dunnetts- test against Col-0 as control. (B-E) Normalized relative transcript levels of SND2a (B), SND2b (C), *At*GET1 (D) and *At*Get3a (E) in Col-0 plants and various single mutants measured by qRT-PCR. PDF2 and SAND serve as reference genes, and expression levels are relative to Col-0. Error bars indicate SD of technical replicates. (n=3).

Simultaneous knockout of both SND2 homologues disturbs plant development

Co-regulation of both genes might be an indication for redundant function. To assess whether there is compensation on transcriptional level, we performed qRT-PCR. Neither loss of SND2a nor SND2b affects the mRNA level of the other homologue (**Fig. S2 C-D**). In humans, silencing hSND2 resulted in elevated SRα and SRβ level (32) underpinning a potential compensatory effect regarding alternative insertion pathways. However, we did not observe this in *Arabidopsis thaliana* when assessing expression levels of the putative homologues of SRα and SRβ (**Fig. S3 C-D**).

To further investigate potential redundancy, we crossed the T-DNA insertion mutants of *snd2a* and *snd2b*. Plants homozygous for one gene and heterozygous for the other did not display any noticeable growth defect, however double homozygous progeny displayed severe growth defects, and lethality at seedling stage at the very latest (**Fig. 4A**). Staining the cell walls of root cells revealed a disorganised structure within the double homozygous mutants compared to wild type or the *snd2a* single mutant. The cells of the double homozygous mutant plants were in parts enlarged and it appears that the root hair maturation zone is closer to the apical meristem compared to normally growing roots. Furthermore, accumulation of propidium iodide clusters of round shape within the cell were observed (**Fig. 4B**). Expression of a genomic version of the *SND2b* gene under the ubiquitin 10 (UBQ10) promoter results in double homozygous T-DNA insertion lines (*snd2a* (-/-)/ *snd2b* (-/-)) with restored WT-like growth (**Fig. S4 A-D**). The complementation with SND2a has not been tested so far.

Genotyping of seedlings derived from single siliques from self-pollinated parental plants homozygous for *snd2a* (-/-) and heterozygous for *snd2b* (+/-) display only a small number of double homozygous mutant plants, with a segregation rate favouring snd2a (-/-)/snd2b (+/+). Selfing of *snd2a* (+/-)/*snd2b* (-/-) plants leads to an almost equal segregation between snd2a (+/+)/snd2b (-/-) and snd2a (+/-)//snd2b (-/-) (**Table 1A**). Nevertheless, the expected Mendelian transmission ratio of 1:2:1 was rejected in both cases indicating a gametophytic defect. To determine whether the gametophytes are affected by the double knockout, reciprocal back-crosses were performed. Pollen of homozygous *snd2a* plants crossed with pistils from *snd2a* (-/-)/*snd2b* (+/-) plants yielded progeny with an approximately 50% segregation ratio of *snd2b*. In contrast, stigma of *snd2a* homozygous plants pollinated with pollen of *snd2a* (-/-)/*snd2b* (+/-) revealed a ratio of 68% (wild type) :32% (*snd2b* (+/-))

(**Table 1B**). This indicates a reduced transmission ratio of 32% for the male gametophyte and normal transmission (of ~50%) for the female gametophyte. This does not entirely match the observed numbers of the selfings probably indicating an impairment of the gametophyte but also the zygote. In contrast, taking pollen of homozygous *snd2b* plants for crossing with pistils from *snd2a* (-/-)/*snd2b* (+/-) plants yield an altered female gametophyte with a transmission ratio of approximately 22%. Additionally, stigma of *snd2b* homozygous plants pollinated with pollen of *snd2a* (+/-)/*snd2b* (-/-) showed a reduction in the male gametophyte transmission ratio with 15% (**Table 1B**). Taking these transmission ratios into account in the self-crossing experiments, similar ratios for the observed numbers for *snd2a (+/-)/snd2b (-/-)* progeny can be calculated (**Table 1A**).

Our findings that male transmission is severely affected in both cases suggests that defects in pollen tube growth may be possible (41, 42). However, evaluation of single knockout *in vitro* and *in vivo* pollen tube growths assays revealed no significant difference in pollen tube length or growth speed (**Fig. 5A-B**). Since no viable double knockouts were obtained, functional redundancy in pollen tube growth cannot be ruled out at this point. Investigation of both homo-/heterozygous double mutant versions showed a decrease in silique length accompanied with reduced numbers of ovules within the siliques (**Fig. 5C-D**).

Table 1: *Double homozygous T-DNA insertion of AtSND2a and AtSND2b results in transmission defects. (A) Data of the genotyping analysis after self-pollination. (B) Reciprocal backcrosses.* [1]*Genotypes were analysed by PCR for only the heterozygous parental gene.*

A

Self-pollinated

parental genotype	No. genotyped	genotypes of progeny[1]			percentage [%]		
		+/+	+/-	-/-	+/+	+/-	-/-
snd2a +/- / snd2b -/-	515	321	185	9	62	36	2
snd2a -/- / snd2b +/-	655	304	297	54	46	45	8

299 B

Reciprocal back-crossing

♂ parent	x	♀ parent	No. genotyped	genotypes of progeny[1]		percentage [%]	
				+/+	-/-	+/+	-/-
snd2a +/- snd2b -/-	x	snd2b -/-	88	75	13	85	15
snd2b -/-	x	snd2a +/- snd2b -/-	45	35	10	78	22
snd2a -/- snd2b +/-	x	snd2a -/-	100	68	32	68	32
snd2a -/-	x	snd2a -/- snd2b +/-	53	26	27	~50	~50

300

301

A

B

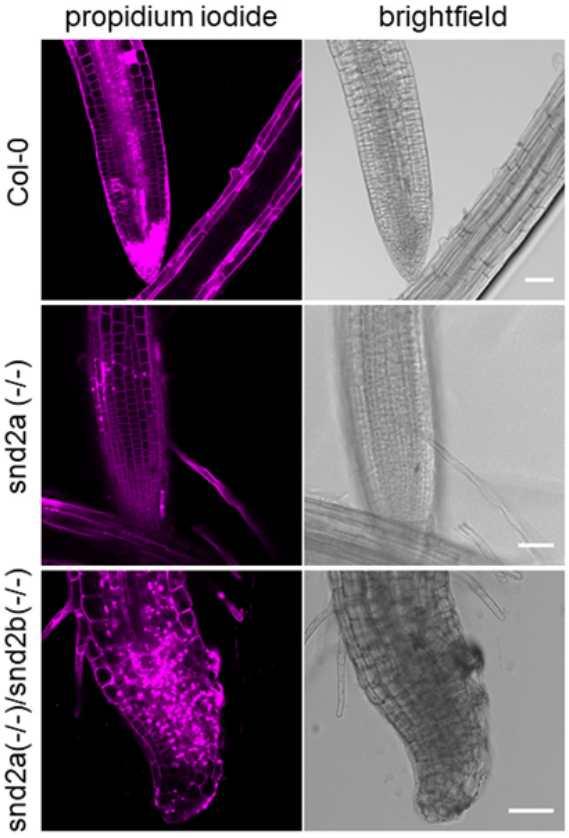

302

Figure 4: Exemplary images of genotypic progenies after self-pollination of *Atsnd2a* +/- *Atsnd2b* -/- or *Atsnd2a* -/- / *Atsnd2b* +/-. (A) Confirmed double homozygous mutants of *Atsnd2a/Atsnd2b* plants display a severe growth defect in seedling stage as shown in the single-lens-reflex camera images compared to homozygous/heterozygous mutant plants. Scale bar = 0.25mm. (B) Propidium iodide-stained Col-0, *Atsnd2a (-/-)*, *Atsnd2a (-/-)/ Atsnd2b (-/-)* root tips. Scale bar = 50µm.

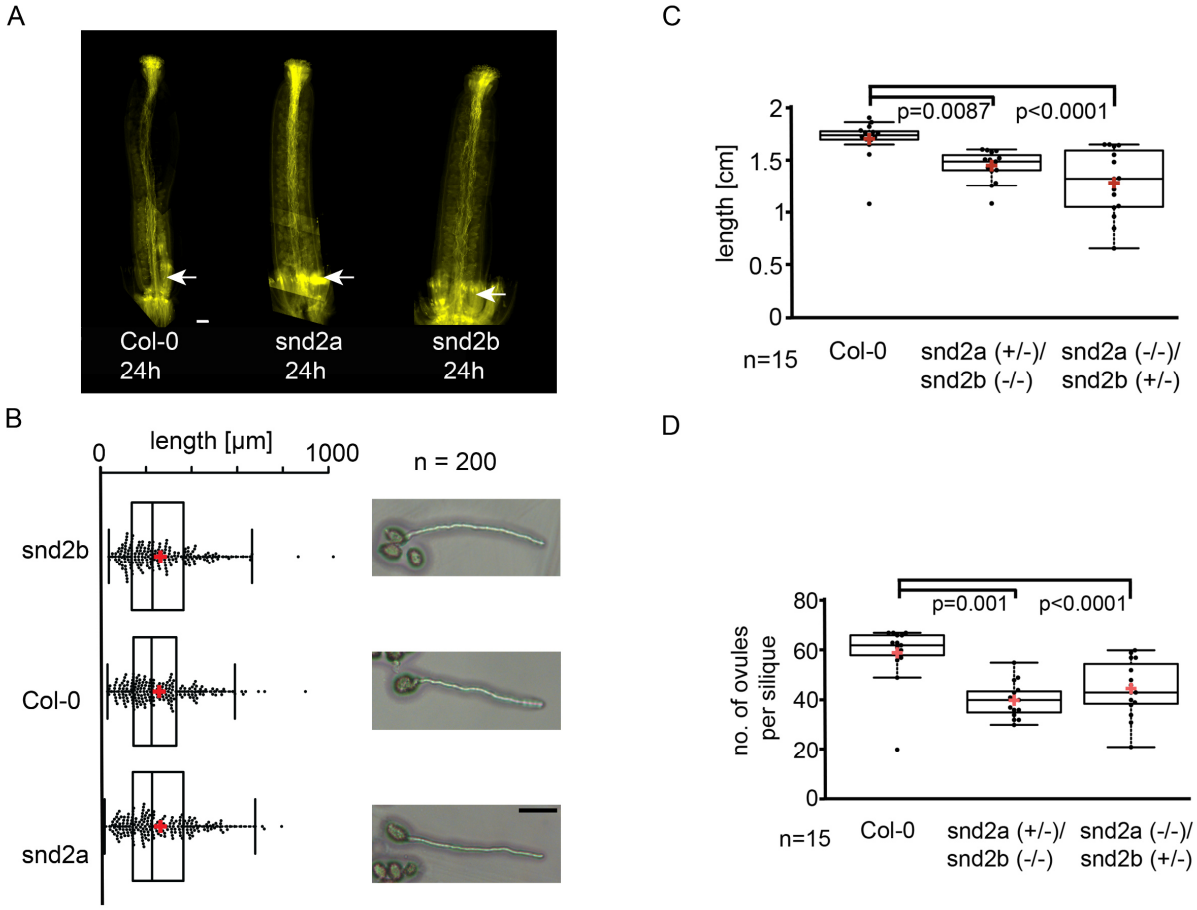

Figure 5: Analysis of pollen tube growth, silique length and number of ovules in single *loss-of function* lines or homo-/heterozygous *snd2a/snd2b* lines.
(A) Aniline blue staining of pollen tubes (WT, *snd2a* and *snd2b* mutants) grown for 24 h after pollination of Col-0 pistils indicate no difference in pollen tube growth. White arrows point to exemplary pollen tube termini that reached ovules. Pictures are composites of individual images along the pistil, the LUT was changed to yellow, and exposure was enhanced to visualize the bright yellow pollen tubes against the darker yellow background. (Scale bar: 100µm) (B) Growth of pollen tubes was measured *in vitro* from 200 individual pollen grains per plant line 7 h post-germination (representative images on the right panel; Scale bar: 50µm). (C) Measurement of silique length in *snd2a* heterozygous *(+/-)/snd2b* homozygous *(-/-)* or *snd2a* homozygous *(-/-)/snd2b* heterozygous *(+/-)* plants in comparison to wild type. The 7th; 8th; and 9th silique of 5 individual approx. 7-week-old plants were used (n=15). (D) Number of ovules per siliques used in (C) (n=15). The central line of box plots represents the median with outer limits at the 25th and 75th percentils. Tukey whiskers extend to 1.5 times the interquartile range. Red crosses mark the mean while black dots show individual values. P – values were obtained from a Dunnett's test to Col-0 as control.

SND2a and SND2b share many interaction partners but are differently regulated upon ER-stress

In mammals, hSND2 interacts with proteins known to assist in ER membrane protein transport (32). To identify potential interaction partners of both plant SND2 orthologues, we employed immunoprecipitation (IP) with subsequent mass spectrometry (MS) analysis. Immunoprecipitants of UBQ10 promoter driven SND2a-GFP or SND2b-GFP from transformed *Arabidopsis* lines together with a negative control (soluble GFP) were analysed for proteins exclusively interacting with either SND2a-GFP, SND2b-GFP or both (**Fig. 6A**). Most of the identified proteins bind to both SND2a and SND2b while other fractions of identified proteins are specific interaction partners for either protein. Among the overlapping pool, proteins associated with protein translocation to the ER membrane can be found (**Fig. 6B, Table S1**), i.e. translocon components as well as auxiliary proteins as the two J proteins ERdj2A and ERdj2B (SEC63 orthologues), multiple subunits of the oligosaccharyltransferase (OST) and putative ER membrane complex (EMC) 8/9 orthologue. Functional differences between the identified proteins binding exclusively to a single SND2 orthologue were revealed in a gene ontology (GO)-Term analysis using GOrilla and PANTHER (http://cbl-gorilla.cs.technion.ac.il/; http://geneontology.org/). Stress response related proteins such as BIP1 and BIP3 were enriched in the subfraction of SND2a-GFP interaction partners. Instead, SND2b-GFP binding partner GO-terms were often associated with transmembrane transport especially to the ER membrane along with SRP related proteins, a possible EMC3 orthologue as well as additional translocon-associated proteins.

We speculated that SND2a might have a diverged function related to stress-response. To test our assumption, we applied ER-stress on Col-0 plants using tunicamycin (43-45) and investigated the expression level of *SND2a* and *SND2b* compared to non-stressed plants. After 6h of tunicamycin exposure, we observed an approximately 5-fold upregulation of *SND2a* (**Fig. 6C**). In contrast, transcription of the SND2b gene was not induced by the treatment (**Fig. 6D**).

We further analysed whether the lack of SND2a or SND2b under ER-stress condition has an impact on known autophagy marker ATG8e (46), ER-phagy related SEC62 (37, 40) or ER-stress response gene BIP3, respectively. However, no difference in the expression pattern was observed (**Fig. S3 A-B, E**), although BIP3 was highly

upregulated by tunicamycin treatment demonstrating successful induction of ER - stress (**Fig. S3 E**).

A

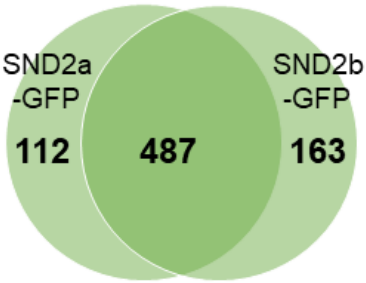

B

Protein	Accession no	Interacts with
ERDj2A	AT1G79940	Both
ERDj2B	AT4G21180	Both
SEC61α2	AT1G29310	Both
SRP54	AT5G03940	SND2b
SRP68	AT5G61970	SND2b
TRAP1	AT2G21160	SND2b[1]
SEC61γ1	AT5G5046	SND2b[1]
BIP1	AT5G28540	SND2a
BIP3	AT1G09080	SND2a

C

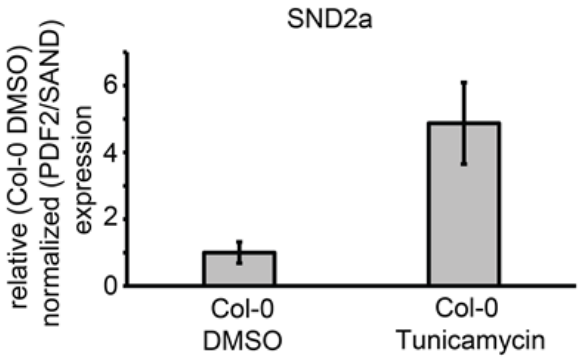

D

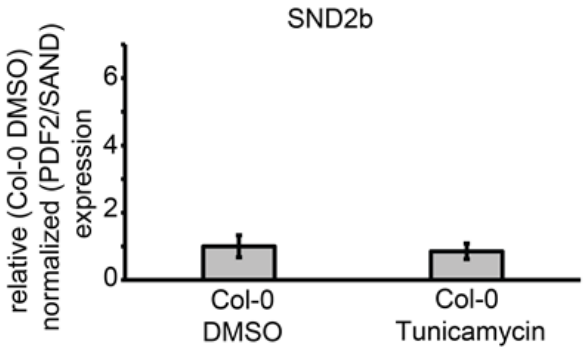

Figure 6: Interactome analysis of SND2a-GFP and SND2b-GFP and different transcriptional activation upon stress. (A) Venn-diagram depicting interacting proteins fished by an IP-MS analysis (3 out of 3 times). (B) Exemplary interaction partners of both or the single proteins. [1] fished one time out of three. (C-D) Normalized relative transcript levels of SND2a (C) or SND2b (D) in Col-0 plants treated either with DMSO or 5µg/ml tunicamycin for 6h measured by qRT-PCR. PDF2 and SAND served as reference genes and expression levels are relative to Col-0. Error bars indicate SD of biological replicates. (n=3).

Discussion and Outlook

Backup pathways to ensure proper protein translocation are important to maintain cellular function. The SRP-independent pathway was shown to function as alternative for some substrates of the SRP/Sec61 and GET pathway in yeast (25). In this study, we sought to find potential conservation of SND orthologues in *Arabidopsis thaliana*. Similar to observations in humans (32), no obvious orthologues for *Sc*SND1 or *Sc*SND3 were found through PSI Blast in different plant species. Instead of one putative *Sc*SND2 orthologue we identified two homologues, SND2a and SND2b, which probably differentiated at the last branching point of the Brassicaceae (**Fig. 1A**). TMHMM prediction designate both proteins as type II membrane proteins oriented with two transmembrane helices, which would contradict findings in yeast and mammals where four TMDs were predicted (25, 32). However, comparison of the sequence alignments revealed that changes of few amino acids within the TMDs might lead to the different prediction in TMHMM. This notion is further supported as orthologues of more basic plants and hSND2 showed similar characteristics (**Fig. S1**). Thus, four TMDs can be presumed.

The C-terminal regions of both SND2a and SND2b contain a KKxx-*like* motif, an ER membrane retention signal of mammalian cells (47). Although nothing is known about such a motif in plants, we showed ER localization of both proteins (**Fig. 1C-N**) which is in line with findings in yeast and mammals (25, 32).

Absence of *Sc*SND2 only in combination with a *Sc*GET-pathway component was shown to cause a synthetic lethal defect in yeast (25). In contrast, double mutants of *snd2a* or *snd2b*, and *get1* are still viable but phenocopy the root hair phenotype of *get1* single mutants (**Fig. 3A**) (23). Although a slight but significant reduction in root hair growth in *snd2a* single mutant was shown, no additive effect on the phenotype was observed in the double mutants. This result might indicate that neither SND2a nor SND2b backup the function of GET1 in root hair growth. This suggestion is further supported as a compensation of GET-pathway components on mRNA level in s*nd2a* or *snd2b* single mutants or vice versa cannot be detected (**Fig. 3B-C**). Moreover, only a limited number of TA proteins have been found to interact with both *At*SND2 proteins in our IP-MS analysis, further supporting the notion that no functional replacement/substitution between *At*SND2a or *At*SND2b and the GET-pathway may

exist. An explanation for the absence of a more severe defect can point towards existence of yet another translocation mechanism. In yeast and mammals, the ER membrane complex (EMC), was recently shown to facilitate insertion of TA proteins with moderately hydrophobic transmembrane domains (29). EMC orthologs are conserved in planta, but their physiological role is elusive, currently. Another explanation for a less severe phenotype in *Arabidopsis thaliana* could be functional redundancy of SND2a and SND2b, albeit the loss of one gene is not transcriptionally compensated by the other gene (**Fig. S2A**). Nevertheless, the lack of a viable double homozygous T-DNA insertion mutant of *snd2a/snd2b* despite no discernibly altered plants in single - or in homozygous/heterozygous mutants, supports the presumption that both proteins might be partially redundant. In line with this, reintroduction of the genomic *SND2b* gene can overcome the strong phenotype (**Fig. S4)**. Similar results are expected for *SND2a* since *snd2a* (+/-)/ *snd2b* (-/-) mutants displayed no detectable growth defect either (**Fig. 4A**). Intracellular propidium iodide clusters observed in *snd2a* (-/-)/ *snd2b* (-/-) mutants might represent stained nuclei as the dye intercalates with DNA (**Fig. 4B**). Most likely, the double homozygous mutant has compromised cell walls or a permeable plasma membrane as only few such round shapes were obtained in singe mutants or Col-0. Both observations are reminiscent of a cytokinesis defect resulting in multinucleate cells. However, other typical characteristics as cell wall stubs in dividing cells or gaps in cell walls as found in the cytokinesis defective *keule* or *keule*-like mutants are missing in our visual analyses(48). As some cytokinesis defects already arise in zygotic stages as seen for *keule* or *knolle* (48-50), assessment of early developmental stages would be relevant. Altered protein translocation to the ER, especially TA proteins were presumed to have strong impact on plant viability (23). As many SNARE proteins, e.g. the cytokinesis specific syntaxin related KNOLLE (SYP111), are tail-anchored proteins (51), defects in their translocation should reveal more pronounced defects (50). So far, the GET-pathway was thought to be an important route of TA proteins to the ER, however the rather mild phenotype of *get* mutants (23, 24) compared to *snd2a/snd2b* double homozygous mutants questions its dominant role in plants. Yet, we found only 9 TA proteins in our IP-MS analysis binding to both SND2a and SND2b, which also argues against a role as a backup mechanism for the GET-pathway let alone for the sole function of TA protein insertion.

In self-pollination experiments and backcrosses, a difference in the transition of SND2a and SND2b was observed. A possible explanation for this observation may be a

sporophytic effect on premeiotic inheritance (52). As seen in our qRT-PCR analysis of organ tissues, SND2a expression is drastically increased in siliques possibly indicating maternal- or paternal-to-zygotic transition of SND2a (53, 54). Differential transition of SND2b compared to SND2a might explain unusual segregation patterns of double homozygous progeny from *snd2a* (-/-)/*snd2b* (+/-). Parental contribution to the zygote transcriptome was shown to be stage dependent and both SND2a and SND2b are among parental transcriptome reads (55). However, individual contribution of parental transition of SND2a or SND2b remains unknown.

Still, a discrepancy between the obtained segregation values from our back-crossing experiment and segregation values of double homozygous progeny from both parental lineages reveals an insufficient percentage of double homozygous progeny (for *snd2a (+/-)/snd2b (-/-)*: 3%; for *snd2a (-/-)/snd2b (+/-)*: 16%). Possibly, the difference stems from an earlier developmental defect as we observed a significant reduction of ovules within the also smaller siliques (**Fig. 5C-D**).

Pollen tube growth speed and length experiments in single *loss-of-function* mutants were carried out to observe an effect on the male gametophyte. However, as discussed above, partial redundancy of both genes likely masks possible effects. To overcome this issue, pollen derived from homo-/heterozygote double mutants would have to be tested. Nevertheless, segregation of the heterozygous gene in the haploid pollen makes it difficult to evaluate such experiments. In case pollen is hampered by the mutated allele, non-altered pollen containing the wild type allele would dominate the experiments, leading to similar results as seen for single mutants. An alternative approach utilizing an additional introduction of a quartet (*qrt1*) mutant would help to analyse morphological differences in pollen and pollen tube growth as the separation of tetrads of microspores derived from a single pollen mother cell is impeded (56). This might also help to understand if different paternal lineages (*snd2a* heterozygous or *snd2b* heterozygous) influence pollen development.

Although functional validation of both proteins is still pending, we propose that SND2a and SND2b might have a function in protein translocation. Similar to hSND2 (32), interaction partners for both proteins are predicted components of translocation machineries as several subunits of SEC61, subunits of oligosaccharyltransferase (OST), translocon-associated proteins and auxiliary proteins as SEC62, ERdj2A and ERdj2B or putative orthologues of the EMC complex (**Fig. 2 and Table S1**). This

establishes an environment where it is likely that SND2a or SND2b assist in the translocation of precursor polypeptides. Quite recently, a role of BIP and Sec63 together with Sec62 in facilitating Sec61 channel assisted co-translational translocation of non-mature proteins with weak signal sequence was identified (31, 57) while Sec62 further supports post-translational insertion of small presecretory proteins (58, 59). It is quite tempting to speculate that both *Arabidopsis thaliana* SND2 paralogues assist in translocation of other pre-proteins on the SEC61-translocon which is favoured by the notion that yeast SND proteins similar associates with Sec62/Sec63 and show a broad substrate spectrum (25).

However, besides their similarities, we presume an additional function of SND2a based on our data. This suggestion is corroborated by the different observations in the expression pattern (**Fig. 1B**), GET1 interaction (**Fig. 2**), root hair phenotype (**Fig. 3A**) and identification of several interaction partners for SND2a related to stress response (**Fig. 6b, Table S1**). In humans it was demonstrated that hSND2 knockdown enhances autophagy and triggers ER-stress (30). It might be possible that SND2a adopted this function which is supported by its transcriptional induction by Tunicamycin-mediated ER-stress (**Fig. 6C)**. Considerable overlap between translocation of nascent proteins and stress responses is often reported, as failure to deliver proteins leads to cytotoxic effects that require a phalanx of stress responsive factors to be available on-demand (60). Quite often components of the diverse translocation machineries are involved in this task (16, 30, 40, 61-64). One of these proteins, SEC62, is proposed to act as a receptor mediating the delivery of misfolded or unfolded proteins into autophagosomes by interacting with ATG8e (40, 61). Although we do not observe an effect on the transcriptional level of ATG8e or SEC62 in *snd2a* mutants, it would be interesting to see if SND2a might act as a co-receptor as interaction with SEC62 was observed, however, this is quite speculative and further investigation needs to address this question.

Our data demonstrate that duplication of a yeast SND2 homologue occurred in Brassicaceae. SND2a and SND2b seems to be at least partially redundant and their interaction profile points to a translocation related function as was demonstrated in yeast and humans (25, 32). Based on our data we hypothesise an additional neofunctionalization of SND2a. Nevertheless, to substantiate our finding, further investigation especially on SND-dependent substrates or crosstalk between different

506 pathways will be essential. As demonstrated, neither SND2a nor SND2b can backup
507 *At*GET1 function while double mutants have a strong phenotype which contradicts the
508 data observed in yeast (25). Therefore, it will be interesting to examine the function of
509 SND2a and SND2b which might provide a broader understanding of protein
510 translocation to the ER membrane in plants.

511

Material and Methods

Plant Material, Growth Conditions and genotyping

T-DNA insertion lines were obtained from the Nottingham Arabidopsis Stock Centre (arabidopsis.info/), and insertion sites were verified by sequencing: *snd2a* (Salk_025845), *snd2b* (Salk_205396C), *Atget1-1* (SAIL_1210_E07) (23).

Seeds were grown either on soil or on ½ Murashige and Skoog (MS) medium including 0.9% plant agar, pH 5.7. Plants were cultivated in a 16-h light/8-h dark cycle at 23 °C in a growth chamber or in a continuous light room at 20°C. Seeds were surface sterilized with chlorine gas or a washing procedure with 70% (v/v) ethanol + 0.1% (v/v) Triton-X100 followed by two washing steps with 70% ethanol and a final washing step with 99% ethanol. Stratification to equalize germination was performed at 4°C for 2 to 3 days in darkness.

gDNA extraction was done using Edwards-buffer (200mM Tris-HC (pH 8), 25mM EDTA, 250mM NaCL, 0.5% (w/v) SDS with an isopropanol precipitation and cleaning of the gDNA in 70% ethanol. Primer combinations according to **Table S2** and **Fig. S2** were used, and PCR-products were analysed by agarose gel electrophoresis.

For the self-pollination experiment, the 7^{th}; 8^{th}; 9^{th} ripe siliques of 5 different plants were separately harvested and each seed were grown on ½ MS medium as described above. All germinated seeds were genotyped, and data were collected for **Table 1**. Exemplary pictures were taken and some plants were used for propidium iodide staining (see below) before their genotype was confirmed.

Construct Generation and Plant Transformation

Constructs were designed using Gateway technology or the Gateway-compatible 2in1 cloning system (36, 38). Constructs were transformed into *Agrobaterium tumefaciens* GV3101 strains and used to transform either Col-0 plants or infiltrate *N. benthamian* leaves (36).

IP-MS Analysis

Protein extracts of pUBQ10 >> SND2a-GFP or SND2b-GFP and as negative control, pUBQ10 >> GFP seedlings grown under continuous light were harvested after 14 d. Three grams of plant tissue was taken for immunoprecipitation according to Park et al. 2012 (65) with slight modifications. Only the second washing buffer (50 mM Tris·HCl, pH 7.5, 150 mM NaCl, 0.1% Triton X-100) was used, but it was used four times; 60 µL GFP-Trap Beads (ChromoTek) were added to each sample. The final precipitate in 2× Laemmli buffer was analysed by MS at the University of Tübingen Proteome Center. Three individual replicates were performed, and candidates that interacted with GFP only were omitted from the final list of interaction partners.

qRT-PCR Analysis and RT-PCR Analysis

For either DMSO or tunicamycin treatments for qRT-PCR, 6-day old plants were incubated on liquid ½ MS medium + 1% sucrose containing 5µg/ml tunicamycin or the respective amount of DMSO solvent control for 6h before harvest. Total RNA was isolated from 100mg of these seedlings using the GeneMATRIX Universal RNA Purification Kit (Roboklon) according to manufacturer`s instructions. The same procedure was applied for samples for organ specific expression analysis. To test for genomic DNA contamination, a PCR using the RNA was performed using primers for the housekeeping gene RAN3 (**Table S2**). Genomic DNA from *Arabidopsis* plants and cDNA without contamination were used as controls. For cDNA synthesis, ProtoScript II–First Strand cDNA Synthesis Kit (NEB; 1 µg RNA) was used. Primer efficiency for all used oligonucleotides (**Table S2**) were performed using different dilutions of Col-0 cDNA. Primer combinations specific for SND2a, SND2b, ATG8e, BIP3, GET1, SEC62 and GET3a were used for the following qRT-PCR (**Table S2**). Reference genes were SAND2 and PDF2 as described in (66). GoTaq® qPCR Master Mix (Promega) was used and qRT-PCR was performed on a One Step Plus Real-Time PCR System (Life technologies). Relative quantification values were calculated using the ΔΔCt method, with SAND2 and PDF2 as normalization control and relativized against Col-0 (DMSO) values according to (67). Values were either from biological replicates comprising technical triplicates each or from technical triplicates directly. Organ specific qRT-PCR was calculated without relativization to an internal control. For semiquantitative RT-

PCR, first strand cDNA was amplified for 30 cycles (23 cycles for RAN3) and verified by agarose gel electrophoresis.

Interaction Assays

rBiFC (38) was applied to test in planta protein–protein interaction as described previously (36). All boxplots were generated using BoxPlotR (68). Statistical analysis was performed using JMP15 (from SAS) with a Tukey HSD all pair test.

Microscopy, propidium iodide staining (PI)

CLSM microscopy was performed using a Leica SP8 at the following laser settings: GFP at 488 nm excitation (ex) and 495- to 520 nm emission (em); YFP at 514 nm ex and 520 to 560 nm em; RFP at 561-nm em and 595 to 620nm ex; mCherry at 587 nm ex and 500 to 620 nm em; PI at (ex) 536 and 600-620 em.

For propidium iodide staining, plants were incubated in 100µg/ml propidium iodide solution (Sigma Aldrich) +/- 0,01% Triton X-100 for 2-3 min before mounted on a slide in water for microscopy.

Root Hair Length Measurements, Pollen Tube Growth, Siliques Analysis

The roots of 7-d-old seedlings grown on ½ MS medium plates were imaged using a camera [Canon EOS 60D; Canon Macro Lens EF 100mm 1:2.8 L IS USM]. Root hair length was measured using Fiji. The 10 longest root hairs from 7 individual roots were examined per WT or T-DNA insertion lines.

Pollination experiments and aniline blue staining for pollen tube growth in pistils were performed as described in (69). *In vitro* pollen germination was performed as reported previously (70). Pollen tubes were imaged 7 h after pollen germination on solid medium, and pollen tube length was quantified using Fiji.

Statistical analysis was performed using JMP15 (from SAS) with a Tukey HSD all pair test.

For siliques analysis, the 7th; 8th; 9th siliques of 50-51day old plants were opened, imaged and all ovules were taken out fur counting. Genotypes of plants were confirmed by PCR before.

In Silico and Phylogenetic Analysis

SND2 orthologues were identified through BLASTp search (National Center for Biotechnology Information) against proteomes of candidate species and using default setting or Phytozome 12 (The Plant Genomic Resource). Accession numbers and FASTA data were downloaded from UniProt, NCBI or Phytozome-12. Multiple sequence alignments were computed using the MUSCLE algorithm with default settings of MEGA-X. Evolutionary history was inferred by using the Maximum Likelihood with settings for the Jones-Taylor-Thornton model, gamma distributed with invariant sites with 5 categories, and partial deletion with 95% site coverage cut off. The rest was default settings.

GO-term analysis was performed on IP-MS data using the given accession numbers from the University of Tübingen Proteome Center or Retrieve/ID mapping from UniProt converting to Araport accession numbers. Those were used either in GOrilla (Gene Ontology enRIchment anaLysis and visuaLizAtion tool) using the two unranked lists of gene settings with once the SND2a interaction partner as background and the SND2b interaction partner as target list and vice versa. Additional, lists of overlapping interacting proteins and of the single lists were analyzed using PANTHER (The Gene Ontology Resource). The *Arabidopsis* genome was set as background with default settings.

References

1. S. Shao, R. S. Hegde, Membrane protein insertion at the endoplasmic reticulum. *Annual review of cell and developmental biology* **27**, 25-56 (2011).
2. David J. Anderson, Peter Walter, G. Blobel, Signal recognition protein is required for the integration of acetylcholine receptor delta subunit, a transmembrane glycoprotein, into the endoplasmic reticulum membrane. *J Cell Biol* **93**, 501-506 (1982).
3. Weiqun Song, David Raden, Elisabet C. Mandon, R. Gilmore, Role of Sec61α in the Regulated Transfer of the Ribosome–Nascent Chain Complex from the Signal Recognition Particle to the Translocation Channel. *Cell* **100**, 333-343 (2000).
4. Asvin K.K. Lakkaraju, Camille Mary, Anne Scherrer, K. S. Arthut E. Johnson, SRP maintains nascent chains translocation-competent by slowing translation rates to match limiting numbers of targeting sites. *Cell* **133**, 400-451 (2008).
5. N. Borgese, S. Colombo, E. Pedrazzini, The tale of tail-anchored proteins: coming from the cytosol and looking for a membrane. *J Cell Biol* **161**, 1013-1019 (2003).
6. S. Stefanovic, R. S. Hegde, Identification of a targeting factor for posttranslational membrane protein insertion into the ER. *Cell* **128**, 1147-1159 (2007).
7. M. Schuldiner *et al.*, The GET complex mediates insertion of tail-anchored proteins into the ER membrane. *Cell* **134**, 634-645 (2008).
8. Y. W. Chang *et al.*, Crystal structure of Get4-Get5 complex and its interactions with Sgt2, Get3, and Ydj1. *J Biol Chem* **285**, 9962-9970 (2010).
9. J. W. Chartron, C. J. Suloway, M. Zaslaver, W. M. Clemons, Jr., Structural characterization of the Get4/Get5 complex and its interaction with Get3. *Proceedings of the National Academy of Sciences of the United States of America* **107**, 12127-12132 (2010).
10. G. S. Gunes Bozkurt, Fabio Vilardi, Stefan Amlacher, Klemens Wild, Gert Bange, Vincenzo Favaloro,, E. H. Karsten Rippe , Bernhard Dobberstein, Irmgard Sinning, Structural insights into tail-anchored protein binding and membrane insertion by Get3. *PNAS* **106**, 21131-21136 (2009).
11. A. Mateja *et al.*, The structural basis of tail-anchored membrane protein recognition by Get3. *Nature* **461**, 361-366 (2009).
12. M. E. Rome, M. Rao, W. M. Clemons, S. O. Shan, Precise timing of ATPase activation drives targeting of tail-anchored proteins. *Proceedings of the National Academy of Sciences of the United States of America* **110**, 7666-7671 (2013).
13. F. Vilardi, H. Lorenz, B. Dobberstein, WRB is the receptor for TRC40/Asna1-mediated insertion of tail-anchored proteins into the ER membrane. *J Cell Sci* **124**, 1301-1307 (2011).
14. F. Wang, C. Chan, N. R. Weir, V. Denic, The Get1/2 transmembrane complex is an endoplasmic-reticulum membrane protein insertase. *Nature* **512**, 441-444 (2014).
15. K. Powis *et al.*, Get3 is a holdase chaperone and moves to deposition sites for aggregated proteins when membrane targeting is blocked. *J Cell Sci* **126**, 473-483 (2013).
16. W. Voth *et al.*, The protein targeting factor Get3 functions as ATP-independent chaperone under oxidative stress conditions. *Mol Cell* **56**, 116-127 (2014).
17. R. Mukhopadhyay, Y. S. Ho, P. J. Swiatek, B. P. Rosen, H. Bhattacharjee, Targeted disruption of the mouse Asna1 gene results in embryonic lethality. *FEBS Lett* **580**, 3889-3894 (2006).
18. L. L. Daniele, F. Emran, G. P. Lobo, R. J. Gaivin, B. D. Perkins, Mutation of wrb, a Component of the Guided Entry of Tail-Anchored Protein Pathway, Disrupts Photoreceptor Synapse Structure and Function. *Invest Ophthalmol Vis Sci* **57**, 2942-2954 (2016).

19. S. Norlin, V. S. Parekh, P. Naredi, H. Edlund, Asna1/TRC40 Controls beta-Cell Function and Endoplasmic Reticulum Homeostasis by Ensuring Retrograde Transport. *Diabetes* **65**, 110-119 (2016).

20. J. Rivera-Monroy *et al.*, Mice lacking WRB reveal differential biogenesis requirements of tail-anchored proteins in vivo. *Sci Rep* **6**, 39464 (2016).

21. C. Vogl *et al.*, Tryptophan-rich basic protein (WRB) mediates insertion of the tail-anchored protein otoferlin and is required for hair cell exocytosis and hearing. *EMBO J* 10.15252/embj.201593565 (2016).

22. R. Srivastava, B. E. Zalisko, R. J. Keenan, S. H. Howell, The GET System Inserts the Tail-Anchored Protein, SYP72, into Endoplasmic Reticulum Membranes. *Plant Physiol* **173**, 1137-1145 (2017).

23. S. Xing *et al.*, Loss of GET pathway orthologs in Arabidopsis thaliana causes root hair growth defects and affects SNARE abundance. *Proceedings of the National Academy of Sciences of the United States of America* **114**, E1544-E1553 (2017).

24. L. Y. Asseck *et al.*, Endoplasmic reticulum membrane receptors of the GET pathway are conserved throughout eukaryotes. *Proceedings of the National Academy of Sciences of the United States of America* **118** (2021).

25. N. Aviram *et al.*, The SND proteins constitute an alternative targeting route to the endoplasmic reticulum. *Nature* **540**, 134-138 (2016).

26. J. Casson *et al.*, Multiple pathways facilitate the biogenesis of mammalian tail-anchored proteins. *J Cell Sci* **130**, 3851-3861 (2017).

27. A. Guna, R. S. Hegde, Transmembrane Domain Recognition during Membrane Protein Biogenesis and Quality Control. *Curr Biol* **28**, R498-R511 (2018).

28. B. M. Abell, M. R. Pool, O. Schlenker, I. Sinning, S. High, Signal recognition particle mediates post-translational targeting in eukaryotes. *EMBO J* **23**, 2755-2764 (2004).

29. A. Guna, N. Volkmar, J. C. Christianson, R. S. Hegde, The ER membrane protein complex is a transmembrane domain insertase. *Science* **359**, 470-473 (2018).

30. Y. Zhao *et al.*, Transmembrane protein 208: a novel ER-localized protein that regulates autophagy and ER stress. *PloS one* **8**, e64228 (2013).

31. S. Hassdenteufel *et al.*, Chaperone-Mediated Sec61 Channel Gating during ER Import of Small Precursor Proteins Overcomes Sec61 Inhibitor-Reinforced Energy Barrier. *Cell Rep* **23**, 1373-1386 (2018).

32. S. Hassdenteufel *et al.*, hSnd2 protein represents an alternative targeting factor to the endoplasmic reticulum in human cells. *FEBS Lett* **591**, 3211-3224 (2017).

33. M. E. Mabry *et al.*, Phylogeny and multiple independent whole-genome duplication events in the Brassicales. *Am J Bot* **107**, 1148-1164 (2020).

34. N. Walden *et al.*, Nested whole-genome duplications coincide with diversification and high morphological disparity in Brassicaceae. *Nat Commun* **11**, 3795 (2020).

35. M. R. Jackson, T. Nilsson, P. A. Peterson, Identification of a consensus motif for retent. *The EMBO Journal* **9**, 3153-3162 (1990).

36. D. G. Mehlhorn, N. Wallmeroth, K. W. Berendzen, C. Grefen, 2in1 Vectors Improve In Planta BiFC and FRET Analyses. *Methods in molecular biology* **1691**, 139-158 (2018).

37. M. J. Mitterreiter, F. A. Bosch, T. Brylok, S. Schwenkert, The ER luminal C-terminus of AtSec62 is critical for male fertility and plant growth in Arabidopsis thaliana. *The Plant journal : for cell and molecular biology* 10.1111/tpj.14483 (2019).

38. C. Grefen, M. R. Blatt, A 2in1 cloning system enables ratiometric bimolecular fluorescence complementation (rBiFC). *BioTechniques* **53**, 311-314 (2012).

39. S. Xing, N. Wallmeroth, K. W. Berendzen, C. Grefen, Techniques for the Analysis of Protein-Protein Interactions in Vivo. *Plant Physiology* **171**, 727–758 (2016).

40. S. Hu, H. Ye, Y. Cui, L. Jiang, AtSec62 is critical for plant development and is involved in ER-phagy in Arabidopsis thaliana. *J Integr Plant Biol* **62**, 181-200 (2020).

41. M. Borg, L. Brownfield, D. Twell, Male gametophyte development: a molecular perspective. *J Exp Bot* **60**, 1465-1478 (2009).

42. Z. Ge, A. Y. Cheung, L. J. Qu, Pollen tube integrity regulation in flowering plants: insights from molecular assemblies on the pollen tube surface. *New Phytologist* **222**, 687-693 (2019).

43. N. Koizumi, T. Ujino, H. Sano, M. J. Chrispeels, Overexpression of a gene that encodes the first enzyme in the biosynthesis of asparagine-linked glycans makes plants resistant to tunicamycin and obviates the tunicamycin-induced unfolded protein response. *Plant Physiology* **121**, 353-361 (1999).

44. Y. Iwata, N. Koizumi, Unfolded protein response followed by induction of cell death in cultured tobacco cells treated with tunicamycin. *Planta* **220**, 804-807 (2005).

45. Y. Cho, K. Kanehara, Endoplasmic Reticulum Stress Response in Arabidopsis Roots. *Front Plant Sci* **8**, 144 (2017).

46. P. Wang, T. M. Nolan, Y. Yin, D. C. Bassham, Identification of transcription factors that regulate ATG8 expression and autophagy in Arabidopsis. *Autophagy* **16**, 123-139 (2020).

47. M. R. Jackson, T. Nilsson, P. A. Peterson, Identification of a consensus motif for retention of transmembrane proteins in the endoplasmic reticulum. *The EMBO Journal* **9**, 3153-3162 (1990).

48. R. Sollner *et al.*, Cytokinesis-defective mutants of Arabidopsis. *Plant Physiol* **129**, 678-690 (2002).

49. W. Lukowitz, U. Mayer, G. Jurgens, Cytokinesis in the Arabidopsis embryo involves the syntaxin-related KNOLLE gene product. *Cell* **84**, 61-71 (1996).

50. M. H. Lauber *et al.*, The *Arabidopsis* KNOLLE Protein Is a Cytokinesis-specific Syntaxin. *J Cell Biol* **139**, 1485-1493 (1997).

51. V. Kriechbaumer *et al.*, Subcellular distribution of tail-anchored proteins in Arabidopsis. *Traffic* **10**, 1753-1764 (2009).

52. S. J. Mazer, D. L. Gorchov, Parental Effects On Progeny Phenotype In Plants: Distinguishing Genetic And Environmental Causes. *Evolution* **50**, 44-53 (1996).

53. M. Ueda *et al.*, Transcriptional integration of paternal andmaternal factors in theArabidopsiszygote. *Genes & Development* **31**, 617-627 (2017).

54. K. Wang, H. Chen, Y. Miao, M. Bayer, Square one: zygote polarity and early embryogenesis in flowering plants. *Current opinion in plant biology* **53**, 128-133 (2020).

55. P. Zhao *et al.*, Two-Step Maternal-to-Zygotic Transition with Two-Phase Parental Genome Contributions. *Dev Cell* **49**, 882-893 e885 (2019).

56. D. Preuss, S. Y. Rhee, R. W. Davis, Tetrad analysis possible in Arabidopsis with mutation of the QUARTET (QRT) genes. *Science* **264**, 1458-1560 (1994).

57. A. Ziska *et al.*, The signal peptide plus a cluster of positive charges in prion protein dictate chaperone-mediated Sec61 channel gating. *Biol Open* **8** (2019).

58. S. Lang *et al.*, Different effects of Sec61alpha, Sec62 and Sec63 depletion on transport of polypeptides into the endoplasmic reticulum of mammalian cells. *J Cell Sci* **125**, 1958-1969 (2012).

59. A. K. Lakkaraju *et al.*, Efficient secretion of small proteins in mammalian cells relies on Sec62-dependent posttranslational translocation. *Mol Biol Cell* **23**, 2712-2722 (2012).

60. J. Casson, M. McKenna, S. High, On the road to nowhere: cross-talk between post-translational protein targeting and cytosolic quality control. *Biochem Soc Trans* **44**, 796-801 (2016).

61. F. Fumagalli *et al.*, Translocon component Sec62 acts in endoplasmic reticulum turnover during stress recovery. *Nature cell biology* **18**, 1173-1184 (2016).

62. K. F. R. Pobre, G. J. Poet, L. M. Hendershot, The endoplasmic reticulum (ER) chaperone BiP is a master regulator of ER functions: Getting by with a little help from ERdj friends. *J Biol Chem* **294**, 2098-2108 (2019).

63. T. Akahane, K. Sahara, H. Yashiroda, K. Tanaka, S. Murata, Involvement of Bag6 and the TRC pathway in proteasome assembly. *Nat Commun* **4**, 2234 (2013).

64. H. Kawahara, R. Minami, N. Yokota, BAG6/BAT3: emerging roles in quality control for nascent polypeptides. *J Biochem* **153**, 147-160 (2013).

65. M. Park, S. Touihri, I. Muller, U. Mayer, G. Jurgens, Sec1/Munc18 protein stabilizes fusion-competent syntaxin for membrane fusion in Arabidopsis cytokinesis. *Dev Cell* **22**, 989-1000 (2012).

66. T. Czechowski, M. Stitt, T. Altmann, M. K. Udvardi, W. R. Scheible, Genome-wide identification and testing of superior reference genes for transcript normalization in Arabidopsis. *Plant Physiol* **139**, 5-17 (2005).

67. M. W. Pfaffl, G. W. Horgan, L. Dempfle, Relative expression software tool (REST©) for group-wise comparison and statistical analysis of relative expression results in real-time PCR. *Nucleic Acids Research* **30** (2002).

68. M. Spitzer, J. Wildenhain, J. Rappsilber, M. Tyers, BoxPlotR: a web tool for generation of box plots. *Nat Methods* **11**, 121-122 (2014).

69. L. Jiang *et al.*, VANGUARD1 encodes a pectin methylesterase that enhances pollen tube growth in the Arabidopsis style and transmitting tract. *The Plant cell* **17**, 584-596 (2005).

70. L. C. Boavida, S. McCormick, Temperature as a determinant factor for increased and reproducible in vitro pollen germination in Arabidopsis thaliana. *The Plant journal : for cell and molecular biology* **52**, 570-582 (2007).

Supporting Information

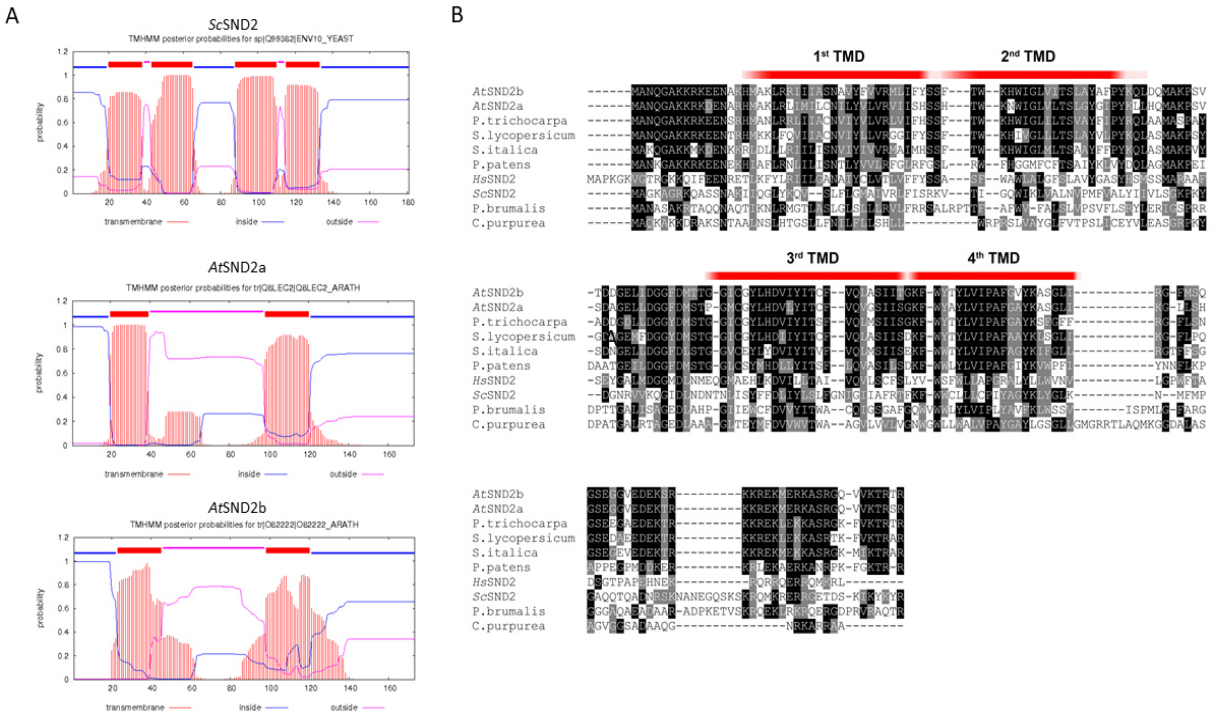

Figure S1: Structural evaluation of SND2 orthologues.
(A) Comparison of TMD prediction of membrane domains of *Sc*SND2, *At*SND2a and *At*SND2b (www.cbs.dtu.dk/services/TMHMM/). (B) Excerpts of multiple sequence alignments of SND2 orthologues of different eukaryotic species showing four conserved TMDs.

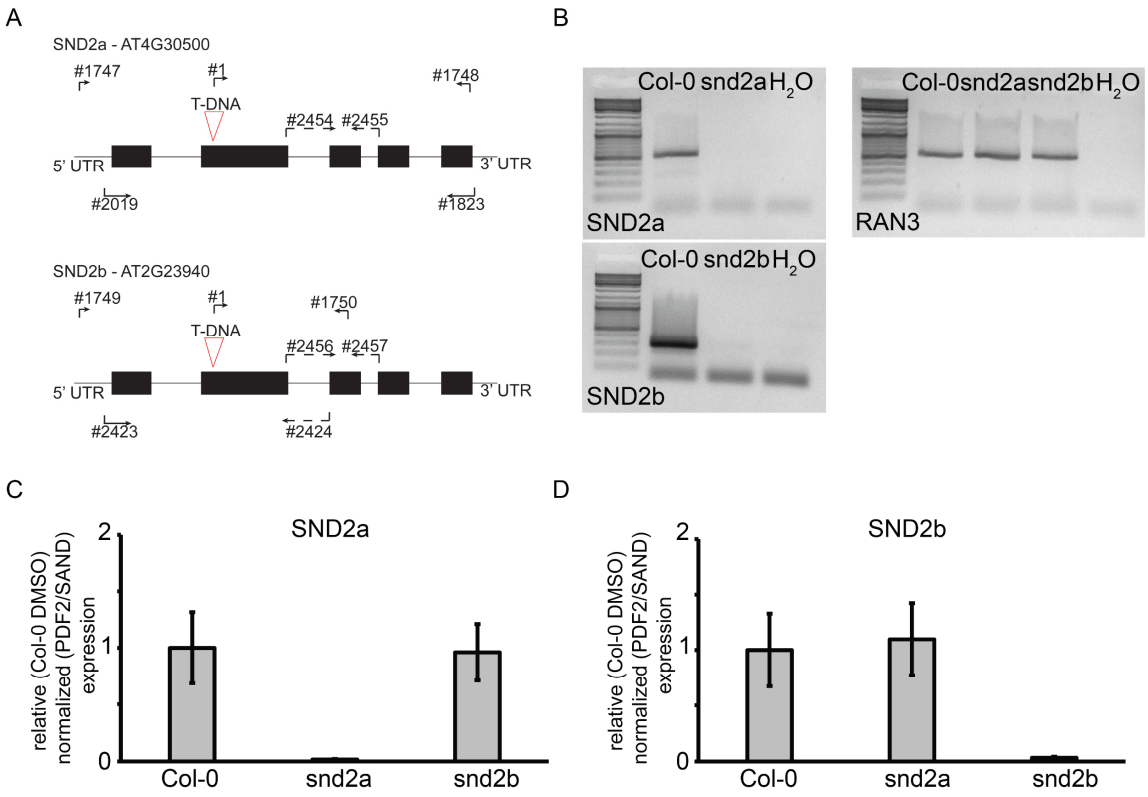

Figure S2: T-DNA insertion line analysis of SND2a and SND2b. (A) Cartoon of the SND2a and SND2b gene. The position of the T-DNA insertion was verified in the 2nd exon in both genes by sequencing. Primer pairs for genotyping, RT-PCR and qRT-PCR are indicated by arrows. RT-PCR primers ranging over an exon-exon junction are specified by dashed arrows. (B) Agarose electrophoresis of semiquantitative RT-PCR confirm lack of transcript in all mutant lines. RAN3 (AT5G55190) transcript was used as control. (C-D) Normalized relative transcript levels of SND2a (C) or SND2b (D) in Col-0 or the single mutant plants measured by quantitative RT-PCR. PDF2 and SAND served as reference genes and expression levels are relative to Col-0. Error bars indicate SD of technical replicates. (n=3).

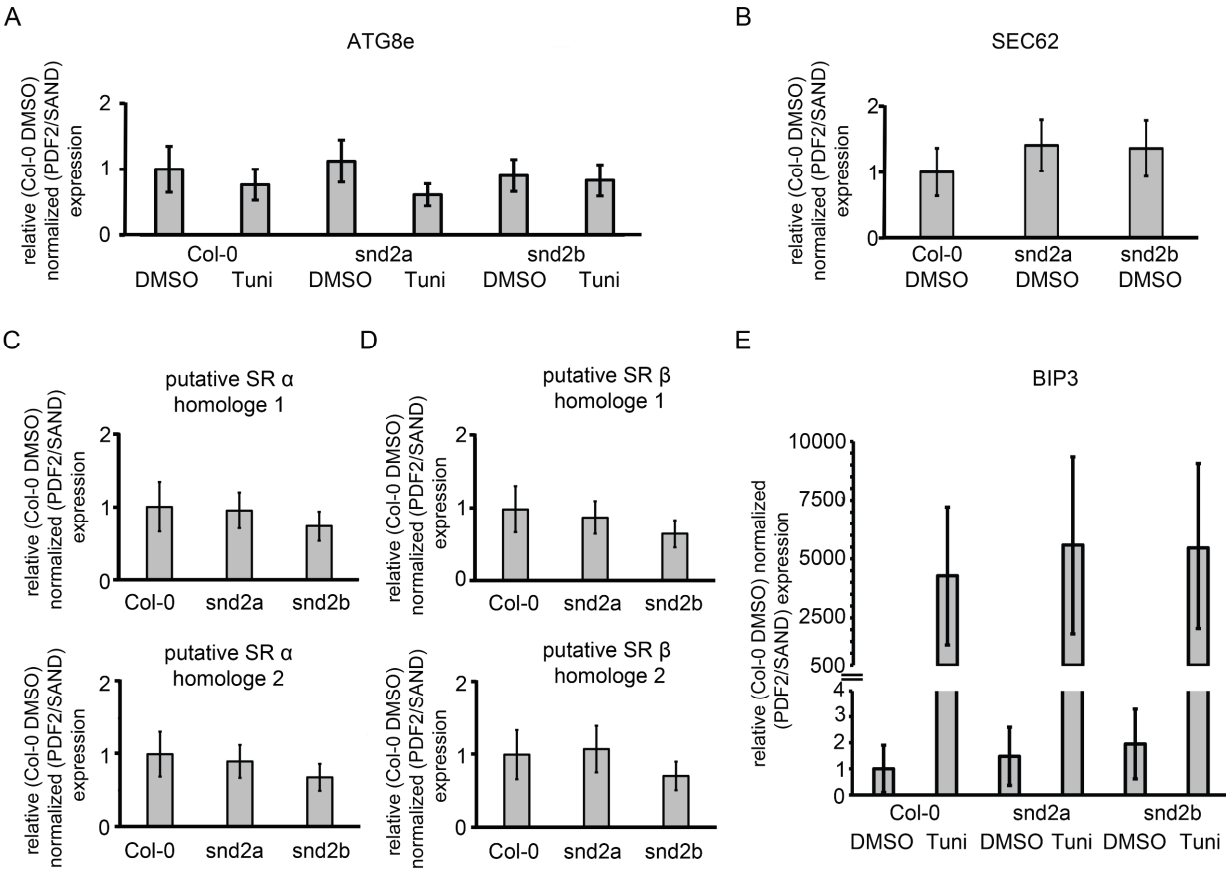

Figure S3: qRT-PCR analysis of *snd2a* and *snd2b* single mutants in comparison to Col-0.

(A-E) Normalized relative transcript levels of ATG8e (A), *At*SEC62 (B), putative SRP-receptor subunit SRα homologue 1 (At4g30600) and 2 (At4g35070) (C), putative SRP-receptor subunit SRβ homologue 1 (At5g05670) and 2 (At2g18770) (D) or BIP3 (E) in Col-0 or the knockout plants measured by quantitative RT-PCR. Where indicated, treatment of either DMSO or 5µg/ml tunicamycin was applied for 6h. PDF2 and SAND served as reference genes and expression levels are relative to Col-0. Error bars indicate SD of biological replicates (n=3 in A; C-E; n=2 in B). (C) Induction with tunicamycin leads to elevated ER-Stress level monitored by BIP3.

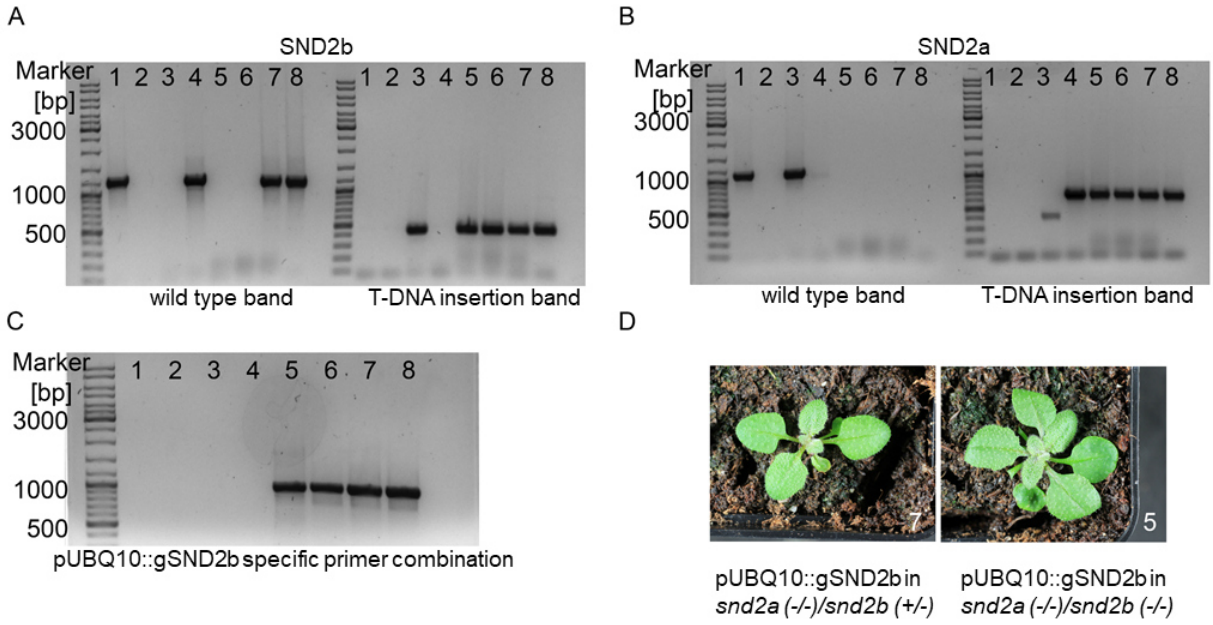

826

827 **Figure S4: Genotyping of *snd2a (-/-)/snd2b (+/-)* progeny transformed with**
828 **pUBQ10::gSND2b.** (A-C) **1**: Col-0, **2**: H_2O control, **3**: *snd2b (-/-)*, **4**: *snd2 a (-/-)*, **5-6**: two
829 independent *snd2a (-/-)/snd2b (-/-)* plants, **7-8**: two independent *snd2a (-/-)/snd2b (+/-)* plants.
830 (A) T-DNA in *snd2b* segregates, double homozygous *snd2a (-/-)/snd2b (-/-)* plants can be
831 observed. (B) Control that no segregation of *snd2a* occurred. (C) Successful transformation of
832 pUBQ10::gSND2b-3xHA confirmed with primer pairs specifically binding in the plasmid. (D)
833 Exemplary pictures of 22-day old plants showed no discernable developmental defect. The
834 number in the right corner represents the corresponding gDNA extracts used in (A-C).
835
836

837 **Table S1: Selection of IP-MS fished interaction partners**

Protein IDs	Protein names	Gene names	[n] detected with SND2a-GFP (max. 3)	[n] detected with SND2b-GFP (max. 3)
Q944K2	Dolichyl-diphosphooligosaccharide-protein glycosyltransferase 48 kDa subunit	OST48	3	3
F4HQE1	DnaJ protein ERDJ2A	ATERDJ2A	3	3
Q9ZUA0	Dolichyl-diphosphooligosaccharide-protein glycosyltransferase subunit 1B	OST1B	3	3
Q9SFX3	Dolichyl-diphosphooligosaccharide-protein glycosyltransferase subunit 1A	OST1A	3	3
F4HQD4	Heat shock 70 kDa protein 14/15	HSP70-15; HSP70-14	3	3
Q9MAH3	Protein DJ-1 homolog B	DJ1B	3	3
Q94AW8	Chaperone protein dnaJ 3; Chaperone protein dnaJ 2	ATJ3; ATJ2	3	3
Q9SYB5	Probable dolichyl-diphosphooligosaccharide-protein glycosyltransferase subunit 3B	OST3B	3	3
A0A1P8B5T4	DnaJ protein ERDJ2B	ERDJ2B	3	3
Q94BY3	Translocon-associated protein subunit beta (TRAB)	At5g14030 [GIP5]	3	3
A0A1P8AMW	Dolichyl-diphosphooligosaccharide-	DAD1	3	3

	protein glycosyltransferase subunit DAD1			
Q27GM7	ERAD-associated E3 ubiquitin-protein ligase HRD1B	At1g65040; HRD1B	3	0
Q9FG71	ER membrane protein complex subunit 8/9 homolog	EMB2731	3	3
Q9M0N1	Plant UBX domain-containing protein 10	PUX10	3	0
A0A1P8ART2	Molecular chaperone Hsp40/DnaJ family protein	At1g80030	3	0
Q9FK81	Stress-response A/B barrel domain-containing protein	At5g22580	3	3
P93042	Protein ROOT HAIR DEFECTIVE 3	RHD3	3	0
A0A1I9LRK5	DNAJ (DUF3353)	At3g51140	0	3
A0A2H1ZEE7	ERAD-associated E3 ubiquitin-protein ligase component HRD3A; HRD3B	HRD3A; HRD3B	1	0
F4IGI4	Translocon-associated protein subunit alpha (TRAP)	At2g21160	0	1
Q8VY97	ER membrane protein complex subunit 7 homolog	AT4G32130	0	1
Q9FJR0	Regulator of nonsense transcripts 1 homolog	UPF1	1	0
Q9SU27	ER membrane protein complex subunit 3 homolog	At4g12590 EMC3	0	2
Q84JM6	ER membrane protein complex subunit-like protein (DUF2012)	At2g25310	0	3

P0DI75	Protein transport protein Sec61 subunit gamma-2; Sec61 subunit gamma-1	SEC61γ2; SEC61γ1	0	1
Q9FH46	Signal recognition particle subunit SRP68	At5g61970	0	3
P37107	Signal recognition particle 54 kDa protein, chloroplastic	FFC	0	3
Q8RWJ5	SecY protein transport family protein	At1g29310; At2g34250	3	3
P53496	Actin-11 (β-actin homologue)	ACT11	3	0
Q9FHB8	PRCE3, PSI-INTERACTING ROOT-CELL ENRICHED 3	AT5g52420	3	3
F4J8C0	Integral membrane HRF1 family protein	HRF1 At1g30890	3	3
Q84TL5	ER lumen protein retaining receptor family protein	At1g75760	0	3
P51414	60S ribosomal protein L26-1	RPL26A	0	3
Q8L953	40S ribosomal protein S27-1, S27-2, S27-3	RPS27A; RPS27B; RPS27D	0	3
Q9FZ76	60S ribosomal protein L6-1	RPL6A	3	3
A0A1P8B2C7	60S acidic ribosomal protein P2-1; P2-2	At2g27710; At2g27720; RPP2A; RPP2B	3	3
Q9LRX8	60S ribosomal protein L13a-2	RPL13AB	3	3
A0A1P8AY36	60S ribosomal protein L18a-1; L18a-2; L18a-3	RPL18AA; RPL18AB; RPL18AC	3	3
Q9SYI0;	Protein translocase subunit SECA1, Protein translocase subunit SecA	SECA1; AGY1	3	3

F4IT48	60S ribosomal protein L7-3; L7-4	At2g44120; RPL7C; RPL7D	3	3
P38666	60S ribosomal protein L24-1; L24-2	RPL24A; RPL24B	3	3
Q9C9C6	60S ribosomal protein L6-2; L6-3	RPL6B; RPL6C	3	3
A8MS28	60S ribosomal protein L27-2; L27-3	At4g15000; RPL27B; RPL27C	3	3
Q9LYK9	40S ribosomal protein S26-1; S26-2; S26-3	RPS26A; RPS26B; RPS26C	3	3
F4KGU2	40S ribosomal protein S6-2	EMB3010; RPS6B	3	3
P42760	Glutathione S-transferase F6; F7	GSTF6; GSTF7	3	0
P93028	Ubiquitin-activating enzyme E1 1	UBA1	3	0
A0A1P8ART2	Molecular chaperone Hsp40/DnaJ family protein	At1g80030	3	0
A0A1P8B159	E3 ubiquitin-protein ligase HOS1	HOS1	3	0
F4JLD1	Guanine nucleotide-binding protein subunit beta; involved in apoptosis	AT4G34460; Gβ	1	0
Q9LP11	P-loop containing nucleoside triphosphate hydrolases superfamily protein	At1g43910	3	0
O81062	homologous to Signal Peptide Peptidases (SPP), required for pollen development and pollen germination	SPP AT2G03120	3	3
F4JQ55	Endoplasmin homologue SDH, ER chaperone	AT4g24190	3	3
Q9LD45	Bax inhibitor 1, involved in apoptosis	AT5G47120, BI1-1	3	3

838

839 **Table S2: List of Oligonucleotides**

#	5'-3' Sequence	Purpose
133	TGAAGGCTTCAAATTTCTGTGAATCC	Genotyping of get1-1
134	AGCCTCTCTCAAAAGCTGCTTAATTTC	Genotyping of get1-1
3	GCCTTTTCAGAAATGGATAAATAGCCTTGCTTCC	Genotyping of get1-1
1	ATTTTGCCGATTTCGGAAC	Genotyping of snd2a and snd2b
1747	AGGTTGTTCTGGCCCATTTAG	Genotyping of snd2a
1748	TGCACAAAGCAGGTGATGTAG	Genotyping of snd2a
1749	TACATGTTGAGTTCATTGCCG	Genotyping of snd2b
1750	CCAGTGATGATGGAAGCTAGC	Genotyping of snd2b
1823	GTTTAAGACATTCATCGAGATCTTGTCT	RT-PCR for SND2a
2019	CTTTTAACTCATGGCGAATCAAGGAG	RT-PCR for SND2a
2423	GAGATTAAGAATGGCGAATCAAGGAG	RT-PCR for SND2b
2424	CATCGTGCAAATATCCGCAGATTC	RT-PCR for SND2b
98	ACCAGCAAACCGTGGATTACCCTAGC	RT-PCR for RAN3
99	ATTCCACAAAGTGAAGATTAGCGTCC	RT-PCR for RAN3
2454	CATGAGCACTCCTGGAATGTG	qRT-PCR for SND2a
2455	GCTCCAAATGCAGGGATCAC	qRT-PCR for SND2a
2456	GGAATCTGCGGATATTTGCACG	qRT-PCR for SND2b
2457	CACCTCCCTCTGAACCTTGTG	qRT-PCR for SND2b
134	AGCCTCTCTCAAAAGCTGCTTAATTTC	qRT-PCR for GET1
439	ATGGAAGGAGAGAAGCTTATAGAAG	qRT-PCR for GET1
1435	TCACAATCTTAGTGATGCCTTTC	qRT-PCR for GET3a
1436	AGAATAAACCATCCATCCCGTC	qRT-PCR for GET3a
2458	TTACTTTTCGTGAGAGCAGTTGC	qRT-PCR for SEC62
2459	GTTCCTTCAATGTGGCTTCCTC	qRT-PCR for SEC62
2460	CACGGTTCCAGCGTATTTCAATG	qRT-PCR for BIP3
2461	CGAGAATGTTTGACTCCCCACC	qRT-PCR for BIP3
2462	GCTAATGTCAAGCGTTTACGAGG	qRT-PCR for ATG8e
2463	CAGAGATTAGATTGAAGAAGCACCGA	qRT-PCR for ATG8e
2425	TAACGTGGCCAAAATGATGC	qRT-PCR for PDF2
2426	GTTCTCCACAACCGCTTGGT	qRT-PCR for PDF2
2427	AACTCTATGCAGCATTTGATCCACT	qRT-PCR for SAND
2428	TGATTGCATATCTTTATCGCCATC	qRT-PCR for SAND
2492	GCTCCTGGTGCTGCCTAC	qRT-PCR for *At*SRα1
2493	GAAAGCAAATCATCCACATAAAGC	qRT-PCR for *At*SRα1
2494	CAAAATACAGAACGAGAGGTTGAG	qRT-PCR for *At*SRα2
2495	GACATTTCTTCTTCCTTCTGACTCA	qRT-PCR for *At*SRα2
2496	CTTCCTATCCATTCGCCTGGTC	qRT-PCR for *At*SRβ1

2497	CTCGGAGTTGGTAAAAGAGCAC	qRT-PCR for *At*SRβ1
2498	ACCATTTGGCTCTTATCTATTCGTTTG	qRT-PCR for *At*SRβ2
2499	CGTTCGGTTCCATTGACGTTAC	qRT-PCR for *At*SRβ2
1751	ggggacaagtttgtacaaaaaagcaggctCTATGGCGAATCAAGGAGCAAAG	DM-SND2a-attB1
1752	ggggacaactttgtataataaagttgCTATGGCGAATCAAGGAGCAAAG	DM-SND2a-attB3
1753	ggggaccactttgtacaagaaagctgggtgTCGAGATCTTGTCTTAACGACTTG	DM-SND2a-attB2-without Stop
1754	ggggacaactttgtatagaaaagttgggtgTCGAGATCTTGTCTTAACGACTTG	DM-SND2a-attB4-without Stop
1755	ggggacaagtttgtacaaaaaagcaggctCTATGGCGAATCAAGGAGCGAAG	DM-SND2b-attB1
1756	ggggacaactttgtataataaagttgCTATGGCGAATCAAGGAGCGAAG	DM-SND2b-attB3
1757	ggggaccactttgtacaagaaagctgggtgTCTTGTTCTCGTCTTGACGACT	DM-SND2b-attB2-without Stop
1758	ggggacaactttgtatagaaaagttgggtgTCTTGTTCTCGTCTTGACGACT	DM-SND2b-attB4-without Stop
363	ACTTTCTCTCAATTCTCTCTACCG	Genotyping UBQ10::gSND2b

840

IV. Mehlhorn et al., 2018:

2in1 vectors improve in planta BiFC and FRET analyses

Chapter 11

2in1 Vectors Improve In Planta BiFC and FRET Analyses

Dietmar G. Mehlhorn, Niklas Wallmeroth, Kenneth W. Berendzen, and Christopher Grefen

Abstract

Protein–protein interactions (PPIs) play vital roles in all subcellular processes and a number of tools have been developed for their detection and analysis. Each method has its unique set of benefits and drawbacks that need to be considered prior to their application. In fact, researchers are spoilt for choice when it comes to deciding which method to use for the initial detection of a PPI, and which to corroborate the findings. With constant improvements in microscope development, the possibilities of techniques to study PPIs in vivo, and in real time, are continuously enhanced, and expanded. Here, we describe three common approaches, their recent improvements incorporating a 2in1-cloning approach, and their application in plant cell biology: ratiometric Bimolecular Fluorescence Complementation (rBiFC), FRET Acceptor Photobleaching (FRET-AB), and Fluorescent Lifetime Imaging (FRET-FLIM), using *Nicotiana benthamiana* leaves and *Arabidopsis thaliana* cell culture protoplasts as transient expression systems.

Key words Protein–protein interaction, rBiFC, FRET, Acceptor photobleaching, FLIM, Gateway, SEC61, 2in1

1 Introduction

Core cellular processes such as signal perception and transduction, vesicle trafficking, transport activities, and metabolic pathways rely on formation of complex protein networks. Analysis of the biochemical mechanisms at the molecular level requires a fundamental understanding of the protein–protein interactions (PPIs) involved. Over the past decades, a number of techniques such as Co-immunoprecipitation (CoIP), the Yeast Two-Hybrid (Y2H), the Split Ubiquitin System (SUS), Förster Resonance Energy Transfer (FRET) and related methods, as well as Bimolecular Fluorescence Complementation (BiFC) have become routine laboratory techniques to dissect PPIs (reviewed in [1]). Technological advancements in microscope development have enhanced possibilities further by facilitating real/life-time imaging of PPIs. Even techniques that were thought to be predominantly in vitro techniques such as

Chris Hawes and Verena Kriechbaumer (eds.), *The Plant Endoplasmic Reticulum: Methods and Protocols*, Methods in Molecular Biology, vol. 1691, DOI 10.1007/978-1-4939-7389-7_11, © Springer Science+Business Media LLC 2018

CoIP are now applicable for microscopy analysis at the single-molecule level [2].

Recently, our lab has introduced 2in1 cloning, a gateway-compatible approach to simultaneously clone two genes-of-interest into two independent expression cassettes on the same T-DNA/plasmid [3] (Fig. 1a). This cloning system is well suited for PPI techniques that rely on transient transfection systems, as a mixture of two (or more) independent *Agrobacteria* each carrying their own plasmid can lead to unequal gene dosage resulting in high variability of coexpression [4]. We have combined the 2in1-cloning system with Bimolecular Fluorescence Complementation [3] as well as with a range of suitable fluorophores for enhanced FRET/FLIM analysis [4].

This chapter describes the application of the optimized 2in1 vector sets that can be used for ratiometric Bimolecular Fluorescence Complementation (rBiFC), FRET-Acceptor Photobleaching (FRET-AB), and Fluorescent Lifetime Imaging (FRET-FLIM), using either *Nicotiana benthamiana* leaves or *Arabidopsis thaliana* cell culture protoplasts as expression system [3, 4].

1.1 Ratiometric Bimolecular Fluorescence Complementation (rBiFC)

Bimolecular Fluorescence Complementation (BiFC) is a protein fragment complementation analysis whose first application was in bacteria [5]. The principle of BiFC is straightforward: a previously split fluorescent protein (FP) reconstitutes due to an interaction of two proteins of interest that are fused to the complementary nonfluorescent fragments (Fig. 1b). One major advantage of BiFC is the applicability of the system to almost all types of proteins (cytosolic, nuclear, organellar, or membrane-bound), and the detection of interaction in an in vivo context. It also allows visualization of PPIs at their site of first interaction—which should not be confused with the subcellular position where these proteins normally reside or are trafficked to—a misconception that is often inferred. Nevertheless, the flaws of the technique almost match the advantages. Overexpression of fusion proteins as well as their FP fragment tag can lead to mis-localization and alter the likelihood of a positive readout. Reassembly of the FP is irreversible, promoting and stabilizing weak or transient interactions, but thereby also causing artifactual results even in the absence of a true interaction [1, 6]. However, the biggest disadvantage in conventional BiFC systems used in the plant field is the use of two individual plasmids and their co-infiltration in transient transformation. This leads to very high variability in gene dosage and only about 70–80% of coexpression ratios [4]. In other words, out of four or five cells analyzed, one does not contain both fusion proteins present making a meaningful interpretation of the results very hard. In addition, classical BiFC constructs do not contain concurrent reference markers making quantification against presumed negative controls (which could be non- or unequally transformed cells) a cherry-picking exercise (Fig. 2).

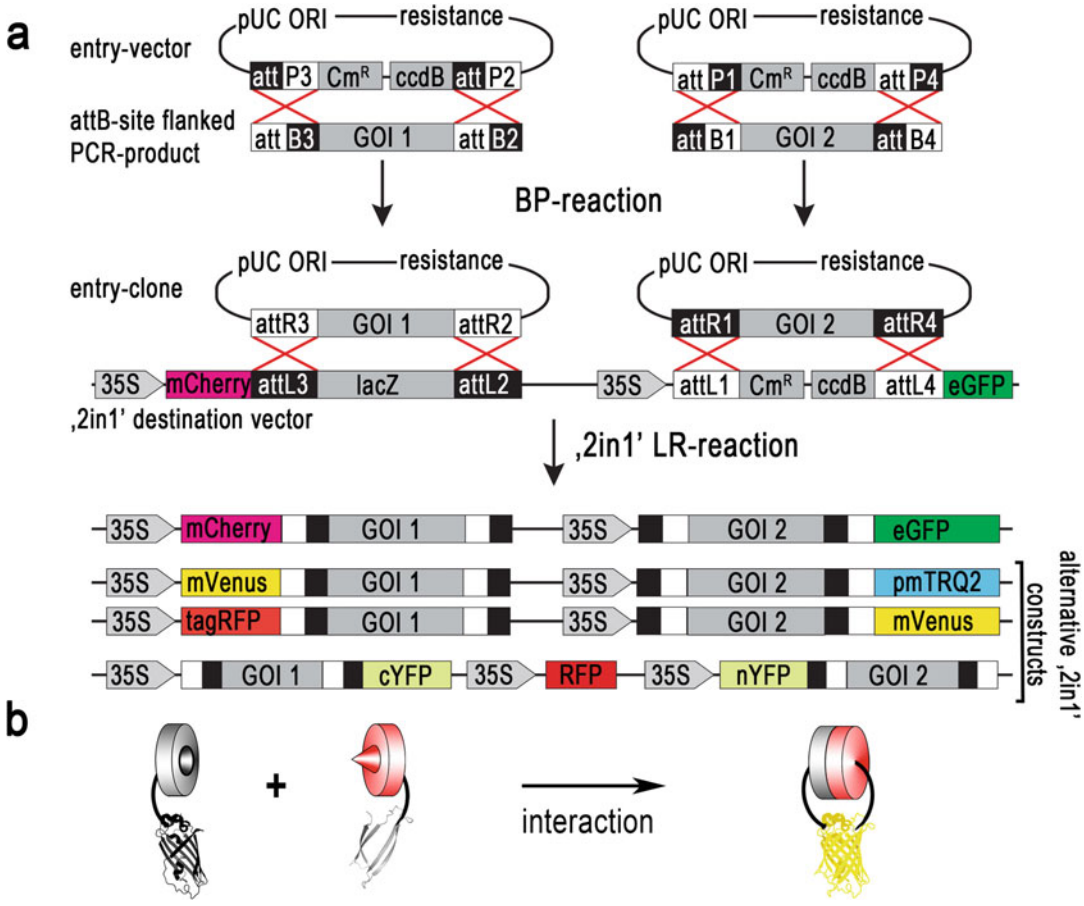

Fig. 1 Concepts of 2in1 cloning, Bimolecular Fluorescence Complementation and Förster Resonance Energy Transfer. (**a**) Site-specific BP recombination of PCR products and Entry vectors generates Entry clones. A subsequent one-step LR reaction recombines the two genes-of-interest (GOI) simultaneously in a 2in1 Destination vector. Depicted are the "2in1" vectors used in this chapter. *See* Table 1 for details. *35S* cauliflower mosaic virus 35S promoter and omega translational enhancer sequence, *pUC ORI* origin of replication, *Cm*^{R} chloramphenicol acetyltransferase resistance gene, *ccdB* gyrase inhibitor gene, *lacZ* lacZ expression cassette. (**b**) Cartoon depicting the concept of bimolecular fluorescence complementation (BiFC). Two proteins (*grey* and *red*) are tagged with nonfluorescent YFP fragments, nYFP and cYFP, respectively. Interaction of both proteins leads to reconstitution of fluorescent YFP. (**c**) Simplified Jablonski diagram depicting the excitation of an electron in a cyan-fluorescing protein (CFP). After internal conversion (*black wavy arrow*) to the S1 ground state (*cyan solid arrow*) a crossing of the energy barrier between S1 and S0 can cause the emission of a photon at a longer wavelength (red shifted, Stokes shift; i.e., fluorescence). If an acceptor molecule is in close enough proximity (here, YFP attached to a red-colored interacting protein), the energy can be transferred non-radiatively to the acceptor molecule. (**d**) Absorbance/fluorescence spectrum of mTurquoise2 and mVenus. The *dark grey surface* depicts the λ^4 weighted overlap integral. Acceptor and donor spectral bleed through are shown in *magenta* and *green*, respectively. (**e**) Example of a FRET acceptor photobleaching experiment. A nucleus expressing two interacting proteins attached to a donor and an acceptor fluorophore. After bleaching (right), the acceptor fluorescence is almost completely lost, but an increase in donor fluorescence can be detected. (**f**) Exemplary fluorescence lifetime decay curve of a putative donor molecule when FRET is occurring (*red solid curve*; *t*1) or in the absence of FRET (*cyan solid line*; *t*2). Fluorescence lifetime *t* is the average time that a fluorescent protein resides in the excited state and at which fluorescence intensity decreased to 1/*e* of its initial value. (**b**–**f**) modified from [1, 4]

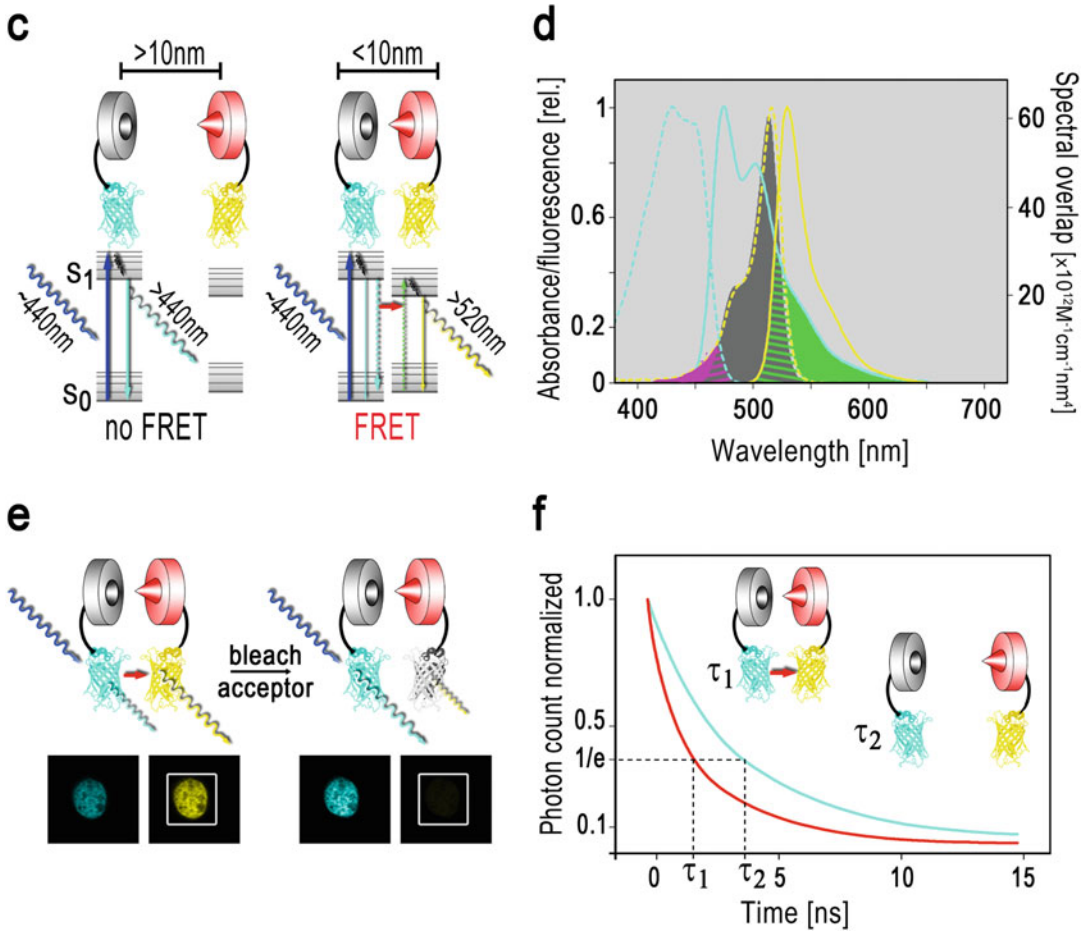

Fig. 1 (continued)

Contrary to classical BiFC, the ratiometric BiFC (rBiFC) approach addresses most of these issues and provides means for internal, ratiometric quantification of results [3]. Placing both FP fragments on the same T-DNA guarantees equal gene dosage of both nonfluorescent fusion proteins and the inclusion of a soluble RFP marker provides a readout for ratiometric analysis and transformation control of the cell under study [3] (Fig. 3). The technique has since been used in a number of studies for the detection of PPIs or their structure-function analysis [7–13, 24] (*see* **Note 1**).

1.2 Förster Resonance Energy Transfer-Acceptor Bleaching (FRET-AB)

An alternative, more reliable, yet sophisticated technique exploits the physical phenomenon of resonance energy transfer which was first postulated by Theodor Förster in 1946 and has been named after him as commemoration [14] (Fig. 1c–f). The principle of FRET is a non-radiative energy transfer from an excited donor fluorophore to an acceptor molecule—often, but not

Table 1
Available 2in1 expression vector sets for rBiFC and FRET experiments[a]

	Origin of replication		Resistance marker				
Name	***E. coli***	***A. tumefaciens***	**Bacteria**	**Plant**	**Promoter**	**FPs[a]**	**Reference**
pBiFC-2in1	ColE1	pVS1	Spectinomycin	None	CaMV35S	nYFP, cYFP, RFP[b]	[3]
pFRETcg-2in1	ColE1	pVS1	Spectinomycin	Basta	CaMV35S	mCherry, mEGFP	[4]
pFRETvt-2in1	ColE1	pVS1	Spectinomycin	Basta	CaMV35S	mVenus, mTRQ2	[4]

[a]Plasmids exist in all possible tag combinations of fluorescent proteins (FPs)
[b]RFP fluorescence serves as transformation control and ratiometric marker

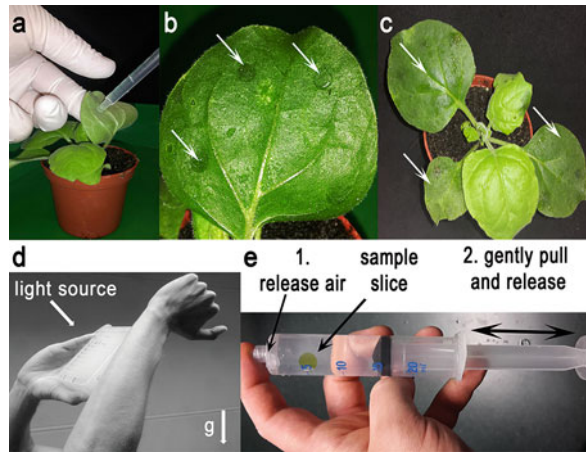

Fig. 2 Method handling. (**a**) Infiltration of 3–4-week-old *N. benthamiana* leaves using a syringe as described in Subheading 3.2. (**b**) *White arrows* point at areas of infiltration at the abaxial side of the leaves. (**c**) The first two youngest (*top*) leaves of a 4–6-week-old *N. benthamiana* plant should *not* be used for infiltration. Instead, slightly older leaves (*white arrows*) are ideal with respect to suitability for injection and transgene expression [23]. (**d**) "Tapping method" for gentle mixing of protoplasts with DNA. (**e**) Preparation of a *N. benthamiana* leaf disc for microscopic analysis. The syringe is filled with water, which – by application of a vacuum – replaces the air in the intercellular space of the leaf epidermis enhancing image quality

necessarily—fluorescent itself. Prerequisite is an overlap of the donor emission with the excitation spectrum of the acceptor. FRET only occurs if donor and acceptor are in close enough proximity of 10 nm or less [15, 16]. Such resolution of molecular distances is more than a magnitude lower than the diffraction limit of light microscopy at 200 nm, allowing distinction of protein co-localization from interaction.

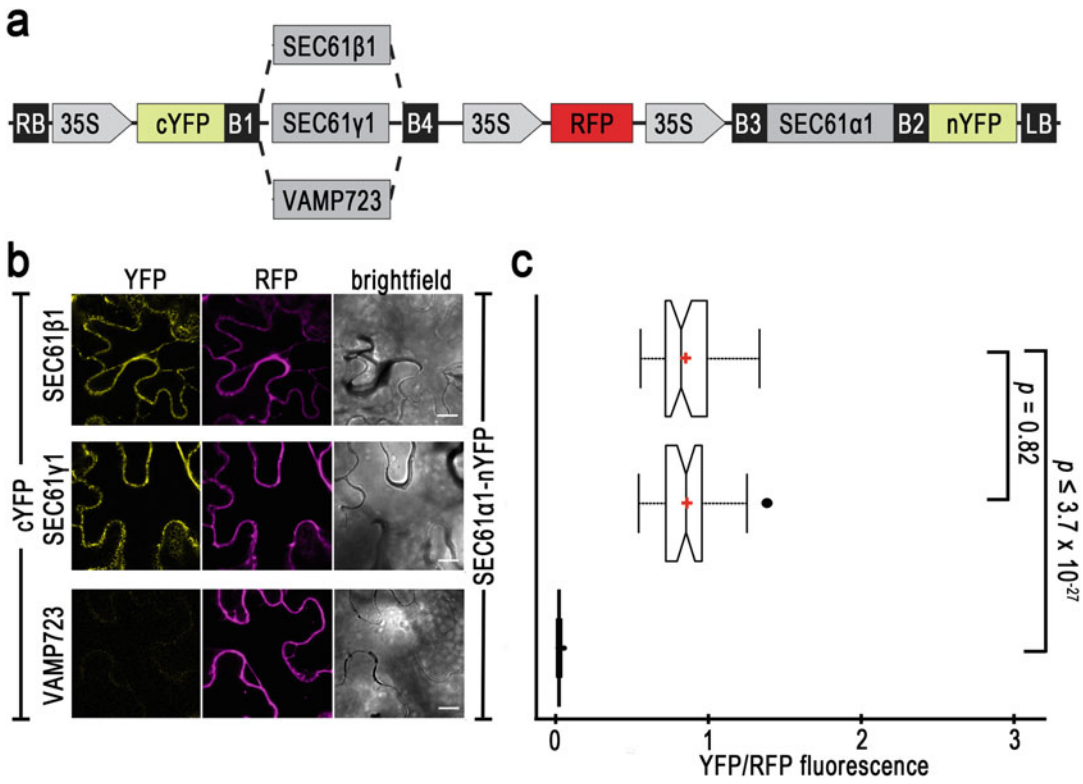

Fig. 3 rBiFC analysis of putative *Arabidopsis* SEC61 subunits in *N. benthamiana* leaves and *A. thaliana* protoplasts. (**a**) Cartoon of the "2in1" rBiFC destination constructs used in this experiment [3]. (**b**) Representative images of *N. benthamiana* leaves expressing SEC61α1-nYFP (At2g34250), RFP, and either cYFP-SEC61β1 (At2g45070), cYFP-SEC61γ (At5g50460), or, cYFP-VAMP723 (At2g33110), respectively. (**d**) At least 40 images were recorded per construct, and YFP/RFP mean fluorescence intensity calculated. *Box plot* depicts the median with outer limits at the 25th and 75th percentile, respectively. Notches indicate the 95% confidence intervals; Tukey whiskers extend to the 1.5× IQR and outliers are depicted as *black dots*. *Red crosses* mark sample means of each dataset. Exemplary *p*-values (*t*-test) are indicated in graph. (**d**) Representative images of *Arabidopsis* protoplasts expressing the same constructs. (**e**) At least ten protoplasts were recorded per construct, and YFP/RFP mean fluorescence intensity calculated. Boxplot as before. (**f**) Immunoblot analysis of HA-tagged SEC61α1, MYC-tagged proteins of interest and soluble RFP expressed in *Arabidopsis* protoplasts used for rBiFC analysis. *Asterisks* indicate expected protein size. Scale bar in (**b**, **d**) = 10 μm

In fluorescence microscopy, the FRET phenomenon can be detected using different approaches. Classical FRET approaches simply measure fluorescence of the acceptor when the donor is excited. However, this can lead to artifactual results due to spectral bleed through, a phenomenon deriving from an overlap of excitation spectrum of the donor with the emission spectrum of the acceptor, which—unfortunately—is a common property with most current FRET FP couples.

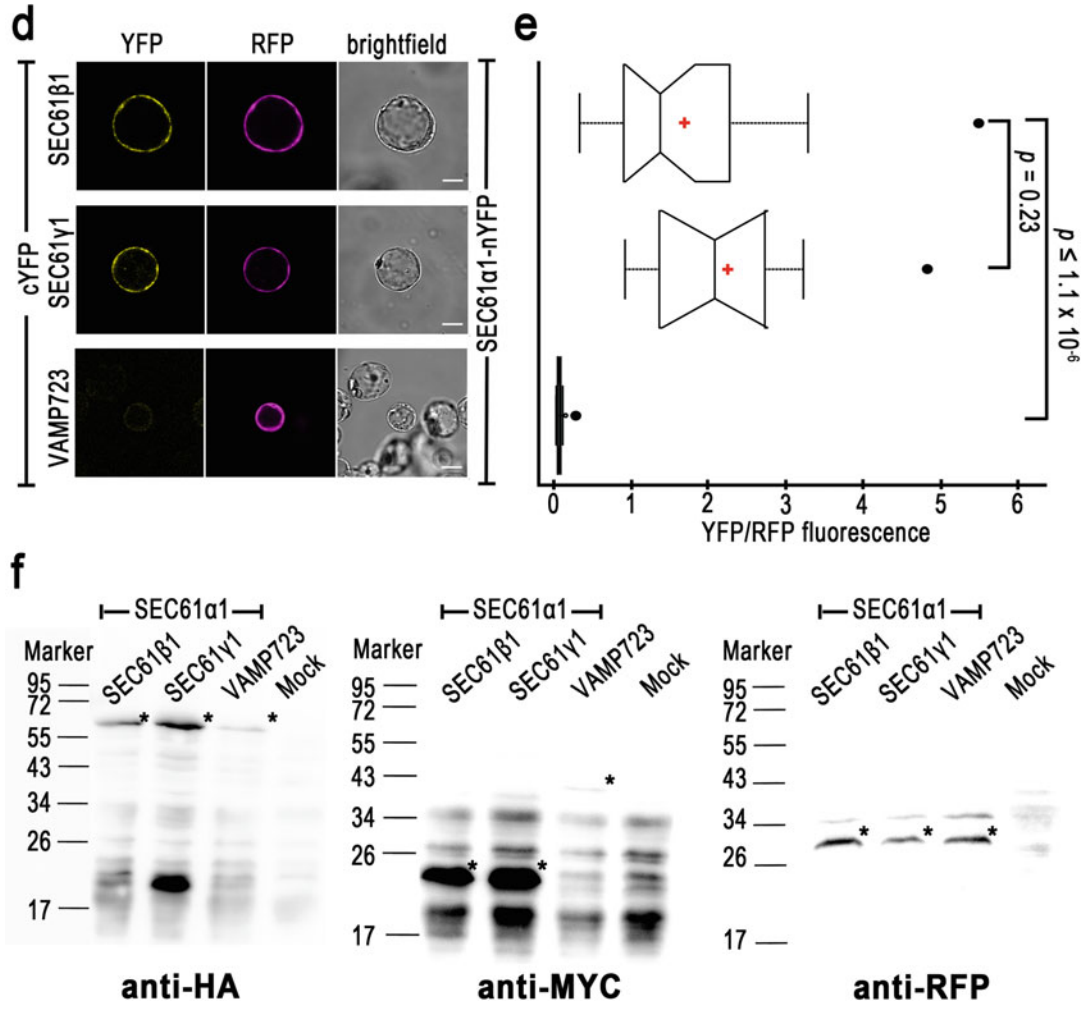

Fig. 3 (continued)

An alternative, more credible method based on FRET is "Acceptor Photobleaching" (FRET-AB). Here, the intensities of the donor fluorophore before and after photobleaching of the acceptor are measured in a specified region of interest (ROI). Bleaching of the acceptor leads to an increase in donor fluorescence in the ROI as the energy that would have been transferred to the acceptor remains within the donor, leading to increased fluorescence of the latter.

AB does not require high-end microscopes and can be carried out at any fluorescence microscope which is an advantage compared to Fluorescence Lifetime Imaging Microscopy (FLIM) measurements [15] (*see* below). However, photobleaching in AB can potentially photo-damage the samples and is therefore not suitable in prolonged time-lapse experiments. Other pitfalls are concomitant bleaching of acceptor and donor, as well as movement of the cytoplasm, both of which may lead to unfeasible results.

1.3 Fluorescence Lifetime Imaging Microscopy (FLIM)

Classical FRET and FRET-AB are both intensity-based methods and—as such—can be compromised by suboptimal fluorophore concentration ratios. Measurement of fluorescence lifetime, however, might overcome this issue [16, 17]. Briefly, irradiation leads to raising of the FP to an excited—S_1—state before relaxation to the ground—S_0—state. The average time the fluorophore resides in the excited state represents its fluorescence lifetime and is unique for each FP [18]. When an acceptor molecule is in close enough range (<10 nm), it can serve as energy sink, resulting in a lifetime "decay" of the donor molecule. Such reduction in lifetime can be compared to negative controls or "donor only" samples which inform on the original lifetime of an FP—the difference between the two informs on PPI (Fig. 4).

Still, while small imbalances in concentration of donor and acceptor do not affect FLIM measurements, the lifetime of fluorophores is affected by other factors such as for example changes in redox state, pH, or temperature. Yet, FRET-FLIM delivers more credible results as it is almost unaffected by concentration differences and spectral properties compared to FRET-AB; but it requires sophisticated and expensive equipment as well as considerable training and experience of the scientist who handles it.

2 Materials

2.1 Bacteria and Plants

For transient transformation of *Nicotiana benthamiana* leaves via infiltration, *Agrobacterium tumefaciens* strain GV3101 pMP90 carrying the selection markers for growth on rifampicin and gentamicin was chosen [19, 20].

2.2 Media and Reagents (Tobacco Leaf Infiltration)

1. Luria-Bertani (LB) medium: 1% tryptone, 0.5% yeast extract, 0.5% NaCl, pH 7.0–7.5 (for solid media add 2% agarose).
2. Antibiotics (1000× stock solution): gentamicin (20 mg/mL in distilled water), spectinomycin (100 mg/mL in distilled water), and rifampicin (50 mg/mL in DMSO).
3. AS medium: 10 mM $MgCl_2$, 10 mM MES-KOH, pH 5.6, 150 μM acetosyringone.
4. Sterile distilled water.

2.3 Media and Reagents (Protoplasts)

2.3.1 Sterile Filtration

The most economic sterile filtration method is to acquire a peristaltic pump and use membrane filters with a Swinnex Filter Holder (Millipore).

2.3.2 Sterile Erlenmeyer Flasks for Cell Culture

250 mL Erlenmeyer flasks are stoppered with Rotilabo®-culture plugs and covered well by aluminum foil. Sub-culturing is performed under highly sterile conditions and the flasks are flamed when opened to prevent contamination.

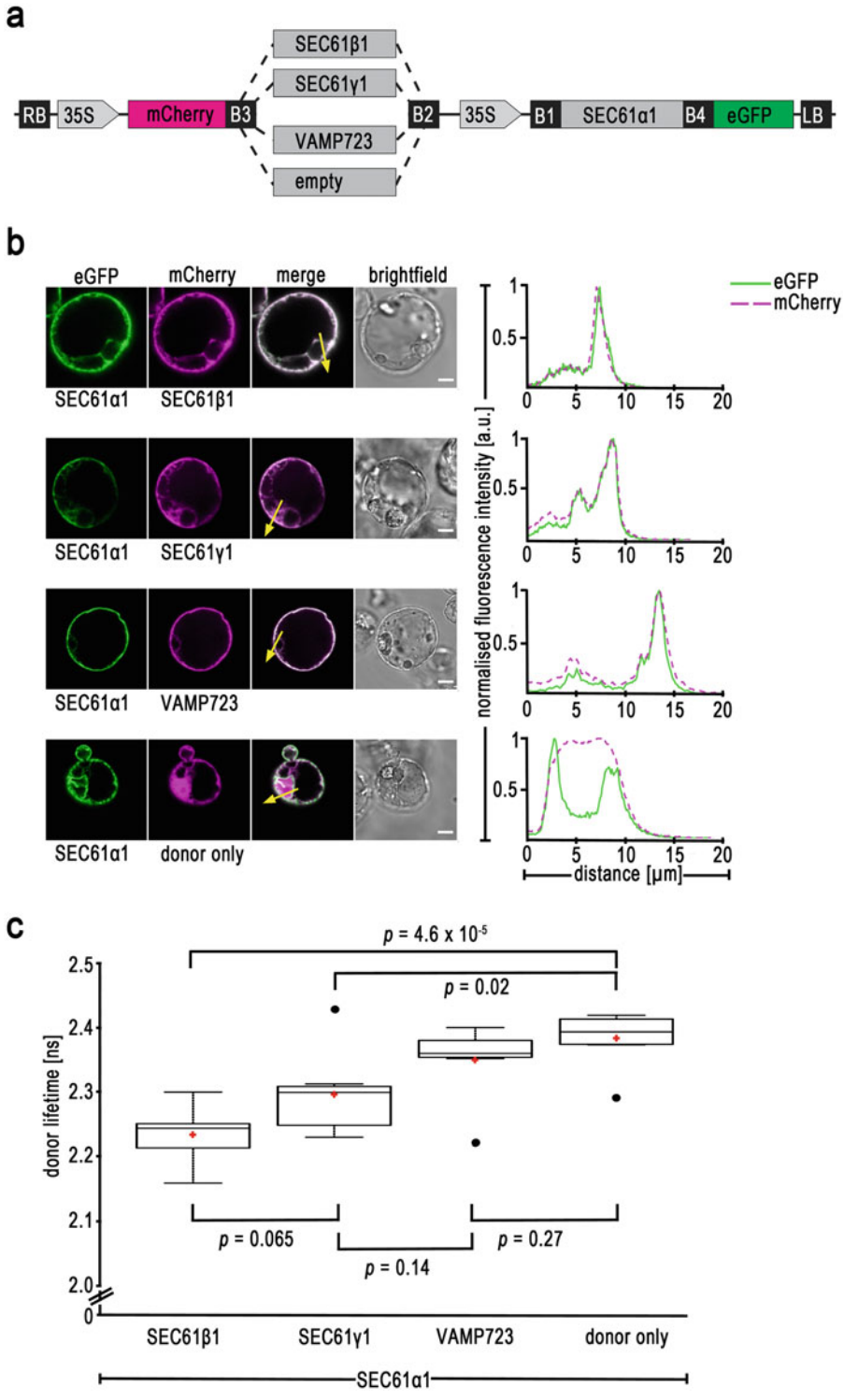

Fig. 4 FRET-FLIM analysis of putative *Arabidopsis* SEC61 subunits in *A. thaliana* protoplasts. (**a**) Cartoon of the "2in1" FRET destination constructs used in this experiment [4]. (**b**) Representative images of *A. thaliana*

2.3.3 Pipetting of Protoplasts

We use 200 μL, cut tips to handle protoplasts and try to aim for a diameter of 2–3 mm. Protoplasts are extremely sensitive to shearing stress and larger tip pore sizes circumvent this.

2.3.4 Cell Culture Maintenance Media

1. MS Col Medium (for 1 L): 4.3 g/L Murashige and Skoog Basal Salt Mixture (MS), 5 mL of NPT-Vitamin Stock, 100 mg/mL *myo*-Inositol, 30 g/L Sucrose, pH 5.8 with KOH. After autoclaving and before use, add 2,4-D to 1 mg/L. Store at 4 °C in the dark.
2. NPT-Vitamin Stock: 1 mg/mL Nicotinic acid, 1 mg/mL Pyridoxine-HCl, 10 mg/mL Thiamine-HCl in dH_2O. Sterilize by filtration (0.22 μm) and store at −20 °C.
3. 2,4-D Stock (for 100 mL): Dissolve 100 mg in 10 mL absolute ethanol and bring to 100 mL with dH_2O. Concentration is 1 mg/mL. Sterilize by filtration (0.22 μm) and store at −20 °C.

2.4 Media for Protoplast Generation

1. Wall digestion solution without enzymes: 8 mM $CaCl_2 \cdot 2H_2O$, 0.4 M Mannitol, pH 5.5 with KOH. Sterilize by filtration (0.22 μm).
2. Wall digestion solution: 1% Cellulase, 0.25% Macerozyme, 8 mM $CaCl_2 \cdot 2H_2O$, 0.4 M Mannitol, pH 5.5 with KOH. Sterilize by filtration (0.22 μm), use immediately or store at −20 °C.
3. W5: 154 mM NaCl, 125 mM $CaCl_2$, 5 mM KCl, 5 mM Glucose, pH 5.8–6.0 with KOH. Sterilize by filtration (0.22 μm) or autoclave.

2.5 Media for Protoplast Transfection

1. 40% PEG-1500: 10 g w/v PEG (1500), 1.275 g Mannitol, 0.413 g $Ca(NO_3)_2 \cdot 4H_2O$, 4 mM MES, pH 6 with KOH. Dissolve mannitol and calcium nitrate in 17.5 mL ddH_2O first and then add the PEG. Thereafter, adjust the pH with KOH. Sterilize by filtration (0.45 μm) and prepare aliquots and store at −20 °C. After defrosting make sure that all salts are

Fig. 4 (continued) protoplasts expressing SEC61α1-eGFP with either mCherry-SEC61β1, mCherry-SEC61γ, mCherry-VAMP723, or, mCherry, respectively. Line histograms to the right show normalized intensities of either eGFP or mCherry fluorescence along *yellow arrows* in merged images. *a.u.* arbitrary units. Scale bar = 10 μm. (**c**) Box plot of SEC61α1-eGFP donor lifetime in ns of at least seven independent measurements for each of the various acceptor samples. *Center lines* of *boxes* represent the median with outer limits at the 25th and 75th percentile, respectively. Notches indicate the 95% confidence intervals; Tukey whiskers extend to the 1.5× IQR and outliers are depicted as *black dots*. *Red crosses* mark sample means of each dataset. Exemplary *p*-values (*t*-test) are indicated in graph

dissolved, if not, shake vigorously until they are; slightly warming of the solution helps.

2. MM: 0.4 M Mannitol, 5 mM MES, pH 6.0 with KOH. Sterilize by filtration (0.22 μm) or autoclave.
3. K3 (for 100 mL)**:** 10 mL macro stock, 0.1 mL micro stock, 0.1 mL vitamin stock, 0.5 mL EDTA stock, 1 mL Ca-Phosphate stock, 10 mg *myo*-Inositol, 25 mg D(+)-Xylose, 13.7 g Sucrose, pH 5.6 with KOH. Sterilize by filtration (0.22 μm), prepare aliquots (15–40 mL) and store at −20 °C.
4. Macro stock (for 1 L): 1.5 g $NaH_2PO_4 \cdot H_2O$, 9 g $CaCl \cdot 2H_2O$, 25 g KNO_3, 2.5 g NH_4NO_3, 1.34 g $(NH_4)_2SO_4$, 2.5 g $MgSO_4 \cdot 7H_2O$, add H_2O up to 1 L and autoclave.
5. Micro stock (for 100 mL): 75 mg KI, 300 mg H_3BO_3, 1 g $MnSO_4 \cdot 7H_2O$ (or 0.6 g $MnSO_4 \cdot H_2O$), 200 mg $ZnSO_4 \cdot 7H_2O$, 25 mg $Na_2MoO_4 \cdot 2H_2O$, 2.5 mg $CuSO_4 \cdot 5H_2O$, 2.5 mg $CoCl_2 \cdot 6H_2O$, add H_2O up to 100 mL. Sterilize by filtration (0.22 μm) and store at −20 °C.
6. Vitamin stock (for 100 mL): 100 mg Nicotinic acid, 100 mg Pyridoxine-HCl, 1 g Thiamine-HCl, add H_2O up to 100 mL. Sterilize by filtration (0.22 μm) and store at −20 °C.
7. EDTA stock (for 1 L): dissolve 7.46 g EDTA in 300 mL pre-warmed H_2O (approx. 30 °C), separately, dissolve 5.56 g Fe (II)$SO_4 \cdot 7H_2O$ in 300 mL pre-warmed H_2O (approx. 30 °C). Combine and add H_2O up to 1 L. Autoclave, aliquot, and store in the dark at 4 °C. Protect from light.
8. Ca-Phosphate stock (for 200 mL): 1.26 g $CaHPO_4 \cdot 2H_2O$, add H_2O up to 200 mL, pH 3 with 25% HCl. Autoclave and keep in the dark at 4 °C. Protect from light.

3 Methods

3.1 Agrobacteria Preparation

1. Select a single colony of transformed *Agrobacteria* which contains the 2in1-vector plasmid or any other plasmid of choice.
2. Inoculate 5 mL LB medium containing the appropriate antibiotics (rifampicin 50 μg/mL, gentamicin 20 μg/mL, and the plasmid specific antibiotic) with the *Agrobacterium* colony and grow it overnight (28 °C, 200–230 rpm) (*see* **Note 2**).
3. Transfer 500 μL of the overnight culture into 4.5 mL of fresh LB medium supplied with rifampicin, gentamycin, and specific antibiotic and grow for another 3–4 h (28 °C, 200 rpm) to an OD_{595} of approximately 0.2–0.8.
4. Determine the OD_{595}.

5. Centrifuge at 4000 × *g* for 15 min at 4 °C and wash the pellet once or twice with 5 mL of 4 °C cold water.
6. Adjust to a final OD_{595} of 0.5 with 4 °C cold AS medium. (Calculation: $OD_{595}/0.5 \times 5$ mL = Volume (in mL) of AS medium needed.)
7. Before proceeding with transient transformation of *Nicotiana benthamiana* leaves, incubate samples at least 1 h on ice.

3.2 Transient Transformation of Nicotiana benthamiana Leaves

1. Water 3–4-week-old (8th–10th leaf stage) *Nicotiana benthamiana* plants 4–6 h prior to infiltration.
2. Start preparation of *Agrobacteria* as mentioned in Subheading 3.1.
3. Inject with a 1 mL syringe (without cannula) *Agrobacterium* suspension into the abaxial side of the third to fifth youngest leaves. For this purpose, position the syringe between leaf-veins and support injection by gentle counter pressure with a finger on the adaxial side (Fig. 2a–c).
4. After infiltration, cover and return plants to the growth chamber.
5. After approximately 36–72 h post-infiltration, proceed to Subheading 3.6.

3.3 Cell Culture Maintenance (Protoplasts)

The particular cell culture in this protocol (*Arabidopsis thaliana*, Col-0, root derived) was generated and donated by Mathur and Koncz [21].

1. Cell cultures are maintained in 250 mL Erlenmeyer flasks under constant shaking (120 rpm) in the dark at 23.5 °C ± 1 °C.
2. The cell culture is propagated by reinoculation every 7 days by transferring 10 mL of a one-week-old (7-day-old) culture to a fresh, sterile 250 mL Erlenmeyer flask with 50 mL MSCol medium. The final, total volume is 60 mL.

3.4 Generation of Protoplasts

1. Protoplasts should be generated from cells 3 days after subcultivation when they are in their peak growth phase (*see* **Note 3**).
2. Aliquot 10 mL of cells into 12 mL Poly-Propylene (PP) round-bottom tubes and collect them at 400 × *g* for 5 min (4–25 °C okay).
3. Wash cells by resuspension with 10 mL "wall digestion solution without enzymes" and spin down at 400 × *g* for 5 min (4–25 °C okay).
4. Re-suspend pellet in 7 mL "wall digestion solution" and dispense into a 90 mm diameter Petri dish.

5. Incubate by shaking at 50 rpm for 6 h at 23.5 °C ± 1 °C in the dark.
6. Collect protoplasts from one Petri dish in a 12 mL PP tube. Centrifuge at 100 × g for 5 min at 4 °C. Discard the supernatant.
7. Wash protoplasts by resuspension in up to 10 mL "wall digestion solution without enzymes" and spin down at 100 × *g* for 5 min at 4 °C. This is Wash #1.
8. Remove supernatant and dissolve pellet in remaining solution. Add up to 10 mL with W5 solution slowly and mix slowly. This is Wash #2. Spin down the cells at 100 × *g* for 5 min at 4 °C.
9. Re-suspend cells in 10 mL W5 solution as in **step 8**. This counts as Wash #3. Take 20 μL (use cut 200 μL tips to handle protoplasts) to determine cell concentration with a hemocytometer.
10. Adjust the cells to 1.5×10^6 cells/mL. Leave cells in the refrigerator (4 °C) for at least 20 min; overnight is also okay.
11. Determine the protoplast concentration you will use. Transfection will occur in ranges of 1.5×10^6 cells/mL up to 6.7×10^6 cells/mL. Our standard concentrations are 6.6×10^6 cells/mL and 3.5×10^6 cells/mL. Use higher cell concentrations when working with multiple plasmid species ($\geq$3) and the lower concentration for $\leq$2 plasmids. It is recommended that you test this for each experimental condition.
12. Collect the protoplasts under 50 × *g* at room temperature (RT).
13. Decant the supernatant (some W5 will remain, $\leq$500 μL) and adjust to the determined cell concentration with MM and incubate cells for 10–30 min (but not longer) at RT.
14. The cells are ready for transfection.

3.5 Protoplast Transfection

This protocol was designed to transfect protoplasts in 96-well plate format (2.2 mL, round-bottom, deep-well) using the "Liquidator™ 96 Manual Pipetting System" (Mettler-Toledo) but it can also be executed using 8- or 12-channel pipettes. It is recommended to mix after each row as soon as you add PEG. A small set of reactions can be performed in 2 mL round-bottom Eppendorfs; mix as soon as you add PEG.

1. Prepare up to 16 μg of high-quality DNA in 20 μL H_2O in each reaction-well.
2. Add 60 μL of cell suspension to the DNA and mix the plate from every side by tapping the plate against your forearm (Fig. 2d) until no cell clumps are visible. Make sure that the DNA is evenly mixed in the total volume.

3. Add 60 μL of PEG and start a timer to a 5 min countdown. Mix the plate from every side by tapping the plate against your forearm until the PEG is evenly dispensed. This will take approximately 1 min. You can see the solution mixing if you hold the plates or tubes against the lighting in your laboratory so that you see light diffraction through the liquid. After 3 min, mix again.
4. Add 60 μL of MM solution and mix as before.
5. Add 500–700 μL of K3 medium, mix gently, and cover the plate with a film that allows gas exchange (e.g., AeraSeal™ film, SIGMA) (*see* **Note 4**).
6. Incubate the cells in the dark at 25 °C from 3 to 24 h depending on your assay (*see* **Note 5**).

3.6 Mounting for Microscopy (Tobacco Leaf Infiltration)

1. Cut a leaf section of approximately 1 cm^2 and transfer it to a 20 mL syringe half filled with water. Use your finger to stop water loss at the syringe's exit, insert the plunger, and carefully remove the remaining air in the syringe (Fig. 2e).
2. Close the tip of the syringe again and pull the plunger back. This will produce a partial vacuum in the syringe.
3. Releasing the plunger gently will replace air space within the leaf slice with water.
4. Repeat **steps 3** and **4** several times until the tissue appears translucent.
5. Take out the slice and mount it upside down on a slide. Drop a bit of water on the slide and place a coverslip over the tissue.
6. Tap coverslips gently to remove air bubbles.

3.7 Mounting for Microscopy (Protoplasts)

Tightly wrap two stripes of tape around a microscope slide with a gap of around 5 mm between them. These will serve as spacers. Put approx. 50–100 μL of cell suspension between the stripes and place a coverslip on top (*see* **Note 6**).

3.8 Confocal Imaging

Our studies are done using the Leica TCS SP8 confocal microscope with laser lines diode 405, pulsed 440, pulsed 470, Argon 488, 496, 514, DPSS 561, HeNe 594, and HeNe 633, respectively. The microscope is equipped with a fast 8 kHz resonant scanner, HyD detectors, and FLIM unit (PicoQuant). Leica Application Suite (LAS) X software was used for image acquisition.

3.8.1 rBiFC

1. Set up the confocal microscope for YFP fluorescence with 514 nm excitation and 520–560 nm emission range and for RFP fluorescence with 561 nm excitation and 570–630 nm emission range. To avoid spectral overlap, sequential scanning should be applied. Include a bright field channel for guidance from transmission of either laser line.

2. Use a 40×/0.75 NA water-immersion objective to focus on epidermal cells. A zoom factor between 3 and 4 is recommended.
3. Start with a positive control and collect several images while adjusting gain and—if necessary—offset, for an optimal dynamic range. Settings should be adjusted to yield a mean fluorescence intensity ratio between YFP and RFP of one (*see* **Note 7**). Once the parameters are adjusted, select and save for quantification of 20–40 images of randomly selected areas (*see* **Note 8**).

3.8.2 Image Analysis

For image analysis, we use the ImageJ software (freely available at http://imagej.net/Downloads) with the Bio-Formats plugin which must be installed separately before using it for the first time.

1. Open the *.lif file with the ImageJ software. Using the Bio-Format tool the first time, choose "view stack with: Hyper-stack" and set a mark in the "split channels" box. Select all series.
2. Close brightfield images.
3. Select the first RFP image and press button M, or STRG-M (measure). A table with different values (Area, Mean, Min, Max) will appear.
4. Select the corresponding YFP image and measure again.
5. Proceed for all images as described in **steps 2–4**. Afterwards you can copy the data table into Microsoft Excel.
6. Calculate the ratio between the mean fluorescence intensity values of YFP and RFP for each image and use for graphical display after/including statistical analysis.

3.8.3 FRET-AB

1. Set up the confocal microscope for eGFP fluorescence with 488 nm excitation and 490–530 nm emission range, and for mCherry fluorescence with 561 nm excitation and 565–610 nm emission range. To avoid spectral overlap, sequential scanning should be applied. Include a bright field channel for guidance from transmission of either laser line.
2. Use a 40×/0.75 NA water-immersion objective.
3. Adjust gain and offset settings for your sample exploiting the full dynamic range.
4. Switch to the FRET-AB mode from the dropdown menu in the LAS X software and adjust donor and acceptor settings as before. Set acceptor-excitation-laser intensity in the "bleach" tab to 100% and frames between 300 and 500.
5. Search an area where both proteins of interest are sufficiently expressed, set up an ROI, and start the bleaching procedure.

LAS X software automatically captures images before and after bleaching and calculates the FRET efficiency (*see* **Note 9**) according to the following formula:

$$\mathrm{FRET}_{\mathrm{eff}} = \left(D_{\mathrm{post}} - D_{\mathrm{pre}}\right)/\left(D_{\mathrm{post}}\right)$$

with D_{pre} and D_{post} as mean fluorescence intensities prior and after bleach, respectively.

3.8.4 Image Analysis

Note the values provided by the LAS X software under the "Quantification" tab for further statistical evaluation and graphical display.

3.8.5 FLIM

For FLIM applications, LAS X software and SymPhoTime 64 (from PicoQuant) software are used.

1. Switch the microscope to FLIM-mode. Start SymPhoTime, and create a new workspace.
2. Start lasers, and set the laser combining unit to 0.
3. Click on the tab "Setup Imaging" in the Leica software, and choose your appropriate laser and detectors.
4. Go to the tab "Setup FLIM", and choose the detector that is connected to the time-correlated single photon counting (TCSPC) module. Choose the wavelength to excite the donor.
5. Under "Acquisition" set resolution to 256 × 256, and scanning speed to 20–50 MHz while adjusting pixel dwell time to approximately 20 μs.
6. Set up the pulsed laser.
7. Choose the number of photons per pixel that should be counted. We recommend 500–1000. Pick a region of interest (ROI), and run a FLIM test. The kilo counts/s should not exceed 10% of the excitation frequency (e.g., 2 kilo counts/s for 20 MHz). If necessary, close the shutter of the laser combining unit to get less counts/s.
8. Run FLIM measurements at 7–10 different positions/cells/protoplasts. Zoom in and define ROIs for measurement. We recommend performing at least three independent biological replicates for FLIM measurements.
9. Measure donor-only samples, as well as a meaningful noninteracting candidate as negative controls.

3.8.6 Measure Instrument Response Function (IRF)

Since the microscope, objective, coverslip, and the pulse type of the laser do have an influence on the detection, the IRF must be measured for later evaluation.

1. Put only a coverslip on the objective without sample.
2. Set the mode from *xyz* to *xzy*, the laser to 5%, and the required wavelength of the donor (e.g., for GFP: 488 nm). Choose one

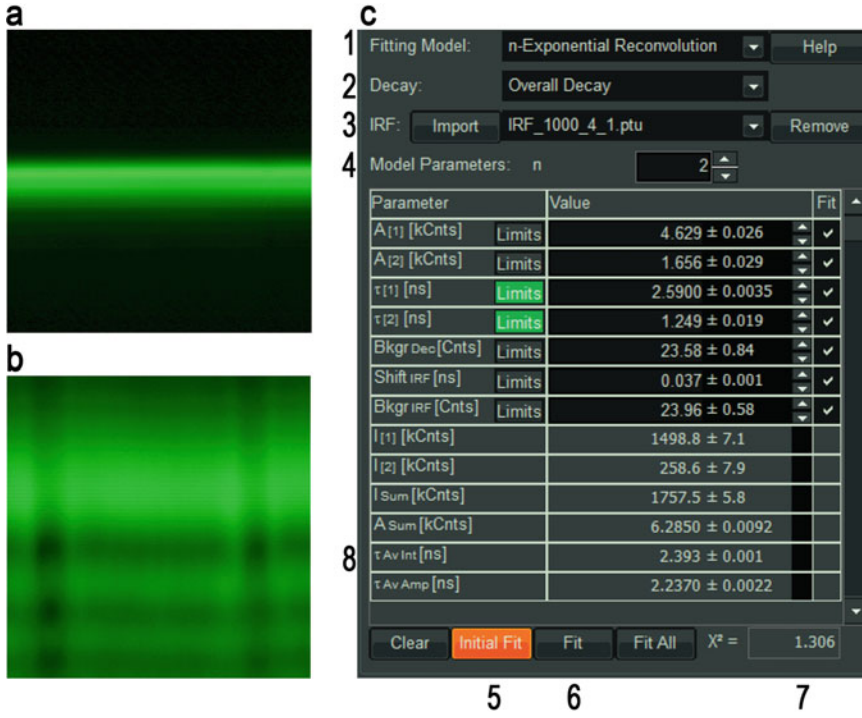

Fig. 5 Comparison between the edge of (**a**) the upper coverslip which is needed for measuring the IRF and (**b**) the edge of the microscope slide which should not be measured. (**c**) Section of SymPhoTime 64 software for evaluation of FRET-FLIM data. (*1*) The "Fitting Model" should be "n-Exponential Reconvolution" while the (*2*) "Decay" should be "Overall Decay." (*3*) The experimentally measured IRF (Subheading 3.8.6) has to be imported here (*4*). "Model Parameters – n" have to be set up according to the decay variant of the donor. Calculation is started with (*5*) "Initial Fit" and (*6*) Fit (*7*). If χ^2 is in the range of approximately 1–2, the fluorescence lifetime τ in [8] can be copied for further evaluation

PMT detector for emission at the same wavelength as the excitation (e.g., GFP: 488 nm).

3. Set the donor fluorescence to reflexion in the tab "AOBS."
4. Set up FLIM as before in Subheading 3.8.5 but use the PMT to detect exactly at the same wavelength as the pulsed laser.
5. Search the upper edge of the coverslip (Fig. 5a).
6. In the tab "fluorifier disc setting," deselect the autoselect and choose an empty position for the filters.
7. Close the laser combining unit.
8. Run a FLIM test with kilo counts per second at approximately 2000.
9. Measure IRF once and save it.

3.8.7 Evaluation

1. Open SymPhoTime and load your data. Choose one ".ptu" file, click Analysis → Imaging → FLIM → Start.

2. Set up "n-Exponential Reconvolution," overall decay and load your measured IRF sample in the designated tab. Choose the "Model Parameter – n" according to the decay variant of your donor fluorophore (e.g., mono- or bi-exponential decay) (Fig. 5).
3. We recommend decreasing the front border-width (e.g., 0.55 ns).
4. Press "Initial FIT" and afterwards "FIT." The χ^2 should be approximately between 1 and 2. Higher values indicate that the measured decay does not correlate to the calculated ideal decay (Fig. 5).
5. Lifetime values for further statistical evaluations are: "τ av. int (ns)" (Fig. 5).
6. Note these values in a .txt file or excel and use them for statistical evaluation and graphical display.

4 Notes

1. For structure-function analysis using alanine-scanning mutagenesis, we routinely design primers using our SDM-assist program that allows—in addition to the desired mutation—introduction of a silent restriction site to distinguish different point mutants via endonuclease digest [22].
2. We recommend construct verification of *Agrobacteria* clones used for transfection through plasmid rescued in *E. coli* followed by restriction analysis [20]. Even antibiotic resistant *Agrobacteria* colonies sometimes do not carry the recombinant plasmid, and we had cases, where plasmid restriction digests revealed significant alterations in plasmids. Verified *Agrobacteria* clones should be stored at −80 °C in 7% DMSO.
3. To gain more *Arabidopsis* protoplasts, it is possible to subculture 10 mL of a 3-day-old culture into 50 mL fresh MSCol medium. Cells for protoplast generation are taken 3 days after this second subculture. These cells are nicknamed "Turbo Cells" and produce finer and smaller protoplasts. You must not use these Turbo Cells for your main culture though, otherwise, the culture will outgrow itself too fast.
4. It is not necessary to wash out the PEG (1500) as its effective concentration is diluted in subsequent steps; alternatively, addition of a washing step with MM or W5 can be included.
5. Reporter assays benefit from shorter incubation times as they have better signal-to-noise ratios when applying treatments, whereas an overnight incubation is sufficient for localization or interaction assays.

6. Living cells will float on the top of the solution when they are in K3. Alternative incubation buffers found in the literature can also be used: for example, WI or TEX.
7. The ratio needs to be set up for a positive control and should be examined on several different epidermal cells. A ratio of 1 is preferred but not always feasible due to overall low expression. It is important that once the parameters are adjusted, there will be no change in settings over the complete set of samples to assure comparability.
8. Even though RFP acts as an expression and transformation/transfection control, verification of protein expression via immunoblot is recommended. The 2in1 plasmid used contains a 3xHA tag as well as a MYC tag fused to the proteins of interest for antibody detection (Fig. 3f).
9. Due to temporal delay in recording caused by the bleaching step, cellular movement leads to a shift of the region of interest out of the focal plane making measurements meaningless. To avoid this issue, we fixed samples in 4% (w/v) paraformaldehyde (PFA) in microtubule stabilization buffer (MTSB) (50 mM PIPES, 5 mM EGTA, 5 mM $MgSO_4 \cdot 7H_2O$, pH ~7 (KOH)).

Acknowledgements

We are grateful to Eva Schwörzer and Laure Grefen for excellent technical support. Work in our lab is supported through seed funding of the SFB1101 and an Emmy Noether fellowship of the German Research Foundation (DFG) to C.G. (GR 4251/1-1).

References

1. Xing S, Wallmeroth N, Berendzen KW, Grefen C (2016) Techniques for the analysis of protein-protein interactions in vivo. Plant Physiol 171:727–758
2. Husbands AY, Aggarwal V, Ha T, Timmermans MC (2016) In planta single-molecule pull-down reveals tetrameric stoichiometry of HD-ZIPIII:LITTLE ZIPPER complexes. Plant Cell 28:1783–1794
3. Grefen C, Blatt MR (2012) A 2in1 cloning system enables ratiometric bimolecular fluorescence complementation (rBiFC). Biotechniques 53:311–314
4. Hecker A, Wallmeroth N, Peter S, Blatt MR, Harter K, Grefen C (2015) Binary 2in1 vectors improve in planta (co-) localisation and dynamic protein interaction studies. Plant Physiol 168:776–787
5. Ghosh I, Hamilton AD, Regan L (2000) Antiparallel leucine zipper-directed protein reassembly: application to the green fluorescent protein. J Am Chem Soc 122:5658–5659
6. Horstman A, Tonaco IA, Boutilier K, Immink RG (2014) A cautionary note on the use of split-YFP/BiFC in plant protein-protein interaction studies. Int J Mol Sci 15:9628–9643
7. Grefen C, Karnik R, Larson E, Lefoulon C, Wang YZ, Waghmare S, Zhang B, Hills A, Blatt MR (2015) A vesicle-trafficking protein commandeers Kv channel voltage sensors for voltage-dependent secretion. Nat Plants 1:15108

8. Lipka E, Gadeyne A, Stockle D, Zimmermann S, De Jaeger G, Ehrhardt DW, Kirik V, Van Damme D, Muller S (2014) The phragmoplast-orienting kinesin-12 class proteins translate the positional information of the preprophase band to establish the cortical division zone in *Arabidopsis thaliana*. Plant Cell 26:2617–2632
9. Albert I, Bohm H, Albert M, Feiler CE, Imkampe J, Wallmeroth N, Brancato C, Raaymakers TM, Oome S, Zhang HQ, Krol E, Grefen C, Gust AA, Chai JJ, Hedrich R, Van den Ackerveken G, Nurnberger T (2015) An RLP23-SOBIR1-BAK1 complex mediates NLP-triggered immunity. Nat Plants 1:15140
10. Karnik R, Zhang B, Waghmare S, Aderhold C, Grefen C, Blatt MR (2015) Binding of SEC11 indicates its role in SNARE recycling after vesicle fusion and identifies two pathways for vesicular traffic to the plasma membrane. Plant Cell 27:675–694
11. Zhang B, Karnik R, Wang Y, Wallmeroth N, Blatt MR, Grefen C (2015) The arabidopsis R-SNARE VAMP721 interacts with KAT1 and KC1 K+ channels to moderate K+ current at the plasma membrane. Plant Cell 27:1697–1717
12. Kumar MN, Hsieh YF, Verslues PE (2015) At14a-Like1 participates in membrane-associated mechanisms promoting growth during drought in *Arabidopsis thaliana*. Proc Natl Acad Sci U S A 112:10545–10550
13. Le CT, Brumbarova T, Ivanov R, Stoof C, Weber E, Mohrbacher J, Fink-Straube C, Bauer P (2016) Zinc finger of Arabidopsis thaliana12 (ZAT12) interacts with FER-Like Iron Deficiency-Induced Transcription Factor (FIT) linking iron deficiency and oxidative stress responses. Plant Physiol 170:540–557
14. Forster T (1946) Energiewanderung und Fluoreszenz. Naturwissenschaften 33:166–175
15. Ishikawa-Ankerhold HC, Ankerhold R, Drummen GP (2012) Advanced fluorescence microscopy techniques—FRAP, FLIP, FLAP, FRET and FLIM. Molecules 17:4047–4132
16. Bucherl CA, Bader A, Westphal AH, Laptenok SP, Borst JW (2014) FRET-FLIM applications in plant systems. Protoplasma 251:383–394
17. Wallrabe H, Periasamy A (2005) Imaging protein molecules using FRET and FLIM microscopy. Curr Opin Biotechnol 16:19–27
18. De Los SC, Chang CW, Mycek MA, Cardullo RA (2015) FRAP, FLIM, and FRET: detection and analysis of cellular dynamics on a molecular scale using fluorescence microscopy. Mol Reprod Dev 82:587–604
19. Koncz C, Schell J (1986) The promoter of Tl-DNA Gene5 controls the tissue-specific expression of chimeric genes carried by a novel type of agrobacterium binary vector. Mol Gen Genet 204:383–396
20. Blatt MR, Grefen C (2014) Applications of fluorescent marker proteins in plant cell biology. Methods Mol Biol 1062:487–507
21. Mathur J, Koncz C (1997) Method for preparation of epidermal imprints using agarose. Biotechniques 22:280–282
22. Karnik A, Karnik R, Grefen C (2013) SDM-assist software to design site-directed mutagenesis primers introducing "silent" restriction sites. BMC Bioinformatics 14:105
23. Sparkes IA, Runions J, Kearns A, Hawes C (2006) Rapid, transient expression of fluorescent fusion proteins in tobacco plants and generation of stably transformed plants. Nat Protoc 1:2019–2025
24. Shuping Xing, Dietmar Gerald Mehlhorn, Niklas Wallmeroth, Lisa Yasmin Asseck, Ritwika Kar, Alessa Voss, Philipp Denninger, Vanessa Aphaia Fiona Schmidt, Markus Schwarzländer, York-Dieter Stierhof, Guido Grossmann, Christopher Grefen, (2017) Loss of GET pathway orthologs in causes root hair growth defects and affects SNARE abundance. Proceedings of the National Academy of Sciences 114(8):E1544–E1553

V. Mehlhorn et al., 2021 (Review):

Looking for a safe haven: tail-anchored proteins and their membrane insertion pathways

Plant Physiology – Invited Update Review (Focus Issue on Transport & Signalling)

Short title: Membrane insertion of tail-anchored proteins

Corresponding Author: Christopher Grefen, christopher.grefen@rub.de

Looking for a Safe Haven: Tail-anchored Proteins and their Membrane Insertion Pathways

Dietmar G. Mehlhorn, Lisa Y. Asseck & Christopher Grefen

Faculty of Biology & Biotechnology, Molecular & Cellular Botany, University of Bochum, Universitätsstraße 150, 44780 Bochum, Germany

One-sentence summary:

Update on the different pathways and candidates that facilitate membrane insertion of tail-anchored proteins in eukaryotes with a special emphasis on recent insights in plant research.

Author contributions:

D.G.M. and C.G. wrote the manuscript with input from L.Y.A.

Funding information: This work was supported by a PhD grant from the Carl-Zeiss Stiftung to D.G.M and grants from the Deutsche Forschungsgemeinschaft to C.G. (DFG GR4251/2-1 and SFB1101-A06).

Number of figures: 1

Number of tables: 1

Keywords: tail-anchored proteins, GET pathway, SND pathway, EMC, Endoplasmic reticulum, *Arabidopsis thaliana*, plants

© The Author(s) (2021) . Published by Oxford University Press on behalf of American Society of Plant Biologists.
This is an Open Access article distributed under the terms of the Creative Commons Attribution License (http://creativecommons.org/licenses/by/4.0/), which permits unrestricted reuse, distribution, and reproduction in any medium, provided the original work is properly cited.

Downloaded from https://academic.oup.com/plphys/advance-article/doi/10.1093/plphys/kiab298/6307274 by guest on 01 July 2021

Abstract:

Insertion of membrane proteins into the lipid bilayer is a crucial step during their biosynthesis. Eukaryotic cells face many challenges in directing these proteins to their predestined target membrane. The hydrophobic signal peptide or transmembrane domain (TMD) of the nascent protein must be shielded from the aqueous cytosol and its target membrane identified followed by transport and insertion. Components that evolved to deal with each of these challenging steps range from chaperones to receptors, insertases and sophisticated translocation complexes. One prominent translocation pathway for most proteins is the signal recognition particle (SRP-) dependent pathway which mediates co-translational translocation of proteins across or into the endoplasmic reticulum (ER) membrane. This textbook example of protein insertion is stretched to its limits when faced with secretory or membrane proteins that lack an amino-terminal signal sequence or TMD. Particularly, a large group of so-called tail-anchored (TA) proteins that harbor a single carboxy-terminal TMD require an alternative, post-translational insertion route into the ER membrane. In this review, we summarize the current research in TA protein insertion with a special focus on plants, address challenges, and highlight future research avenues.

Downloaded from https://academic.oup.com/plphys/advance-article/doi/10.1093/plphys/kiab298/6307274 by guest on 01 July 2021

Diversity of membrane proteins

Roughly one third of the average eukaryotic proteome comprises integral membrane proteins (IMPs) that act for example as channels, transporters or receptors (Hegde and Keenan, 2011). IMPs are found in all organellar membranes within the cell. They reside in the lipid bilayers of the endomembrane system (endoplasmic reticulum (ER), Golgi, TGN/MVC, vacuole, peroxisomes and plasmamembrane (PM)) as well as in the membranes of the semiautonomous cell organelles of chloroplast and mitochondria. To maintain membrane integrity and cellular function, correct targeting and insertion of newly synthesized IMPs has to be guaranteed. For this purpose, dedicated signal sequences and insertion pathways have evolved.

Shared features of all IMPs are strongly hydrophobic transmembrane domains (TMDs); yet these vary in their sequence, number and final topology, and thereby define the different types of membrane proteins (Guna and Hegde, 2018). However, all IMPs face three fundamental challenges in their biogenesis:

(1) The nascent protein including its non-polar TMD(s) must navigate through the aqueous cytosolic environment before reaching the membrane. As exposure of the lipophilic TMDs within the cytosol would lead to premature aggregation, chaperoning proteins are needed which recognize and shield the TMDs until their insertion into the hydrophobic bilayer.

(2) IMPs with varying numbers of TMDs and either luminally or cytosolically facing peptide stretches require membrane-bound receptors that aid in the insertion process and guarantee correct orientation within the membrane.

(3) Finally, targeting sequences (e.g. retention motifs) within the protein need to be recognized to facilitate delivery to the corresponding target membrane (ER & secretory pathway vs. organellar membranes) (Pedrazzini et al., 1996).

Of signal recognition and translocons

To cope with the challenges mentioned above, various strategies evolved in eukaryotes and were described by scientists in the past decades. Günter Blobel was awarded the 1999 Nobel Prize in Physiology or Medicine "*For the discovery that proteins have intrinsic signals that govern their transport and localization in the cell*" (Celebrating 20 years of cell biology, 2019). Together with David Sabatini, Blobel had

Downloaded from https://academic.oup.com/plphys/advance-article/doi/10.1093/plphys/kiab298/6307274 by guest on 01 July 2021

postulated the “signal hypothesis” some 30 years earlier (Sabatini and Blobel, 1970). Although a hypothesis at first and rejected by many at the time it turned out to be correct and found its way into the textbooks. The majority of secretory proteins or IMPs utilize this signal recognition particle (SRP-) dependent pathway and enter the ER through the Sec61 translocon which was later discovered and likewise earned its discoverer Randy Schekman a Nobel prize (Novick et al., 1980; Deshaies et al., 1991) shared with James Rothman and Thomas Südhof “*for their discoveries of machinery regulating vesicle traffic, a major transport system in our cells*” (Wickner, 2013). The pathway is also referred to as ‘co-translational’ as it targets and inserts proteins into the ER during their synthesis (Anderson et al., 1982).

Translocation starts with the extrusion of a nascent polypeptide chain from the ribosome exit channel. SRP recognizes ribosomes with either an N-terminal signal sequence or TMD of a nascent protein (Ogg and Walter, 1995; Shao and Hegde, 2011). Subsequent binding of SRP to the ribosome transiently arrests protein synthesis by blocking further tRNA entry (Lakkaraju et al., 2008; Richter and Coller, 2015). Targeting to the ER membrane of the SRP/ribosome-nascent chain (RNC) complex is induced by the binding to the SRP receptor (SR) in a GTP-dependent manner (Gilmore et al., 1982; Gilmore et al., 1982). Subsequent conformational changes lead to interaction with the Sec61 translocon, unloading of RNC from SRP to Sec61 and determine the duration of the translational pause. GTP hydrolysis triggers the disassembly of SRP from SR and recycling of the components for additional rounds of protein targeting (Song et al., 2000; Shao and Hegde, 2011).

During co-translational insertion, two mechanisms protect the TMD from the aqueous cytosol:

(1) early targeting of the TMD by SRP and maintenance of this connection until docking at the Sec61 channel to ensure minimal exposure to the cytosol prior to integration,

(2) translational slowdown that prevents translation of additional, subsequent TMDs into the cytosol (Walter and Blobel, 1981; Pechmann et al., 2014).

Little is known about an Archaeplastida Sec61 translocon, although such a fundamental mechanism is undoubtedly conserved in plants. Three homologs of each, the central pore Sec61α as well as the two subunits Sec61β and Sec61γ, are

Downloaded from https://academic.oup.com/plphys/advance-article/doi/10.1093/plphys/kiab298/6307274 by guest on 01 July 2021

encoded in the Arabidopsis (*Arabidopsis thaliana*) genome. While functional data is lacking, physical interaction of *At*Sec61α1 with *At*Sec61β1 and *At*Sec61γ1 was shown by our group (Mehlhorn et al., 2018). In addition, the translocon associated proteins *At*Sec62 and Sec63 (*At*ErdjA and *At*Erdj2B) are conserved as well (Mitterreiter et al., 2020). Together with the tetratricopeptide repeat protein *At*TPR7, both are probably involved in a chaperone-assisted post-translational import of small peptides in Arabidopsis (Schweiger et al., 2012).

Tail-anchored proteins

The SRP/Sec61 co-translational pathway reaches its limits, though, when signal sequences or TMDs are lacking within the N-terminal part of the protein. This is in particular the case for type II orientated membrane proteins that feature a TMD close to their C-terminal end and are referred to as tail-anchored (TA) proteins (Borgese et al., 2003). To distinguish these from other type II proteins, the C-terminal (after translocation: luminal) stretch should by definition be no longer than ~30 amino acids (Borgese et al., 2003). This is roughly the length of a peptide stretch within the ribosomal exit channel (Voss et al., 2006). Proteins with such feature are released from the ribosome when their TMD is disclosed to the cytosolic environment. To prevent aggregation of the hydrophobic TMD within the aqueous cytosol immediate action of chaperones is required aiding in shuttling and post-translational translocation. (Pedrazzini, 2009; Johnson et al., 2013).

TA proteins make up to ~3-5% of all IMPs and can be found in almost all cellular membranes (Abell and Mullen, 2011). In Arabidopsis, around 500 TA proteins were predicted *in silico* (Kriechbaumer et al., 2009). They play key roles in many vital processes such as vesicle trafficking, apoptosis, translocation of other proteins, ubiquitination, signal transduction, enzymatic reactions or regulation of transcription (Borgese et al., 2003; Kriechbaumer et al., 2009). Some TA proteins even take part in translocation of other membrane proteins as subunits of translocation machineries such as the Sec61β subunit of the SEC61 translocon, or Translocase of outer membrane 22 (Tom22) and Translocase of chloroplast 33 (Toc33) of the mitochondrial and chloroplast import machineries. Additionally, most of the soluble N-ethylmaleimide-sensitive factor attachment receptors (SNAREs) which facilitate vesicle fusion in eukaryotic cells, are TA proteins (Neveu et al., 2020). Their prominent role in many physiological processes is reflected by the dramatic

Downloaded from https://academic.oup.com/plphys/advance-article/doi/10.1093/plphys/kiab298/6307274 by guest on 01 July 2021

phenotypes associated with their *loss-of-function* lines, ranging from conditional sensitivity towards pathogens to embryonic lethality (Lipka et al. 2007).

Anchoring in the ER membrane

The seemingly textbook example for post-translational membrane insertion of TA proteins into the ER is the **Guided Entry of Tail-anchored proteins** (GET) pathway (Figure 1) which was initially identified in mammals and yeast (Stefanovic and Hegde, 2007; Schuldiner et al., 2008).

In yeast, nascent TA proteins are recognized immediately after emergence from the ribosomal exit tunnel through a tripartite pre-targeting complex consisting of small glutamine-rich tetratricopeptide cochaperone 2 (Sgt2), Get4 and Get5 (Chang et al., 2010; Wang et al., 2010). A functional mammalian homologue of Get4/5 is the BAG6 complex comprising BCL2-associated athanogene cochaperone 6 (BAG6), transmembrane domain recognition complex 35 (TRC35) and ubiquitin-like domain (UBL)-containing protein 4A (UBL4A), which works in cooperation with Small glutamine-rich tetratricopeptide repeat-containing protein α (SGTA), the mammalian Sgt2 orthologue (Mariappan et al., 2010; Johnson et al., 2013). While Sgt2 alone is ineffective in binding TA proteins, Get4/5 assist this process by bridging and facilitating TA protein transfer from Sgt2 to the cytosolic ATPase Get3 (in mammals TRC40 or Asna1) (Suloway et al., 2009; Simpson et al., 2010; Chartron et al., 2011; Gristick et al., 2014). BAG6 triages nascent TA proteins in either an insertion competent fraction, or destined for proteasomal degradation (Leznicki and High, 2012; Shao et al., 2017). Recent work has now demonstrated that polyubiquitinated TA proteins can circumvent recognition by BAG6 and still be inserted via the (mammalian) TRC40 pathway and subsequent deubiquitination (Culver and Mariappan, 2021).

Key-component of the pathway is the dimeric ATPase Get3. Its subunit interaction is stabilized by a Zn^{2+} ion coordinated by a CxxC motif (Mateja et al., 2009; Simpson et al., 2010). Get3 consists of a nucleotide-binding pocket and a TA protein binding domain and undergoes conformational changes dependent on its nucleotide-binding state (Wereszczynski and McCammon, 2012). In a nucleotide-free state, Get3 is in an open conformation while binding of ATP leads to a closed dimer, thereby creating a hydrophobic groove which binds and shields the TMD of TA proteins (Mateja et al.,

Downloaded from https://academic.oup.com/plphys/advance-article/doi/10.1093/plphys/kiab298/6307274 by guest on 01 July 2021

2009; Wereszczynski and McCammon, 2012; Mateja et al., 2015). It was demonstrated that unlike SRP, Get3 does not associate with ribosomes (Stefanovic and Hegde, 2007). Get3 shuttles the client protein to the ER membrane receptors consisting of a heteromeric complex of Get1 (WRB in mammals (Vilardi et al., 2011; McDowell et al., 2020)) and Get2 (CAML in mammals (Yamamoto and Sakisaka, 2012; Vilardi et al., 2014)). The long cytosolic N-terminal domain of Get2 mediates tethering of the Get3-TA protein complex (Mariappan et al., 2011; Wang et al., 2011). Interaction of Get2 only takes place with a nucleotide-bound Get3 which is also compatible with TA protein binding (Denic et al., 2013). Hydrolysis of ATP opens the Get3 dimer. This conformational change disrupts the hydrophobic groove releasing the bound TA protein and providing it for insertion by the Get1-Get2 insertase (Wang et al., 2014; Zalisko et al., 2017). Intriguingly, Get1 and Get2 compete for Get3 binding via overlapping binding sites (Stefer et al., 2011; Denic et al., 2013), although interaction between Get3 and a coiled-coil domain of Get1 occurs only with an open, nucleotide-free Get3 (Mariappan et al., 2011). Rebinding of ATP returns Get3 into a closed conformation, thereby weakening the Get3-Get1 interaction which leads to dissociation of Get3 from the membrane and recycling for another round of TA protein loading via the pre-targeting complex Sgt2/Get4/Get5 (Stefer et al., 2011; Suloway et al., 2012).

It is noteworthy that TA protein recognition from ribosome to membrane is assisted by heat-shock proteins (Rabu et al., 2008; Craig, 2018). Recently, the involvement of J-domain proteins involved in the TA protein handover from Hsp70 to Sgt2 in yeast has been demonstrated (Cho and Shan, 2018; Cho et al., 2021).

It GET's complicated in plants

In Arabidopsis, a high degree of conservation was presumed from an *in silico* search of GET components (Abell and Mullen, 2011; Duncan et al., 2013). Four years later, the existence and function of a plant GET pathway was demonstrated by two groups, independently (Srivastava et al., 2017; Xing et al., 2017) although some of its components still remain elusive. While a functional Get4 orthologue (At5g63220) was identified in plants, its partner proteins within a putative pre-targeting complex could not be determined as too many potential candidates exist. Based on sequence similarities, there are multiple putative Sgt2 and Get5 orthologs in Arabidopsis, the latter features a ubiquitin-like domain which is present in a wide range of proteins

Downloaded from https://academic.oup.com/plphys/advance-article/doi/10.1093/plphys/kiab298/6307274 by guest on 01 July 2021

(Paul et al., 2013; Srivastava et al., 2017; Xing et al., 2017). BAG6, the protein that bridges the interaction of Ubl4A to TRC35 within a mammalian pre-targeting complex, is lacking in yeast (Leznicki et al., 2013). Interestingly, a putative BAG6 ortholog (Table 1) exists in Arabidopsis and is involved in triggering autophagy in response to pathogen attack (Li et al., 2016), however, an involvement in a plant GET pathway remains elusive, currently.

Other than Get1/WRB, Get2/CAML has no sequence orthologue in plants. However, only recently, a functional Get2/CAML homologue has been identified in Arabidopsis using affinity purification-mass spectrometry (Asseck et al., 2021). Despite low sequence similarity, the overall structure comprising three TMDs and a cytosolic N-terminal stretch of basic amino acid residues seem to be evolutionary conserved to maintain a common function (Asseck et al., 2021). Position-specific iterative (PSI)-basic local alignment search tool (BLAST) analysis of the human CAML sequence revealed co-selection of the two functional domains, allowing the identification of orthologous genes also in distant phyla (Borgese, 2020; Asseck et al., 2021). In mammals, the two subunits of the GET receptor complex have been shown to depend on each other for expression and are degraded in the absence of the binding partner (Carvalho et al., 2019; Inglis et al., 2020). Similarly, Get1 deficiency in yeast leads to a reduced protein level of Get2 and *vice versa*, demonstrating reciprocal regulation of these two proteins (Schuldiner et al., 2008; Stefer et al., 2011). In Arabidopsis, however, the relationship between the receptor components seems to be distinct from that in Opisthokonts. In the absence of its co-receptor, *At*GET2 is still expressed but no longer interacts with the targeting factor *At*GET3a (Asseck et al., 2021).

There are additional, intriguing differences among Archaeplastida GET components such as three different GET3 proteins that were identified in Arabidopsis (namely *At*GET3a, *At*GET3b and *At*GET3c). *In silico* comparison of these three paralogues revealed two distinct clades (GET3a and GET3bc) present in the Archaeplastida and SAR supergroup but not in Opisthokonts and Amoebozoa indicating a duplication event in the evolution of eukaryotes (Xing et al., 2017; Farkas et al., 2019). However, orthologues of *At*GET3c seem to be *Brassicaceae*-specific whereas several copies of *At*GET3b orthologues can exist in other plant species (Bodensohn et al., 2019).

Downloaded from https://academic.oup.com/plphys/advance-article/doi/10.1093/plphys/kiab298/6307274 by guest on 01 July 2021

Obvious differences between Archaeplastida GET3 proteins and Opisthokont Get3 include:

(1) The conserved CxxC motif necessary for the coordination of a zinc ion and dimer formation (*see* **above**) is lacking in GET3a but not in the GET3bc clade despite *At*GET3a retaining the ability to form dimers (Xing et al., 2017). Instead, in GET3a an ExxE motif and additional acidic residues adjacent to the site that usually bears the CxxC motif in other species' sequences may take over metal ion coordination and dimer stabilization (Farkas et al., 2019).

(2) An approximately 30 amino acid long, strongly charged extension was only found in the GET3a clade and suggested to be involved in dimerization (Farkas et al., 2019).

(3) *At*GET3a is targeted to the cytosol and probably recruited to the ER membrane, as it can be found in microsomal fractions (Srivastava et al., 2017; Bodensohn et al., 2019) which might represent the receptor bound state. *At*GET3b, however, is located within the stroma of chloroplasts and *At*GET3c in the matrix of mitochondria (Xing et al., 2017). Their organellar function is currently not understood (Zhuang et al., 2017; Bodensohn et al., 2019).

(4) While all three orthologues possess the ATPase motif, GET1 and GET4 binding residues are only conserved in *At*GET3a. Consistent with this finding, only *At*GET3a interact with *At*GET4 and *At*GET1 but neither *At*GET3b nor *At*GET3c (even in truncated, cytosolic forms) (Xing et al., 2017). This suggests that only the cytosolic *At*GET3a plays a role in a canonical ER GET pathway in plants.

GETting knocked out – phenotypic consequences

But there remain more mysteries. So far only two TA proteins have been identified that show reduced membrane insertion in *Atget* mutants, the pollen-specific SNARE protein SYP72 (Srivastava et al., 2017) and the root-hair specific SNARE protein SYP123 (Xing et al., 2017). The GET pathway is considered as the main route for post-translational TA protein insertion into the ER. Contrary to such an implied vital role, yeast *loss-of-function* strains are viable under normal growth conditions (Schuldiner et al., 2008) and the lethality under oxidative stress likely relates to the function of *Sc*Get3 as chaperone for unfolding soluble proteins (Voth et al., 2014). A later analysis of yeast TA proteins revealed that only two out of 46 potential client

Downloaded from https://academic.oup.com/plphys/advance-article/doi/10.1093/plphys/kiab298/6307274 by guest on 01 July 2021

proteins show dependency on the presence of an intact GET pathway. Nonetheless, knockout of the mammalian orthologue TRC40 leads to embryo lethality in mice (Mukhopadhyay et al., 2006) and severe organ defects in induced *get* mutants (Lin et al., 2016; Norlin et al., 2016; Vogl et al., 2016). One could conclude from this that among multicellular Opisthokonts an intact GET pathway became indispensable for survival.

The data in other multicellular organisms such as plants, however, rules out such general conclusion. In Arabidopsis loss of GET pathway function clearly causes effects such as increased ER-stress levels (Srivastava et al., 2017) and reduced root hair length (Xing et al., 2017), yet no pleiotropic phenotypes, let alone seedling or embryo lethality, was observed. Such strong phenotypes, however, should be expected considering that certain vital TA proteins such as the cytokinesis-specific SNARE KNOLLE (Lauber et al., 1997) do not reach their target membrane.

With the implication that the GET pathway is the major hub for TA protein insertion in the ER, the question is justified whether this can hold true with respect to such mild phenotypes and whether or not backup systems have evolved. An alternative explanation would be that a plant GET pathway evolved additional/alternative function(s) instead/apart from TA protein insertion. The latter suggestion is supported by an IP-MS analysis where only 23 TA proteins interacted with *At*GET3a-GFP (Xing et al., 2017) which is less than 5% of all predicted TA proteins in Arabidopsis (Kriechbaumer et al., 2009). Thus, it seems that in plants, the GET pathway might not play a – not to mention *the* - major role in TA protein insertion; or at least that plants have evolved alternative mechanisms to secure TA protein insertion in case one route breaks down.

GET Alternatives

The dispensability of Arabidopsis GET components for general plant growth and survival with merely an effect on root hair growth (Xing et al., 2017; Asseck et al., 2021) allows speculation regarding the existence of yet undiscovered alternative insertion pathways in plants that might redundantly substitute TA protein insertion into the ER membrane.

In a pioneering effort, an SRP-independent targeting (SND) pathway consisting of three genetically linked proteins localizing to the cytosol (Snd1) or ER membrane

Downloaded from https://academic.oup.com/plphys/advance-article/doi/10.1093/plphys/kiab298/6307274 by guest on 01 July 2021

(Snd2 and Snd3) was identified in yeast (Aviram et al., 2016). Here, cytosolic Snd1 is predicted to interact with ribosomes, co-translationally capturing nascent proteins while Snd2 and Snd3 associate with the Sec61 translocon acting as putative receptors. The SND pathway was initially described as a pathway for IMPs harboring an internal TMD, and its loss leads to mislocalisation of these proteins. It was shown that all three Snd proteins act in the same pathway and it additionally serves as safeguard for both SRP-dependent insertion and the GET pathway. As for the get knockouts, *SND* deletion did not affect the viability of *Saccharomyces* under normal growth conditions. Interestingly, double knockouts between *SND* and *GET* are non-viable, suggesting a compensatory role of TA protein delivery to the ER (Aviram et al., 2016).

In mammals, homologues of SND1 and SND3 have not been found, yet an SND2 homologue (TMEM208, or hSND2) was identified and its localization to the ER confirmed (Hassdenteufel et al., 2017). In two independent studies, the function of hSND2 in TA protein biogenesis was shown as deletion leads to decreased TA protein insertion (Casson et al., 2017; Hassdenteufel et al., 2017). Interestingly, loss of hSND2 is compensated by upregulation of the SRP receptor SRα which was shown to aid in an SRP dependent post-translational insertion of some client TA proteins (Casson et al., 2017; Hassdenteufel et al., 2017). In Arabidopsis two sequence paralogs for Snd2 can be identified via BLAST search, but no obvious orthologs for Snd1 or Snd3 (Table 1). It remains to be seen whether an SND pathway is functionally conserved and which proteins pair up with SND2 in plants to facilitate such function.

Another recently discovered post-translational insertase for ER-destined TA proteins with TMDs of moderate to low hydrophobicity is the ER membrane complex (EMC). In semi-permeabilized cells silenced for EMC components, integration of the mammalian ER-resident enzyme squalene synthase (SQS) and four other TA proteins with similar hydrophobic TMD characteristics failed. Calmodulin seems to play a role as chaperone in this pathway (Guna et al., 2018; Volkmar et al., 2019).

Putative orthologs for all 9-10 components of the mammalian EMC can be found in plants through sequence homology (Table 1). Whether a similar function is associated with these proteins in Arabidopsis or which other proteins are involved within a putative plant EMC complex is currently unresolved. It is noteworthy, that

Downloaded from https://academic.oup.com/plphys/advance-article/doi/10.1093/plphys/kiab298/6307274 by guest on 01 July 2021

EMC3 as well as Get1 are ER resident homologs of the Oxa1/Alb3/YidC family of insertases that facilitate co- and posttranslational insertion of transmembrane proteins into the inner mitochondrial membrane (Oxa1), the thylakoid membrane (Alb3) and the inner membrane of bacteria (YidC), respectively (Samuelson et al., 2000; Anghel et al., 2017).

The SEC61 translocon and its auxiliary proteins SEC62/SEC63 make use of heat shock proteins to provide an additional post-translation pathway (Abell et al., 2007; Wu et al., 2019). In Arabidopsis, *At*TPR7 together with the translocon associated proteins *At*Sec62 and *At*Erdj2 (*At*SEC63) seem to facilitate heat-shock protein mediated delivery of proteins for post-translational translocation (Schweiger et al., 2012; Schweiger and Schwenkert, 2013). Loss of *At*Sec62 impairs plant growth and reduces male fertility (Mitterreiter et al., 2020) yet it remains to be dissected whether the causative effect of this phenotype is an impairment in translocation or an interference in ER-phagy (Fumagalli et al., 2016; Hu et al., 2020).

Insertion of TA-proteins in other organelles

Translocation to the ER may be the major route for most TA proteins, yet post-translational insertion requires recognition of the target membrane ahead of distribution. This is even more challenging for plants with one additional endomembrane compared to other eukaryotic cells. To distinguish between the different destination membranes targeting information is required within the TA protein.

More than two decades of research in TA proteins has unveiled properties and motives that seem important for endomembrane distinction, however, many candidates still seem to be exempt from rules (Borgese et al., 2001; Borgese et al., 2019). These rules comprise targeting signals encoded in the hydrophobicity of the TMD as well as charge and length of the adjacent C-terminal element (CTE) (Beilharz et al., 2003; Borgese et al., 2007; Abell and Mullen, 2011; Marty et al., 2014; Rao et al., 2016; Costello et al., 2017).

For ER targeting, the consensus motif seems to be a long and hydrophobic TMD followed by non-polar, negative or no residues in the CTE (Rao et al., 2016).

It is currently proposed that TA proteins of the outer mitochondrial membrane (OMM) show less hydrophobic and shorter TMDs with reduced helical content compared to

Downloaded from https://academic.oup.com/plphys/advance-article/doi/10.1093/plphys/kiab298/6307274 by guest on 01 July 2021

TA proteins destined to the ER or secretory pathway (Kriechbaumer et al., 2009; Lee et al., 2014; Rao et al., 2016; Chio et al., 2017).

Targeting of some mitochondrial TA proteins to the OMM is also conducted by a moderately positively charged CTE (Marty et al., 2014; Rao et al., 2016). For Fis1, it could be demonstrated that a minimum of four basic residues are needed for mitochondrial localization while mutation of the basic residues in the CTE of some OMM TA proteins changes their destination (Rao et al., 2016). For example, mammalian ER localized cytb5 with a negatively charged CTE localizes to the OMM when artificially reverted to a positive net charge. This same construct expressed in plant cells, however, is directed to the chloroplast highlighting the challenges associated with the discrimination of multiple destination membranes (Maggio et al., 2007). It was also demonstrated that two cytochrome b5 (cytb5) isoforms – both with positive net charges in their CTE, but a number of putative phosphorylation sites – localize to either the ER, or the chloroplast outer envelope (Maggio et al., 2007) which leads to the speculation of phosphorylation as a cue to aid in discriminating target membranes through reversion of a positive net charge. Mitochondrial targeting is also dependent on the distance between TMD and CTE (Marty et al., 2014). Another potent indicator of plant OMM TA proteins is found in the dibasic motif adjacent to the C-terminal part of the TMD (Marty et al., 2014).

In mammals and yeast no unambiguous amino acid motif for TA protein targeting had been found so far. A recent study in Arabidopsis*,* however*,* showed that some plastid outer envelope membrane (OEM) TA proteins harbor a CTE with a RK/ST sequence motif. OEP7.2, which localizes to the OEM was used for swapping experiments with CTEs of other TA proteins with and without this motif. Only CTE with RK/ST motifs were functionally interchangeable. Thus, they concluded that for a subset of OEM TA proteins there is a conserved element for plastid targeting (Moog, 2019; Teresinski et al., 2019).

Overall, it seems that length and hydrophobicity of the TMD with a combination of charge dictates the localization of TA proteins within the cell while plant OEM TA proteins with a specific motif might be more of an exception.

However, dually targeted TA proteins such as *At*PMD1 to mitochondria and peroxisomes (Aung and Hu, 2011), *At*PAP2 to chloroplast and mitochondria (Sun et al., 2012), or proteins which display multiple targeting [chloroplast, mitochondria, and

Downloaded from https://academic.oup.com/plphys/advance-article/doi/10.1093/plphys/kiab298/6307274 by guest on 01 July 2021

peroxisomes] as *At*FIS1A (Ruberti et al., 2014), highlight that topogenic information (alone) cannot suffice to discern targeting routes. Nonetheless, the specificity of targeting motifs is interlinked with the binding properties of the different chaperones that shepherd their substrate to their destination membrane.

Potentially as consequence of ambiguous signals, mistargeting occurs against which fail-safe mechanisms evolved: in yeast, the AAA-ATPase Msp1 (Okreglak and Walter, 2014; Wang et al., 2020) recognizes TA proteins wrongly delivered to the OMM and either hands them over for proteasome mediated degradation or extracts them for correct rerouting (thoroughly reviewed in (Wang and Walter, 2020)). While such dislocase function also exists in animals (ATAD1, (Chen et al., 2014)) a similar function has not been found in plants where a large number of AAA-ATPases exist (Ogura and Wilkinson, 2001).

1. Insertion into chloroplasts

The translocation mechanism of TA proteins into the OEM of chloroplasts is currently not well understood. Unassisted insertion dependent on the lipid composition of the membrane and the TA protein CTE has been observed (Qbadou et al., 2003; Pedrazzini, 2009; Dhanoa et al., 2010). . Additionally, a cytosolic OEM chaperone, ankyrin repeat-containing protein (AKR2a) was found to play a role for the targeting of some TA proteins to chloroplasts and the delivery of dual targeted APX3 to peroxisomes (Bae et al., 2008; Shen et al., 2010). This observation would argue against its role as a specific chloroplast TA protein insertion factor indicating AKR2a as a rather unspecific chaperone.

Recently, another putative chaperone was detected in the green algae *Chlamydomonas reinhardtii*. Here, an arsenite transporter (*Cr*ArsA1) binds Toc34 and delivers it to chloroplasts (Maestre-Reyna et al., 2017). Intriguingly, two ArsA paralogous genes can be found in the *C. reinhardtii* genome, *Cr*ArsA1 and *Cr*ArsA2. Both are homologs of the cytosolic targeting factors TRC40 and Get3 (Formighieri et al., 2013). *Cr*ArsA1 and *Cr*ArsA2 have a discrete ligand preference, with *Cr*ArsA1 supposedly carrying TA proteins to the OEM and *Cr*ArsA2 to the ER (Maestre-Reyna et al., 2017). The subcellular localization of ArsA1 homologues in Chlorophytes is a matter of debate. While Formighieri et al. propose *Cr*ArsA1 to be cytoplasmic (Formighieri et al., 2013), its protein sequence clearly features an organellar transit

Downloaded from https://academic.oup.com/plphys/advance-article/doi/10.1093/plphys/kiab298/6307274 by guest on 01 July 2021

peptide at the N-terminus (Xing et al., 2017; Farkas et al., 2019). Its sequence also suggests high similarity to other GET3bc clade homologs of Archaeplastida which are also organellar localized (Xing et al., 2017; Lin et al., 2019). In addition, a recent affinity purification mass spectrometry of the chloroplastic ribosome interactome of *Chlamydomonas reinhardtii* revealed *Cr*ArsA1 lending further support to its stroma rather than cytosolic localization (Westrich et al., 2021).

The Arabidopsis homologue of *Cr*ArsA1 is *At*GET3b, which also features an N-terminal transit peptide and localizes to the stroma of chloroplasts (Xing et al., 2017). However, localizing within the stroma precludes a possible involvement in TA protein insertion at the OEM. One could speculate that AtGET3b is involved in TA protein targeting to the inner envelope membrane or thylakoids (Anderson et al., 2019; Bodensohn et al., 2019). While *At*GET3b does not bind to ER-resident *At*GET1 (Xing et al., 2017), interaction assays should first elucidate whether *At*GET3b could potentially bind to the Get1 orthologue Alb3 (At2g28800) or Alb4 (At1g24490), which facilitates membrane protein biogenesis in endosymbiontic organelles (Anghel et al., 2017; McDowell et al., 2021).

2. Insertion into mitochondria

Mitochondria have a small semi-autonomous genome, albeit most of the mitochondrial proteins are encoded by the nuclear genome, synthesized by cytosolic ribosomes and transported post-translationally into the mitochondria (Neupert, 1997; Pfanner and Geissler, 2001). There are many mitochondrial TA proteins, yet the pathway(s) responsible for their insertion are not clear. It had been reported that insertion of mitochondrial TA proteins depended on the unique lipid composition of the OMM, especially the ergosterol levels (Setoguchi et al., 2006; Kemper et al., 2008; Krumpe et al., 2012) and with the help of peroxisome import factor Pex19 (Cichocki et al., 2018). Moreover, translocation of TA proteins was moderately affected with hampered mitochondrial import complex (MIM) or Tom20 receptors (Thornton et al., 2010; Doan et al., 2020). It is conceivable that Tom20 acts as receptor while the MIM complex mediates insertion (Drwesh and Rapaport, 2020). Also, N-terminally GFP labelled OMM protein Mcp3 mislocalises to the ER in wildtype yeast but not in *get* knockout strains (Vitali et al., 2018). Apparently, when mitochondrial import is compromised, TA proteins intended for the OMM are

Downloaded from https://academic.oup.com/plphys/advance-article/doi/10.1093/plphys/kiab298/6307274 by guest on 01 July 2021

mistargeted to the ER membrane by the GET pathway. This implies that in yeast insertion pathways may compete for client delivery.

*At*Get3c, a homologue of Get3 is found in the mitochondrial matrix of Arabidopsis. Whether or not it is involved in TA protein insertion into the inner membrane of mitochondria is currently unknown. However, its *loss-of-function* line seems to show no obvious growth or cellular defects (Xing et al., 2017). It was speculated that the GET3c variants are *Brassicaceae*-specific while some GET3b homologues (that localize to chloroplasts in Arabidopsis) were mitochondria localized in the *Fabidae* (Bodensohn et al., 2019). Similar to chloroplasts, a Get1 orthologue is present in the mitochondrial inner membrane (Oxa1). As discussed above, the GET3bc clade lacks the GET1 binding motif (Anghel et al., 2017; Farkas et al., 2019) and has not been demonstrated to interact with or depend on Oxa1 so far.

3. Insertion into peroxisomes

Peroxisomes are single membrane, multifunctional organelles with essential roles in development such as scavenging of reactive oxygen species or peroxides, photorespiration, glycolate cycle and fatty acid β-oxidation (Aung and Hu, 2011; Kao et al., 2018). In contrast to chloroplasts and mitochondria they neither contain DNA nor possess a protein-synthesizing machinery. Peroxisomes are discussed to be ER-derived and early acting peroxin (PEX) proteins such as PEX3, PEX16 and PEX19 help in the peroxisomal genesis but also division by fission is possible (Kao et al., 2018). Therefore, the acquisition of protein delivery machineries is of great importance for peroxisomal identity.

In mammals and yeast, it was shown that peroxisomal-targeted TA proteins can take two distinct routes, (1) directly from the cytosol or (2) via the ER (Borgese et al., 2019). Both ways depend on the peroxisomal import proteins Pex19 and Pex3. Cytosolic Pex19 binds nascent peroxisomal TA proteins within a hydrophobic groove thereby stabilizing them. Recognition occurs via the TMD and basic CTE of the TA proteins (Halbach et al., 2006; Yagita et al., 2013; Chen et al., 2014). Binding of its membrane receptor Pex3 leads to direct insertion into the membrane (Cichocki et al., 2018).

ER-dependent insertion is partially carried out by the GET machinery. For instance, yeast Pex15 is ER-inserted via the GET pathway (Schuldiner et al., 2008; van der

Downloaded from https://academic.oup.com/plphys/advance-article/doi/10.1093/plphys/kiab298/6307274 by guest on 01 July 2021

Zand et al., 2010). Here, a specialized subdomain within the ER is formed, the so-called peroxisomal ER (pER). Localized budding of peroxisomal vesicles carrying TA proteins and subsequent fusion to existing peroxisomes requires Pex3, Pex19, ATP and additional yet unidentified cytosolic factors (van der Zand et al., 2010; Lam et al., 2011). Studies on these events proposed a dual functionality of Pex3. Its luminal sequence harbors a sorting signal for delivering Pex3 to the pER whereas the TMD of Pex3 is important for later directing of the vesicles to peroxisomes (Tam et al., 2005; Fakieh et al., 2013; Chio et al., 2017).

In plants, the peroxisomal targeted TA protein ascorbate peroxidase (APX) was shown to insert post-translationally dependent on ATP, Hsp70 and an additional, unknown receptor via pER (Mullen and Trelease, 2000). Unassisted insertion can also be observed for some peroxisomal TA proteins as MDAR4 (Lisenbee et al., 2005; Abell and Mullen, 2011). A conserved mechanism for translocation of plant TA proteins as seen in *Opisthokonts* is conceivable, however, exact information are lacking (Cross et al., 2016).

Future Perspectives

The most puzzling discovery in TA protein insertion in plants is certainly the rather mild phenotype associated with GET *loss-of-function* lines. How can this be reconciled with the notion that the GET pathway is universally conserved and acts as *the* textbook pathway for TA protein insertion into the ER? A non-lethal phenotype of a plant that lacks a general membrane insertion pathway of an important subclass of membrane proteins would surely lead to more pleiotropic growth defects. Failure to insert TA proteins – among them the trafficking facilitating SNARE proteins which are required for polar growth and cytokinesis – should lead to embryo lethality “at best”, or developmental arrests in earlier stages such as compromised pollen tube growth. Their absence suggests one or more backup system(s) in place. Existence, identity and conservation of such systems (eg. SND, EMC, Table 1) are a major avenue for future research as well as the identification of further GET pathway substrates which may also aid in understanding additional function(s) of a plant GET pathway.

Another obvious question is the precise targeting and distinction of TA proteins to their various destination membranes. A complex combination of physico-chemical properties or as in case of some plant OEM TA proteins, a specific motif (Teresinski

Downloaded from https://academic.oup.com/plphys/advance-article/doi/10.1093/plphys/kiab298/6307274 by guest on 01 July 2021

et al., 2019) might be the answer. Yet, how exactly dual-targeted TA proteins are sorted is still not clear and a simple solution unlikely.

A puzzling observation are the additional GET3 paralogs in Archaeplastida (Xing et al., 2017; Farkas et al., 2019). While clade *a* GET3 appears to be functionally related to yeast Get3 and mammalian TRC40, the roles of clade *bc* GET3 remain elusive. It is likely that all plants possess at least one copy of a chloroplast GET3b which might be involved in TA protein targeting to the inner envelope or thylakoids. However, the mitochondrial GET3c seems absent in most plant species which begs questions to its functional role and evolution (Bodensohn et al., 2019).

These are just some points that require addressing in future research and there is a lot to learn in terms of TA protein insertion in plants (see Outstanding Questions). Other fundamental homeostatic pathways such as cytokinesis (Jurgens, 2005) have significantly diverged among Opisthokonts and Archaeplastida – an evolutionary divide of more than 1.5 billion years – and validated the importance of research into different model species. Nonetheless, evidence for functional conservation of important fundamental processes such as membrane protein insertion remains limited in plants. The vast amount of data gained from research in single-celled models such as bacteria, yeast and cell culture should be used to inform on hypothesis-driven research in plants. Especially, the model plant Arabidopsis and the palette of modern genomic tools established therein, will allow a more organismal-focussed, phenotypic analyses of these pathways in the context of a multi-cellular organism.

Acknowledgments

We are grateful to Sonja Mehlhorn for detailed comments on this review. This work was supported by a PhD grant from the Carl-Zeiss Stiftung to D.G.M and DFG grants to C.G. (GR4251/2-1 and SFB1101-A06).

Downloaded from https://academic.oup.com/plphys/advance-article/doi/10.1093/plphys/kiab298/6307274 by guest on 01 July 2021

Table 1: Arabidopsis orthologs of yeast and mammalian TA protein insertion pathways

GET pathway				
Yeast/ Mammalian	**AGI code**	**Gene name[1]**	**Protein localisation**	**Reference**
GET1/WRB	At4g16444	AtGET1	ER membrane[2]	(Srivastava et al., 2017; Xing et al., 2017)
GET2/CAML	At4g32680	AtGET2	ER membrane[2]	(Asseck et al., 2021)
GET3/TRC40	At1g01910 At3g10350 At5g60730	AtGET3a AtGET3b AtGET3c	Cytosol[2] Chloroplast stroma[2] Mitochondria matrix[2]	(Srivastava et al., 2017; Xing et al., 2017)
GET4/TRC35	At5g63220	AtGET4	Cytosol[2]	(Srivastava et al., 2017; Xing et al., 2017)
GET5/UBL4A	At1g55060	UBQ12	Cytosol[3]	(Srivastava et al., 2017)
SGT2/SGTA	At4g08320	TPR8	Nucleus[3]	(Srivastava et al., 2017)
BAG6	At2g46240	BAG6	Nucleus[3]	PSI-Blast, TAIR
SND pathway				
SND1	*not found*	-	-	PSI-Blast
SND2	At4g30500 At2g23940	AtSND2a AtSND2b	Plasma membrane[3] ER membrane[3]	PSI-Blast
SND3	*not found*	-	-	PSI-Blast
ER Membrane Complex (EMC)				
EMC1	At5g11560	PNET5	ER membrane[3]	PSI-Blast, TAIR
EMC2	At3g04830 At5g28220	AtEMC2a AtEMC2b	ER membrane[3] Cytosol[3]	PSI-Blast, TAIR
EMC3	At4g12590	AtEMC3	ER membrane[3]	PSI-Blast, TAIR
EMC4	At5g10780	AtEMC4	ER membrane[3]	PSI-Blast, TAIR
EMC5	At5g03345	PRCE2	ER membrane[3]	PSI-Blast, TAIR
EMC6	At5g49540	AtEMC6	Plasma membrane[3]	PSI-Blast, TAIR
EMC7	At2g25310 At4g32130	AtEMC7a AtEMC7b	ER membrane[3] ER membrane[3]	PSI-Blast, TAIR
EMC8/9	At5g55940	EMB2731	ER membrane[3]	PSI-Blast, TAIR
EMC10	*not found*	-	-	PSI-Blast

[1]Found annotated at TAIR (Arabidopsis.org) or – if designated as unknown protein – our suggestion for future use. [2]Experimentally validated, see referenced publication for details. [3]Predicted using SUBA (suba.live).

Downloaded from https://academic.oup.com/plphys/advance-article/doi/10.1093/plphys/kiab298/6307274 by guest on 01 July 2021

564 **Figure Legends**

565 **Figure 1: Graphical summary depicting translocation pathways of TA-proteins**
566 **in plants.** Detailed description of the pathways can be found in the text. ER-destined
567 TA-proteins (yellow), peroxisomal TA proteins (blue), mitochondrial TA-proteins (red),
568 chloroplastidic TA-proteins (green), dual-targeted TA proteins
569 (mitochondria/peroxisomes, dashed arrow, red-blue TA-protein). Opaqueness
570 generally refers to proposed mechanisms/proteins/complexes which may be involved
571 in TA-protein translocation in plants but still require experimental validation.

572

Downloaded from https://academic.oup.com/plphys/advance-article/doi/10.1093/plphys/kiab298/6307274 by guest on 01 July 2021

References:

Abell BM, Mullen RT (2011) Tail-anchored membrane proteins: exploring the complex diversity of tail-anchored-protein targeting in plant cells. Plant Cell Rep **30:** 137-151

Abell BM, Rabu C, Leznicki P, Young JC, High S (2007) Post-translational integration of tail-anchored proteins is facilitated by defined molecular chaperones. J Cell Sci **120:** 1743-1751

Anderson DJ, Walter P, Blobel G (1982) Signal recognition protein is required for the integration of acetylcholine receptor delta subunit, a transmembrane glycoprotein, into the endoplasmic reticulum membrane. J Cell Biol **93:** 501-506

Anderson SA, Singhal R, Fernandez DE (2019) Membrane-Specific Targeting of Tail-Anchored Proteins SECE1 and SECE2 Within Chloroplasts. Front Plant Sci **10:** 1401

Anghel SA, McGilvray PT, Hegde RS, Keenan RJ (2017) Identification of Oxa1 Homologs Operating in the Eukaryotic Endoplasmic Reticulum. Cell Rep **21:** 3708-3716

Asseck LY, Mehlhorn DG, Monroy JR, Ricardi MM, Breuninger H, Wallmeroth N, Berendzen KW, Nowrousian M, Xing S, Schwappach B, Bayer M, Grefen C (2021) Endoplasmic reticulum membrane receptors of the GET pathway are conserved throughout eukaryotes. Proc Natl Acad Sci U S A **118**

Aung K, Hu J (2011) The Arabidopsis tail-anchored protein PEROXISOMAL AND MITOCHONDRIAL DIVISION FACTOR1 is involved in the morphogenesis and proliferation of peroxisomes and mitochondria. Plant Cell **23:** 4446-4461

Aviram N, Ast T, Costa EA, Arakel EC, Chuartzman SG, Jan CH, Hassdenteufel S, Dudek J, Jung M, Schorr S, Zimmermann R, Schwappach B, Weissman JS, Schuldiner M (2016) The SND proteins constitute an alternative targeting route to the endoplasmic reticulum. Nature **540:** 134-138

Bae W, Lee YJ, Kim DH, Lee J, Kim S, Sohn EJ, Hwang I (2008) AKR2A-mediated import of chloroplast outer membrane proteins is essential for chloroplast biogenesis. Nat Cell Biol **10:** 220-227

Beilharz T, Egan B, Silver PA, Hofmann K, Lithgow T (2003) Bipartite signals mediate subcellular targeting of tail-anchored membrane proteins in Saccharomyces cerevisiae. J Biol Chem **278:** 8219-8223

Bodensohn US, Simm S, Fischer K, Jaschke M, Gross LE, Kramer K, Ehmann C, Rensing SA, Ladig R, Schleiff E (2019) The intracellular distribution of the components of the GET system in vascular plants. Biochim Biophys Acta Mol Cell Res **1866:** 1650-1662

Borgese N (2020) Searching for Remote Homologs of Caml among Eukaryotes. Traffic

Borgese N, Brambillasca S, Colombo S (2007) How tails guide tail-anchored proteins to their destinations. Curr Opin Cell Biol **19:** 368-375

Borgese N, Colombo S, Pedrazzini E (2003) The tale of tail-anchored proteins: coming from the cytosol and looking for a membrane. J Cell Biol **161:** 1013-1019

Borgese N, Coy-Vergara J, Colombo SF, Schwappach B (2019) The Ways of Tails: the GET Pathway and more. Protein J **38:** 289-305

Borgese N, Gazzoni I, Barberi M, Colombo S, Pedrazzini E (2001) Targeting of a tail-anchored protein to endoplasmic reticulum and mitochondrial outer membrane by independent but competing pathways. Mol Biol Cell **12:** 2482-2496

Carvalho HJF, Del Bondio A, Maltecca F, Colombo SF, Borgese N (2019) The WRB Subunit of the Get3 Receptor is Required for the Correct Integration of its Partner CAML into the ER. Sci Rep **9:** 11887

Casson J, McKenna M, Hassdenteufel S, Aviram N, Zimmerman R, High S (2017) Multiple pathways facilitate the biogenesis of mammalian tail-anchored proteins. J Cell Sci **130:** 3851-3861

Celebrating 20 years of cell biology. (2019) Nat Cell Biol **21:** 1

Chang YW, Chuang YC, Ho YC, Cheng MY, Sun YJ, Hsiao CD, Wang C (2010) Crystal structure of Get4-Get5 complex and its interactions with Sgt2, Get3, and Ydj1. J Biol Chem **285:** 9962-9970

Chartron JW, Gonzalez GM, Clemons WM, Jr. (2011) A structural model of the Sgt2 protein and its interactions with chaperones and the Get4/Get5 complex. J Biol Chem **286:** 34325-34334

Downloaded from https://academic.oup.com/plphys/advance-article/doi/10.1093/plphys/kiab298/6307274 by guest on 01 July 2021

Chen Y, Pieuchot L, Loh RA, Yang J, Kari TM, Wong JY, Jedd G (2014) Hydrophobic handoff for direct delivery of peroxisome tail-anchored proteins. Nat Commun **5:** 5790
Chen YC, Umanah GK, Dephoure N, Andrabi SA, Gygi SP, Dawson TM, Dawson VL, Rutter J (2014) Msp1/ATAD1 maintains mitochondrial function by facilitating the degradation of mislocalized tail-anchored proteins. EMBO J **33:** 1548-1564
Chio US, Cho H, Shan SO (2017) Mechanisms of Tail-Anchored Membrane Protein Targeting and Insertion. Annu Rev Cell Dev Biol **33:** 417-438
Cho H, Shan SO (2018) Substrate relay in an Hsp70-cochaperone cascade safeguards tail-anchored membrane protein targeting. EMBO J **37**
Cho H, Shim WJ, Liu Y, Shan SO (2021) J-domain proteins promote client relay from Hsp70 during tail-anchored membrane protein targeting. J Biol Chem**:** 100546
Cichocki BA, Krumpe K, Vitali DG, Rapaport D (2018) Pex19 is involved in importing dually targeted tail-anchored proteins to both mitochondria and peroxisomes. Traffic **19:** 770-785
Costello JL, Castro IG, Camoes F, Schrader TA, McNeall D, Yang J, Giannopoulou EA, Gomes S, Pogenberg V, Bonekamp NA, Ribeiro D, Wilmanns M, Jedd G, Islinger M, Schrader M (2017) Predicting the targeting of tail-anchored proteins to subcellular compartments in mammalian cells. J Cell Sci **130:** 1675-1687
Craig EA (2018) Hsp70 at the membrane: driving protein translocation. BMC Biol **16:** 11
Cross LL, Ebeed HT, Baker A (2016) Peroxisome biogenesis, protein targeting mechanisms and PEX gene functions in plants. Biochim Biophys Acta **1863:** 850-862
Culver JA, Mariappan M (2021) Deubiquitinases USP20/33 promote the biogenesis of tail-anchored membrane proteins. J Cell Biol **220**
Denic V, Dotsch V, Sinning I (2013) Endoplasmic reticulum targeting and insertion of tail-anchored membrane proteins by the GET pathway. Cold Spring Harb Perspect Biol **5:** a013334
Deshaies RJ, Sanders SL, Feldheim DA, Schekman R (1991) Assembly of yeast Sec proteins involved in translocation into the endoplasmic reticulum into a membrane-bound multisubunit complex. Nature **349:** 806-808
Dhanoa PK, Richardson LG, Smith MD, Gidda SK, Henderson MP, Andrews DW, Mullen RT (2010) Distinct pathways mediate the sorting of tail-anchored proteins to the plastid outer envelope. PLoS One **5:** e10098
Doan KN, Grevel A, Martensson CU, Ellenrieder L, Thornton N, Wenz LS, Opalinski L, Guiard B, Pfanner N, Becker T (2020) The Mitochondrial Import Complex MIM Functions as Main Translocase for alpha-Helical Outer Membrane Proteins. Cell Rep **31:** 107567
Drwesh L, Rapaport D (2020) Biogenesis pathways of alpha-helical mitochondrial outer membrane proteins. Biol Chem **401:** 677-686
Duncan O, van der Merwe MJ, Daley DO, Whelan J (2013) The outer mitochondrial membrane in higher plants. Trends Plant Sci **18:** 207-217
Fakieh MH, Drake PJ, Lacey J, Munck JM, Motley AM, Hettema EH (2013) Intra-ER sorting of the peroxisomal membrane protein Pex3 relies on its luminal domain. Biol Open **2:** 829-837
Farkas A, De Laurentiis EI, Schwappach B (2019) The natural history of Get3-like chaperones. Traffic **20:** 311-324
Formighieri C, Cazzaniga S, Kuras R, Bassi R (2013) Biogenesis of photosynthetic complexes in the chloroplast of Chlamydomonas reinhardtii requires ARSA1, a homolog of prokaryotic arsenite transporter and eukaryotic TRC40 for guided entry of tail-anchored proteins. Plant J **73:** 850-861
Fumagalli F, Noack J, Bergmann TJ, Cebollero E, Pisoni GB, Fasana E, Fregno I, Galli C, Loi M, Solda T, D'Antuono R, Raimondi A, Jung M, Melnyk A, Schorr S, Schreiber A, Simonelli L, Varani L, Wilson-Zbinden C, Zerbe O, Hofmann K, Peter M, Quadroni M, Zimmermann R, Molinari M (2016) Translocon component Sec62 acts in endoplasmic reticulum turnover during stress recovery. Nat Cell Biol **18:** 1173-1184

Downloaded from https://academic.oup.com/plphys/advance-article/doi/10.1093/plphys/kiab298/6307274 by guest on 01 July 2021

Gilmore R, Blobel G, Walter P (1982) Protein translocation across the endoplasmic reticulum. I. Detection in the microsomal membrane of a receptor for the signal recognition particle. J Cell Biol **95:** 463-469

Gilmore R, Walter P, Blobel G (1982) Protein translocation across the endoplasmic reticulum. II. Isolation and characterization of the signal recognition particle receptor. J Cell Biol **95:** 470-477

Gristick HB, Rao M, Chartron JW, Rome ME, Shan SO, Clemons WM, Jr. (2014) Crystal structure of ATP-bound Get3-Get4-Get5 complex reveals regulation of Get3 by Get4. Nat Struct Mol Biol **21:** 437-442

Guna A, Hegde RS (2018) Transmembrane Domain Recognition during Membrane Protein Biogenesis and Quality Control. Curr Biol **28:** R498-R511

Guna A, Volkmar N, Christianson JC, Hegde RS (2018) The ER membrane protein complex is a transmembrane domain insertase. Science **359:** 470-473

Halbach A, Landgraf C, Lorenzen S, Rosenkranz K, Volkmer-Engert R, Erdmann R, Rottensteiner H (2006) Targeting of the tail-anchored peroxisomal membrane proteins PEX26 and PEX15 occurs through C-terminal PEX19-binding sites. J Cell Sci **119:** 2508-2517

Hassdenteufel S, Sicking M, Schorr S, Aviram N, Fecher-Trost C, Schuldiner M, Jung M, Zimmermann R, Lang S (2017) hSnd2 protein represents an alternative targeting factor to the endoplasmic reticulum in human cells. FEBS Lett **591:** 3211-3224

Hegde RS, Keenan RJ (2011) Tail-anchored membrane protein insertion into the endoplasmic reticulum. Nat Rev Mol Cell Biol **12:** 787-798

Hu S, Ye H, Cui Y, Jiang L (2020) AtSec62 is critical for plant development and is involved in ER-phagy in Arabidopsis thaliana. J Integr Plant Biol **62:** 181-200

Inglis AJ, Page KR, Guna A, Voorhees RM (2020) Differential Modes of Orphan Subunit Recognition for the WRB/CAML Complex. Cell Rep **30:** 3691-3698 e3695

Johnson N, Powis K, High S (2013) Post-translational translocation into the endoplasmic reticulum. Biochim Biophys Acta **1833:** 2403-2409

Jurgens G (2005) Cytokinesis in higher plants. Annu Rev Plant Biol **56:** 281-299

Kao YT, Gonzalez KL, Bartel B (2018) Peroxisome Function, Biogenesis, and Dynamics in Plants. Plant Physiol **176:** 162-177

Kemper C, Habib SJ, Engl G, Heckmeyer P, Dimmer KS, Rapaport D (2008) Integration of tail-anchored proteins into the mitochondrial outer membrane does not require any known import components. J Cell Sci **121:** 1990-1998

Kriechbaumer V, Shaw R, Mukherjee J, Bowsher CG, Harrison AM, Abell BM (2009) Subcellular distribution of tail-anchored proteins in Arabidopsis. Traffic **10:** 1753-1764

Krumpe K, Frumkin I, Herzig Y, Rimon N, Ozbalci C, Brugger B, Rapaport D, Schuldiner M (2012) Ergosterol content specifies targeting of tail-anchored proteins to mitochondrial outer membranes. Mol Biol Cell **23:** 3927-3935

Lakkaraju AK, Mary C, Scherrer A, Johnson AE, Strub K (2008) SRP keeps polypeptides translocation-competent by slowing translation to match limiting ER-targeting sites. Cell **133:** 440-451

Lam SK, Yoda N, Schekman R (2011) A vesicle carrier that mediates peroxisome protein traffic from the endoplasmic reticulum. Proc Natl Acad Sci U S A **108:** E51-52

Lauber MH, Waizenegger I, Steinmann T, Schwarz H, Mayer U, Hwang I, Lukowitz W, Jurgens G (1997) The Arabidopsis KNOLLE protein is a cytokinesis-specific syntaxin. J Cell Biol **139:** 1485-1493

Lee J, Kim DH, Hwang I (2014) Specific targeting of proteins to outer envelope membranes of endosymbiotic organelles, chloroplasts, and mitochondria. Front Plant Sci **5:** 173

Leznicki P, High S (2012) SGTA antagonizes BAG6-mediated protein triage. Proc Natl Acad Sci U S A **109:** 19214-19219

Leznicki P, Roebuck QP, Wunderley L, Clancy A, Krysztofinska EM, Isaacson RL, Warwicker J, Schwappach B, High S (2013) The association of BAG6 with SGTA and tail-anchored proteins. PLoS One **8:** e59590

Downloaded from https://academic.oup.com/plphys/advance-article/doi/10.1093/plphys/kiab298/6307274 by guest on 01 July 2021

Li Y, Kabbage M, Liu W, Dickman MB (2016) Aspartyl Protease-Mediated Cleavage of BAG6 Is Necessary for Autophagy and Fungal Resistance in Plants. Plant Cell **28:** 233-247

Lin SY, Vollrath MA, Mangosing S, Shen J, Cardenas E, Corey DP (2016) The zebrafish pinball wizard gene encodes WRB, a tail-anchored-protein receptor essential for inner-ear hair cells and retinal photoreceptors. J Physiol **594:** 895-914

Lin TW, Chen CC, Wu SM, Chang YC, Li YC, Su YW, Hsiao CD, Chang HY (2019) Structural analysis of chloroplast tail-anchored membrane protein recognition by ArsA1. Plant J **99:** 128-143

Lisenbee CS, Lingard MJ, Trelease RN (2005) Arabidopsis peroxisomes possess functionally redundant membrane and matrix isoforms of monodehydroascorbate reductase. Plant J **43:** 900-914

Maestre-Reyna M, Wu SM, Chang YC, Chen CC, Maestre-Reyna A, Wang AH, Chang HY (2017) In search of tail-anchored protein machinery in plants: reevaluating the role of arsenite transporters. Sci Rep **7:** 46022

Maggio C, Barbante A, Ferro F, Frigerio L, Pedrazzini E (2007) Intracellular sorting of the tail-anchored protein cytochrome b5 in plants: a comparative study using different isoforms from rabbit and Arabidopsis. J Exp Bot **58:** 1365-1379

Mariappan M, Li X, Stefanovic S, Sharma A, Mateja A, Keenan RJ, Hegde RS (2010) A ribosome-associating factor chaperones tail-anchored membrane proteins. Nature **466:** 1120-1124

Mariappan M, Mateja A, Dobosz M, Bove E, Hegde RS, Keenan RJ (2011) The mechanism of membrane-associated steps in tail-anchored protein insertion. Nature **477:** 61-66

Marty NJ, Teresinski HJ, Hwang YT, Clendening EA, Gidda SK, Sliwinska E, Zhang D, Miernyk JA, Brito GC, Andrews DW, Dyer JM, Mullen RT (2014) New insights into the targeting of a subset of tail-anchored proteins to the outer mitochondrial membrane. Front Plant Sci **5:** 426

Mateja A, Paduch M, Chang HY, Szydlowska A, Kossiakoff AA, Hegde RS, Keenan RJ (2015) Protein targeting. Structure of the Get3 targeting factor in complex with its membrane protein cargo. Science **347:** 1152-1155

Mateja A, Szlachcic A, Downing ME, Dobosz M, Mariappan M, Hegde RS, Keenan RJ (2009) The structural basis of tail-anchored membrane protein recognition by Get3. Nature **461:** 361-366

McDowell MA, Heimes M, Fiorentino F, Mehmood S, Farkas A, Coy-Vergara J, Wu D, Bolla JR, Schmid V, Heinze R, Wild K, Flemming D, Pfeffer S, Schwappach B, Robinson CV, Sinning I (2020) Structural Basis of Tail-Anchored Membrane Protein Biogenesis by the GET Insertase Complex. Mol Cell **80:** 72-86 e77

McDowell MA, Heimes M, Sinning I (2021) Structural and molecular mechanisms for membrane protein biogenesis by the Oxa1 superfamily. Nat Struct Mol Biol **28:** 234-239

Mehlhorn DG, Wallmeroth N, Berendzen KW, Grefen C (2018) 2in1 Vectors Improve In Planta BiFC and FRET Analyses. Methods Mol Biol **1691:** 139-158

Mitterreiter MJ, Bosch FA, Brylok T, Schwenkert S (2020) The ER luminal C-terminus of AtSec62 is critical for male fertility and plant growth in Arabidopsis thaliana. Plant J **101:** 5-17

Moog D (2019) Higher Complexity Requires Higher Accuracy: Tail-Anchored Protein Targeting to the Outer Envelope Membrane of Plant Plastids via a Specific C-Terminal Motif. Plant Cell Physiol **60:** 489-491

Mukhopadhyay R, Ho YS, Swiatek PJ, Rosen BP, Bhattacharjee H (2006) Targeted disruption of the mouse Asna1 gene results in embryonic lethality. FEBS Lett **580:** 3889-3894

Mullen RT, Trelease RN (2000) The sorting signals for peroxisomal membrane-bound ascorbate peroxidase are within its C-terminal tail. J Biol Chem **275:** 16337-16344

Neupert W (1997) Protein import into mitochondria. Annu Rev Biochem **66:** 863-917

Neveu E, Khalifeh D, Salamin N, Fasshauer D (2020) Prototypic SNARE Proteins Are Encoded in the Genomes of Heimdallarchaeota, Potentially Bridging the Gap between the Prokaryotes and Eukaryotes. Curr Biol **30:** 2468-2480 e2465

Norlin S, Parekh VS, Naredi P, Edlund H (2016) Asna1/TRC40 Controls beta-Cell Function and Endoplasmic Reticulum Homeostasis by Ensuring Retrograde Transport. Diabetes **65:** 110-119

Downloaded from https://academic.oup.com/plphys/advance-article/doi/10.1093/plphys/kiab298/6307274 by guest on 01 July 2021

Novick P, Field C, Schekman R (1980) Identification of 23 complementation groups required for post-translational events in the yeast secretory pathway. Cell **21:** 205-215
Ogg SC, Walter P (1995) SRP samples nascent chains for the presence of signal sequences by interacting with ribosomes at a discrete step during translation elongation. Cell **81:** 1075-1084
Ogura T, Wilkinson AJ (2001) AAA+ superfamily ATPases: common structure--diverse function. Genes Cells **6:** 575-597
Okreglak V, Walter P (2014) The conserved AAA-ATPase Msp1 confers organelle specificity to tail-anchored proteins. Proc Natl Acad Sci U S A **111:** 8019-8024
Paul P, Simm S, Blaumeiser A, Scharf KD, Fragkostefanakis S, Mirus O, Schleiff E (2013) The protein translocation systems in plants - composition and variability on the example of Solanum lycopersicum. BMC Genomics **14:** 189
Pechmann S, Chartron JW, Frydman J (2014) Local slowdown of translation by nonoptimal codons promotes nascent-chain recognition by SRP in vivo. Nat Struct Mol Biol **21:** 1100-1105
Pedrazzini E (2009) Tail-Anchored Proteins in Plants. Journal of Plant Biology **52:** 88-101
Pedrazzini E, Villa A, Borgese N (1996) A mutant cytochrome b5 with a lengthened membrane anchor escapes from the endoplasmic reticulum and reaches the plasma membrane. Proc Natl Acad Sci U S A **93:** 4207-4212
Pfanner N, Geissler A (2001) Versatility of the mitochondrial protein import machinery. Nat Rev Mol Cell Biol **2:** 339-349
Qbadou S, Tien R, Soll J, Schleiff E (2003) Membrane insertion of the chloroplast outer envelope protein, Toc34: constrains for insertion and topology. J Cell Sci **116:** 837-846
Rabu C, Wipf P, Brodsky JL, High S (2008) A precursor-specific role for Hsp40/Hsc70 during tail-anchored protein integration at the endoplasmic reticulum. J Biol Chem **283:** 27504-27513
Rao M, Okreglak V, Chio US, Cho H, Walter P, Shan SO (2016) Multiple selection filters ensure accurate tail-anchored membrane protein targeting. Elife **5**
Richter JD, Coller J (2015) Pausing on Polyribosomes: Make Way for Elongation in Translational Control. Cell **163:** 292-300
Ruberti C, Costa A, Pedrazzini E, Lo Schiavo F, Zottini M (2014) FISSION1A, an Arabidopsis tail-anchored protein, is localized to three subcellular compartments. Mol Plant **7:** 1393-1396
Sabatini DD, Blobel G (1970) Controlled proteolysis of nascent polypeptides in rat liver cell fractions. II. Location of the polypeptides in rough microsomes. J Cell Biol **45:** 146-157
Samuelson JC, Chen M, Jiang F, Moller I, Wiedmann M, Kuhn A, Phillips GJ, Dalbey RE (2000) YidC mediates membrane protein insertion in bacteria. Nature **406:** 637-641
Schuldiner M, Metz J, Schmid V, Denic V, Rakwalska M, Schmitt HD, Schwappach B, Weissman JS (2008) The GET complex mediates insertion of tail-anchored proteins into the ER membrane. Cell **134:** 634-645
Schweiger R, Muller NC, Schmitt MJ, Soll J, Schwenkert S (2012) AtTPR7 is a chaperone-docking protein of the Sec translocon in Arabidopsis. J Cell Sci **125:** 5196-5207
Schweiger R, Schwenkert S (2013) AtTPR7 as part of the Arabidopsis Sec post-translocon. Plant Signal Behav **8**
Setoguchi K, Otera H, Mihara K (2006) Cytosolic factor- and TOM-independent import of C-tail-anchored mitochondrial outer membrane proteins. EMBO J **25:** 5635-5647
Shao S, Hegde RS (2011) Membrane protein insertion at the endoplasmic reticulum. Annu Rev Cell Dev Biol **27:** 25-56
Shao S, Rodrigo-Brenni MC, Kivlen MH, Hegde RS (2017) Mechanistic basis for a molecular triage reaction. Science **355:** 298-302
Shen G, Kuppu S, Venkataramani S, Wang J, Yan J, Qiu X, Zhang H (2010) ANKYRIN REPEAT-CONTAINING PROTEIN 2A is an essential molecular chaperone for peroxisomal membrane-bound ASCORBATE PEROXIDASE3 in Arabidopsis. Plant Cell **22:** 811-831
Simpson PJ, Schwappach B, Dohlman HG, Isaacson RL (2010) Structures of Get3, Get4, and Get5 provide new models for TA membrane protein targeting. Structure **18:** 897-902

Downloaded from https://academic.oup.com/plphys/advance-article/doi/10.1093/plphys/kiab298/6307274 by guest on 01 July 2021

Song W, Raden D, Mandon EC, Gilmore R (2000) Role of Sec61alpha in the regulated transfer of the ribosome-nascent chain complex from the signal recognition particle to the translocation channel. Cell **100:** 333-343

Srivastava R, Zalisko BE, Keenan RJ, Howell SH (2017) The GET System Inserts the Tail-Anchored Protein, SYP72, into Endoplasmic Reticulum Membranes. Plant Physiol **173:** 1137-1145

Stefanovic S, Hegde RS (2007) Identification of a targeting factor for posttranslational membrane protein insertion into the ER. Cell **128:** 1147-1159

Stefer S, Reitz S, Wang F, Wild K, Pang YY, Schwarz D, Bomke J, Hein C, Lohr F, Bernhard F, Denic V, Dotsch V, Sinning I (2011) Structural basis for tail-anchored membrane protein biogenesis by the Get3-receptor complex. Science **333:** 758-762

Suloway CJ, Chartron JW, Zaslaver M, Clemons WM, Jr. (2009) Model for eukaryotic tail-anchored protein binding based on the structure of Get3. Proc Natl Acad Sci U S A **106:** 14849-14854

Suloway CJ, Rome ME, Clemons WM, Jr. (2012) Tail-anchor targeting by a Get3 tetramer: the structure of an archaeal homologue. EMBO J **31:** 707-719

Sun F, Carrie C, Law S, Murcha MW, Zhang R, Law YS, Suen PK, Whelan J, Lim BL (2012) AtPAP2 is a tail-anchored protein in the outer membrane of chloroplasts and mitochondria. Plant Signal Behav **7:** 927-932

Tam YY, Fagarasanu A, Fagarasanu M, Rachubinski RA (2005) Pex3p initiates the formation of a preperoxisomal compartment from a subdomain of the endoplasmic reticulum in Saccharomyces cerevisiae. J Biol Chem **280:** 34933-34939

Teresinski HJ, Gidda SK, Nguyen TND, Howard NJM, Porter BK, Grimberg N, Smith MD, Andrews DW, Dyer JM, Mullen RT (2019) An RK/ST C-Terminal Motif is Required for Targeting of OEP7.2 and a Subset of Other Arabidopsis Tail-Anchored Proteins to the Plastid Outer Envelope Membrane. Plant Cell Physiol **60:** 516-537

Thornton N, Stroud DA, Milenkovic D, Guiard B, Pfanner N, Becker T (2010) Two modular forms of the mitochondrial sorting and assembly machinery are involved in biogenesis of alpha-helical outer membrane proteins. J Mol Biol **396:** 540-549

van der Zand A, Braakman I, Tabak HF (2010) Peroxisomal membrane proteins insert into the endoplasmic reticulum. Mol Biol Cell **21:** 2057-2065

Vilardi F, Lorenz H, Dobberstein B (2011) WRB is the receptor for TRC40/Asna1-mediated insertion of tail-anchored proteins into the ER membrane. J Cell Sci **124:** 1301-1307

Vilardi F, Stephan M, Clancy A, Janshoff A, Schwappach B (2014) WRB and CAML are necessary and sufficient to mediate tail-anchored protein targeting to the ER membrane. PLoS One **9:** e85033

Vitali DG, Sinzel M, Bulthuis EP, Kolb A, Zabel S, Mehlhorn DG, Figueiredo Costa B, Farkas A, Clancy A, Schuldiner M, Grefen C, Schwappach B, Borgese N, Rapaport D (2018) The GET pathway can increase the risk of mitochondrial outer membrane proteins to be mistargeted to the ER. J Cell Sci **131**

Vogl C, Panou I, Yamanbaeva G, Wichmann C, Mangosing SJ, Vilardi F, Indzhykulian AA, Pangrsic T, Santarelli R, Rodriguez-Ballesteros M, Weber T, Jung S, Cardenas E, Wu X, Wojcik SM, Kwan KY, Del Castillo I, Schwappach B, Strenzke N, Corey DP, Lin SY, Moser T (2016) Tryptophan-rich basic protein (WRB) mediates insertion of the tail-anchored protein otoferlin and is required for hair cell exocytosis and hearing. EMBO J

Volkmar N, Thezenas ML, Louie SM, Juszkiewicz S, Nomura DK, Hegde RS, Kessler BM, Christianson JC (2019) The ER membrane protein complex promotes biogenesis of sterol-related enzymes maintaining cholesterol homeostasis. J Cell Sci **132**

Voss NR, Gerstein M, Steitz TA, Moore PB (2006) The geometry of the ribosomal polypeptide exit tunnel. J Mol Biol **360:** 893-906

Voth W, Schick M, Gates S, Li S, Vilardi F, Gostimskaya I, Southworth DR, Schwappach B, Jakob U (2014) The protein targeting factor Get3 functions as ATP-independent chaperone under oxidative stress conditions. Mol Cell **56:** 116-127

Downloaded from https://academic.oup.com/plphys/advance-article/doi/10.1093/plphys/kiab298/6307274 by guest on 01 July 2021

Walter P, Blobel G (1981) Translocation of proteins across the endoplasmic reticulum III. Signal recognition protein (SRP) causes signal sequence-dependent and site-specific arrest of chain elongation that is released by microsomal membranes. J Cell Biol **91:** 557-561

Wang F, Brown EC, Mak G, Zhuang J, Denic V (2010) A chaperone cascade sorts proteins for posttranslational membrane insertion into the endoplasmic reticulum. Mol Cell **40:** 159-171

Wang F, Chan C, Weir NR, Denic V (2014) The Get1/2 transmembrane complex is an endoplasmic-reticulum membrane protein insertase. Nature **512:** 441-444

Wang F, Whynot A, Tung M, Denic V (2011) The mechanism of tail-anchored protein insertion into the ER membrane. Mol Cell **43:** 738-750

Wang L, Myasnikov A, Pan X, Walter P (2020) Structure of the AAA protein Msp1 reveals mechanism of mislocalized membrane protein extraction. Elife **9**

Wang L, Walter P (2020) Msp1/ATAD1 in Protein Quality Control and Regulation of Synaptic Activities. Annu Rev Cell Dev Biol **36:** 141-164

Wereszczynski J, McCammon JA (2012) Nucleotide-dependent mechanism of Get3 as elucidated from free energy calculations. Proc Natl Acad Sci U S A **109:** 7759-7764

Westrich LD, Gotsmann VL, Herkt C, Ries F, Kazek T, Trosch R, Armbruster L, Muhlenbeck JS, Ramundo S, Nickelsen J, Finkemeier I, Wirtz M, Storchova Z, Raschle M, Willmund F (2021) The versatile interactome of chloroplast ribosomes revealed by affinity purification mass spectrometry. Nucleic Acids Res **49:** 400-415

Wickner WT (2013) Profile of Thomas Sudhof, James Rothman, And Randy Schekman, 2013 Nobel Laureates in Physiology or Medicine. Proc Natl Acad Sci U S A **110:** 18349-18350

Wu X, Cabanos C, Rapoport TA (2019) Structure of the post-translational protein translocation machinery of the ER membrane. Nature **566:** 136-139

Xing S, Mehlhorn DG, Wallmeroth N, Asseck LY, Kar R, Voss A, Denninger P, Schmidt VA, Schwarzlander M, Stierhof YD, Grossmann G, Grefen C (2017) Loss of GET pathway orthologs in Arabidopsis thaliana causes root hair growth defects and affects SNARE abundance. Proc Natl Acad Sci U S A **114:** E1544-E1553

Yagita Y, Hiromasa T, Fujiki Y (2013) Tail-anchored PEX26 targets peroxisomes via a PEX19-dependent and TRC40-independent class I pathway. J Cell Biol **200:** 651-666

Yamamoto Y, Sakisaka T (2012) Molecular machinery for insertion of tail-anchored membrane proteins into the endoplasmic reticulum membrane in mammalian cells. Mol Cell **48:** 387-397

Zalisko BE, Chan C, Denic V, Rock RS, Keenan RJ (2017) Tail-Anchored Protein Insertion by a Single Get1/2 Heterodimer. Cell Rep **20:** 2287-2293

Zhuang X, Chung KP, Jiang L (2017) Targeting tail-anchored proteins into plant organelles. Proc Natl Acad Sci U S A **114:** 1762-1764

Downloaded from https://academic.oup.com/plphys/advance-article/doi/10.1093/plphys/kiab298/6307274 by guest on 01 July 2021

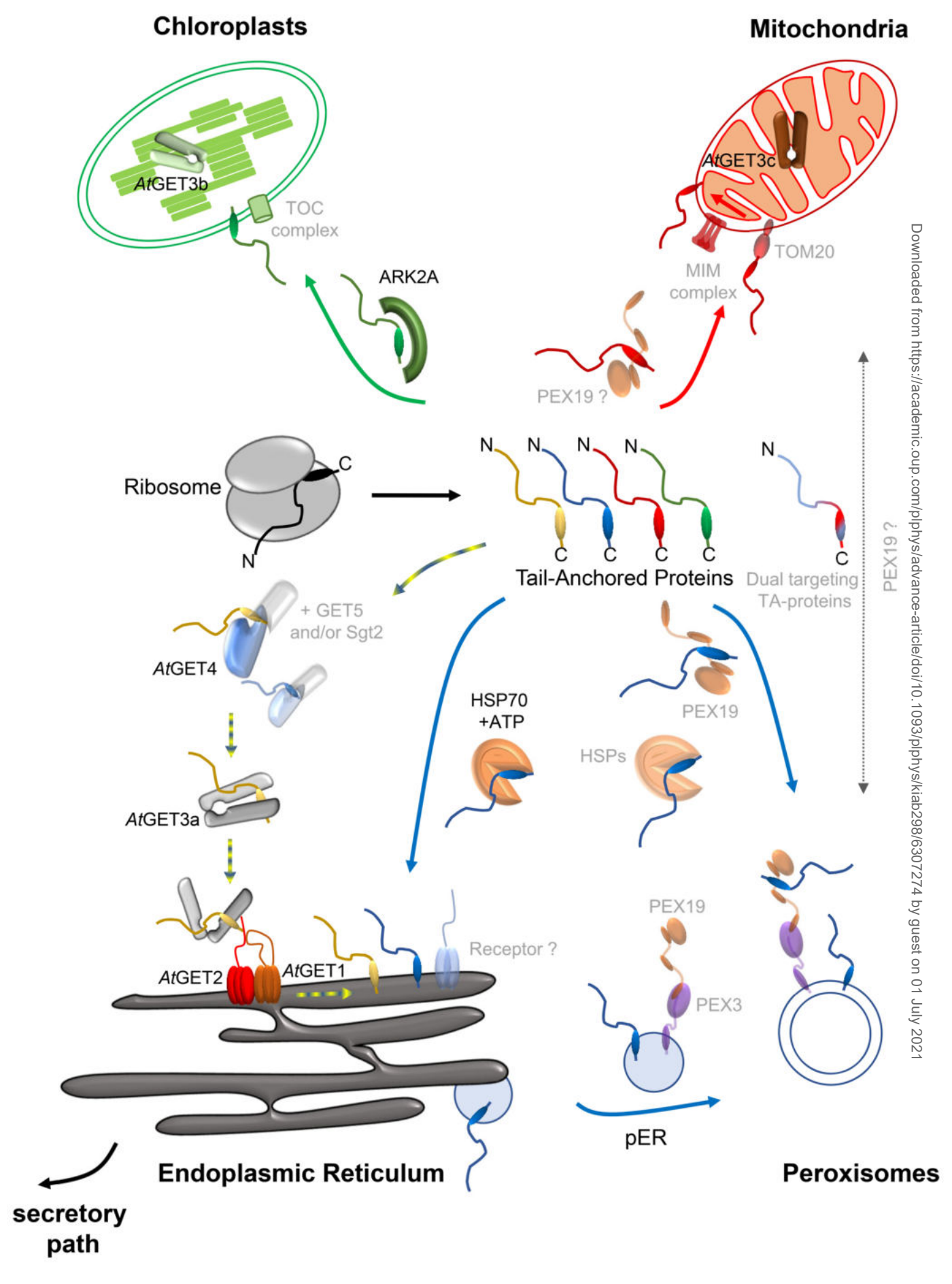

Downloaded from https://academic.oup.com/plphys/advance-article/doi/10.1093/plphys/kiab298/6307274 by guest on 01 July 2021

ADVANCES

- Research in the last decade revealed several different targeting routes for TA protein transport and translocation into the ER and organellar membranes of eukaryotes.
- The GET pathway described for TA protein insertion in yeast and mammals is partially conserved in Arabidopsis where loss of function leads to defects in root hair growth.
- Absence of the coreceptor for TA protein docking and insertion at the ER membrane in the context of the GET pathway in plants phenocopies other *get* lines.
- Sequence information confirms conservation of alternative yeast pathways in plants while functional data currently remains elusive.
- TA protein import into the ER membrane was mainly studied in yeast and mammalian cell culture, but plants have proven ideal models to gain a deeper understanding of these pathways in an organismal context and to study their functional impact on multicellular systems.

Downloaded from https://academic.oup.com/plphys/advance-article/doi/10.1093/plphys/kia

OUTSTANDING QUESTIONS

- Which additional pathways for TA protein insertion exist in plants?
- What alternative functions have evolved for the GET pathway components in Arabidopsis or more generally in plants?
- Why did Archaeplastida evolve organellar variants of the GET3 ATPase and what is (are) their function(s)?
- Is a post-translational pre-targeting complex conserved in archaeplastida?

Downloaded from https://a